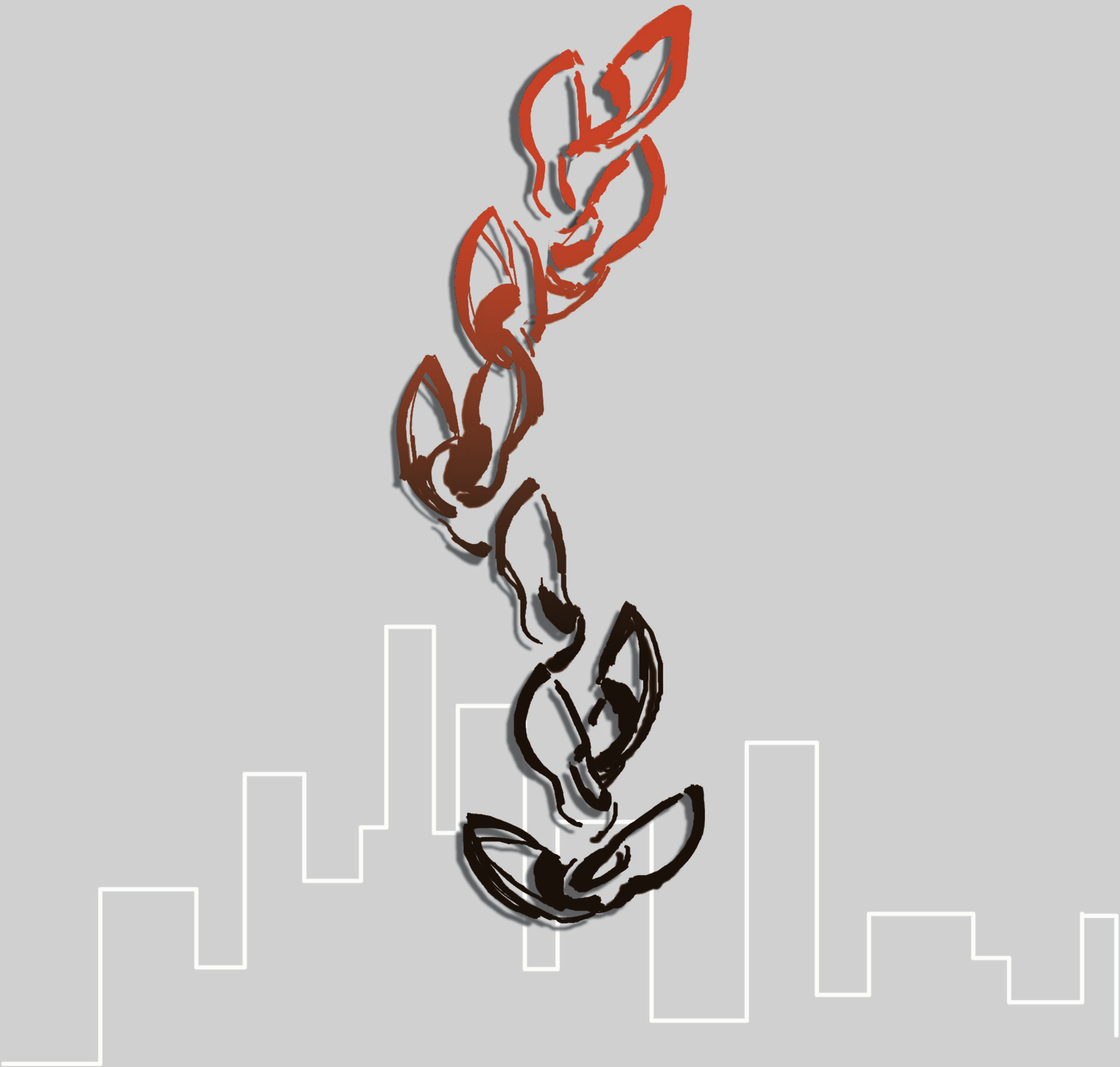

Rice husk ash as a mineral admixture for Ultra High Performance Concrete

NGUYEN VAN TUAN

Rice Husk Ash as a Mineral Admixture for Ultra High Performance Concrete

Cover designed by Nguyễn Minh Quân

Rice Husk Ash as a Mineral Admixture for Ultra High Performance Concrete

Proefschrift

ter verkrijging van de graad van doctor
aan de Technische Universiteit Delft,
op gezag van de Rector Magnificus prof. ir. K.C.A.M. Luyben,
voorzitter van het College voor Promoties,
in het openbaar te verdedigen op dinsdag 20 september 2011 om 10.00 uur

door Văn Tuấn NGUYỄN
Master of Engineering, National University of Civil Engineering
geboren te Thái Bình, Vietnam

Dit proefschrift is goedgekeurd door de promotor:
Prof. dr. ir. K. van Breugel

Copromotor: Dr. G. Ye

Samenstelling promotiecommissie:

Rector Magnificus,	voorzitter
Prof. dr. ir. K. van Breugel,	Technische Universiteit Delft, promotor
Dr. G. Ye,	Technische Universiteit Delft, copromotor
Prof. dr. ir. E. M. Haas,	Technische Universiteit Delft
Prof. dr. G. De Schutter,	Universiteit Gent, België
Prof. dr. M.H. Zhang,	National University of Singapore, Singapore
Dr. ir. E.A.B. Koenders,	Technische Universiteit Delft / COPPE-UFRJ, Brazilië
Dr. D.D. Bui,	National University of Civil Engineering, Vietnam
Prof. dr. R.B. Polder,	Technische Universiteit Delft, reservelid

ISBN: 978-94-6191-024-0

Keywords: rice husk ash, silica fume, ultra high performance concrete

Printed in the Netherlands.

Acknowledgements

I would like to express my deep gratitude to some people who have been supporting me during this thesis accomplishment.

I wish to express my thanks to the PhD scholarship sponsored by the Vietnamese Overseas Scholarship Program of Vietnamese Government (322 Project). The financial supports from CICAT and Section of Materials and Environment, TU Delft are highly appreciated.

I would like to express my greatest gratitude to my promotor Prof. Klaas van Breugel for his guidance, advice, and invaluable support throughout my PhD period, especially the challenges he let me think independently in studying. I admire his profound knowledge, experience, and enthusiasm in research.

I express my sincerest acknowledgement to my co-promotor Ass. Prof. Ye Guang for all his excellent supervision, tireless assistance, patience, encouragement, and his thorough understanding that helps me balance my private and professional life. I will always be grateful for the lessons learnt through numerous discussions.

I am also most grateful to my supervisor, Dr. Zhanqi Guo, for his constructive guidance, generous support and inspired suggestions during the first two years.

My sincere appreciation goes to Drs. H.P.S. Althuis, the director of CICAT, especially to Veronique van de Varst for her consideration and support during my stay in Delft and Holland.

I would like to thank my colleagues in the section of Materials and Environments including all PhD colleagues, especially Jian Zhou, Phùng Trọng Quyền, Sonja Scher, Sonja Fennis; post-doc researchers Alvaro Garcia Hernandez, Kritsada Sisomphon, Dessi Koleva; a MSc colleague Madiha Ahammout for her translation; technicians Fred Schilperoort, Arjan Thijssen, Gerrit Nagtegaal, Gerard Timmers, John van der Berg, Ron Penners; secretaries Iris, Claudia, Nynke; and Dr. Alex Fraaij, Dr. Mario de Rooij, Dr. Oguzhan Copuroglu, Dr. Erick Schlangen, Dr. Henk Jonkers for their friendship, assistance and discussions throughout the course of this work. I am grateful for numerous discussions with my two office-roommates Liu Lin and Jie Zhao. My special thank goes to Dr. Eddy Koenders for his invaluable discussions on the HYMOSTRUC3D model and Zhang Qi who helped me to implement the simulation part.

The supply of materials from ENCI, ELKEM, BASF, and FILCOM companies for this project is also highly appreciated.

I gratefully acknowledge my English teachers Ana Reeves, Claire Taylor, my wife Nguyễn Hải Yến, my ping-pong group member Adam Pel and Nguyễn Vĩnh Phú who help in correcting my written English of the papers and the PhD thesis.

I feel very lucky to have many close friends from my ping-pong group. The funny games and discussions from them are very valuable for me to release stress after the hard and intensive working days, especially for my final PhD studying phase.

I would like to express my many thanks to all my dear Vietnamese friends in Rotterdam and Delft, which were too many to mention in this list, for their precious kindness and warm friendliness especially during the time my wife and my son lived in the Netherlands. You are always in my mind.

My thanks also go to my teachers and my colleagues Prof. Phùng Văn Lự, Ass. Prof. Phạm Hữu Hanh, Ass. Prof. Nguyễn Mạnh Phát, Dr. Lê Trung Thành in the Department of Building Materials, National University of Civil Engineering, Hanoi, Vietnam, especially to Dr. Bùi Danh Đại who has given me invaluable discussions on the cement-based materials containing rice husk ash. A special thank to Công Thắng who helped me for the preparation of the rice husk ash sample.

I take this opportunity to convey my sincere thanks to Dr. Nguyễn Bỉnh Thìn for his suggestion in my very first studying years at university, which brought me to a world of a fruitful land of research (i.e. building materials).

I express my deepest gratitude to my family for all their love, support, and encouragement throughout my life to this point. Without their encouragement this work would not have been possible. I especially want to thank my parents Nguyễn Văn Kép and Đặng Thị Nuột, my parents-in-law Nguyễn Thế Bình and Nguyễn Thị Kim Liên, and my sister Nguyễn Thị Thanh Bình for their many sacrifices and supports for us during the time I and my wife studied, and my son was born and lived in the Netherlands. I will always be grateful for everything they have done and owe them a debt that never can be repaid - Thank you for everything.

Last but not least, I owe this thesis to Nguyễn Hải Yến for her love, unwavering support, patience and companion through many ups and downs, and to our little beloved children, Nguyễn Thế Trung and Nguyễn Ngân Hà, for bringing the happiness to my family everyday. They all truly share in this accomplishment.

Nguyễn Văn Tuấn
Delft, Sept. 2011

Table of contents

List of Symbols

b, n	the Rosin-Rammler constants
C_{CH}	a repair factor in HYMOSTRUC
Ea	activation energy
F_i	the influence factors of temperature of the hydration process
G(x)	the particle size distribution of material
K_0	the basic rate factor of the boundary reaction in HYMOSTRUC
N	the number of particles
Po_{RHA}	the factor accounting for the reaction of CH phase with RHA
R	the radius of the particle
V	the volume of phase
W(x)	the mass of material
x	the diameter of the particle
$\alpha(t)$	the degree of hydration at time t
β_i	the empirical factors in HYMOSTRUC
γ	the correction factor in HYMOSTRUC
δ_{tr}	the transition thickness in HYMOSTRUC
ζ_{pa}	the volumetric density of the paste
ζ_x	the volumetric density of the cell
ζ_{sh}	the shell density
λ	the factor in HYMOSTRUC
ν	the ratio between the volume of the gel and that of the reactant
ρ	the specific mass
ω_b	the water/binder ratio
ω_0	the water/cement ratio
ϕ	the diameter of the pore
Ω_i	the effect factors of water on the cement hydration mechanisms

List of Abbreviations

AFm	Mono-sulphate
AFt	Ettringite
BSE	Backscattered electron
CH	Calcium hydroxide
CPM	Compressible packing model
CSH	Calcium Silicate Hydrates
ESEM	Environmental Scanning Electron Microscope
HSC	High strength concrete
HPC	High performance concrete
ITZ	Interfacial Transition Zone
LPM	Linear packing model
MIP	Mercury Intrusion Porosimetry
NSC	Normal strength concrete
PSD	Particle size distribution
RH	Relative humidity
RHA	Rice husk ash
RPC	Reactive powder concrete
SE	Secondary electron
SEM	Scanning Electron Microscope
SF	Silica fume
TGA	Thermogravimetric analysis
UHPC	Ultra high performance concrete
w/c	water-to-cement
w/b	water-to-binder

1

Introduction

1.1 Background to the research

Recent work carried out on the formulation and manufacture of concretes has led to the development of ultra-high performance concretes (UHPC), which is considered to be one of the latest advances in concrete technology. This concrete presents superior mechanical and durability properties [Richard and Cheyrezy 1995; AFGC-SETRA 2002]. In general, UHPC is a fiber-reinforced, superplasticized, silica fume-cement mixture with a very low water-cement ratio (w/c) characterized by the presence of very fine quartz sand (0.15-0.60 mm) instead of ordinary aggregate. Depending on its composition and the treating temperature its compressive strength ranges between 150 and up to 800 MPa [Richard and Cheyrezy 1995].

The high amount of cement in UHPC, 900-1000 kg/m^3, and very high silica fume (SF) content, 150-250 kg/m^3 (10-30% by weight of cement) [Richard and Cheyrezy 1994; 1995; Long *et al.* 2002] cause not only the high cost of powders in UHPC [Bonneau *et al.* 1996; Aïtcin 2000], but also some drawbacks when sustainable development is considered. The production of cement increases the content of CO_2, which impacts on global warming. In this respect, using the mineral admixtures can be an attractive alternative.

Silica fume with an extreme fineness and a high amorphous silica content becomes an essential constituent in UHPC because of its physical- (filler, lubrication) and pozzolanic-effects. Thanks to its exceptional characteristics and properties, the presence of SF explains its contribution to the mechanical properties and durability of UHPCs [Long *et al.* 2002]. As a result, the limited available resource and the high cost of SF constrain its application in modern construction industry, especially in developing countries. For these reasons, it gives a motivation for searching for other materials with similar functions to substitute SF partially or fully in producing UHPC.

It should be noted that in fact, the SF in the original ‘as collected’ form as used in this study is light and of low bulk density, which may cause difficulty and expense for transportation and handling. Commercial suppliers have responded by processing SF using different methods of densification and compaction in order to improve the handling and transport properties of the material, such as dry-densified, slurried or dry-pelletized to increase its bulk density [Malhotra *et al.* 1987; Boddy *et al.* 2000]. The dry-densified SF is by far the most common form of SF used in current concrete practice [Diamond and Sahu 2006] and makes up more than 75% of the commercial market in the western hemisphere [Wolsiefer Sr. 2007]. The particle size of this type of SF is relatively big, between 10 µm and several mm [Diamond *et al.* 2004; Diamond and Sahu 2006]. These SF particles cannot be easily broken up due to the high inter-particle forces, for example, forces due to electrostatic charging, Van der Waal's forces and forces due to moisture. Some studies have raised concerns about the dispersibility of SF and the potential for development of the alkali-silica reaction associated with the presence of undispersed agglomerates of SF in cement matrices. In this respect, the substitution for SF by rice husk ash (RHA) is very promising in terms of technical, economical, and environmental feasibility.

One possibility for these alternatives is using rice husk ash (RHA), which is obtained by burning rice husk, an agricultural waste. Rice husk constitutes about one fifth of the 690 million metric tons of rice paddy produced annually in the world [FAO 2010]. When completely incinerating the husk in appropriate conditions, the residue, RHA, contains 90-96% silica in an amorphous form. RHA is also classified in the same category of highly active pozzolans as SF [Mehta 1983]. The mean particle size of RHA generally ranges from 5 to 10 µm [Siddique 2008], whereas the SF mean particle size is only about 0.1-1 µm. However, RHA has a very high specific surface area ranging from 20 to 260 m^2/g [Bui 2001] which is attributed to its porous structure [Cook 1986; Mehta 1994], whereas the specific surface area of SF is about 18-20 m^2/g [Jayakumar 2004] which mainly comes from the ultra-fine particles. Therefore, with a similar chemical composition of RHA and SF, the difference in particle characteristics will be expected to produce different effects on the hydration and microstructure development of cement paste. This aspect so far, however, has not been considered at all.

Although RHA has good prospects from a technical, environmental and economical point of view, there are a number of concerns which should be considered as follows.

1) RHA has a very high water demand due to its porous structure. When added to a concrete mix, RHA particles, like a sponge, absorb water into their pores. In order to obtain a given workable concrete mix, it is necessary to use a considerably larger amount of mixing water. Introduction of superplasticizers into a concrete mix can offset this negative effect of RHA on workability. Normally, the combination of RHA and superplasticizers may reduce the water-to-binder (w/b) ratio of the concrete mix with an acceptable workability. It should be noted that the w/b ratio of UHPC mixture is very low (0.10-0.25, by weight) [Vande Voort *et al.* 2008]. The effect of RHA on the workability of UHPC mixtures with such a low w/b ratio has not been explicitly accounted for.

It is well-known that the addition of a low SF replacement content can improve both the workability and the packing density of UHPC mixtures due to the spherical shape of its ultra-fine particles [Domone and Soutsos 1995; Richard and Cheyrezy 1995; Lea 2004]. This gives rise to the idea that the combination of SF and RHA may compensate for the high water demand of RHA in low w/b mixtures. In fact, the positive effect of the blend of RHA and SF on the rheological performance of HPC was reported by experimental results in comparison to those of single mineral admixtures of either RHA or SF [Laskar and Talukdar 2008]. However, the effect of the combination of RHA and SF on the workability and the packing density of UHPC mixtures where the w/b ratio is very low still remains unknown.

2) The reactivity of RHA is attributed to both its high amorphous silica content and its very large surface area. Mehta [1994] suggested that the RHA particles do not need to be very fine

since the activity of RHA mainly originates from the internal surface area of the particles. In fact, the RHA particle size decreases with increasing the degree of grinding, but an intensive grinding may cause the porous structure of RHA particles to collapse [Sugita *et al.* 1997; Bui 2001; Bui *et al.* 2005]. This collapse will lead to a change in the influence of RHA on the hydration and microstructure development of cement paste. On the other hand, the collapse of the RHA pore structure reduces the water demand as well as the need to increase the superplasticizer dosage [Bui *et al.* 2005]. In addition, the fineness of RHA concerns the energy required for grinding rice husk in which more grinding energy was consumed for a greater fineness of RHA. However, if long periods of grinding are required, either the production output will be reduced or larger milling capacity will be required for a given output. The latter obviously results in higher capital costs for plant, especially in developing countries [Mehta 1994]. This means that an appropriate fineness of RHA should be evaluated, which is advantageous to the optimization of grinding energy, to the enhancement of its pozzolanic activity, and to the improvement of the workability of RHA blended concrete.

3) The high autogenous shrinkage of UHPC is caused by the high chemical volume contraction during cement hydration and the high self-desiccation due to the use of high contents of both cement and SF, and the very low w/c ratios in UHPC as well. What makes RHA a unique pozzolan is its multi-layered, micro-porous surface which differs from SF's spherical solid particles. The porous structure of RHA particles is responsible for reducing the bleeding of mixtures through the water absorption ability of RHA [Hwang and Wu 1989]. Besides, the absorbed water in RHA particles can also compensate for the drop of relative humidity in cement paste during the hydration of cement, as suggested by De Sensale *et al.* [2008]. These results give rise to the idea that RHA can act as an internal curing agent that might mitigate the high autogenous shrinkage of UHPC. This positive effect should be evaluated when the use of internal curing is one of very important methods to enhance the properties of concrete, especially with low w/b ratio mixes [Kovler and Jensen 2007; Bentz and Weiss 2011].

4) With respect to improving the strength of concrete mixtures by using RHA, Mehta [1994] revealed a very interesting point that the addition of RHA will enhance the compressive strength of low w/b ratio samples at later stages, after 28 days and 1 year. For example, the 28-day compressive strength increases approximately 14% compared to that of the control sample when 20% RHA is added. Similar results were also found by Zhang *et al.* [1996] and Bui [2001]. More interestingly, with 0.30 w/b ratio mixtures, the development of the compressive strength of the RHA sample is even similar to that of the SF sample after 90 days [Zhang *et al.* 1996]. To date, the effect of RHA on the compressive strength of UHPC has not yet been exhaustively investigated.

5) As discussed above, the w/b ratio of UHPC is very low, from 0.10 to 0.25 by weight of binder [Vande Voort *et al.* 2008]. Estimates of the final hydration percentage of the cement in UHPC range from 31 to 60% [Cheyrezy *et al.* 1995; Habel *et al.* 2006]. The cores of unhydrated cement particles then work as micro-aggregates. Therefore, being a very expensive 'filler', the substitution for cement by mineral admixtures, i.e. RHA, SF, fly ash, blast furnace slag, etc., is desirable to give a larger packing effect and to increase both the strength and durability of concrete. Furthermore, because of the very high cement content in UHPC, many other beneficial effects can be achieved from this substitution, such as improving the environment and the resulting enhanced sustainability of UHPC. In this respect, the maximum content of the cement replacement by these mineral admixtures, especially for RHA in this research, should be given more attention.

1.2 Objective and scope of this thesis

The particular aim of this thesis is to investigate the possibility of using RHA to produce UHPC. With this aim, the research focuses on the following aspects:

1. The effect of RHA in comparison with SF on the hydration and microstructure development of cement paste is studied in order to evaluate the possibility of RHA to substitute for SF in the low w/b ratio mixtures is evaluated.
2. Numerical simulation studies of the hydration and microstructure development of cement paste containing RHA in order to optimize the use of RHA in cement paste are evaluated. This aspect is very important in designing the UHPC mixtures containing RHA.
3. The mix design of UHPC incorporating RHA including the optimization of the packing density of the granular mixture will be accounted for.
4. The effect of RHA in combination with or without SF on the workability and the compressive strength of UHPC, one of the most important aspects to evaluate the possibility of using RHA to produce UHPC, is considered.
5. The effect of RHA on the hydration and microstructure development of cement paste as well as on the interfacial transition zone between cement paste and sand particles in UHPC at a very low w/b ratio is also taken into account.
6. The effect of RHA on autogenous shrinkage of UHPC is dealt with. This aspect will prove the positive effect of the absorbed water in the porous RHA particles to mitigate the high autogenous shrinkage of UHPC.

In this research, cement paste and concrete incorporating RHA were studied with the following restrictions (see Table 1.1):

Table 1.1 Scope of the thesis

Cement paste	Concrete
- W/b ratios ranging from 0.25 to 0.60	- W/b ratios ranging from 0.15 to 0.23
- Curing age from casting up to 1 year	- Curing age from casting up to 91 days
- Curing in a sealed condition at 20°C	- Curing in a fog room at 20±2°C and with relative humidity of over 95%
- Superplasticizer was used with a w/b ratio of 0.25	- Superplasticizer was used

1.3 Research methodology

In order to reach such goals, the experimental studies focus on the influence of RHA, not only on the hydration and microstructure development of cement paste at a low w/b ratio, but also on autogenous shrinkage and the compressive strength of UHPC.

With respect to the experimental program, isothermal calorimetry was used to measure the heat evolution of cement paste; mercury intrusion porosimetry was applied to determine the pore volume and pore size distribution; scanning electron microscopy was employed to examine the phase distribution; and thermogravimetric analysis was utilized to determine the content of calcium hydroxide, which is one of the main hydration products. The sealed corrugated moulds were used to measure the autogenous shrinkage of UHPC mixtures. The compressive strength of UHPC was determined by the compression test.

With respect to the numerical simulation, the effect of RHA on the hydration and microstructure development was simulated and verified in order to optimize the use of RHA in cement paste.

1.4 Outline of this thesis

This thesis consists of six chapters describing the study of using RHA to produce UHPC. A summary of the content of each chapter is presented below and in Figure 1.1.

In the first chapter, a brief introduction, the objective and scope of this thesis are given. A literature review on UHPC and the potential of RHA to produce UHPC are introduced in the second chapter. In the third chapter, the experiments on the hydration and microstructure development of cement blended with RHA are shown and discussed in detail. The effect of RHA in comparison with that of SF on the hydration process and microstructure development was studied by means of isothermal calorimetry, mercury intrusion porosimetry (MIP), scanning electron microscopy (SEM), and thermogravimetric analysis (TGA).

Apart from empirical approaches, in the fourth chapter, a model of the hydration and microstructure development of cement blended with RHA was developed based on the original HYMOSTRUC3D model [Breugel 1991; Koenders 1997; Ye 2003] in which the chemical reactions and the degree of hydration of four main cement phases, i.e. C_3S, C_2S, C_3A, C_4AF and the reaction of RHA, were dealt with. This model is able to account for a number of aspects of the effect of the RHA particle size, the amorphous phase content and the RHA content on the degree of RHA reaction and the volume fraction of hydration products. From this simulation, the optimal RHA content which is used in cement paste was evaluated.

In the fifth chapter, the possibility of using RHA in combination with or without SF to produce UHPC is investigated. The optimization of the packing density of the UHPC granular mixture and UHPC mix design is dealt with. In addition, the effect of RHA on the hydration and microstructure development, on the compressive strength, and on autogenous shrinkage of UHPC is taken into account. These results are compared to those of the samples made with SF.

In the last chapter, the conclusions and recommendations on the use of RHA as a mineral admixture to produce UHPC are highlighted and discussed.

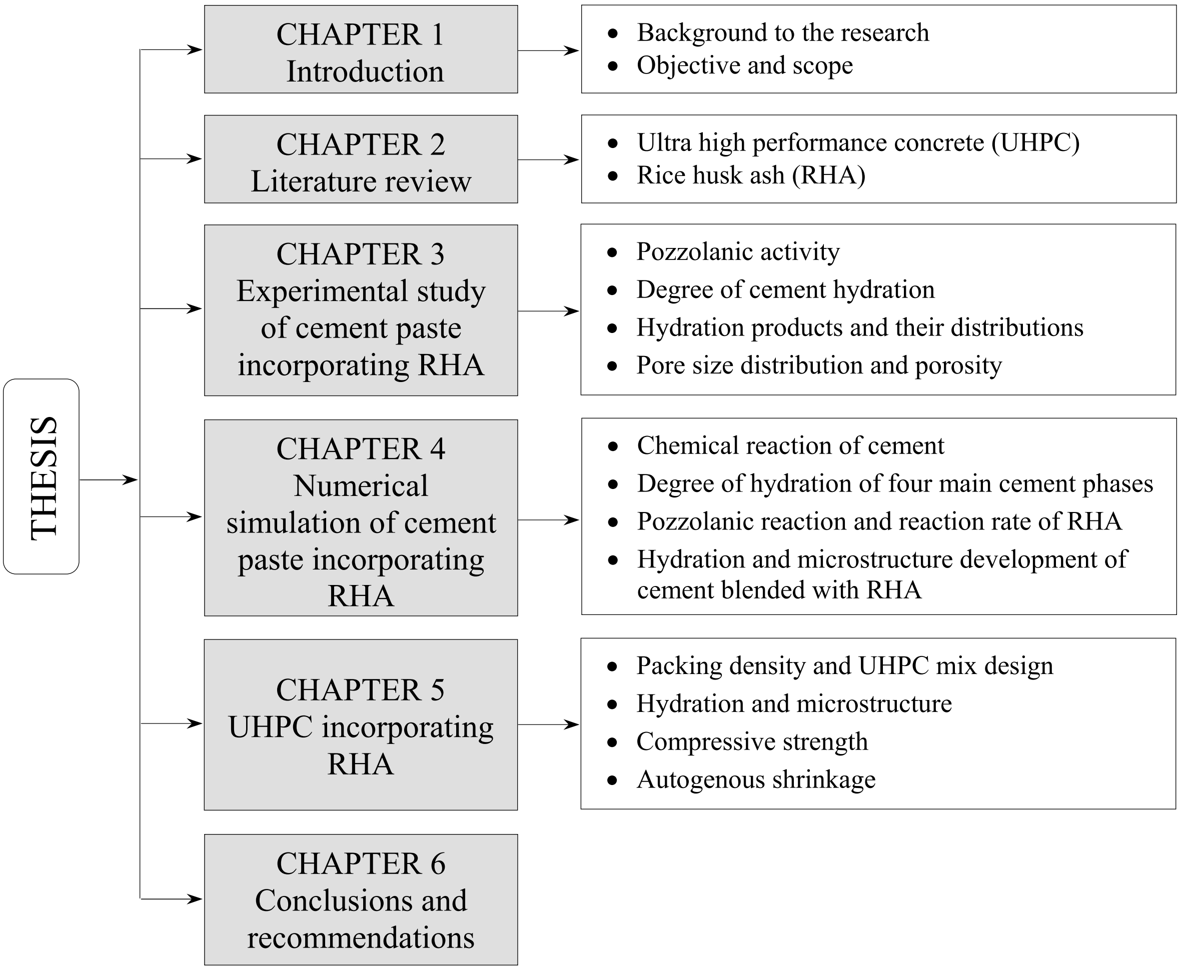

Figure 1.1 Outline of this thesis

2

Literature Review on Ultra-High Performance Concrete and Rice Husk Ash

In this chapter, a brief overview on ultra-high performance concrete (UHPC) will be given. In fact, UHPC is a special concrete with exceptional properties, such as flowability, mechanical properties, and durability, which is distinguished from normal concrete and high performance concrete both in terms of the mix composition, requirements, and principles of production. As a result, the hydration process and microstructure development of UHPC is different from ordinary concrete. During hydration, UHPC mixtures also show a very high autogenous shrinkage due to the high amount of both cement and SF used.

With respect to the material constituents of UHPC, SF plays an important role in making UHPC with its outstandingly physical and chemical effects, but it also has some limitations in terms of cost and availability. This constrains its applications in concrete production in particularly UHPC, especially in developing countries. Due to this reason, it gives rise to an idea to search for other substitutions for SF. Among the mineral admixtures, RHA is a very promising candidate considered as a highly reactive pozzolan such as SF. A summary of the properties of RHA, the effect of RHA on the hydration and the formation of the microstructure of cement paste, and its utilization in concrete are discussed in the second main part. Seen from the hydration and microstructural points of view, RHA has demonstrated a potential to replace SF in low w/b ratio mixtures. This is very important for the following experimental studies in the next chapters.

2.1 Ultra-high performance concrete

2.1.1 Definition

UHPC is a new generation of high performance concrete with a very high strength, a very high ductility, and a very high durability. It is defined worldwide as a concrete with a compressive strength exceeding of 150 MPa [AFGC-SETRA 2002; Schmidt and Fehling 2005], possibly attaining 250 MPa and with a sufficient fiber content to achieve a ductile behaviour under tension. Normally, the term UHPC has been used to describe a fiber-reinforced, superplasticized, silica fume-cement mixture with a very low water-cement ratio (w/c) characterized by the presence of a very fine quartz sand (0.15-0.60 mm) instead of the ordinary aggregate.

In fact, UHPC is not a concrete, because there is no coarse aggregate in the mixture [Sadrekarimi 2004a]. However, Blais and Couture [1999] suggested that the term ‘concrete’ is used rather than ‘mortar’ to describe UHPC with the addition of fine steel fibres to enhance the ductility. Considering the scale effect helps to understand the significance of these fibres. If UHPC, whose maximum particle size is 0.60 mm, is compared to concrete made with the maximum coarse aggregate of 25 mm, the scale is 25 mm to 0.60 mm, or 42 to 1. Adding a steel fiber with the size of 0.2×25 mm to the UHPC is like adding an 8 mm×1 m reinforcing bar to the ordinary reinforced concrete with the 25 mm-coarse aggregate. In practice, several types of UHPC have been developed in different countries and by different manufacturers. The main difference between the types of UHPC is the type and amount of fibres used. To date, there are four main types of UHPC including Ceracem/BSI, compact reinforced composites (CRC), multi-scale cement composite (MSCC), and reactive powder concrete (RPC) [Vande Voort *et al.* 2008]. Ceracem/BSI includes coarse aggregates, which are eliminated in the other types of UHPC [Jungwirth and Muttoni 2004]. CRC and MSCC both use high amounts of fiber and use different fiber sizes than those used in RPC [Rossi 2005]. RPC’s steel fibres occupy two per cent of the concrete mixture by volume. RPC has become one of the leading types of UHPC, and one such product is marketed under the name Ductal® by the French companies Lafarge, Bouygues, and Rhodia. Since RPC is the most commonly available type of UHPC and was used for the laboratory and field experiments in the current study, the term ‘UHPC’ refers exclusively to RPC for the remainder of this thesis.

The basic principles used in UHPC have been identified by several authors [Richard and Cheyrezy 1995; Ma and Schneider 2002; Schmidt and Fehling 2005; Spasojevic 2008], which can be summarized as follows:

1. Enhancement of the homogeneity by eliminating the coarse aggregate resulting in a decrease in the mechanical effects of heterogeneity.
2. Enhancement of the packing density by optimizing the granular mixture through a wide distribution of powder size classes.
3. Improvement of the properties of the matrix by adding a pozzolanic admixture, such as silica fume.
4. Improvement of the matrix properties by reducing the water-to-binder (w/b) ratio.
5. Enhancement of the microstructure by the post-set heat-treatment.
6. Enhancement of the ductility by including small steel fibres.

Application of the first five principles leads to a concrete with a very high compressive strength. The addition of the steel fibres helps to improve both the tensile strength and the ductility [Richard and Cheyrezy 1995].

2.1.2 Development of UHPC

Concrete is generally considered an appropriate construction material for many civil and military applications. It can be strong and durable, can be placed in many shapes, and is economical. Since it is much stronger in compression than it is in tension, concrete is primarily used for its compressive strength [O'Neil *et al.* 2001]. Therefore, intensive research efforts began in the 1930s and attained an improvement in the compressive strength of concretes. The significant achievements of concrete technology in the last 40 years can be seen in Figure 2.1. In addition, the development of the compressive strength of concrete over 100 years is presented in Figure 2.2.

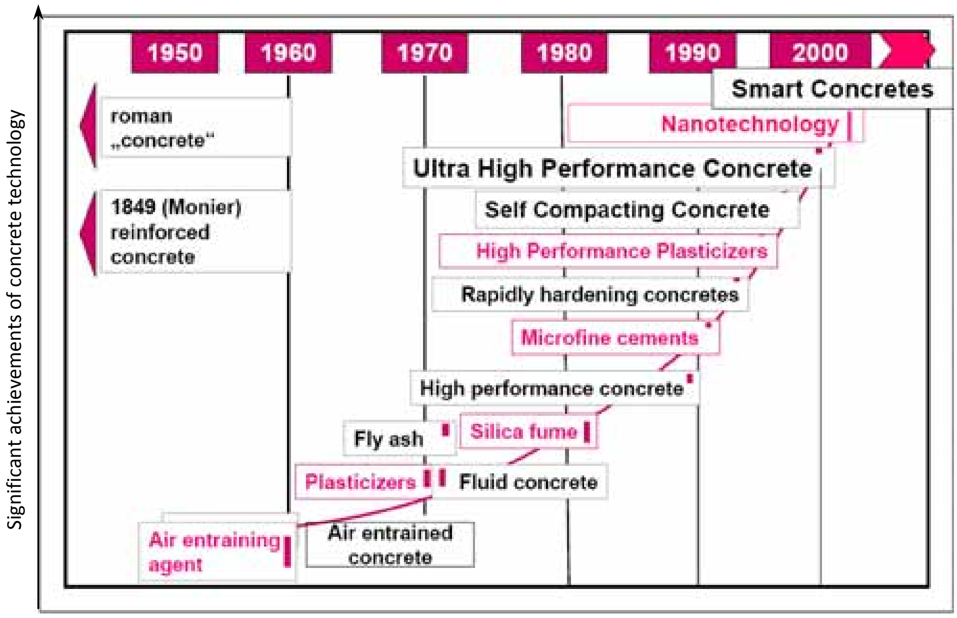

Figure 2.1 Significant developments in concrete technology in the last 40 years [Schmidt 2006]

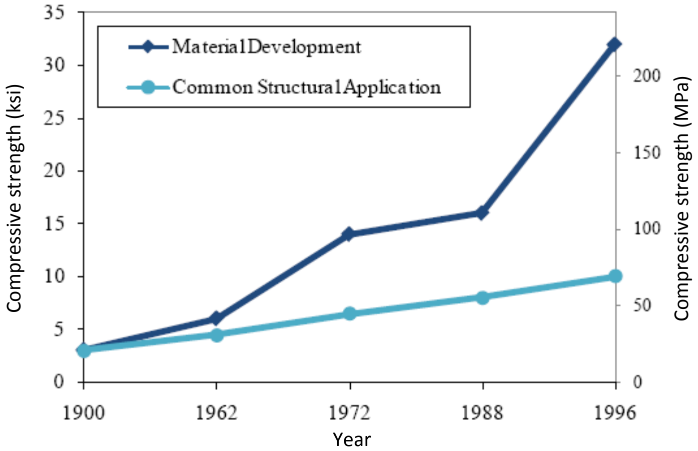

Figure 2.2 The development of the compressive strength of concrete over 100 years [Spasojevic 2008]

It can be seen that the concrete technology progress evolved slowly during the 1960s with the maximum compressive strength of 15-20 MPa. It was multiplied by three to 45-60 MPa over a period of about 10 years with an important advance by using water reducers. Concrete compressive strengths stopped increasing at about 60 MPa by the early 1970s, when a technological barrier was reached that could not be surmounted with the raw materials then available. In addition the water reducers that were normally available at that time were not capable of reducing the w/b ratio any further [Aïtcin 1998]. During the 1980s, it began to be realized that the high-range water reducers, called superplasticizers, were more powerful than lignosulfonates and could be used to progressively reduce w/b ratios down to 0.30. Reducing the w/b ratio below this was taboo until Bache [1981] reported that by lowering the w/b ratio of a particular concrete down to 0.16, using a very high dosage of superplasticizer and a new ultrafine cement substitute (silica fume), he had been able to reach a compressive strength of 280 MPa within the compacted granular materials by optimizing the grain size distribution of the granular skeleton. About 100 years after first being proposed by Féret, the w/b law concerning the compressive strength can be said to have been extended! [Aïtcin 1998].

The results of careful thinking how to exploit these technological breakthroughs and/or some fundamental knowledge about low-porosity materials has led to the development over the past 30 years of a number of Portland cement-based materials that present remarkable mechanical properties. Recently, reactive powdered concrete (RPC), which was developed by Richard and Cheyrezy [1994], is the latest ultra-high-strength Portland cement-based material that has been developed. It can achieve a compressive strength of up to 800 MPa, though this is not the ultimate strength that is likely to be achieved. All these materials have one thing in common: their w/c ratio is much lower than that of high-performance concrete. It lies in the 0.10 to 0.20 range in order to achieve the densest packing possible in the hardened product. They are only different in the way in which this increased packing is achieved. Aïtcin [2000] gave a very useful brief look at how UHPC is able to attain such high strength: 'We know how to make 150 MPa concrete on an industrial basis. Because at such a level of strength it is the coarse aggregate which becomes the weakest link in concrete, it is only necessary to take out coarse aggregate, to be able to increase the concrete compressive strength and make RPC having a compressive strength of 200 MPa; it is only necessary to confine this RPC in thin-walled stainless steel tubes to see the compressive strength increased to 375 MPa; and when the sand is replaced by a metallic powder, the compressive strength of concrete increases to 800 MPa'.

2.1.3 Material selection

As mentioned in the definition section, UHPC is composed of materials such as sand, cement, silica fume, fiber, superplasticizer and water. In this thesis, the properties of a UHPC mix may be assumed to be characteristic of UHPC regardless of fiber content or curing process of the post-heat treatment. The following sections present a further detailed description of the role of each constituent in the UHPC mix.

Sand Quartz sand is usually used as this material is readily available, has low cost, and is very strong. Moreover, this sand has excellent paste/aggregate interfaces. The maximum particle size of sand used in UHPC is limited to 600 μm. For the minimum value, particle sizes below 150 μm are avoided in order to prevent the interference with the largest cement particles (80-l00 μm) [Richard and Cheyrezy 1995].

Cement A typical Portland cement or other similar cements can be used in UHPC.

Mineral admixtures Fine-grained mineral additions can help improve many qualities of concrete. There can be physical effects, such as the increased packing, or chemical-physical effects, such as new reaction products formed during the pozzolanic reaction. In both cases, the end effect is similar: the concrete porosity decreases and the pore size distribution shifts towards smaller size fractions. The use of pozzolans can modify any or all rheological, mechanical, and durability properties of concrete. In HPC and UHPC, the primary aim is to optimize the grain size distribution, especially for fine particles. The use of superplasticizers and mineral admixtures permits fluid mixes with a very low w/b ratio. The resulting concrete has a very high strength and density, and a very low porosity.

Silica fume or microsilica is an amorphous type of silica dust mostly collected in baghouse filters as a by-product of the silicon and ferro-silicon production. Thanks to its exceptional characteristics and properties, SF has become a top-of-the-range product for which demand is constantly increasing [Tafraoui *et al.* 2009]. SF is composed of ultra-fine, amorphous silica particles which are perfectly spherical. This leads to the fact that SF is a principal constituent of the new generation HPC and UHPC. Normally, SF is used in UHPC for three main functions [Richard and Cheyrezy 1995; Ma and Schneider 2002]:

1. Filling the voids between the next larger granular class particles (cement).
2. Enhancing rheological characteristics by the lubrication effect resulting from the perfect sphericity of the particles.
3. Producing secondary hydrates by the pozzolanic reaction with calcium hydroxide generated from the primary hydration of Portland cement.

It was recognized that these functions correspond to the different ‘optimum’ amounts of SF. For example, the amount of SF theoretically required for total consumption of $Ca(OH)_2$ released from cement hydration is 18% by weight of cement [Papadakis 1999]. However, the optimum SF content increases to about 25% to get the densest mixture, and tests reveal that the greatest compressive strength could be achieved with 30% SF [Ma and Schneider 2002; Ma *et al.* 2003]. Therefore, the silica fume content in UHPC is normally 25-30% of cement in regard to these functions.

It should be noted that SFs used in UHPC should be pure with a low carbon content, since carbon increases the water requirement and decreases the flowability [Schmidt *et al.* 2003]. Also, SF slurry cannot be used because the quantity of water in the slurry often exceeds the total water required for the UHPC mix [Richard and Cheyrezy 1995].

Despite its outstanding properties, SF still has many drawbacks. Firstly, SF is initially considered as an industrial waste, and hence its availability is limited, especially in developing countries, which constrains its applications in concrete production. Secondly, SF also causes an aesthetic problem as it sometimes gives a dark colour to the concrete, which is due to the unburnt coal contained in it. However, specially treated silica fumes are available, but they are expensive. Besides, being an industrial by-product, homogeneity of the product can vary [Chandra and Bergqvist 1997]. Thirdly, owing to the fact that the particle size of SF is very small, about 0.1-1 μm, SF is generally considered a nuisance dust of low toxicity. Use and handling of SF represent a health risk when normal safety rules are not observed.

The disadvantages of SF give a motivation for searching for other materials with similar performances, especially in developing countries. To date, many ultrafines other than SF, such as pulverized fly ash, ground granulated blast furnace slag, metakaolin, and limestone microfiller have been studied successfully to make UHPC [Long *et al.* 2002; Rougeau and Borys 2004; Le 2008; Tafraoui *et al.* 2009]. However, the use of mineral admixtures in UHPC still opens the door for other materials, especially for waste materials to substitute SF, i.e. RHA. So far, the possibility of using RHA to make UHPC still remains doubtful in term of its big particle size and high water demand. These aspects are investigated in this study.

Superplasticizer Superplasticizers are high-range water reducers composed of powerful organic polymers used to disperse cement particles and SF, and therefore to improve the flowability of UHPC mixes [Aïtcin 2000]. Thus, superplasticizers can allow a lower w/b ratio to be used without sacrificing the workability of the mix. Since UHPC uses such low w/b ratios, the optimum amount of superplasticizer is relatively high, with a solid content of approximately 1.6% of the cement content [Richard and Cheyrezy 1995].

2.1.4 Composition of UHPC

For comparison, the typical compositions and properties of normal strength concrete (NSC), high strength concrete (HSC), and UHPC are listed in Table 2.1. UHPC is distinguished as a fine-grained concrete with a very high binder content and a very low w/c ratio.

The selection of the components of UHPC is applied by using the optimization principle of the packing density. The mix is also proportioned in such a way that the fine aggregates will be a set of movable inclusions in the matrix, rather than a rigid skeleton. Use of smaller particles only to fill the voids between sand particles would lead to the packing optimization, but a rigid skeleton of sand particles would still remain. According to the results from Reschke, cited by Ma *et al.* [2002], a mixture with a large size distribution has a low porosity. This means that the powder mixture should be composed of a number of classes of granular powder. In UHPC, the wide distribution of granular classes from sand (0.15-0.6 mm) to SF (0.1-1 μm) helps to maximize the density and to create a more uniform stress distribution when the matrix is loaded. Moreover, the smaller grains, i.e. SF, serve as a lubricant, allowing sand particles of the same size to move easily and to pass one another, reducing the inter-particle friction. This improves the flowability of UHPC mixes. Usually, UHPC mixes can be made to be self-compacting, requiring no vibration to cast.

The w/c ratio has typically been used as an indicator of the concrete strength. Schmidt *et al.* [2003], however, claim that the compressive strength of UHPC cannot be accurately characterized by w/c ratio alone. They note that UHPC can be developed with a w/c ratio as high as 0.40 without a reduction in strength, though the porosity may be greatly increased with such a comparatively high w/c ratio. The link between porosity and compression strength is also questioned by Larrard and Sedran [1994], who regard the porosity as a better indicator of strength. Regardless, the w/c ratio does affect the porosity and has a significant effect on the compressive strength, even if it is not the only factor [Aïtcin 2000; van Breugel and Ye 2004].

Table 2.1 Examples of composition and properties of NSC, HSC and UHPC [Spasojevic 2008; Vande Voort *et al.* 2008]

Material characteristics	NSC	HSC	UHPC
Component (kg/m^3)			
Portland cement	< 400	400	600 - 1000
Coarse aggregate	≈ 1000	900	-
Sand	≈ 700	600	1000 - 2000
Silica fume	-	40	50 - 300
Reinforcement/Fibres	designed	designed	40 - 250
Superplasticizer	-	5	10 - 70
Water	> 200	100 - 150	110 - 260
Maximum aggregate size (mm)	19.0-25.5	9.5-12.5	0.15-0.6
w/c ratio (by weight)	0.40-0.70	0.24-0.38	0.14-0.27
w/b ratio (by weight)	-	< 0. 38	< 0.27
Properties (at 28 days)			
Density (kg/m^3)	2000 - 2800	2000 - 2800	2320 - 2760
Porosity (%)	20-25	10-15	2-6
Compression strength (MPa)	< 60	60 - 100	> 150
Tensile strength (MPa)	< 3	< 5	> 8
Initial modulus of elasticity (GPa)	≈ 30	< 45	50 - 70
Fracture energy (J/m^2)	30 - 200	< 150	< 90 without fibres > 10000 with fibres

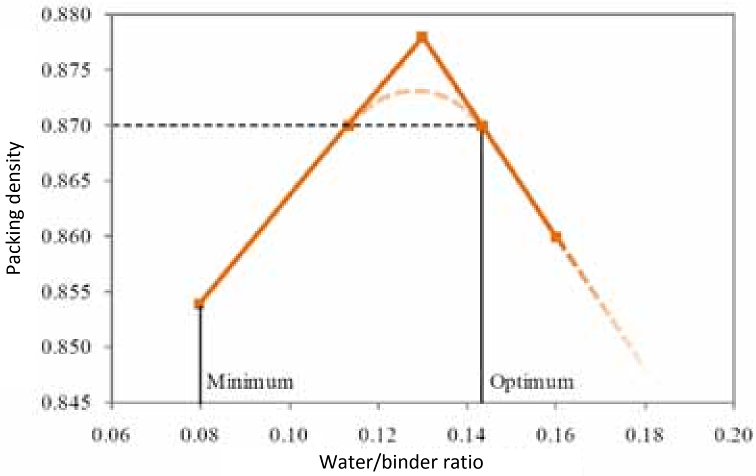

Figure 2.3 Packing density versus the w/b ratio [Richard and Cheyrezy 1995]

The goal in a UHPC mix is not only to minimize the water content, but also to maximize the packing density. In UHPC, the range of w/b ratios that can be applied to make UHPC can vary from 0.08 to 0.25 [Richard and Cheyrezy 1995; Vande Voort *et al.* 2008]. The packing density, however, is not maximized at a very low w/b ratio, as can be seen in Figure 2.3. As the w/b ratio is increased above the 0.10 minimum, water replaces air without increasing the volume of the mixture up to a w/b ratio of about 0.13. If the w/b ratio is increased beyond this point, additional water increases the volume and thus decreases the density of the mixture. In Figure 2.3, the mixtures represented by the descending branch of the graph have a superior performance and workability to those represented by the ascending branch, so the practical optimal w/b ratio used is chosen slightly biased towards the higher values of w/b ratio to ensure that the w/b ratio of the actual mixture is slightly higher than the theoretical optimum. Some investigations have found the optimal w/b ratios in UHPC ranging from 0.14 to 0.16 from experimental tests [de Larrard and Sedran 1994; Richard and Cheyrezy 1995; Wen-yu *et al.* 2004; Gao *et al.* 2006]. This aspect is also dealt with in the experimental study of UHPC incorporating RHA.

2.1.5 Packing density

UHPCs are characterized by extremely high packing densities [Richard and Cheyrezy 1995; Ma and Schneider 2002; Schmidt and Fehling 2005; Spasojevic 2008]. These densities can be achieved by optimizing the proportioning of components. The particles should be selected to fill up the voids between large particles with smaller particles and so on, leading to a smaller volume of gaps within the aggregate skeleton. The concept of packing density, i.e. the ratio of the volume of solids to a given volume, is introduced to evaluate the arrangement of granular mixture. Figure 2.4 illustrates how the concept of packing density can be applied with three granular systems, i.e. single-, binary-, and ternary- systems [Stovall *et al.* 1986]. The single-sized aggregate can be packed together to occupy only a limited space, i.e. can achieve only a relatively low packing density. However, the multi-sized aggregate can be packed together much more effectively to achieve a much higher packing density, i.e. binary and ternary mixtures. With the paste volume fixed, the increase in packing density of the aggregate could be employed to increase the workability of concrete at the same w/b ratio, or increase the strength of concrete by reducing the w/b ratio at a given workability.

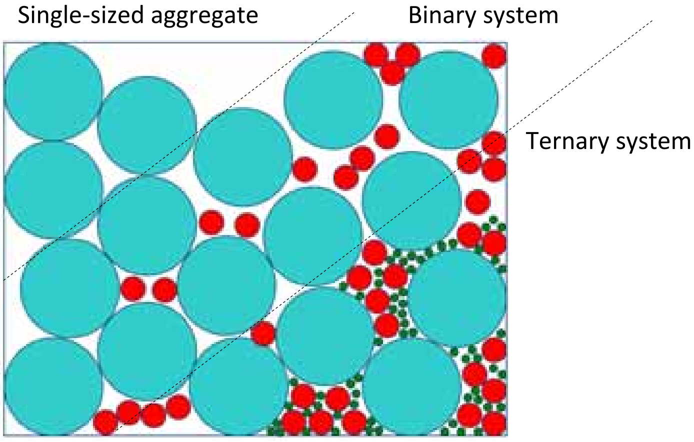

Figure 2.4 Typical packing arrangements of binary and ternary mixtures [Stovall *et al.* 1986]

In the history of concrete, the concept of packing of aggregates already received attention in the 19th century. Nowadays, the packing density of aggregate has become one of the most important parameters influencing the performance of concrete, i.e. increasing the strength, reducing the permeability and bleeding of the fresh cement paste, and reducing the porosity of the transition zone. To date, the methods for optimizing the granular mixtures can be divided into three groups:

1. Optimization curves: Particle groups are combined in such a way that the total particle size distribution of the mixture is closest to the 'ideal' grading curves to achieve the highest packing density. These 'ideal' curves were worked out on the basis of practical experiments and theoretical calculations.
2. Particle packing models: These models are analytical models which calculate the overall packing density of a mixture based on the geometry of the combined particle groups.
3. Discrete element models: This type of computer models generates a 'virtual' particle structure from a given particle size distribution.

Among these models, the model developed by Larrard [1999], called the Compressible Packing Model (CPM), is the most accurate model as it considers the mutual influence of compaction and interactions in the particle structure. These interactions are ascribed by the wall effect (when the fine particles are butting into the surfaces of very large size particles) and the loosening effect (when the fine particles cannot fit themselves perfectly into the gaps of the larger size particles), as depicted in Figure 2.5 [de Larrard 1999]. This model has been found useful to optimize the packing density of granular mixtures of UHPC [de Larrard and Sedran 1994].

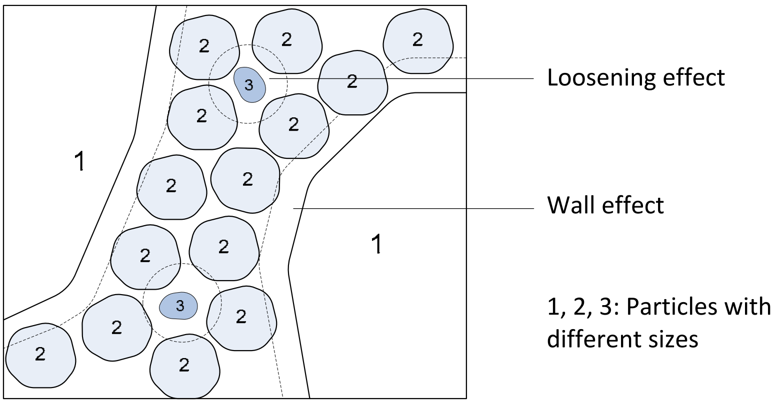

Figure 2.5 Wall and loosening effects in a ternary system of the granular mixture [de Larrard 1999]

2.1.6 Hydration and microstructure

The hydration and microstructural investigation of UHPC is to help understand how to further enhance the performance of this type of concrete. Unfortunately, so far, only a few studies on these aspects have been published [Cheyrezy *et al.* 1995; Vernet *et al.* 1998; Loukili *et al.* 1999; Reda *et al.* 1999; Schmidt and Fehling 2005; Habel *et al.* 2006; Möser and Pfeifer 2008]. A brief description of these aspects is presented below.

Hydration of UHPC As mentioned previously, the w/b ratio of UHPC is very low, from 0.10 to 0.25 by weight [Vande Voort *et al.* 2008]. It was observed in practice that the maximum degree of hydration of cement for this w/c ratio range is between 30% and 55% (Figure 2.6) [Mills 1966], which is similar to the estimated value in UHPC [Cheyrezy *et al.* 1995; Habel *et al.* 2006].

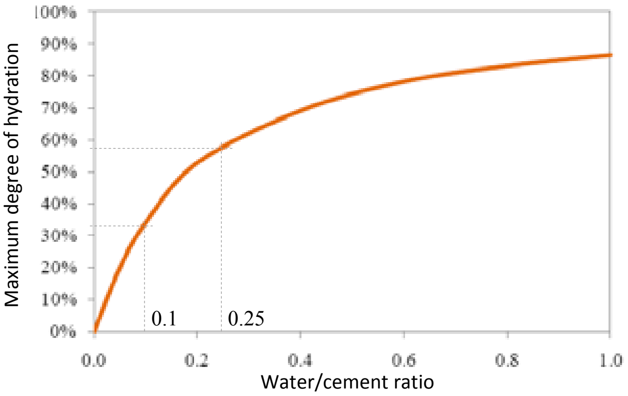

Figure 2.6 Maximum degree of hydration of cement observed in practice vs. the w/c ratio [Mills 1966]

Microstructure development of UHPC UHPC with very low w/b ratios and optimized granular mixtures shows a very dense microstructure [Reda *et al.* 1999; Schmidt and Fehling 2005].

The extremely dense microstructures of UHPC can be observed by means of electron microscopy. The image sequence (Figure 2.7a-d) shows the hydration process and the development of the UHPC microstructure observed by ESEM [Möser and Pfeifer 2008].

Up to a hydration time of eight hours and beyond, the microstructure of UHPC is dominated by spherical SF particles (Figure 2.7a). Isolated ettringite crystals with a short prismatic (length up to 400 nm) are visible between the SF spheres. The hydration of the clinker phase alite is retarded up to this point in time by the superplasticizer used, so that no CSH phases are observed. With the hydration process, after a time of 18 hours, CSH phases with a length of up to 200 nm are visible (see Figure 2.7b).

After a hydration time of 4 days (heat-treated sample) the clinker grain shows only a marginal, heterogeneous dissolution structure of the alite phase (Figure 2.7c). On the other hand, after a hydration time of 28 days (Figure 2.7d) the clinker grain shows a strongly dissolved area of the alite phase (reaction zone approximately 1 µm as shown under the white line in Figure 2.7d) [Möser and Pfeifer 2008].

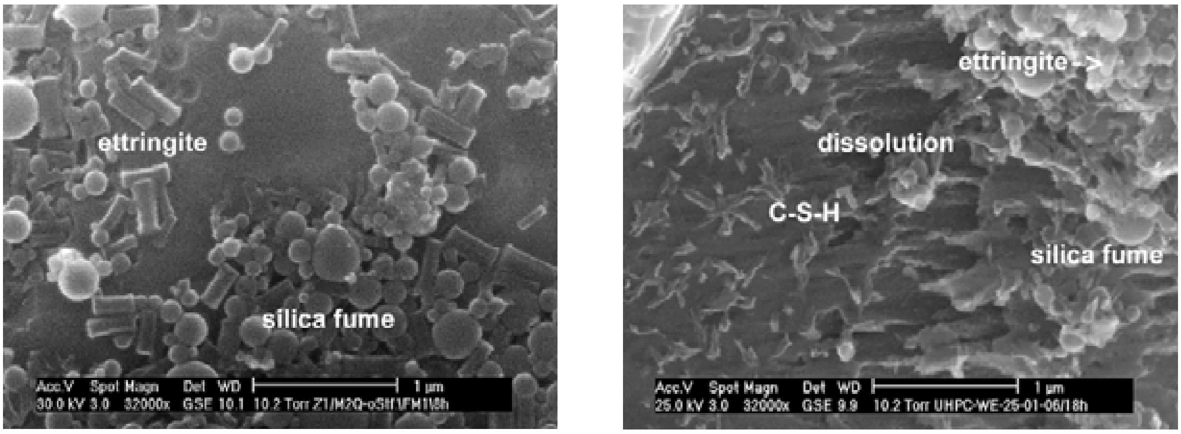

(a) Hydration at 8 hours: spherical SF particles and short prismatic (length up to 400 nm) ettringite crystals

(b) Hydration at 18 hours: needle-like CSH phases (length up to 200 nm) and cavities on the surface of an alite grain

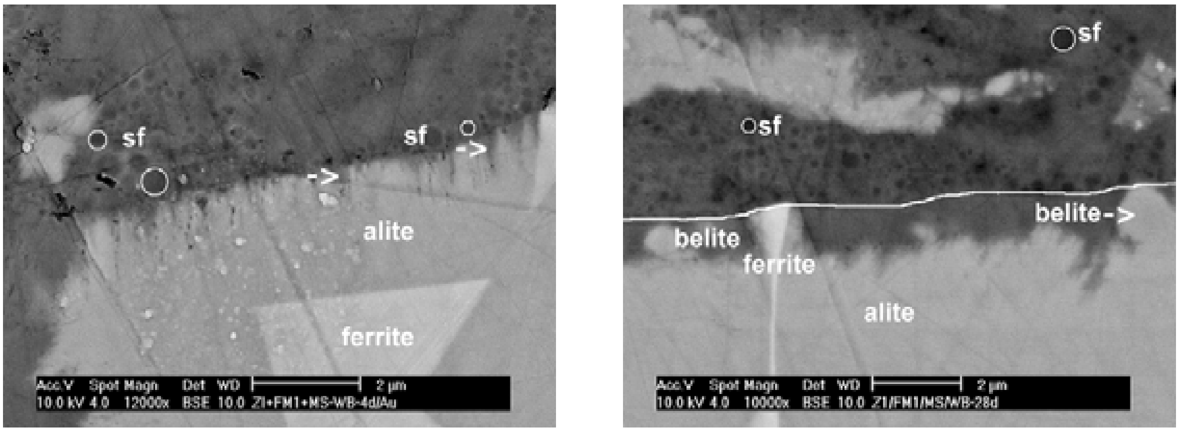

(c) Heat-treated sample after 4 days: marginal heterogeneous dissolution of alite (see arrows); SF- dark spherical particles (see white circles)

(d) Heat-treated sample after 28 days: phases of a clinker grain with different reactivity - the white line marks the former grain size

Figure 2.7 Hydration of UHPC over time (a) 8 hours, (b) 18 hours, (c) 4 days, and (d) 28 days [Möser and Pfeifer 2008]

With respect to the *interfacial transition zone* (ITZ) between the cement paste and sand particles in UHPC, the thickness of this zone was found to be very small compared to that of conventional concrete [Reda *et al.* 1999]. This is due to the absence of coarse aggregate in UHPC resulting in a significant reduction of the wall effect normally occurring around the surface of larger size particles. A comparison of transition zones of normal concrete and UHPC are shown in Figure 2.8 [Droll 2004]. It can be seen that broad gaps between the cement matrix and aggregate grains up to 20 µm are clearly visible in a C45/55 concrete and a direct adhesion takes place only at a part of the complete contact surface in the normal concrete, but is very small in the UHPCs.

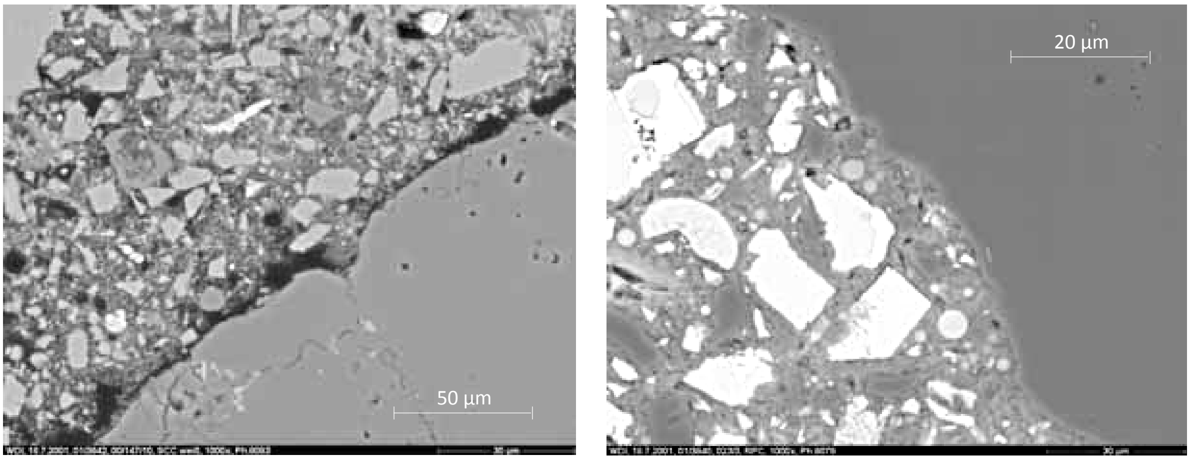

(a) C45/55 (b) UHPC

Figure 2.8 Interfacial transition zone in a normal concrete C45/55 and in UHPC [Droll 2004] with magnification of 1000×

One further aspect in the microstructure of UHPC is its *pore size distribution and porosity*. Given the very low w/b ratio and the dense packing of the solids in the matrix, the porosity of UHPC is characterized by the absence of capillary pores (Figure 2.9) [Schmidt and Fehling 2005] and the very small cumulative porosity (Figure 2.10) [Cheyrezy *et al.* 1995] tested by mercury intrusion. This is the real reason why properly manufactured UHPC has a particularly high resistance to carbonization and penetration of chloride ion, as well as to attacks of frost and frost/de-icing salt [Schmidt *et al.* 2003].

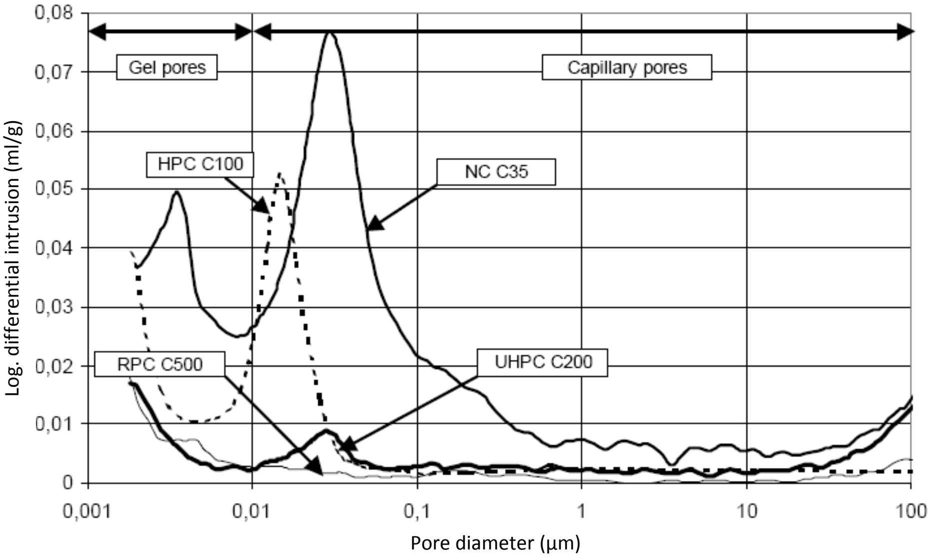

Figure 2.9 Pore size distribution of UHPC, HPC and Normal Strength Concrete (NC) [Schmidt and Fehling 2005]

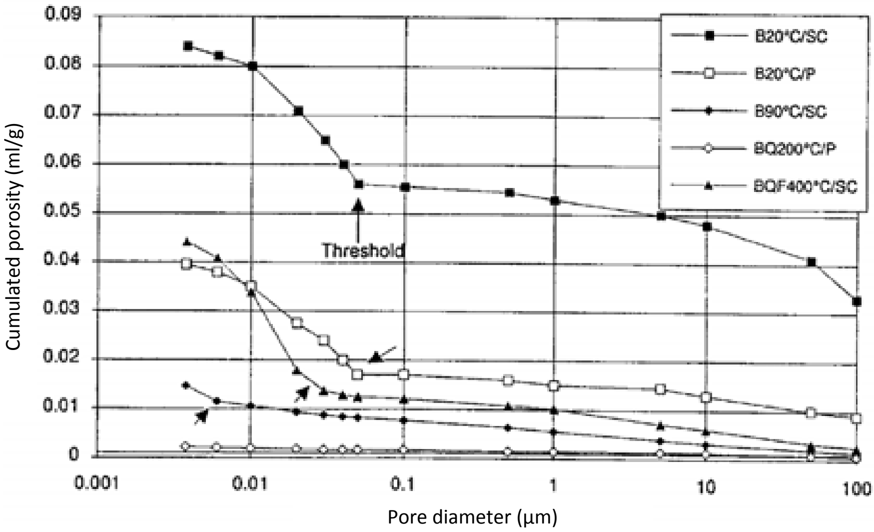

Figure 2.10 UHPC cumulative porosity versus the pore diameter [Cheyrezy *et al.* 1995]. The samples with different heat treatment temperatures and setting pressures: soft cast (SC), setting pressure at 310 atm or 625 atm (P); normal composition or basic formulation (B), normal composition with crushed quartz and steel fibres (BQF)

The addition of mineral admixtures, in particular SF, is believed to modify the hydration and microstructure development of UHPC. Unfortunately, to date, the effects of these mineral admixtures on both aspects in UHPC have been discussed very little. This is one of the main objectives of this research, in which the effect of RHA on the hydration and microstructure development of UHPC in comparison with that of SF will be investigated.

2.1.7 UHPC with sustainability

Material Requirements The use of UHPC may save the total amount of materials required for building various structures. Although UHPC uses a larger amount of cement per cubic meter compared to normal concrete, structural members typically require fewer cubic meters of material. As a result, the total quantity of cement used is comparable or even less for UHPC design solutions. Racky [2004], in his own study, determined that while the cement content in UHPC may be as much as twice that in normal concrete, the volume of UHPC required for a large column application was only 44% of the normal concrete alternative. Regarding the high cement content required to produce UHPC, the use of more mineral admixtures instead of cement is a useful solution to reduce the cement demand, and it contributes to sustainable development.

Lifecycle Although too few applications of UHPC currently exist to allow a reliable comparison with normal concrete for average life-cycle durations and costs, most researchers agree that the excellent durability properties of UHPC should increase the longevity of structures while minimizing maintenance costs [Blais and Couture 1999; Racky 2004]. Aïtcin [2000] notes that, unlike normal concrete, UHPC can be recycled several times before being used as granular road base. This recyclability is attributed to the fact that not all of the cement in UHPC is hydrated during hardening, and anhydrous cement is therefore available for future reactions.

2.1.8 Shrinkage of UHPC

Two types of shrinkage contribute to the total shrinkage in concrete: autogenous shrinkage and drying shrinkage. Autogenous shrinkage is defined as ‘the bulk deformation of a closed, isothermal, cementitious material system not subjected to external forces’ [Jensen and Hansen 2001]. Drying shrinkage refers to the volume reduction in the cement matrix resulting from an overall loss of water to the environment through evaporation.

UHPC exhibits large shrinkage values, but, unlike normal concrete, autogenous shrinkage makes up a larger portion of the total shrinkage in UHPC than drying shrinkage [Schmidt *et al.* 2003]. In fact, UHPC shows a very high autogenous shrinkage already in the first one or two days after mixing, which points to a considerable cracking potential at early ages. Such early age cracking due to restrained autogenous shrinkage tends to negate the numerous advantageous properties of UHPC and significantly limits its prospective utilization in construction. The very high autogenous shrinkage of UHPC is due to the very low w/b ratio and very high amount of SF used in UHPC which causes a significant drop in the internal relative humidity (RH) in the cement paste during the hardening, and self-desiccation occurs in the absence of an external source of water [Jensen and Hansen 2001].

Mitigation of autogenous shrinkage using external curing is not effective, due to the fact that the very dense microstructure of UHPC enables only very slow water ingress into the interior of concrete members. Because of this, internal water curing is considered to be an effective solution to counteract self-desiccation and autogenous shrinkage for the low permeability of the low w/b ratio cementitious system, thereby reducing the likelihood of early-age cracking. The most popular methods of internal curing for concrete are using water-saturated aggregates and super-absorbent polymers (SAPs) [Kovler and Jensen 2007]. Unfortunately, because of strict requirements on mechanical behaviours and the maximum size of aggregate, only the SAPs have been proposed to be used as an internal curing agent to mitigate the autogenous shrinkage of UHPC up to now. It has been shown that the technology also works in practice [Mechtcherine *et al.* 2008]. However, SAPs may easily make the concrete heterogeneous, because it will leave voids even as big as 600 μm [Dudziak and Mechtcherine 2008], equal to the maximum sand size in concrete during hydration, which might negatively influence the properties of UHPC. Searching for the internal curing method of UHPC still remains a motivation for researchers to explore in this field. One of the very interesting questions is that whether or not one material can play 'a duplex role' to replace both SF and SAPs to make UHPC. If possible, it will give a big advantage in producing UHPC. This concern is dealt with in the later section of autogenous shrinkage of UHPC incorporating RHA in this research.

2.1.9 Applications of UHPC

As mentioned in Chapter 1, UHPC has a lot of potential as a material in terms of its mechanical behaviour and durability. The general advantages of UHPC can be summarized as below [Lubbers 2003; Buitelaar 2004; Sadrekarimi 2004b; Vande Voort *et al.* 2008]:

1. UHPC is a better alternative to HPC and has the potential to compete structurally with steel.
2. UHPC with its superior strength combined with higher shear capacity results in a significant dead-load reduction and less limited shapes of its structural members. UHPC can lead to longer span structures with reduced member sizes compared to normal or high-strength concrete, and to a significant reduction in the volume and the self-weight with UHPC members. For example, Figure 2.11 shows beams made from UHPC, steel, pre-stressed, and reinforced concrete with equal moment capacities [Perry 2006]. Interestingly, the UHPC beam requires only half the section depth of the reinforced or pre-stressed concrete beams, which in turn reduces its weight by 70% or more. The UHPC beam also has a same section depth as the steel beam which, in this case, is only slightly lighter than the UHPC member.
3. The superior durability properties of UHPC are also advantageous in terms of service life and reduced maintenance costs.

The development of UHPC with such advantages offers many attractive applications in the construction industry. The applications of UHPC can be separated into various aspects: wear protection; concrete repair, offshore, security industry, prefab structures, industrial floors, pavements and new applications. Their details can be found elsewhere [Buitelaar 2004; Sadrekarimi 2004b; Schmidt and Fehling 2005]. By combining UHPC with other materials, large ceramic metal-based hybrid structures can be made that exhibit unique combinations of great strength in all directions, an extreme hardness, and very high fracture toughness. This makes it not only possible to design and to build gigantic structures and extremely slender, elegant and daringly designed structures, but also to make non-brittle ceramics for medical (implants and bone replacements) and industrial applications (tooling, pumps, and engines).

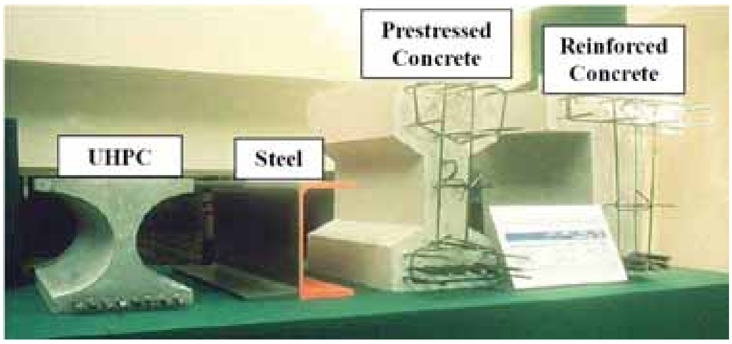

Material	UHPC	Steel	Pre-stressed Concrete	Reinforced Concrete
Depth, mm	360	360	700	700
Weight, kg/m	141	110	466	528

Figure 2.11 UHPC, steel, pre-stressed, and reinforced concrete beams with equal moment capacities [Perry 2006]

2.2 RHA - a potential substitute for condensed SF in producing UHPC

Portland cement, the principal hydraulic binder used worldwide in modern concrete, is not only a product of an energy-intensive industry (4 GJ/ton of cement), but also responsible for large emissions of CO_2, thereby contributing to global warming. Manufacturing one ton of Portland-cement clinker releases nearly one ton of CO_2 into the atmosphere, while nowadays the world's yearly cement output of 1.5 billion tons of mostly Portland cement accounts for nearly 7% of the global CO_2 emissions [Mehta 2002].

To obtain a major reduction in the CO_2 emission associated with cement production, the clinker content of the final product must be lowered as much as possible by maximizing the proportion of mineral admixtures in cement, and to increase the use of blended cements in general construction [Mehta 2002,2009]. Among the technically acceptable and economically available mineral admixtures produced every year, such as fly ash (500 million tons), limestone (170 million tons), and blast-furnace slag (75 million tons), RHA with about 28 million tons also offers a potential for reducing a considerable amount of the CO_2 emission attributable to the cementitious materials used in concrete.

Rice is one of the major crops grown throughout the world, sharing equal importance with wheat as the principal staple food and provider of nourishment for the world's population. Rice husk is a by-product of rice processing, and constitutes about one fifth of the 690 million tons of rice paddy produced annually in the world [FAO 2010]. During rice cultivation, the bulky nature of rice husk could cause difficulty for storage and transportation. When rice husk is not treated properly, such as dumping into ponds or streams, it becomes a huge quantity waste which seriously pollutes the environment. One of the useful solutions is to use the ash obtained from the husk combustion as a mineral admixture in concrete. As a result, the problems and costs associated with the environmentally safe disposal of this waste can be reduced or sometimes entirely eliminated. The socio-economic benefits, achieved by the utilization of RHA as a mineral admixture in concrete, is now well recognized by all those concerned with the production, disposal, and utilization of this waste.

In this section, a brief overview of the potential utilization of RHA will be presented in some aspects of the properties of RHA, the effect of RHA on the hydration and microstructure development of cement paste, and the use of RHA in concrete.

2.2.1 Properties of RHA

The utilization of rice husk for use as a cementitious material in cement and concrete depends on the pozzolanic property of its ash. The pozzolanic reactivity of the ash is closely related to the form of silica present and the carbon content. Since the physico-chemical properties of silica in RHA are strongly influenced by the temperature and the duration of thermal treatment, the yield of a highly reactive ash requires a burning method that can remain a low firing temperature and a short retention period in order to give ash with a low carbon content and a high surface area [Bui 2001; Nair 2006].

RHA production For every 1000 kg of milled paddy, about 200 kg (20%) of husk is produced. When this husk is completely burnt, about 50 kg (25%) of RHA is generated. The husk contains about 50% cellulose, 25-30% lignin, and 15-20% of silica. Upon burning, cellulose and lignin are removed, leaving behind silica ash. The use of RHA as a supplementary cementing material requires silica in an amorphous reactive form. Crystalline phases of silica have a negligible pozzolanic reactivity with lime. Generally, the quality of RHA relates to the amorphous SiO_2 content, the porous structure of ash particles and the specific surface area. The amorphous SiO_2 content and the porous structure of RHA depend on the temperature, the duration, and the environment of thermal treatment, as well as the pre-treatment of husk before combustion [Bui 2001]. Analysis of the reports on the influence of combustion conditions on the nature of silica suggests that temperatures below 750°C will be sufficiently safe to produce rice husk ash with high reactivity [Boateng and Skeete 1990; Bui 2001].

There are several methods to convert rice husks to ash that have been suggested by some authors, such as a cyclone-type furnace developed by Mehta-Pitt in 1976, a fluidized bed system by Takuma, a tub-in basket type rice husk burner designed by Kapur in 1981, a brick incinerator by the Cement Research Institute of India, and a drum incinerator by the Pakistan Council of Specific and Industrial Research (PCSIR) in 1979 [Cook 1984; Bui 2001; Bui *et al.* 2005; Nair 2006]. In this thesis, the drum incinerator by PCSIR [Cook 1984] which was modified to increase its capacity to 1 m^3 by Bui [2001] was chosen to burn the rice husk. This method is very suitable for a laboratory scale. It takes almost 12 hours for complete burning to get about 15-20 kg RHA. The husks burn by themselves once ignited. No control is required during the burning process. RHA samples are collected after the complete cooling of ash samples. The details of this incinerator can be found elsewhere [Bui 2001]. The drum and detachable chimney of the incinerator were easily made from galvanized iron sheet. The incinerator is light and can easily be carried by two persons. The fire is started from the bottom using a small amount of waste paper or wood. The highest temperature recorded in this incinerator was 780^{o}C. The carbon content of the ashes was found to fluctuate from 4 to 7%.

Microstructure and fineness of RHA Upon combustion, the cellulose-lignin matrix of the rice husk burns away leaving behind a porous silica skeleton. The highly porous structure (see Figure 2.12 and Figure 2.13) of the ash gives rise to a large surface area. The actual specific surface area determined by the BET nitrogen absorption method of RHA ranges from 20 to 270 m^2/g [Bui 2001], while that of SF is around 18-23 m^2/g [Swamy 1986; Malhotra *et al.* 1987].

Rice husk ash, being porous in nature, has an extremely high surface area, while its average size is still fairly high. This is a difference in particle characteristics between RHA and SF. Compared to SF with a mean particle size of 0.1-1 μm [Swamy 1986; Malhotra *et al.* 1987], RHA with a mean particle size around 45 μm has a three times higher surface area [Chandrasekhar *et al.* 2003]. Mehta [1994] suggested that since RHA derives its pozzolanicity from its internal surface area, grinding of RHA to a high degree of fineness should be avoided. Additionally, the long periods of grinding do not increase the economical benefits, especially in developing countries where electricity is comparatively expensive and frequently intermittent in supply [Cook 1984]. This means that there is an appropriate fineness of RHA which is not only advantageous to the enhancement of its pozzolanic activity, but also economically beneficial. Unfortunately, this value has been investigated very little [Bui *et al.*

2005; Habeeb and Fayyadh 2009]. In this research, the effect of RHA fineness on the pozzolanic activity and properties of UHPC is one of the important aspects to be studied and discussed in detail in Chapter 3 and Chapter 5.

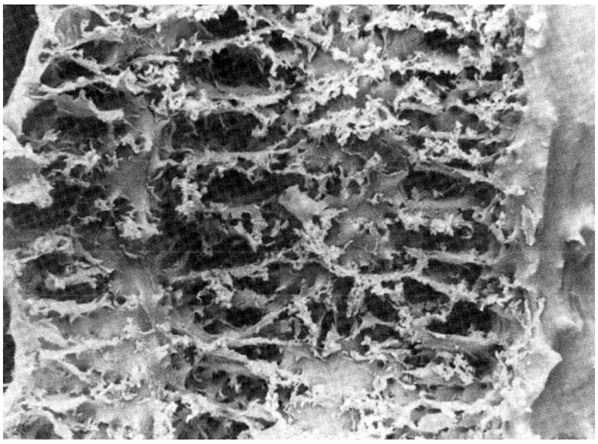

Figure 2.12 Skeletal structure of RHA (736×) [Cook 1984]

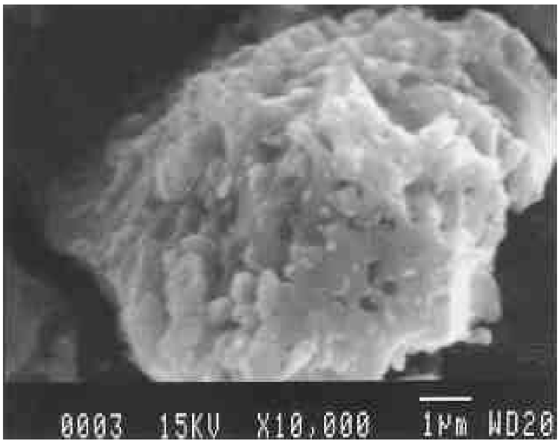

Figure 2.13 SEM image of RHA particle [Zhang and Malhotra 1996]

With respect to the porous structure of RHA, Sugita *et al.* [1997] revealed that the specific pore volume of coarse RHA is as much as 0.16 cm^3/g, and the pores in it are mainly distributed in the region of 2–40 nm with an average radius of 12.3 nm. The authors suggested that with so many such pores, RHA has a characteristic of high water absorption and this high demand for water is a drawback for RHA mixtures. In fact, the pore structure of RHA will be changed with the degree of grinding [Sugita *et al.* 1992; Bui 2001]. According to Sugita *et al.* [1997] and Real *et al.* [1996], the pore size distribution of the ground RHA is small with a range of 2–5 nm and an average radius of 4 nm. Also, the specific pore volume of this RHA is decreased to 0.13 cm^3/g. The reductions in pore volume and pore size will decrease the ability of water absorption of RHA and therewith change the resulting properties of RHA mixtures.

Physical and chemical composition of RHA RHA is a very fine material with a mean particle size ranging from 5 to 10 μm [Siddique 2008b]. The physical properties and chemical composition of RHA, in comparison with those of SF as reported by several authors, are given in Table 2.2 and Table 2.3, respectively. It also can be seen that RHA is very rich in silica content and has a high alkali amount (mainly K_2O). For RHA to be used as a pozzolan in cement and concrete, it should satisfy requirements for chemical composition of pozzolans as ASTM C618, in which the combined proportion of silicon dioxide (SiO_2), aluminium oxide ($A1_2O_3$) and iron oxide (Fe_2O_3) in the ash should not be less than 70%, and loss on ignition (LOI) should not exceed 12% [Siddique 2008b].

Table 2.2 Physical properties of RHA [Siddique 2008b]

Property	Value				
	RHA	RHA	RHA	RHA	SF
	[Mehta 1994]	[Zhang *et al.* 1996]	[Feng *et al.* 2004]	[Bui *et al.* 2005]	[Jayakumar 2004]
Mean particle size (μm)	-	-	7.4	5.0	0.1-1.0
Specific gravity (g/cm^3)	2.06	2.06	2.10	2.10	2.20
Fineness, passing 45 μm (%)	99	99	-	-	-

Table 2.3 Chemical composition of RHA [Siddique 2008b]

	Percentage by weight			
	RHA	RHA	RHA	SF
	[Mehta 1994]	[Zhang *et al.* 1996]	[Bui *et al.* 2005]	[Jayakumar 2004]
Silica (SiO_2)	87.2	87.3	86.98	90 - 96
Alumina (Al_2O_3)	0.15	0.15	0.84	0.5 - 0.8
Iron Oxide (Fe_2O_3)	0.16	0.16	0.73	0.2 - 0.8
Calcium Oxide (CaO)	0.55	0.55	1.4	0.1 - 0.5
Magnesium Oxide (MgO)	0.35	0.35	0.57	0.5 - 1.5
Sodium Oxide (Na_2O)	1.12	1.12	0.11	0.2 - 0.7
Potassium Oxide (K_2O)	3.68	3.68	2.46	0.4 - 1.0
Sulphur Oxide (SO_3)	0.24	0.24	-	-
Loss on ignition (LOI)	8.55	8.55	5.14	0.7 - 2.5

2.2.2 Hydration and microstructure development of Portland cement

The addition of RHA changes the hydration process and microstructure development of Portland cement. In this section, first a brief review of hydration and microstructure of Portland cement is presented. Afterwards, in Section 2.2.3, the effect of RHA on the hydration and microstructure development of Portland cement will be discussed.

Hydration of Portland cement After cement is mixed with water, the water-cement mixture ultimately converts into a stone-like material, which serves as the matrix phase for mortar and concrete. This process is the so-called cement hydration process. During this conversion period, a number of complex chemical and physical reactions take place. The chemical reactions show the phase changes of hydration products, while the physical reactions reveal the spatial re-distribution of the hydration products. The final cement hydration product is a porous rigid material, which directly determines the mechanical and transport properties of cement-based materials.

The hydration process of cement is a transformation from a high energy state to a lower one, where energy is transmitted as heat [Mindess *et al.* 2003]. Observations of the heat of hydration can therefore reveal information about the chemical reactions taking place in the cement during hydration. Through a typical heat evolution curve as shown in Figure 2.14 the paste hydration of Portland cement may be characterized by several stages [Mindess *et al.* 2003] with appearance of numbered peaks [Pratt and Ghose 1983; Taylor 1997].

1. Pre-induction period (stage I): Upon contact with water, cement grains immediately start to react. In this early stage C_3A is the most active phase.

2. Dormant stage (stage II): The rapid early reactions in the first minutes are followed by a period of low reactivity, known as the dormant stage.

3. Acceleration stage (stage III): The reaction occurs actively and accelerates with time, reaching a maximum rate at the end of stage III.

4. Post-acceleration stage (stage IV): In this period the rate of heat release slows down gradually, as the amount of available material to still react declines. The CSH phase continues to be formed and the relative contribution of C_2S to this process increases with time.

Many cements show a shoulder at about 16 hours. This peak is associated with a renewed formation of ettringite as a result of further hydration of C_3A [Pratt and Ghose 1983; Scrivener 1989]. A further, less distinct shoulder has been associated with the hydration of the ferrite phase or conversion of ettringite to mono-sulphate phase, which may correspond to a peak at about 50 hours [Taylor 1997; Mindess *et al.* 2003].

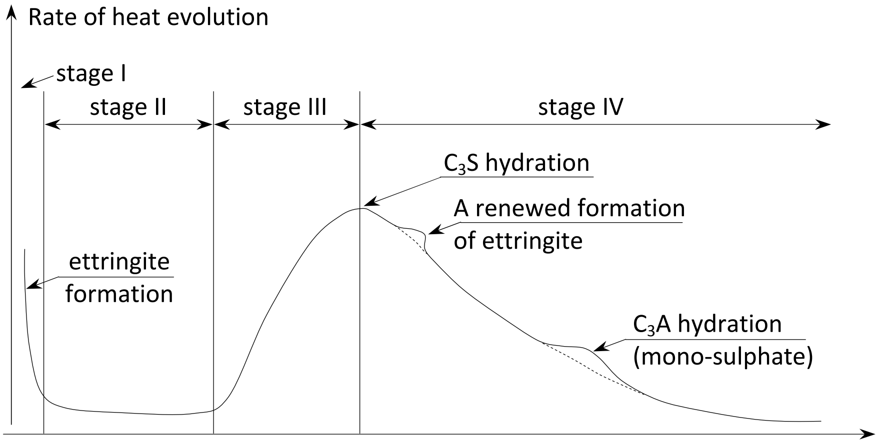

Figure 2.14 Rate of heat evolution during the hydration of Portland cement with the significance of peaks [Taylor 1997; Mindess *et al.* 2003]

Development of microstructure of Portland cement The development of the microstructure in cement paste includes the formation of hydration products (solid phases) and the distribution of the pore structure network (pore phase). Three main hydration products, calcium silicate hydrates (CSH), calcium hydroxide (CH) and calcium trisulfoaluminate hydrate, called ettringite (AFt), together with other minor products formed during the hydration process are diagrammatically shown in Figure 2.15 [Locher *et al.* 1976].

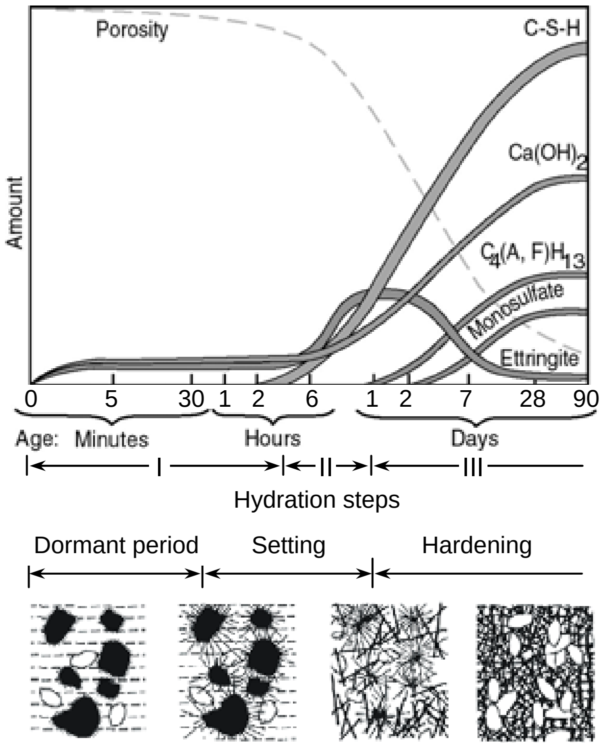

Figure 2.15 Formation of hydration products in Portland cement paste as a function of hydration time at an ambient temperature [Locher *et al.* 1976]

2.2.3 Hydration and microstructure development of cement blended with RHA

Hydration mechanisms of cement blended with RHA Many investigators have explored the hydration mechanisms of cement blended with RHA [Cook *et al.* 1976; James and Subba Rao 1986; Hwang and Wu 1989; Yu *et al.* 1999; Ordóñez *et al.* 2002; Feng *et al.* 2004; Sivakumar and Ravibaskar 2009]. They suggested that RHA containing a considerable amount of SiO_2 can react with $Ca(OH)_2$ to produce the CSH gel. Because of the pozzolanic reaction, the paste containing RHA has a lower $Ca(OH)_2$ content than the pure Portland cement paste. In general, the hydration mechanism of paste made with RHA can be hypothesized by Hwang *et al.* [Hwang and Chandra 1997] as shown schematically in Figure 2.16. This mechanism may be described as follows:

The penetration resistance coincides with the growth of calcium hydroxide (CH) up to 8 hours. This is similar to the behaviour of ordinary Portland cement paste. The early resistance may be primarily due to the formation of the CH crystal. This formation at the surface of RHA may be due to the adsorption by the cellular structure of RHA. The water which is adsorbed previously and available in RHA particles will enhance the pozzolanic reaction inside the inner cellular spaces.

After 40 hours, the pozzolanic reaction further binds Si in RHA with CH to form the CSH gel and solid structures. This means that RHA fills the finer pores and reduces the permeability, which may be beneficial for the durability.

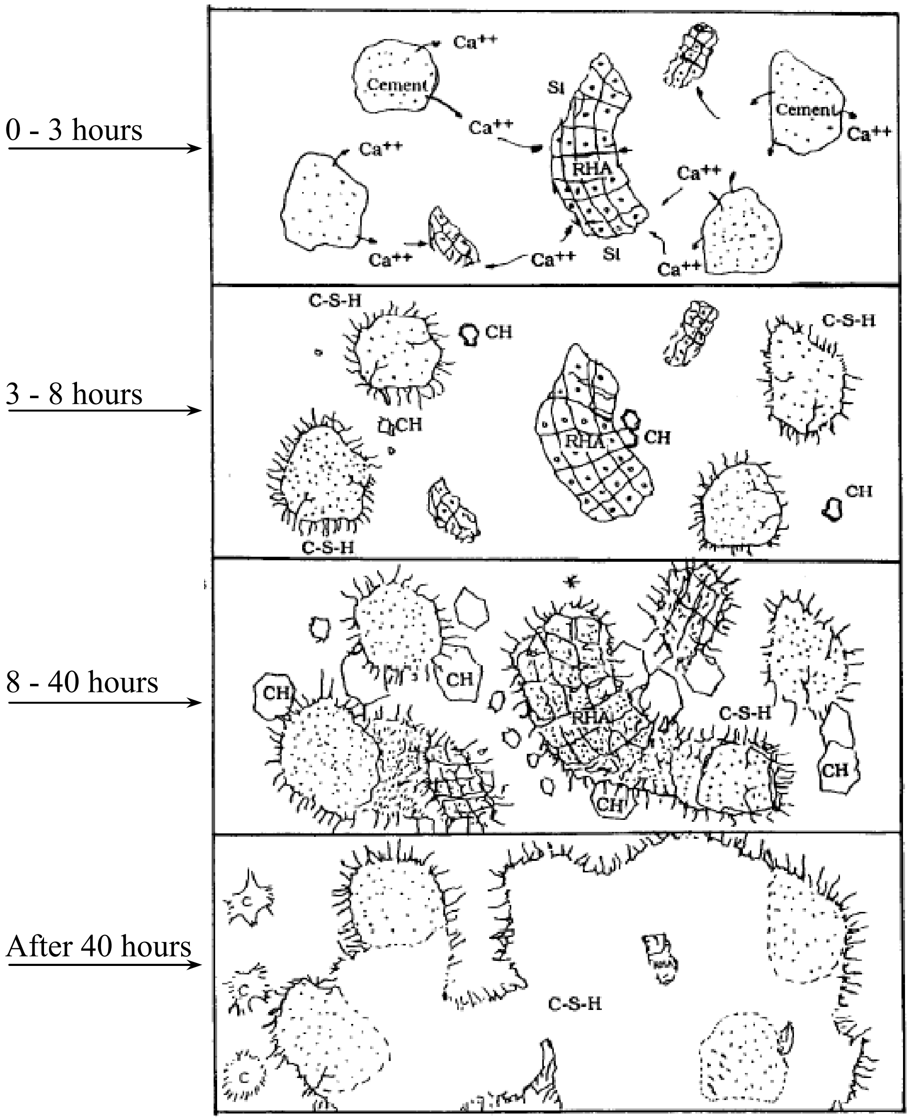

Figure 2.16 Schematic drawing of the hydration of cement paste containing RHA, suggested by Hwang *et al.*, cited in [Hwang and Chandra 1997]

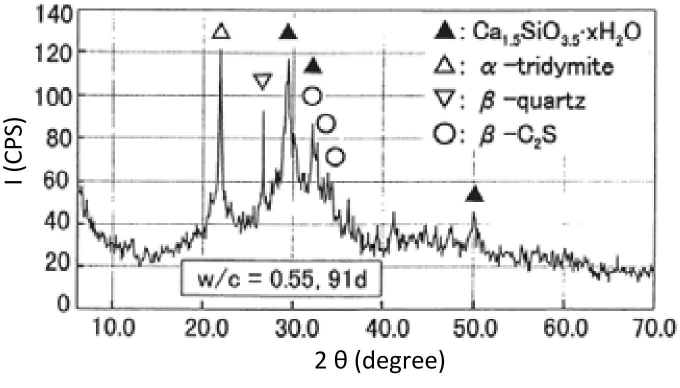

Figure 2.17 XRD patterns of paste with w/c ratio of 0.55 and 20% RHA, the reaction products in the presence of water $Ca_{1.5}SiO_{3.5}\cdot xH_2O$ (CSH gel) at $20\pm1^{o}C$ for 91 days [Yu *et al.* 1999]

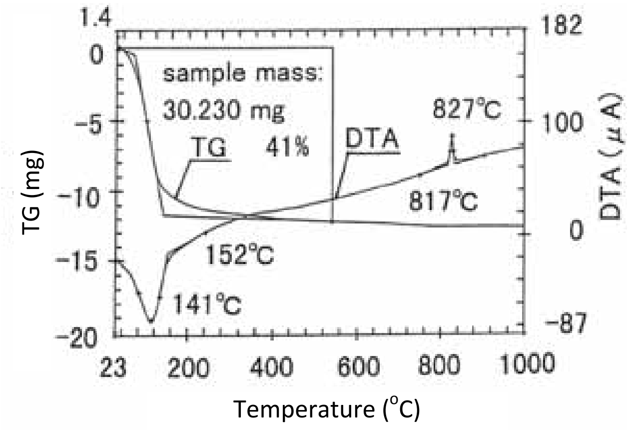

Figure 2.18 TG-DTA curves of the product generated from the pozzolanic reaction of RHA [Yu *et al.* 1999]

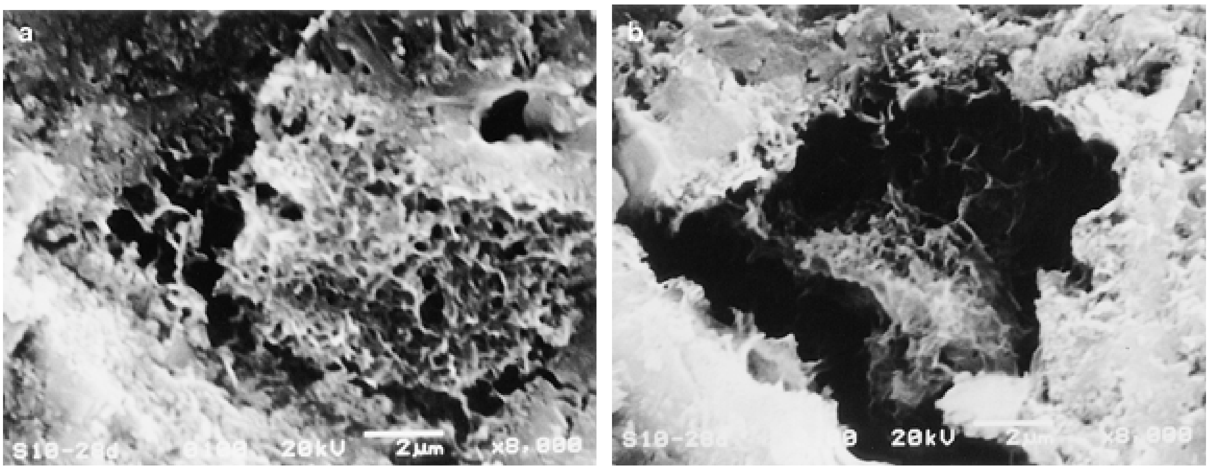

Figure 2.19 SEM images of the CSH gel in the paste containing 10% RHA at 20±1°C for 28 days, the CSH gel observed in the paste (left) and in the pore (right), 8,000× [Yu *et al.* 1999]

Hydration products In general terms, the CSH formed in the pozzolanic reaction between RHA and CH is of the CSH(I) type [Cook 1984]. In fact, RHA has both hydraulic and pozzolanic properties. RHA itself can react with water to form CSH [James and Subba Rao 1986]. There is some evidence to suggest that CSH (II) is also produced under certain circumstances, but these appear to be very unstable and reversion to CSH (I) occurs [Cook 1984]. In 1999, Yu *et al.* [1999] suggested that in the presence of water, RHA could react with $Ca(OH)_2$ to form a kind of the fine CSH gel ($Ca_{1.5}SiO_{3.5}.xH_2O$) ([Yu *et al.* 1999]). They also suggested that the average particle size of the reaction products, ranging between 4.8 and 7.9 μm, varied slightly with the condition under which the reaction occurs. The CSH gel appears to be flocs in morphology and be small round grains with a porous structure and a large N_2-specific surface. The pores in the gel are mainly between 1 and 10 nm with an average radius of about 2 nm. The SEM images (Figure 2.19) show that the CSH gel formed from the pozzolanic reaction of RHA fills in the pores and plays a bridging role between hydrates and anhydrous cement particles. Being porous in structure and large in specific surface, these products contain much absorbed water. Therefore, it has a marked weight loss up until 141°C, in [Yu *et al.* 1999], because of evaporation of absorbed water. When the product is heated, it gradually loses the water, but it still keeps an amorphous form up to 750°C. Above 780°C, it will be transformed to crystalline $CaSiO_3$, which can be seen at 827°C.

Hydration kinetics In general, the heat evolution curve of cement paste made with RHA is similar in shape to that of Portland cement paste (see Figure 2.20) [Hwang and Wu 1989].

It can be seen that the first peak is higher than the second peak. The larger the amount of RHA was added, the lower the amount of heat produced. To explain this phenomenon, the authors suggested that SiO_2 of RHA reacts with Ca^{2+} to reduce both the first and second peak. A higher w/c ratio may also reduce the heat of hydration due to the diluting effect of water. At the second stage of the hydration (the dormant period), the concentration of Ca^{2+} decreases, which increases the saturation time of ions and thus delays the second peak. However, the pH value increases primarily due to the potassium content in RHA dissolved in water. This compensates for the alkali concentration consumed by Ca^{2+} to nucleate earlier and to accelerate the second peak.

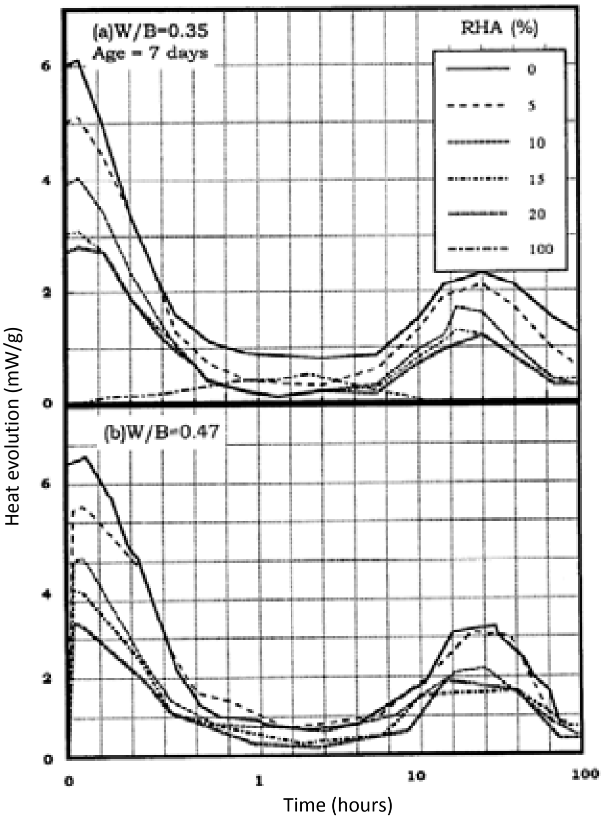

Figure 2.20 Heat evolution of cement paste made with RHA [Hwang and Wu 1989]

Microstructure of cement blended with RHA Adding of RHA changes the microstructure development of Portland cement paste. This can normally be observed by means of a scanning electron microscope (SEM). From SEM observations, Hwang and Wu [1989] revealed that a CH crystal in the cement paste containing RHA appears between anhydrous cores, and that the CSH gel appears after 5 hours. The size of this crystal will increase up to 4, 8 and 26 times after 6.5, 7.5 and 12.5 hours, respectively, compared to that after 5 hours. However, such a phenomenon does not occur in cement paste without RHA.

Also from SEM observations, Sivakumar and Ravibaskar [2009] found that after just 1 hour, the surface of RHA particles are covered by hydration products. After 1 day, most of the CH may have reacted with RHA; some hexagonal plates (about 0.1 μm) grow on the surface of RHA particles similar to that of monosulfoaluminate (AFm). The ettringite (AFt) needles disappear and the CH crystals diminish due to the pozzolanic reaction. After 3 days, the dense fibres bond with the matrix within large pores, and in 1 week, these pores are filled with the

CSH gel [Hwang and Chandra 1997]. After 4 weeks, the matrix has become denser and the non-decomposed CH crystal clogs the matrix. After 60 days, the matrix bonds together, and the presence of CH becomes unclear [Hwang and Wu 1989; Sivakumar and Ravibaskar 2009].

Regarding the interfacial zone between the aggregate and paste in concrete, normally both the hydration and the microstructure of ITZ is partly influenced by the ‘wall effect’ within the vicinity of aggregate surfaces. In normal concrete, this region may extend some 50 µm from the interface into the cement paste [Maso 1996]. In fact, the addition of RHA was found to improve both the hydration and microstructure of this zone [Zhang *et al.* 1996], in which the porosity and the $Ca(OH)_2$ amount is reduced, as well as the thickness of this zone, compared to that in the Portland cement paste. However, in UHPC, the coarse aggregates are absent and only sand is used as the main aggregate. This reduces the ‘wall effect’ and the resulting thickness of ITZ. However, how this zone is changed, especially in the presence of RHA, has still not been investigated exhaustively. This issue will be mentioned later in this thesis in the experimental part on the development of the microstructure of UHPC.

2.2.4 The use of RHA in concrete

The use of RHA in concrete was found very early with two German patents from 1924 [Swamy 1986]. However, the utilization of RHA as a pozzolanic material in cement and concrete was significantly advanced after the 1970s when many positive results were achieved [Mehta 1994]. It was recognized that RHA provides several advantages, such as improving compressive and flexural strengths [Ismail and Waliuddin 1996; Zhang and Malhotra 1996; Rodríguez 2006; Sata *et al.* 2007; Habeeb and Fayyadh 2009], reducing the permeability [Zhang and Malhotra 1996; Ganesan *et al.* 2008], increasing the resistance to chemical attack [Chindaprasirt and Rukzon 2008], increasing the durability [Coutinho 2003; Mahmud *et al.* 2009], reducing the effects of alkali-silica reactivity (ASR) [Nicole *et al.* 2000], reducing the shrinkage, and making concrete denser [de Sensale *et al.* 2008; Habeeb and Fayyadh 2009]. Besides, from an economical and environmental point of view, RHA can reduce costs due to cement savings, and has environmental benefits related to the disposal of waste materials and reduction of carbon dioxide emissions.

2.2.5 RHA as a potential substitute for condensed SF in HPC and UHPC

The limited resource and high cost of SF for HPC and UHPC applications, especially in developing countries, require the blending of Portland cement with a cheap alternative for condensed SF. Since rice is produced in a significant share of the developing countries, RHA, an agro-waste from the rice processing, has the potential of becoming one of the most appropriate candidates.

RHA is classified in the same category of highly pozzolanic materials as SF [Mehta 1994]. With a similar chemical composition of RHA and SF, the main differences between the two mineral admixtures are their size, morphology, and particle characteristics. As mentioned ealier, condensed SF, an industrial by-product in silicon and ferrosilicon manufacture, is reported to be a mineral composed of ultrafine particles with an average diameter of 0.1 µm (about 20 m^2/g surface area by nitrogen absorption), and amorphous glassy spheres of SiO_2 [Swamy 1986; Malhotra *et al.* 1987; Mehta 1994].

RHA is normally obtained by a controlled combustion of rice husks and retains the porous structure of the husk. It consists essentially of silica in the amorphous form. The average particle size of RHA ranges from 5 to 10 µm [Siddique 2008a], which is much larger than that of SF, but RHA also has a very large surface area originated from the porous structure of its particles [Cook 1984; Mehta 1994]. In fact, increasing the fineness of a pozzolanic material also increases its reactivity. It is expected that the RHA when pulverized can give finer particles in order to get the required size distribution for a higher reactivity. However, Mehta [1994] has suggested that grinding RHA to a high degree of fineness should be avoided since it derives its pozzolanic activity mainly from the internal surface area of the particles which in turn depends on the obtained porous structure of RHA.

Regarding the pore structure of RHA, as discussed in Section 2.2.1, the distribution of the pores in the ground RHA is narrowed to the range of 2–5 nm, with an average radius of 4 nm, and its specific pore volume is decreased to 0.13 cm^3/g. During the mixing process, a certain amount of water is needed to cover external and internal surfaces of ash particles and to fill up their pores. Normally, this causes high water demand for concrete mixtures containing RHA [Bui 2001]. This disadvantage can be compensated, like SF, by the use of superplasticizers.

Due to the fact that both RHA and SF are highly pozzolanic materials with a similar amount of SiO_2, RHA has been found to be useful to substitute SF to make HSC and HPC. The possibility for this substitution was analysed by Chandrasekhar *et al.* [2002; 2003], and in practice RHA has been proven to achieve HSC/HPC [Dalhuisen *et al.* 1996; Zhang *et al.* 1996; Sata *et al.* 2007].

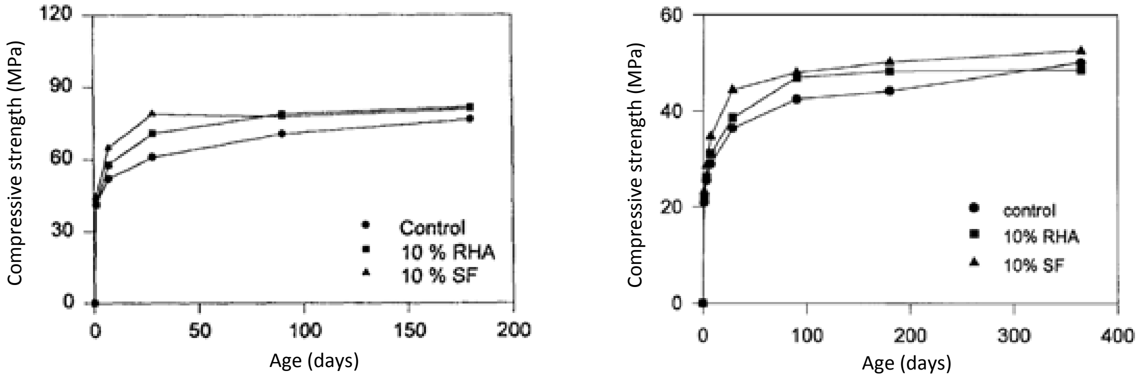

(a) w/c, w/(c+RHA), or w/(c+SF) = 0.30 (b) w/c, w/(c+RHA), or w/(c+SF) = 0.40

Figure 2.21 Development of the compressive strength of concrete made with RHA and SF [Zhang *et al.* 1996; Zhang and Malhotra 1996]

With respect to the low w/b ratio mixtures, Mehta [1994] reported that the strength contribution of RHA is larger at later ages, after 28 days and 1 year. With 20% cement replacement by RHA, the 28-day compressive strength increased with approximately 14% compared to that of the control sample, which is in close agreement with the results by Zhang *et al.* [1996; 1996] (see Figure 2.21). In particular for 0.30 w/b ratio mixtures, the development of the compressive strength of the RHA modified sample is even similar to that of the SF modified sample at 90 days and 180 days (Figure 2.21a). The authors also recognized from image analysis that the area percentage of anhydrous cement after 28 days in the RHA modified sample is lower than that in both the control sample and the SF modified sample. It indicates a possible acceleration of hydration of cement in the presence of RHA at later ages. It suggests that there is another mechanism governing the hydration process which may be caused by the porous structure of RHA. The water absorbed in the porous RHA particles will be released with the progress of cement hydration process, and increase the degree of hydration of cement and the resulting compressive strength. This mechanism will be further discussed in the section pertaining to the experiments on UHPC.

2.3 Concluding remarks

2.3.1 Summary

In this chapter, a brief introduction to UHPC was presented including the definition, the material selection with some favourable mineral admixtures common used to make UHPC, the mix composition, the packing density of granular mixtures, the hydration and microstructure development, and the shrinkage of UHPC. Regarding the material constituents, SF is a principal component in UHPC. However, the use of SF has some limitations such as the high cost and the available resource. This limits its applications in concrete production, especially in developing countries. This has given rise to the idea to search for other substitutions with similar functions. Among the mineral admixtures, RHA, an agro-waste with a high amount of amorphous SiO_2 and extremely high specific surface area like SF, has a very high potential. The literature survey also provides some clues about the feasibility of the substitution of SF by RHA in low w/b ration mixtures. This is very important for the experimental studies in the next chapters relating to cement paste and UHPC containing RHA.

2.3.2 Intention for new research

Given a similar chemical composition of RHA and SF, the differences of particle characteristics between RHA and SF are expected to be the same differences in both the hydration and microstructure development of cement paste. These aspects are investigated by isothermal calorimetry, image analysis, pore size distribution, thermogravimetric analysis of the paste (Chapter 3). An evaluation of the possibility for substituting SF by RHA to make UHPC through the experimental results of cement paste is accounted for. The optimal amount of RHA in regard of the hydration and microstructure development of cement paste is evaluated by simulation in Chapter 4.

One of the most important principles for designing UHPC is the optimization of granular mixtures. The packing density of ternary and quaternary systems of sand, cement, RHA and/or SF is predicted and verified by experimental results. The effect of RHA on the workability of UHPC mixtures is also discussed. Furthermore, the possibility for using RHA in combination with or without SF to make UHPC is evaluated based on the experimental results of the hydration and microstructure development of UHPC as well as the development of the compressive strength and autogenous shrinkage of UHPC. All of these aspects are dealt with in Chapter 5.

3

Experimental Study of the Hydration and Microstructure Development of Cement Paste incorporating Rice Husk Ash

3.1 Introduction

It is well known that the addition of pozzolans, such as RHA and SF, changes the properties of cement paste. With a similar chemical composition and specific surface area of RHA and SF, the different particle characteristics may cause differences in the development of the hydration process and microstructure development of cement paste. This is the main objective of this chapter which is to evaluate the possibility for using RHA as a substitute for SF in low w/b ratio cement pastes. The evaluation was based on the investigation of the pozzolanic activity, degree of hydration, phases and the phase distribution, pore size distribution, and the change of the amount of hydration products in cement paste containing either RHA or SF. Different experimental techniques, i.e. a pH meter, electrical conductivity, isothermal calorimetry, image analysis, mercury intrusion porosimetry, and thermogravimetric analysis are used for these experimental studies.

Two main w/b ratios of 0.25 and 0.40 were employed. Cement pastes made with different amounts of RHA and SF additions, from 5 to 20%, were cured at 10-40^{o}C.

3.2 Materials and Methods

3.2.1 Materials

The materials used in this study were Portland cement (CEM I 52.5N), RHA, condensed SF, and a polycarboxylate-based superplasticizer (Glenium 51) with 35% solid content by weight. As discussed in the previous chapter, rice husk, an agricultural waste material from Vietnam, was burnt in a drum incinerator developed by PCSIR [Cook 1984] and modified by Bui

[2001]. The obtained ash was ground in a vibrating ball mill for 45 minutes. The properties of cement, RHA, and SF are shown in Table 3.1. The mineral composition of cement was calculated by the modified Bogue equation [van Breugel 1991] as presented in Table 3.2.

Table 3.1 Properties of cement, RHA, and SF used in this study

Components	Cement*	RHA**	SF**
Chemical properties, % by weight			
CaO	64.00	1.14	0.39
SiO_2	20.00	87.96	97.20
Al_2O_3	5.00	0.30	0.51
Fe_2O_3	3.00	0.52	0.18
SO_3	2.40	0.47	0.26
Na_2O	0.30	-	-
K_2O	-	3.29	1.04
Loss on ignition (LOI)	1.30	3.81	-
Physical properties			
Specific gravity, g/cm^3	3.15	2.10	2.20
Specific surface area, m^2/g (Blaine)	4500	-	-
Specific surface area, m^2/g (nitrogen absorption- BET)	-	19.2	19.5
Mean particle size, µm	13.7	7.30	0.15

*) Data provided from the company
**) Chemical composition determined by X-Ray Fluorescence Spectrometry method

Table 3.2 The mineral composition of cement CEM I 52.5 N, % by weight

Mineral composition, % by weight (calculated by the modified Bogue equation [van Breugel 1991])			
C_3S	C_2S	C_3A	C_4AF
63.77	9.24	8.18	9.13

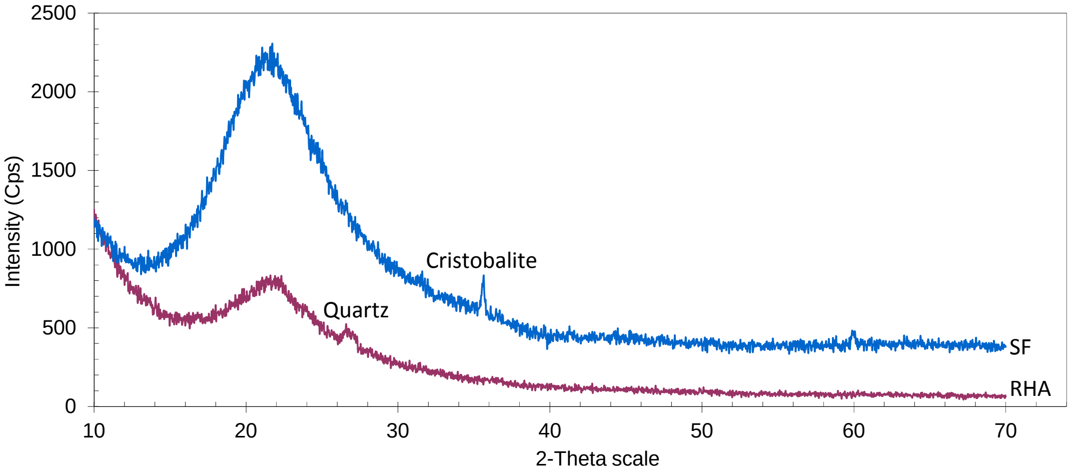

Figure 3.1 XRD patterns of RHA and SF

Figure 3.1 shows X-Ray diffraction patterns of RHA and SF. The RHA modified sample contains a small amount of quartz, while the bulk of the ash is amorphous, similar to the SF sample.

The particle size distribution of cement, RHA, and SF used in this study is shown in Figure 3.2. The particle size distribution and the mean particle size of materials were determined by laser diffraction (Mastersizer 2000).

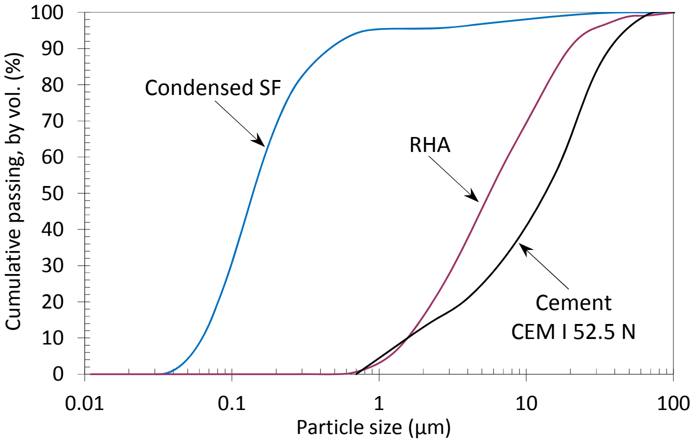

Figure 3.2 Particle size distribution of cement, RHA, and SF used in this study

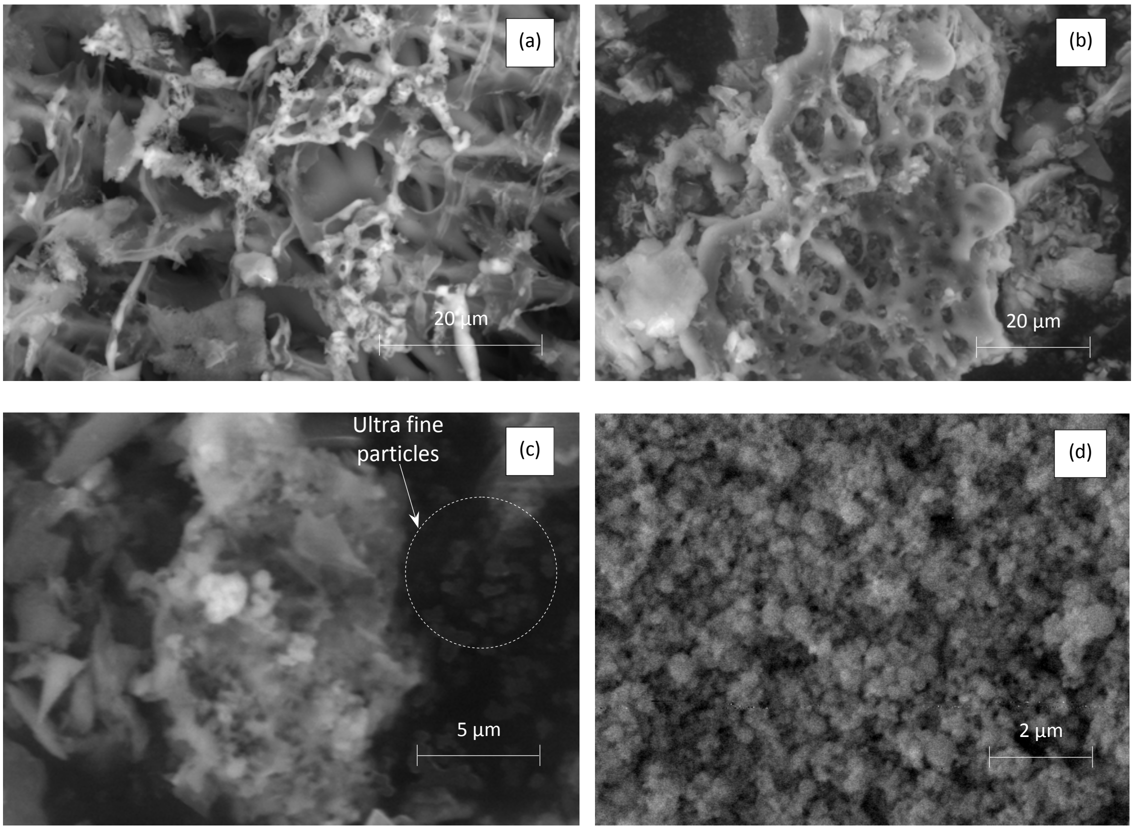

Figure 3.3 SEM images of RHA before grinding (a); RHA after grinding (b)-(c); and SF (d)

The SEM images of RHA and SF are shown in Figure 3.3. It can be seen that both the original RHA obtained after combustion (Figure 3.3a) and the ground RHA have the porous structure (Figure 3.3b-c). The ground RHA also contains ultra-fine particles (Figure 3.3c) with a size falling into the size range of SF particles.

To study the effect of RHA fineness on the hydration and microstructure development of cement paste, other types of RHA with different mean particles sizes were selected, i.e. 15.5, 9.0, 6.3, 5.6, and 3.6 μm. These RHAs were obtained by grinding the original RHA obtained after combustion for different times. The particle size distribution of these RHAs is shown in Figure 3.4. The corresponding specific surface areas determined by the BET nitrogen absorption method are 13.4, 18.3, 19.7, 20.6, and 14.6 m^2/g.

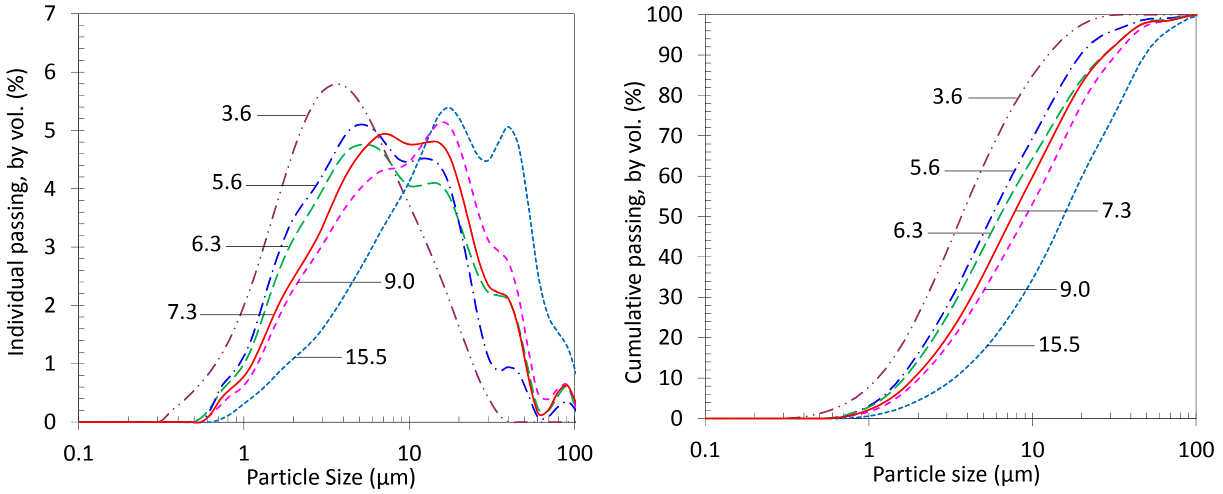

Figure 3.4 Particle size distribution of different RHA types, the numbers indicate the mean particle sizes of RHAs

3.2.2 Experimental methods

The effect of RHA on the pH value of the pore solution of cement paste and concrete was evaluated by the change of the pH value of demineralized water with the addition of RHA. A digital pH meter recorded the pH values. The pozzolanic activity of RHA was evaluated by using an electrical conductivity meter. The rate of hydration of cement paste was measured by isothermal calorimetry. Two main techniques were used to examine the microstructure of the paste, i.e. Mercury Intrusion Porosimetry (MIP) for pore size distribution and porosity, and an Environmental Scanning Electron Microscope (ESEM) for phases and phase distribution. Thermogravimetric analysis (TGA) was used to determine the calcium hydroxide content of samples.

The digital pH meter and electrical conductivity meter

To study the effect of RHA on the change of the pH value of demineralized water, a digital pH meter (827 pH lab Metrohm) was used. In this study, 200 ml of demineralized water at 20±1^{o}C was prepared and 10.0 g of RHA was added. This condition was kept constant while stirring.

To evaluate the pozzolanic activity of RHA, a rapid indirect method proposed by Luxan *et al.* [1989] was applied. This method is based on the change in the electrical conductivity of a calcium hydroxide saturated solution in which a particular pozzolanic material is dispersed. The electrical conductivity is a function of the concentration of Ca^{2+} in the calcium hydroxide solution. When a pozzolanic material is added to the solution, its active constituents will react with calcium hydroxide leading to a decrease in the concentration of Ca^{2+} and, hence, to a decrease in the electrical conductivity. A suspension with RHA and $Ca(OH)_2$ was prepared at a solid-water ratio of 0.05 g/ml. The solutions were placed in a sealed beaker which was then placed on a stirring device which was heated up to 40 ± 1^oC. According to this method, 5.0 g of RHA which was dried at 105^oC was added to 200 ml of saturated $Ca(OH)_2$ solution. After two minutes of constant stirring, the value of the electrical conductivity of the solution was recorded. The change of this value for the first two minutes was calculated. This result was used to evaluate the pozzolanic activity of RHA and SF.

Isothermal calorimetry The rates of heat evolution of all the cement mixes were measured in a Thermometric isothermal conduction calorimeter (TAM-Air-314) (Figure 3.5), using 10±0.01g samples and appropriate amounts of mixing water. Before mixing, all the materials were placed in an oven for at least 12 hours at the desired testing temperature. The cement pastes were cast into capped glass vials and the vials were inserted in the calorimeter. For this reason it was not possible to register the first hydration peak, which occurs immediately after water addition (Chapter 2). The tests were performed on 2 parallel samples at 10, 20, 30 and 40^oC. Each test lasted 120 hours starting from mixing. The isothermal heat of hydration was derived by integration of the rate of heat evolution.

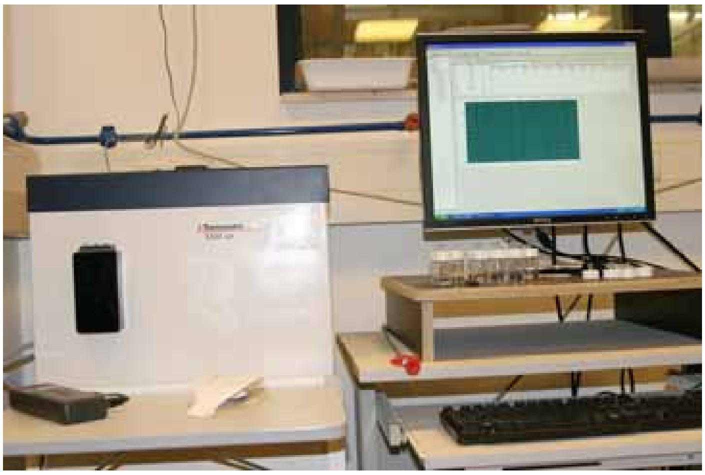

Figure 3.5 TAM-Air-314 used to measure the rate of heat evolution of cement

Based on the result of isothermal heat of hydration, the degree of hydration at time *t* can be approximated as the heat released at time *t* divided by the maximum heat [van Breugel 1991], viz.

$$\alpha(t) = Q(t) / Q_{max} \tag{3.1}$$

where Q(t) is the heat liberated at time t, Q_{max} is the maximum heat when all the cement has hydrated. The maximum heat of the binder (cement and RHA/SF) is calculated as follows:

$$Q_{max} = P_{Cem}.Q_{Cem} + P_{Poz}.Q_{Poz} \qquad (3.2)$$

P_{Cem}, P_{Poz} are the percentages of cement and pozzolan (RHA or SF), respectively; Q_{Cem} is the maximum heat of hydration of cement calculated according to Bogue [van Breugel 1991]; Q_{Poz} is the maximum heat of RHA or SF calculated from the amount of amorphous SiO_2 in RHA or SF, where Q_{SiO2} = 780 J/g [Waller *et al.* 1996].

In addition, the activation energy is calculated from the rate of hydration [Kada-Benameur *et al.* 2000; D'Aloia and Chanvillard 2002]:

$$Ea(\alpha) = R\left[\frac{T_1.T_2}{T_1 - T_2}.\ln\left(\frac{\frac{d\alpha_1}{dt}}{\frac{d\alpha_2}{dt}}\right)\right] \qquad (3.3)$$

where R is the gas constant (8.314 J/mol K); T_1 and T_2 the curing temperatures (K); $d\alpha_1/dt$, $d\alpha_2/dt$: the rate of hydration at T_1 and T_2, respectively.

Sample preparation for SEM, MIP and TGA The studies on SEM, MIP, and TGA were performed on cement pastes with two w/b ratios of 0.25 and 0.40 by weight. A constant dosage of superplasticizer (0.8% by weight of the cement) was employed for pastes with a w/b ratio of 0.25. In addition, in order to compare with the effect of RHA on the hydration and microstructure development of cement paste, these experiments were also applied for SF.

All pastes were prepared in a three-litre Hobart mixer. After mixing for 3 minutes in total, the pastes were first poured into 500 ml plastic bottles and then sealed with a plastic lid. The samples were cured at 20°C until testing, i.e. 6 hours, 1, 3, 7, 28 and 91 days. At the end of each curing period, the cover of the plastic bottle was removed. Samples were split into small pieces of about 1 cm^3 by hammer. The cement hydration was stopped by immersing the samples into liquid nitrogen at a temperature of -195°C. The samples were then dried in a freeze-drying chamber. These samples were used for the MIP test. With the SEM test, the dried samples were epoxy-impregnated, and then cut and polished. Details of this method were proposed and described by Ye [2003]. For TGA, the samples were first dried and then ground to a particle size less than 125 μm before analysis.

MIP MIP is the most common method to measure a pore size distribution and porosity in cement paste. The pore diameters that can be measured by MIP vary from 0.001 μm to 1000 μm according to the pressure used. Although MIP provides a fast method to obtain the pore structure, the result from MIP is influenced by some conditions such as pore shape, the ink-bottle effect, the damaged fine structure during measuring, surface tension and contact angle, the sample preparation, i.e. drying treatment [Diamond 1971; Cook and Hover 1993; Ye 2003].

Mercury intrusion measurements were performed with Micrometrics PoroSizer® 9320 (Figure 3.6). The PoreSizer-9320 is a 207 MPa mercury intrusion porosimeter, which determines pore sizes in the range from 7 nm to 500 µm. The apparatus has two low-pressure chambers and one high pressure chamber. A measurement is conducted in two stages: a manual low pressure run from 0 to 0.170 MPa and an automated high pressure run from 0.170 to 205 MPa.

Figure 3.6 PoreSizer-9320 used to measure the pore size distribution of cement paste

For each test, two or three samples with a total weight of approximately 4-6 g per sample were used. The relation between the pressure p (MPa) and the pore diameter d (µm) is described by the Washburn equation (3.4), cited by Ye [2003], based on a model of cylindrical pores:

$$p = -\frac{4\gamma \times \cos\theta}{d} \tag{3.4}$$

where γ is the surface tension of the mercury (mN/m) and θ (-) is the contact angle between the mercury and the pore wall surface of the cement. In this study, the mercury contact angle and surface tension used were 139^{o} and 480 mN/m, respectively [Ye 2003]. By applying the Washburn equation, mercury intrusion data can be converted into a pore size distribution.

SEM SEM has become one of the most widely utilized instruments for materials characterization. Two common modes used to obtain images with SEM are the secondary electron (SE) and the backscattered electron (BSE) modes. The former can be used to observe individual particles or fracture surfaces, hydrate surface morphology, and pore structure. The latter can yield information on the distribution of phases and composition of hydrated cement paste.

In this study, the BSE mode was used to investigate the microstructure of cement blended with RHA, i.e., phases and phase distribution. The observations were conducted on a Philips-XL30-ESEM in a gaseous (water vapour) environment (Figure 3.7). The acceleration voltage of 15-20 kV was used. To analyse the BSE image, the size of the image and its magnification were chosen, 1424×968 pixels and 540×, respectively. The calculated resolution of these images was 0.185 µm/pixel. For each sample, 12 images were captured in order to provide a good level of statistical confidence in the results of the image analysis [Ye 2003].

BSE observation can provide two-dimensional information of the microstructure. A typical BSE image of the hardening Portland cement paste and its grey level histogram are shown in Figure 3.8. Depending on the density, the phases will appear with different grey levels. The main phases in the microstructure of cement paste, i.e. pore, hydration products and anhydrous cement can be distinguished by their grey levels. As observed, the anhydrous core of cement particles appear bright, the calcium hydroxide shows light grey and the other hydration products (i.e. CSH) are various shades of darker grey. Due to the low average atomic number of the epoxy that is filling the pores, the pores do not scatter electrons and appear uniformly black. With a commercial image processing program, the area of each phase can be determined by counting the number of pixels. In this study, only anhydrous cement was considered in order to determine the degree of hydration of cement in cement paste. Samples were tested at the ages of 1, 3, 7, and 28 days.

Figure 3.7 Philips-XL30-ESEM used for microstructural observation

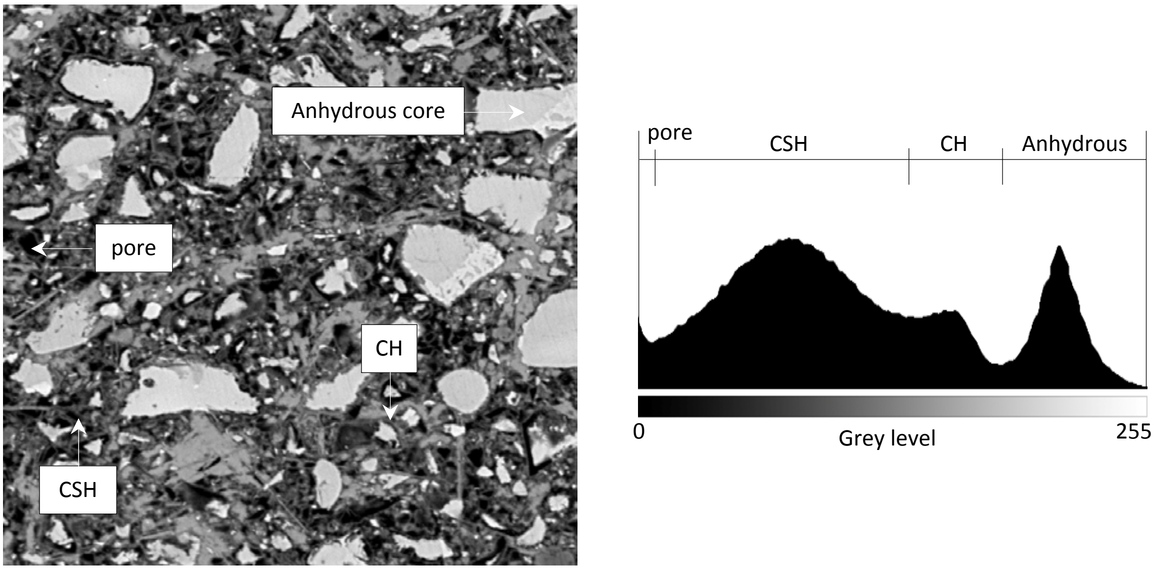

Figure 3.8 A typical BSE image of the Portland cement paste and its grey level histogram

According to stereology analysis [Diamond and Leeman 1995], with sufficient sampling, the volume fraction can be assumed to be equal to the area fraction in BSE images. From this, the percentage of anhydrous Portland cement and the resulting degree of hydration of cement can be calculated.

TGA The amount of calcium hydroxide (CH) of samples was determined by TGA which has been widely accepted as an accurate method [Midgley 1979]. Analyses were conducted using a TG-449-F3-Jupiter® instrument (Figure 3.9) at a heating rate of 10°C/min from 35°C to 1100°C under flowing nitrogen. Before measuring, the sample was ground until the particle size was smaller than 125 μm. The mass of sample for each test was between 75 and 90 mg.

A typical weight-loss versus temperature curve obtained by TGA for hardened cement paste can generally be seen in Figure 3.10. This curve can be separated into [Bhatty and Reid 1985; Marsh and Day 1988]: (a) an abrupt weight loss near 450°C, associated with the dehydration of CH, illustrated as CH_{loss}; (b) another fairly sudden, but less distinct weight loss about 700°C, labelled CO_{loss}. This was ascribed to the decomposition of calcium carbonate (this may not be present if care has been taken to prevent carbonation), and (c) a continuous weight loss over the whole range from 105 to 1000°C, but most pronounced before 500°C; this loss is due to the dehydration of calcium silicate hydrates, calcium aluminate hydrates and other minor hydrates.

The methods for interpretation of thermograms, however, have varied among researchers [Marsh and Day 1988]. In this study, the CH content was determined from the weight loss curve during thermal analysis by a graphical technique as illustrated in Figure 3.11 [Marsh and Day 1988; Haines 2002]. This method can be briefly described through an example of a typical abrupt weight loss on the TG curve. It occurs between initial (T_i) and final (T_f) temperatures. The determination requires drawing of tangents to the curve at the initial baseline and the steepest part of the curve and making their intersection of the extrapolated onset temperature (T_e) and the extrapolated offset one (T_o). The mid-point $T_{0.5}$ is created by these points. A weight loss is defined as the distance between two intersections generated by the vertical line from $T_{0.5}$ with initial and final baselines.

Figure 3.9 TG-449-F3-Jupiter® used for thermogravimetric analysis

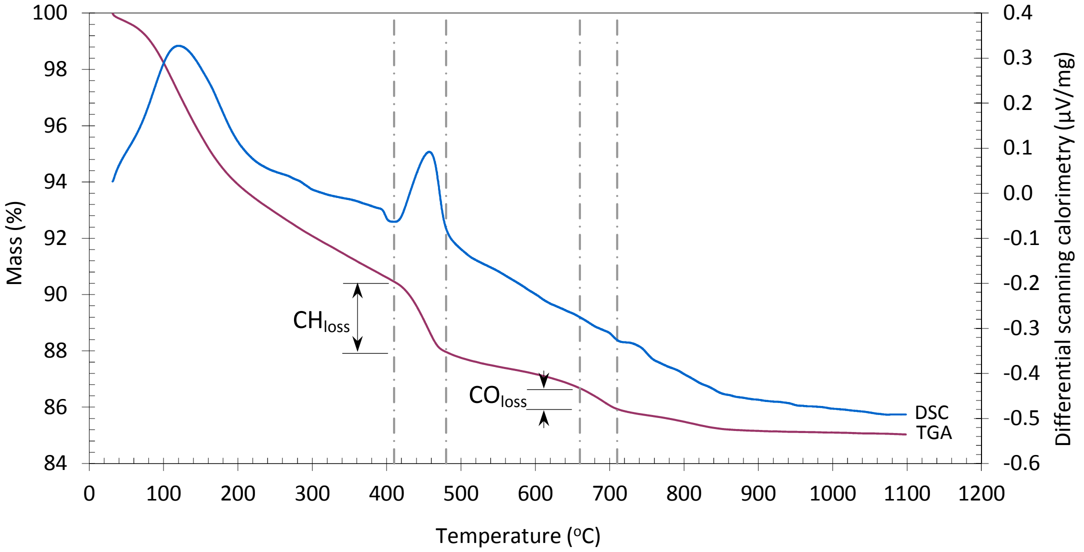

Figure 3.10 DSC/TGA data and the measured hydration quantities

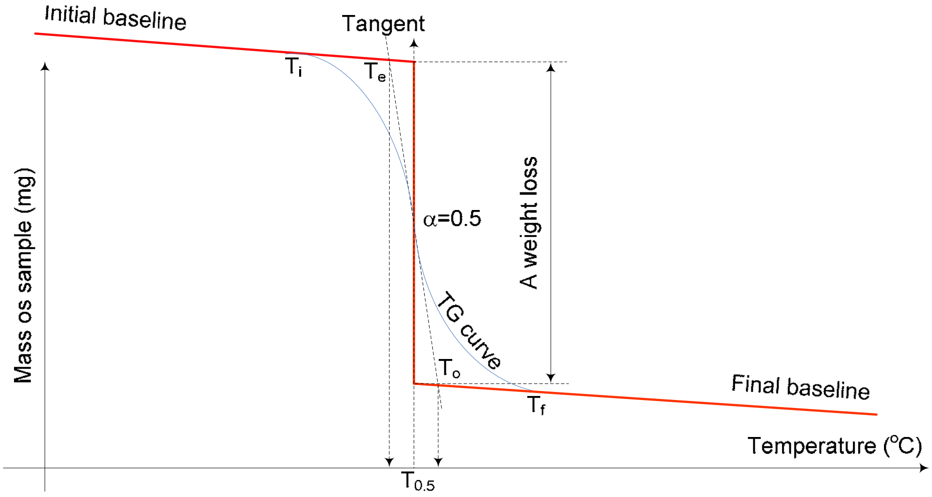

Figure 3.11 Method used to calculate the content from a weight loss curve during thermal analysis [Marsh and Day 1988; Haines 2002]

3.3 Experimental results

3.3.1 The pH value of RHA dispersed in the demineralized water

With regard to the chemical composition of the RHA powder, one notable point in the properties of RHA in comparison with SF is that RHA has a high content of K_2O. This possibly causes a different effect of the pH value of the pore solution in the cement paste or concrete, when RHA or SF is added in the system. In fact, the high content of K_2O in RHA will contribute a high alkalinity of the pore solution and may help to offset the decrease in pH value of the pore solution due to the pozzolanic reaction between the silica of RHA and the calcium hydroxide [Hwang and Wu 1989; Bui 2001] whereas the pH value of the pore solution will decrease continuously. The change of the pH value of the solution with the addition of either RHA or SF was studied in this section.

The change of the pH value of the demineralised water with time in the presence of either RHA or SF can be seen in Table 3.3. It is clear that the RHA dissolves very fast and the maximum pH value of 9.79 was reached within 30 minutes. This value then fell slightly to 9.58 after 24 hours. The increase in the pH value of the SF solution was slower. The maximum pH value of the SF solution achieved was 8.26 after 90 minutes.

Table 3.3 Evolution of the pH value of the RHA and SF solutions with solid-water ratio of 0.05 g/ml

	pH value with time								
	0 min.	5 min.	10 min.	20 min.	30 min.	60 min.	90 min.	120 min.	24 hours
RHA	5.87	9.67	9.76	9.83	9.79	9.77	9.76	9.76	9.58
SF	5.87	6.62	7.01	8.02	8.15	8.23	8.26	8.23	8.03

3.3.2 **Pozzolanic activity**

Pozzolanic activity is the extent of the chemical reaction occurring between the active constitutes of pozzolana, calcium hydroxide, and water. In this study, RHA contains amorphous silica as an active component, thus the pozzolanic activity of RHA is directly related to the degree of amorphousness of the silica in the ash. This aspect was evaluated by the indirect method through the variation in the electrical conductivity in the first two minutes as introduced in the experimental method part 3.2.2.

Table 3.4 shows the variation in the electrical conductivity of the RHA solution using RHAs with different mean particle sizes of RHA. In this table, SF was also used to compare with RHA. The results indicate that the reactivity of RHA increases with a decrease in its particle size. However the change is not significant with a particle size of RHA of less than 5.6 µm. This may be caused by the grinding level, which influences the exposed surface area of RHA particles and also the porous structure of RHA, i.e. collapsing the structure of particles as suggested by Mehta [1994], Bui *et al.* [2005], Nguyen *et al.* [2010b]. Moreover, RHA has a same reactivity in terms of the variation in the electrical conductivity like SF when the particle size of RHA is less than 7.3 µm.

Table 3.4 Variation in the electrical conductivity in the RHA and SF solutions

	RHA with different mean particle sizes				SF
	15.0 µm	7.3 µm	5.6 µm	3.6 µm	0.15 µm
Variation in the electrical conductivity (mS/cm)	0.67	0.91	1.05	1.08	0.90

To further understand the pozzolanic reaction of RHA, the test was recorded for 600 minutes. The pH meter was also used to evaluate the reactivity of RHA. In this section, only RHA with a mean particle size of 7.3 µm was selected to study in detail. The pH value and the variation in the electrical conductivity of saturated $Ca(OH)_2$ from 0 to 600 min. in the presence of RHA is shown in Figure 3.12. These initial values at 40 ± 1°C were 12.02 and 7.05 mS/cm. After adding RHA to the solution, both the pH value and the electrical conductivity gradually decreased with time, which indicates that both the Ca^{2+} and OH^- concentrations of the solution reduce with time. The reason for the decrease in the concentration of Ca^{2+} and OH^- ions can probably be attributed to the interaction between them and RHA that was added [Yu *et al.* 1999].

Tests performed also reveal that the pozzolanic reaction of RHA occurs slower and later than the reaction of SF. This may be caused by the difference in particle characteristics. As discussed previously, with a same specific surface area of RHA and SF, the surface of the RHA comes from its porous structure whereas in the case of SF it comes from the ultra-fine particles. According to Chandra and Bergqvist [1997], a material is in a finer dispersion form which enables its quick access to the calcium hydroxide in the solution and thus the reactivity of this material is higher than that of the coarser one. In this respect, the mean particle size of RHA is much bigger than that of SF which leads to a lower reactivity of RHA compared to that of SF. Additionally, the cellular porous structure of RHA particles possibly delays the pozzolanic reaction of RHA because the silica inside the RHA particles have to first diffuse to the surface of these particles and then diffuse to the solution. The similar phenomenon also occurs with the access of the calcium hydroxide in the solution through the pore inside the RHA particles. On the contrary, SF is in a finer dispersion form which enables its quick access to the calcium hydroxide in the solution which results in a faster pozzolanic reaction of SF compared to that of RHA.

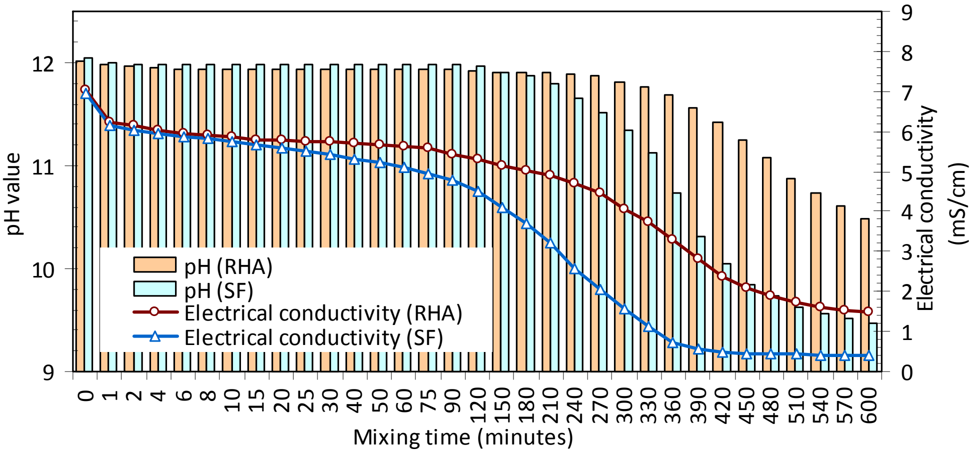

Figure 3.12 Variation of the pH value and the electrical conductivity of the saturated $Ca(OH)_2$ solution with time in the presence of RHA and SF

3.3.3 Effect of RHA on the content of calcium hydroxide of cement paste

The sequence of different phases in the hydration process of cement can be followed by determining the amount of the products formed at different times. Calcium hydroxide is considered as one of the major phases in the hardened Portland cement paste [Midgley 1979]. The addition of RHA in cement paste leads to a reduced CH content caused by its pozzolanic reaction. Moreover, the difference in particle characteristics between RHA and SF is expected to result in different effects in the pozzolanic reaction and in the resulting decrease of the CH content.

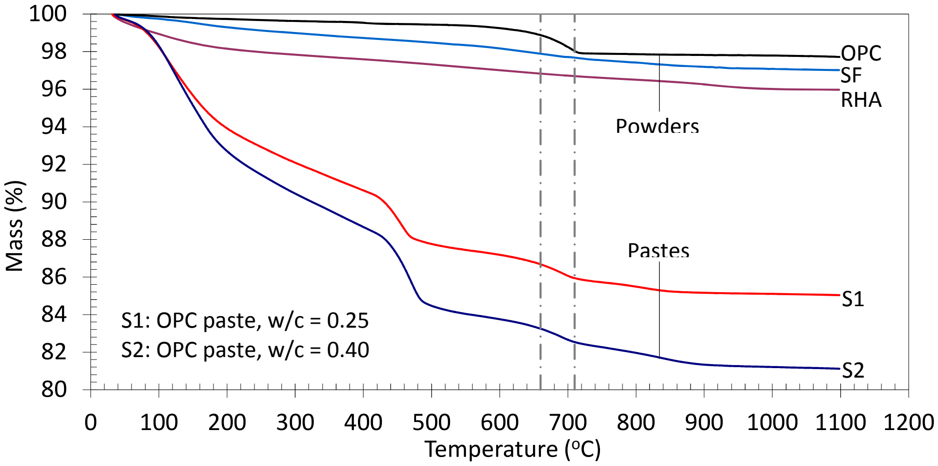

Figure 3.13 TGA data for powders of OPC, SF and RHA, and the OPC cement paste at w/b ratios of 0.25 and 0.40

Figure 3.13 shows the TGA data for powders of OPC, SF, RHA. It can be seen that an abrupt weight loss occurs only with the OPC powder at the temperature range between 660°C and 710°C, which is due to the existence of limestone filler, about 1% by weight of cement. This filler was added in the cement manufacturing process. The results for cement paste, i.e. OPC pastes with w/c ratios of 0.25 and 0.40, also exhibit this abrupt weight loss at this temperature range. Therefore, the quantity of the weight loss at this temperature range was not taken into account in the calculation of CH content.

The amount of $Ca(OH)_2$ formed from 0.25 to 360 days of cement paste with or without RHA and SF is shown in Figure 3.14. It can be seen that the addition of RHA strongly reduces the amount of $Ca(OH)_2$ in cement paste beyond 3 days for both w/b ratios of 0.25 and 0.40. The $Ca(OH)_2$ content falls to a minimum at the age of 91 days.

Compared with the SF modified paste, the RHA modified paste had the same CH contents from 0.25 to 3 days, but higher values after 7 days. A higher amount of SF strongly decreases the CH content in the cement paste. The minimum of the CH content in the SF modified pastes also occurs at about 91 days. The value of the CH content of all samples at that day is presented in Table 3.5.

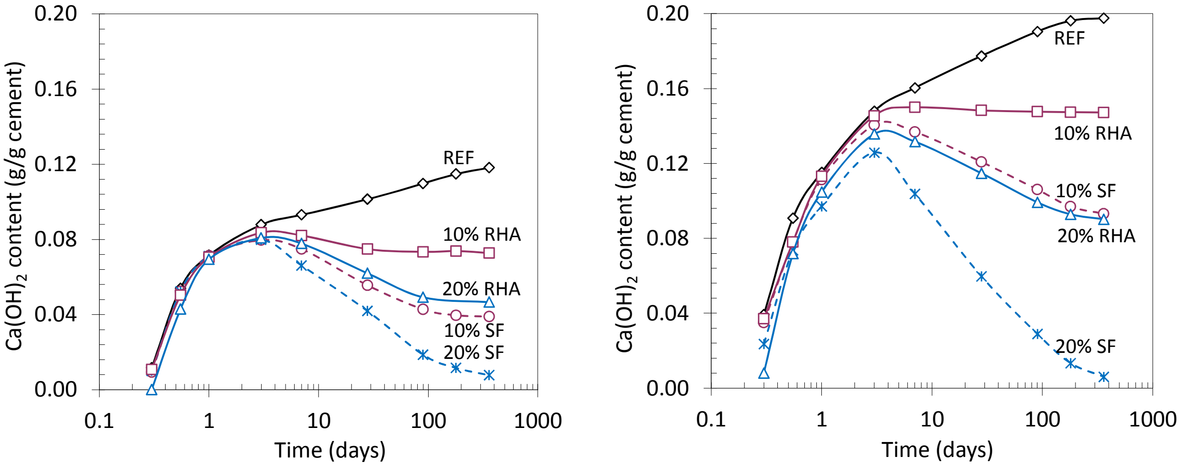

(a) w/b = 0.25 (b) w/b = 0.40

Figure 3.14 The content of Ca(OH)$_2$ of cement blended with 0, 10 and 20% RHA or SF at ages from 0.25 to 360 days

From the result of the CH content calculated by weight, the volume fraction of CH can be determined with its specific gravity of 2.24 g/cm^3 [Bentz *et al.* 1994] and shown in Figure 3.15. This result will be used to verify the numerical simulation result in Chapter 4.

Table 3.5 Content of Ca(OH)$_2$ of cement paste with or without RHA and SF at 91 days

w/b ratio, by weight	The content of Ca(OH)$_2$ of cement paste, g/g cement				
	The control	10% RHA	20% RHA	10% SF	20% SF
0.25	10.8	7.3	4.9	4.3	1.9
0.40	19.0	14.8	9.9	10.6	2.9

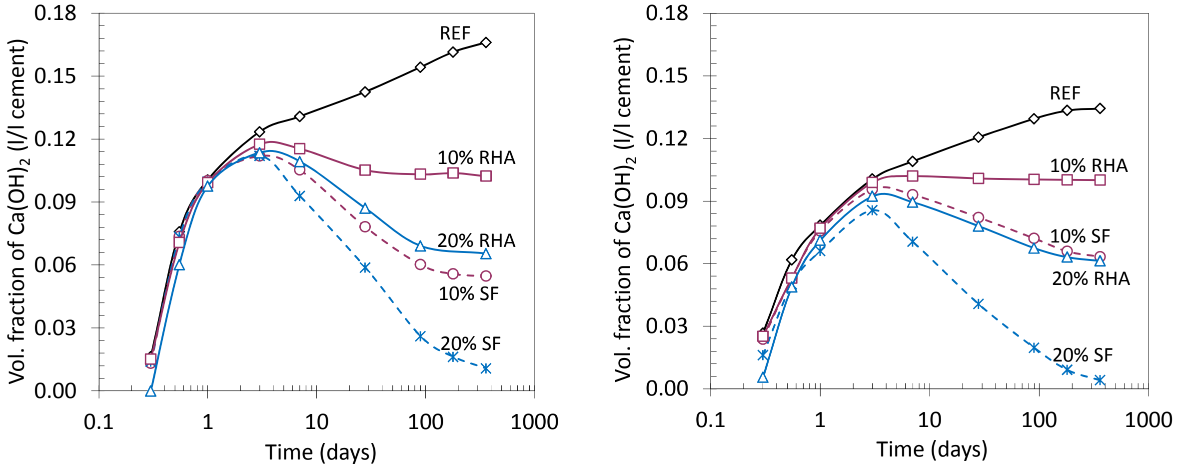

(a) w/b = 0.25 (b) w/b = 0.40

Figure 3.15 The volume fraction of Ca(OH)$_2$ of cement blended with 0, 10 and 20% RHA or SF at ages from 0.25 to 360 days

3.3.4 Effect of RHA on the kinetic of hydration of cement process

Heat evolution The effect of RHA contents on the rate of heat evolution of cement paste determined by isothermal calorimetry at 20°C curing is shown in Figure 3.16. Measurements were made with pastes at w/b ratios of 0.25, 0.40 and 0.60 for 120 minutes.

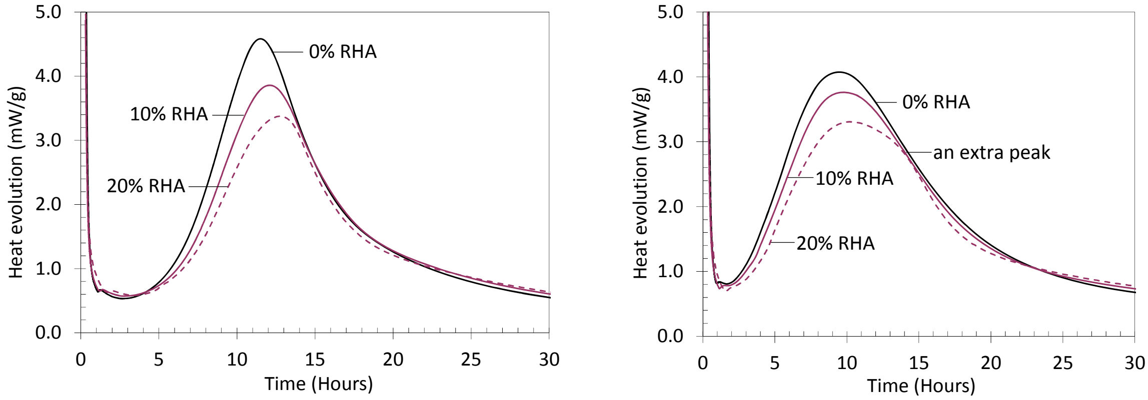

(a) w/b = 0.25 (b) w/b = 0.40

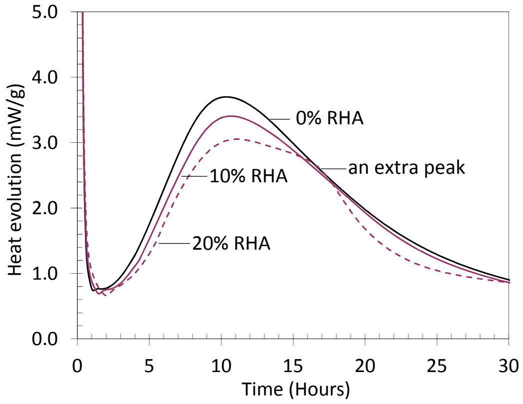

(c) w/b = 0.60

Figure 3.16 Heat evolution of cement paste made with RHA and w/b ratios from 0.25 to 0.60

The result reveals that the heat evolution curve of cement paste with RHA is similar to the control paste without RHA. The addition of RHA, however, lowers the amount of heat evolved. There is a small effect on the dormant period which occurs at about 2 hours. As the w/b ratio increases, the acceleration peak, or main peak, of the heat evolution curve of the RHA modified sample offsets to the right. An extra peak occurs at about 14 to 17 hours and the intensity of this peak is greater if the w/b ratio is higher and more RHA is added.

The main peak can be associated with C_3S hydration, which occurs at a later time than that of the control paste. The more prominent extra peak occurring in the RHA modified paste is due to the pozzolanic reaction of RHA.

The effect of RHA on the hydration of cement can be explained by several reasons. First, when more RHA is added, the amount of cement in the paste decreases and therefore the heat evolution would be decreased (dilution effect). Second, the pozzolanic reaction of RHA affects the precipitation of $Ca(OH)_2$, the formation of CSH, and the resulting heat evolution of cement paste.

Normally, during the hydration of a pure cement, the concentration of Ca^{2+} ions increases rapidly and reaches a supersaturation level within the first few minutes [Mindess *et al.* 2003]. For the RHA modified paste, this supersaturation state may or may not be reached depending on the amount of RHA present. The amount of RHA influences the migration of Ca^{2+} ions from the grain surface to the solution, which in turn influences the rate of hydration of cement. The rate of hydration of cement also depends on the precipitation of $Ca(OH)_2$ and the formation of CSH.

When water is added to cement, there is an exchange of ions between the solid particles and the solution. With the progress of the hydration process, the pore solution consists of some main ions such as Ca^{2+}, Na^{+}, K^{+}, and OH^{-} ions. The concentration of Ca^{2+} ions depends on the alkalinity of the solution, which is determined by the concentration of OH^{-} ions. Within the first few minutes of hydration, the Ca^{2+}, K^{+}, Na^{+}, and OH^{-} ions are rapidly absorbed at the surface of RHA particles, which serve as precipitation sites. The coordination number of the silicon atom on the surface increases due to the absorbed OH^{-} ion. As a result, this weakens the oxygen bonds to the underlying silicon atoms. The silicon ions go into the solution as silica. The dissolution of silica will result in lowering the concentration of OH^{-} ions and more Ca^{2+} ions to come into the solution [Wu and Young 1984b; Urhan 1987]. Therefore the rate of dissolution of cement grains is accelerated, especially with an increase in the RHA content. This leads to a higher heat evolution in the early period.

After that, CH nuclei simultaneously form on the sites and outside of the original grain boundaries in the water-filled space. The large surfaces of RHA particles increase the number of CH nuclei. In the literature, there is evidence that silicate species retard the growth of CH and possibly poison the nucleation of CH, and a silicate-rich surface causes the same effect, known as 'the silicate poisoning theory' [Young 1972; Skalny and Young 1980; Wu and Young 1984a]. This theory proposes that CH nuclei are 'poisoned' by the adsorbed silicate species, and can only grow spontaneously from a solution supersaturated with respect to the pure CH phase. This gives a delay in the formation of stable CH nuclei and crystals. This delay is greater with an increase of the RHA content.

One notable point of RHA's properties is its high potassium content. This primarily increases the pH value of the solution in the presence of RHA, see Table 3.3. This compensates for the alkali concentration consumed by Ca^{2+} to nucleate earlier and to accelerate the second peak.

The final result of both effects of delaying and enhancing the cement hydration is shown in Figure 3.16c. The main peak on the hydration curve of the RHA modified paste with a w/b ratio of 0.60 appears at the same time with the neat sample. In a low w/b ratio cement paste, less water is available for cement hydration. This would also reduce the amount of the silica to dissolve. For significant amounts of silica to go into solution, the concentration of OH^{-} ions per unit surface of silica must be sufficiently high. Due to the lower amount of water in the paste, the OH^{-} ion concentration on the surface of RHA may never reach the concentration to initiate the dissolution of RHA within the first few minutes of hydration. In addition, the very fine RHA particles can also adhere to the surface of the cement particles creating a layer of reactive silica. Upon contact with water, the ions, i.e. Ca^{2+} ion released by hydrating cement or the OH^{-} ion from the pore solution, have to pass through this layer. The low w/b ratio cement paste will encounter a larger number of silica particles in the vicinity of the surface of cement particles.

This influences the rate of diffusion of ions and results in the delayed and reduced rate of heat evolution. This effect can be seen for the low w/b ratio pastes in Figure 3.16.

In principle, the effect of SF on heat evolution of cement paste is the same as that of RHA because both of them mainly contain the amorphous silica. However, the SF-modified pastes reveal different effects in which the addition of SF accelerates the hydration of cement pastes with a high w/b ratio and the main peaks shift towards the left (Figure 3.17).

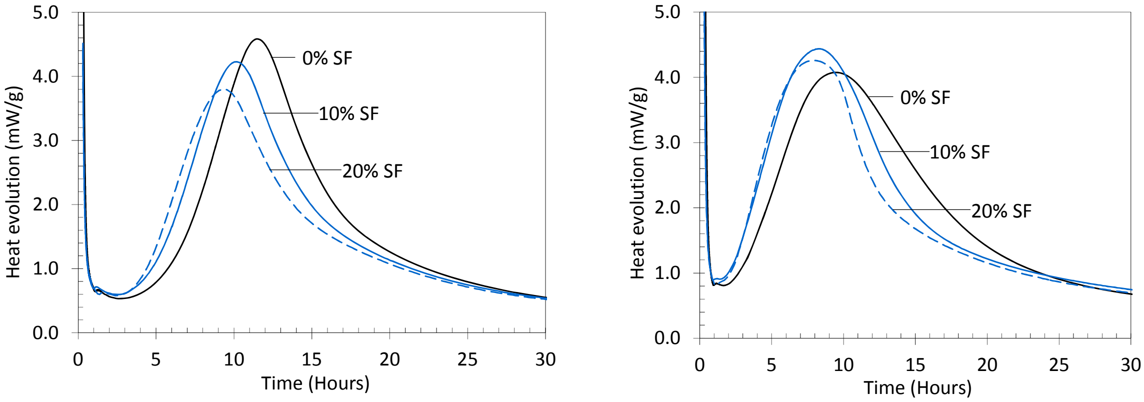

(a) w/b = 0.25 (b) w/b = 0.40

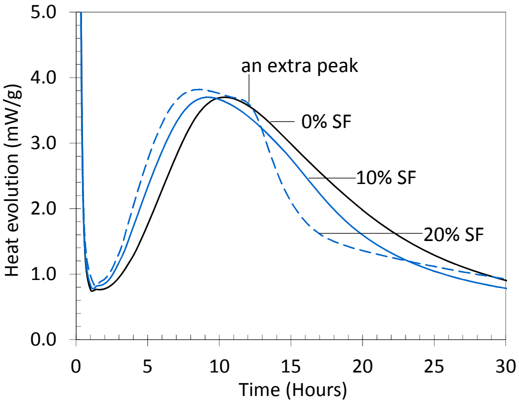

(c) w/b = 0.60

Figure 3.17 Heat evolution of cement paste made with SF and w/b ratios from 0.25 to 0.60

These different effects may be caused by the fact that RHA and SF has a different particle characteristic. The ultra-fine particles of SF will have an easier accessibility of ions from the surface of these particles to the pore solution than that of RHA particles. The surface area of RHA is originated from inside its particles. This leads to a larger dissolution of silica, a larger precipitation site, and a larger nucleation site of SF than that of RHA even with a similar specific surface area. Consequently, the hydration of cement is stimulated and more heat is produced. However, because SF particles are ultra-fine, a large number of them, i.e. approximately 100,000 [Chatterji *et al.* 1982], tend to attach around each cement particle creating a dense SF layer. This layer constrains ions passing through and the rate of heat evolution is thus reduced. On the contrary, the particle size of RHA is much bigger than that of SF. So, the effect of RHA particles to make a dense layer around the cement particles is not extensive compared to that of SF ones, especially at a low w/b ratio.

It is noticed that although both RHA and SF have a similar amount of SiO_2, the amount of K_2O in RHA is higher than that in SF. As a result, a higher resulting pH value of the pore solution of the RHA modified paste will compensate for the alkali which is consumed by Ca^{2+}. This may accelerate the second peak.

In summary, the different particle characteristic and chemical composition result in the differences of hydration of cement of RHA- and SF- modified pastes. The addition of RHA lowers and delays the main hydration peak of cement paste and vice versa with the addition of SF. For the high w/b ratio paste, the main hydration peak is lower with an increased cement replacement percentage by either RHA or SF. This may be caused by the dilution effect. The lower peak value of the low w/b ratio paste containing SF may be attributed to the higher concentration of silica around the cement particles.

The detail of these results can be found in Appendixes A1.1 and A1.2.

Degree of hydration of cement paste incorporating RHA The degree of hydration of cement made with RHA and SF is calculated following the equation (3.1). A comparison of degree of hydration of the RHA- and SF- modified pastes is shown in Figure 3.18. In this figure, only pastes with w/b ratios of 0.25 and 0.60 are presented. A notable point is that the degree of hydration of the RHA modified pastes is higher than that of the SF modified samples at the low w/b ratio.

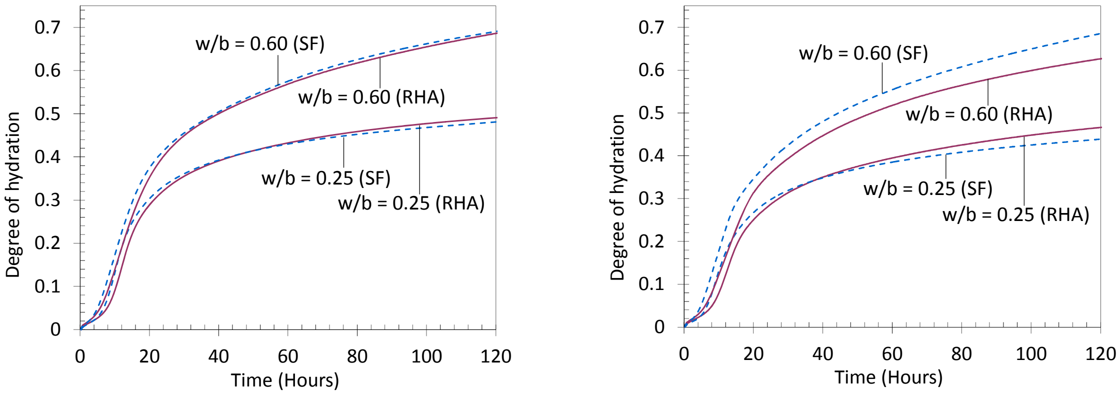

(a) 10% cement replacement (b) 20% cement replacement

Figure 3.18 Degree of hydration of cement made with (a) 10% and (b) 20% either RHA or SF

The increase of hydration of cement with the addition of RHA at the later period can be explained by the porous structure of RHA particles. The pores in RHA particles may absorb a certain amount of free water into its pores during mixing. On the one hand, this adsorbed water decreases the rate of hydration of cement at an early stage. This is because of the smaller amount of water available for cement to hydrate, especially with low w/b ratio mixtures. However, at the later stage, the relative humidity in cement paste drops and this absorbed water will release from the porous RHA particles can compensate this drop. In addition, the release of water also promotes the hydration of cement. This effect is larger with a lower w/b ratio. The mechanism is similar to the suggestion by Weber and Reinhardt [1997] and Van Breugel *et al.* [1999] when using saturated lightweight aggregates, and from Jensen and Hansen [2001,2002] when using SAP particles for internal curing of concrete. Besides, the experimental result on mitigation of autogenous shrinkage and on the relative humidity in the RHA-modified paste [de Sensale *et al.* 2008] also supports this idea: the more RHA is added, the higher the relative humidity is observed.

From this result, it can be concluded that the effect of RHA on increasing the degree of hydration of cement in the low w/b ratio mixtures is larger than that of SF at the later period.

Activation energy of cement paste made with RHA The temperature sensitivity of the hydration process can be quantified with the Arrhenius function. By using the Arrhenius function with an appropriate value of the apparent activation energy Ea, the influence of temperature on the rate of hydration of Portland cement can be described. It should be noted that the Ea of the hydration process of Portland cement is the minimum amount of energy needed for this material to hydrate. Thus, the influence of temperature on the development of any concrete property, which is related to the degree of hydration of cement, can be estimated. This approach has been used to predict compressive strength as a function of the curing temperatures [Hansen and Pedersen 1977].

The Ea can be determined from heat evolution curves measured in, for example, isothermal calorimeter. In fact, in calculations of temperature distributions in concrete structures the *Ea* is considered to be different. Ma *et al.* [1994] considered the Ea as a constant. Several studies, however, reveal the Ea not to be constant at all. Schindler [2004] proposed an equation for the Ea that considers the chemical composition and fineness of cement. Hansen and Pedersen [1977] recommended that the Ea is only a function of curing temperature. Van Breugel [1991] proposed an equation for the Ea as a function of chemical composition of cement, curing temperature and the degree of hydration. In addition, the addition of mineral admixtures possibly has an influence on the Ea. Therefore, the objective of this section is to study the activation energy of cement blended with RHA. The effect of the degree of hydration, the curing temperature, the w/b ratio and the RHA content was accounted for in the determination of the Ea. Isothermal calorimetry was used to study the heat evolution of blended cement at curing temperatures from 10 to 40^{o}C. The result was also compared to that of cement blended with SF.

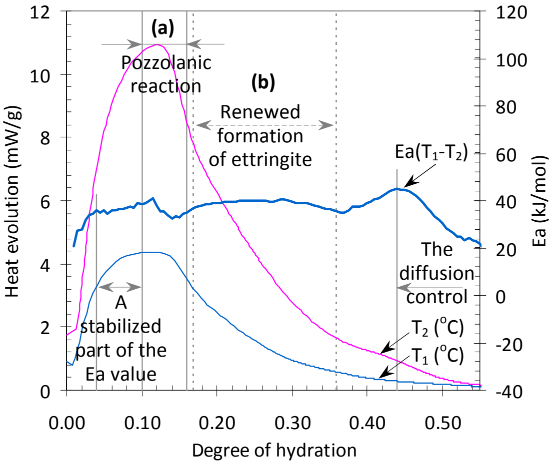

Figure 3.19 A typical curve of the calculated Ea values of the RHA modified paste for the temperature range of T_1-T_2 (^{o}C) with two phenomena (a) Pozzolanic reaction, (b) the renewed formation of ettringite, w/b = 0.40

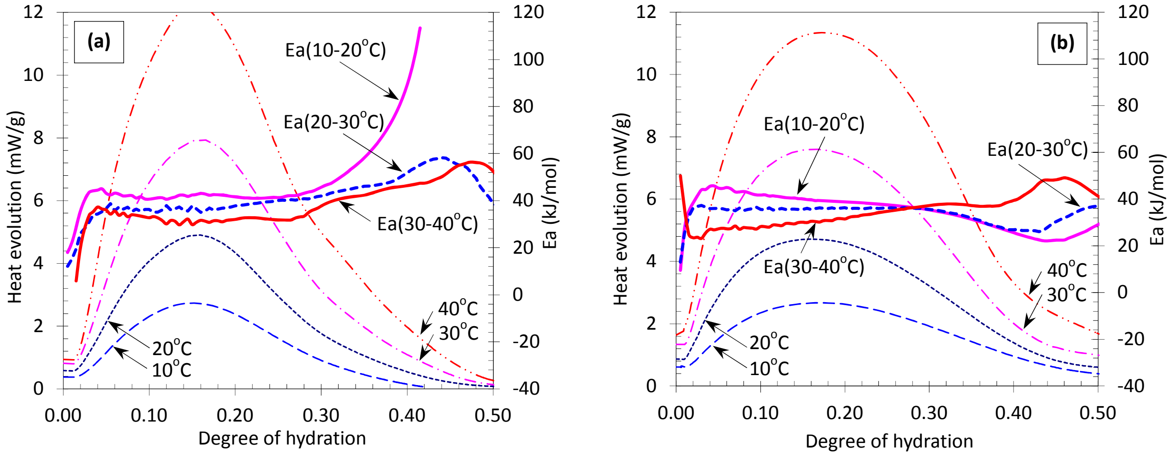

Figure 3.20 Heat evolution and the calculated Ea of control samples without RHA, w/b = 0.25 (a) and 0.40 (b)

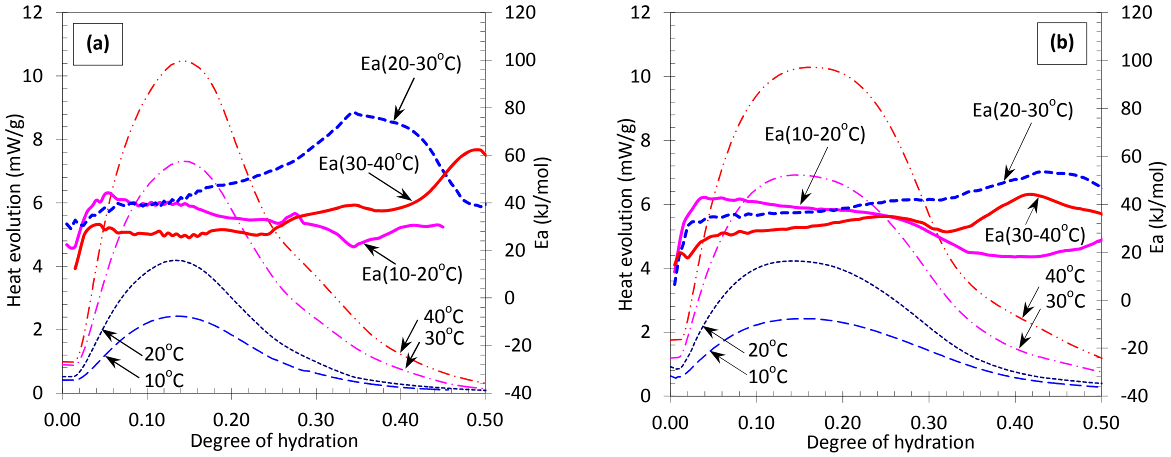

Figure 3.21 Heat evolution and the calculated Ea of samples containing 10% RHA, w/b = 0.25 (a) and 0.40 (b)

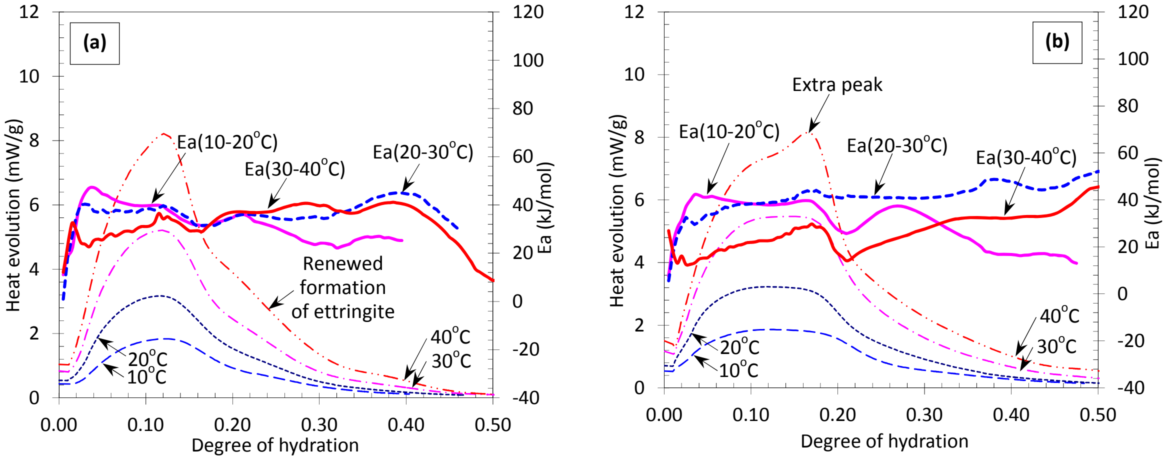

Figure 3.22 Heat evolution and the calculated Ea of samples containing 30% RHA, w/b = 0.25 (a) and 0.40 (b)

In this research, the Ea is calculated from the rate of hydration, as mentioned in Section 3.2.2. A typical result of activation energy of cement paste blended with RHA in one temperature range (T_1-T_2, $T_1<T_2$) can be observed as seen in Figure 3.19. The temperature noticeably accelerates the heat evolution of cement. The Ea is observed to be more or less 'constant' at a degree of hydration ranging from 0.05 to 0.20-0.40. Outside this range, the Ea varies considerably and then decrease gradually. Additionally, two phenomena can be observed from the Ea curves. First, the pozzolanic reaction of RHA causes an extra peak on the heat evolution curve. This leads to a jump on the calculated Ea curve. Second, a shoulder in the deceleration period on the heat evolution curve which causes a considerable variation of the calculated Ea values. This shoulder which appears at about 16 hours on the heat evolution curve can be ascribed to a renewed formation of ettringite [Pratt and Ghose 1983; Scrivener 1989].

Figure 3.20 to Figure 3.22 show the results of heat evolution and the calculated Ea of control pastes and pastes containing 5 to 30% RHA replacement. The three ranges of temperature studied were 10-20, 20-30, and 30-40°C. The detail of the effect of RHA or SF on heat evolution of cement paste can be found in Appendixes A1.3 and A1.4.

In the RHA modified paste, the phenomenon of the renewed ettringite formation appears earlier with increasing the RHA content, especially for low w/b ratio mixtures (Figure 3.20 to Figure 3.22). When the renewed formation of ettringite appears, the Ea gradually decreases. This change is ascribed to the change in mechanism of hydration of cement, in which the chemical reaction control will switch to the diffusion control in this period, as suggested by Kjellsen and Detwiler [1992]. The Arrhenius law cannot be applied in this case [Kada-Benameur et al. 2000].

In comparison with RHA, SF has the same effect on cement hydration and a similar value for the Ea. The detail of these results can be found in Appendixes A1.5 and A1.6. In this section, only the calculated Ea of cement paste containing 30% SF is presented (Figure 3.23) in order to compare to the Ea of the RHA modified paste. In comparison with the result in Figure 3.22, the phenomenon of the renewed formation of ettringite in SF modified pastes appears earlier than that in RHA modified pastes, which leads to a shorter stabilized part of the calculated Ea values.

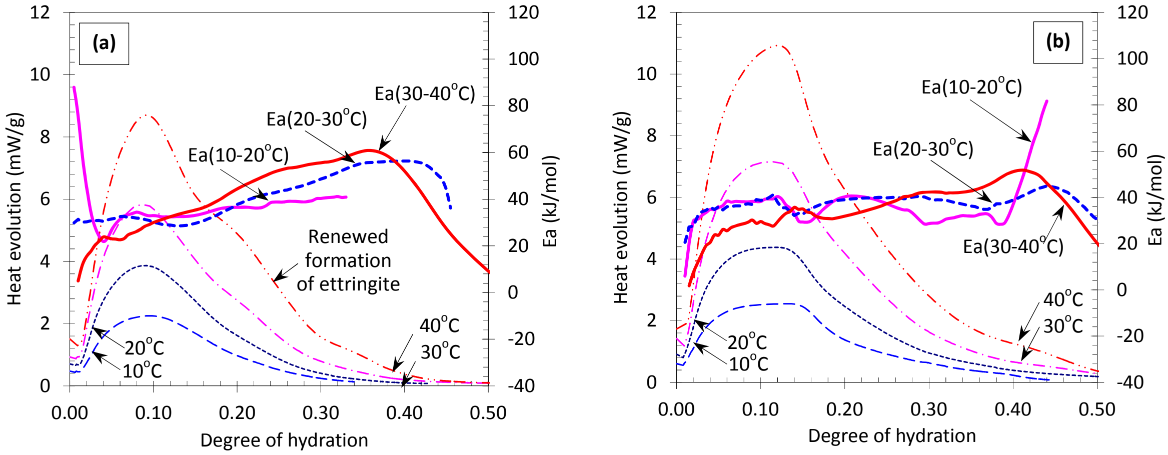

Figure 3.23 Heat evolution and the calculated Ea of samples containing 30% SF, w/b = 0.25 (a) and 0.40 (b)

The mean calculated values of the Ea are calculated from the stabilized part, which is considered from a corresponding degree of hydration of 0.05 to a value at which the renewed ettringite formation appears. In this part, the pozzolanic reaction takes place. The detail of the results can be seen in Table 3.6. The calculated values of the Ea are almost independent of the amount of RHA as long as one temperature range is considered, i.e. 10-20, 20-30, and 30-40°C. However, the values of Ea vary with the temperature and are lower at a high temperature.

Table 3.6 The Ea calculated by equation (3.3) obtained for degree of hydration α from 0.05 to 0.2-0.4 for three ranges of temperature (10-20, 20-30, 30-40°C)

Sample	% RHA or SF, by weight	The mean *Ea* value							
		w/b = 0.25				w/b = 0.40			
		α from 0.05 to	10-20°C	20-30°C	30-40°C	α from 0.05 to	10-20°C	20-30°C	30-40°C
REF	0	0.285	41.87	37.57	32.39	0.380	37.82	35.04	32.81
RHA	5	0.270	37.93	36.71	34.81	0.365	43.37	34.55	31.44
	10	0.250	37.38	44.07	27.34	0.335	36.10	38.59	31.01
	20	0.205	38.00	34.43	31.52	0.285	38.90	35.71	30.73
	30	0.175	37.77	36.39	30.55	0.220	36.60	39.63	22.12
SF	5	0.255	34.61	36.95	31.41	0.330	38.25	36.05	31.55
	10	0.240	36.51	37.89	27.80	0.300	40.31	34.08	33.02
	20	0.195	33.88	34.51	30.28	0.235	40.36	35.04	31.68
	30	0.150	32.44	30.41	29.26	0.180	36.05	36.38	30.18

Table 3.7 Average values of the Ea of blended cement paste with different RHA and SF replacement percentages calculated over the total temperature range from 10 to 40°C

w/b ratio, by weight	The average calculated Ea value of the blended cement								
	Control sample	% RHA, by weight				% SF, by weight			
		5	10	20	30	5	10	20	30
0.25	37.28	36.48	36.26	34.65	34.90	34.32	34.06	32.89	30.71
0.40	35.22	36.45	35.23	35.12	32.79	35.28	35.81	35.69	34.20

The average calculated values of the Ea over the whole temperature range from 10 to 40°C are presented in Table 3.7. These values are in consensus with the ones calculated following the ASTM C 1074 method [Nguyen *et al.* 2009; Nguyen *et al.* 2010a]. It can be seen that the average calculated Ea values of both of RHA and SF modified pastes are quite similar. In addition, these average calculated values do not change significantly with different amounts of cement replacement or at different w/b ratios.

3.3.5 Effect of RHA on the pore structure of cement paste

Effect of the RHA content The cumulative and differential pore size distribution curves for the w/b ratio 0.25 and 0.40 mixes containing 0, 5, 10, and 20% RHA or SF are shown in Figure 3.24 to Figure 3.26 for the periods of 1, 3, 7, 28, and 91 days. The detail of these results can be found in Appendix A2. The total porosity of these pastes is presented in Table 3.8. In this table, the results indicate that the total porosity of cement paste decreases with progress of the hydration process. It was observed that the initial peak exhibited on the differential MIP curve, which is called one of the ‘critical pore diameters’ [Cook and Hover 1999; Ye 2003], shifts to the smaller pores with the progress of the hydration process. This means that the pore structure became increasingly finer. In this study, the critical pore size of mixes with w/b ratios of 0.25 and 0.40 is larger than 0.04 μm and 0.2 μm, respectively. Additionally, the total pore volume decreases drastically with longer curing times.

The addition of RHA does not change the typical shape of the pore size distribution curves significantly. However, the fine pores increases with increasing the RHA content, especially after 3 days, although the total pore volume is a little higher than in the OPC paste (Table 3.8). The reduction in total porosity of the RHA modified sample over time can be attributed to the pozzolanic reaction of RHA and calcium hydroxide (Figure 3.14).

Table 3.8 The total porosity of samples with or without RHA and SF

	Age, days	The total porosity of samples, %						
		Control sample	The RHA modified samples			The SF modified samples		
			5% RHA	10% RHA	20% RHA	5% SF	10% SF	20% SF
w/b = 0.25	1	18.76	18.98	19.19	21.70	18.13	18.75	19.60
	3	14.61	15.89	15.68	15.04	12.69	11.37	12.14
	7	11.08	12.47	11.68	11.89	10.74	9.73	8.88
	28	10.61	10.87	10.50	8.95	7.52	6.23	4.53
	90	10.99	10.51	10.24	9.32	6.94	5.32	3.77
w/b = 0.40	1	34.34	34.20	32.96	33.09	31.91	32.66	32.60
	3	27.40	26.05	26.90	26.54	22.34	21.73	21.53
	7	22.96	21.69	21.19	20.93	16.04	16.04	15.90
	28	17.46	16.18	16.70	16.80	13.27	12.91	13.26
	90	14.65	13.41	15.41	16.67	12.64	11.88	8.53

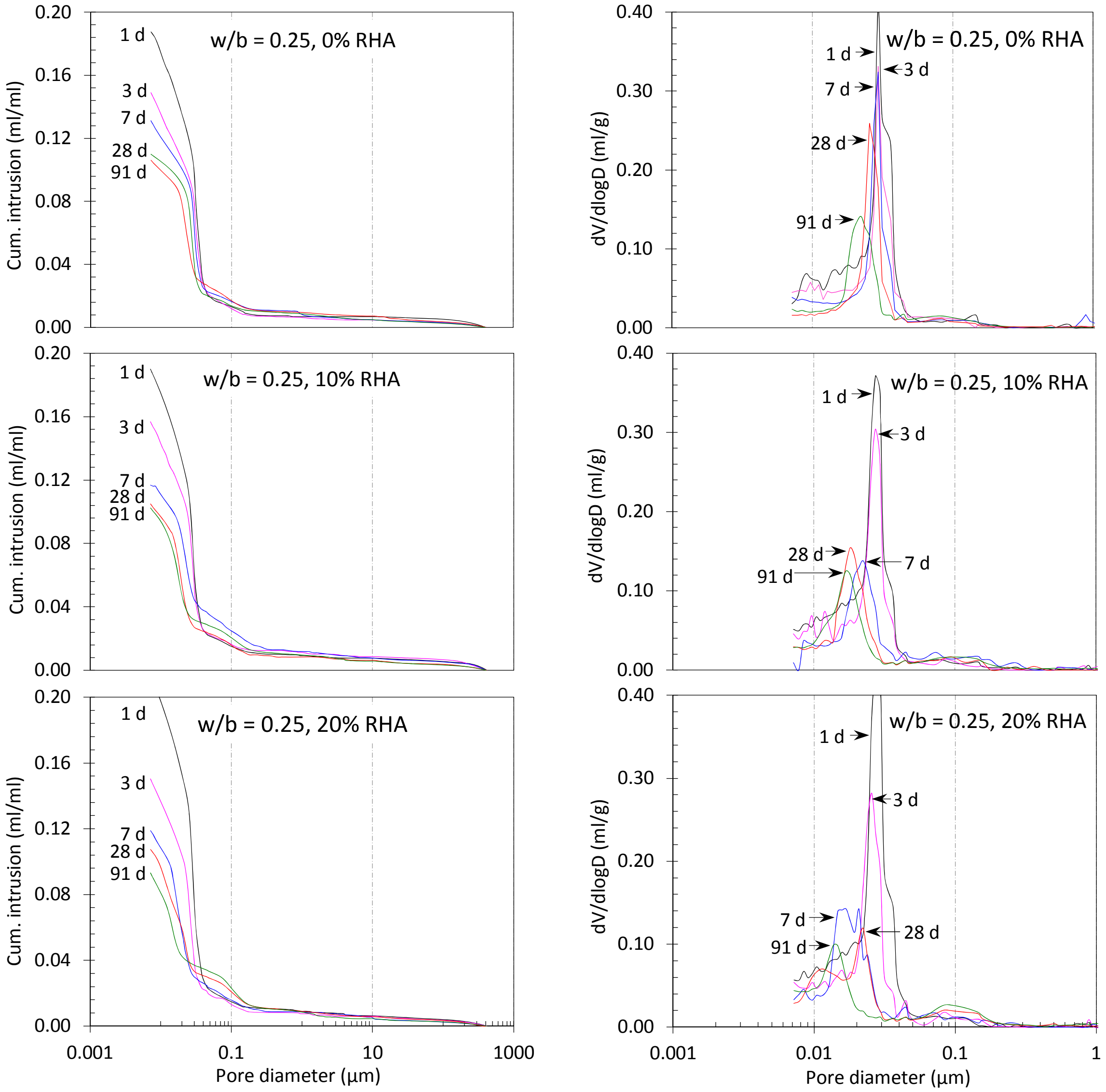

Figure 3.24 Pore size distribution of cement blended with 0, 5, 10 and 20% RHA at ages from 1 to 91 days, w/b = 0.25

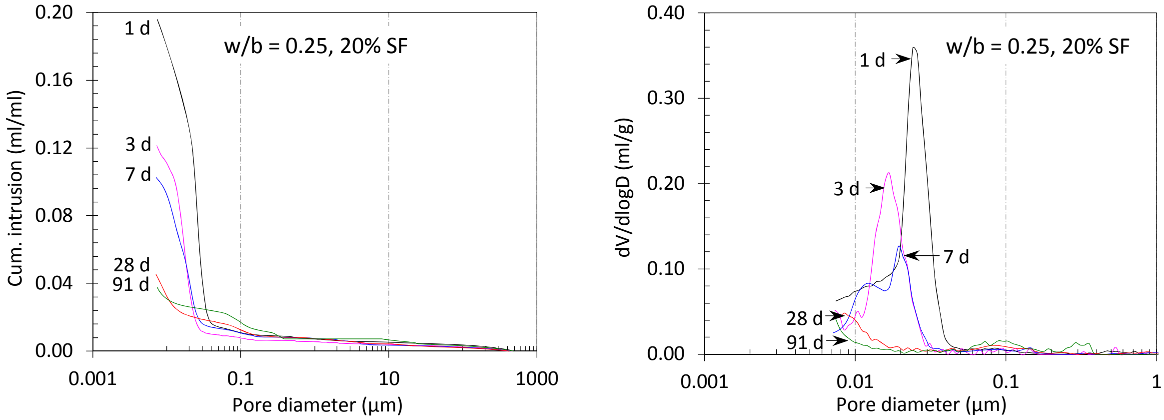

Figure 3.25 Pore size distribution of cement blended with 20% SF at ages from 1 to 91 days, w/b = 0.25

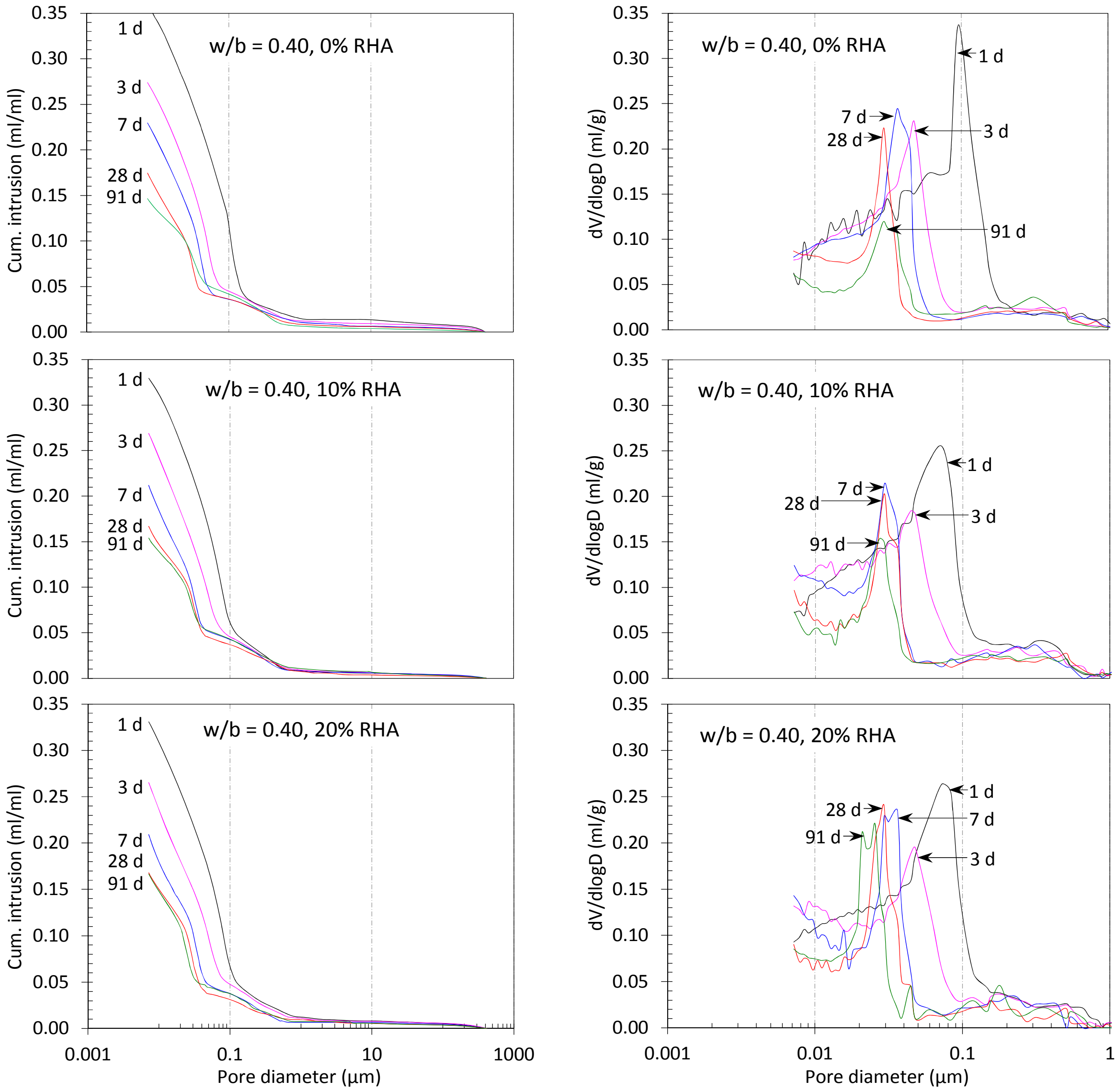

Figure 3.26 Pore size distribution of cement blended with 0, 5, 10 and 20% RHA at ages from 1 to 91 days, w/b = 0.40

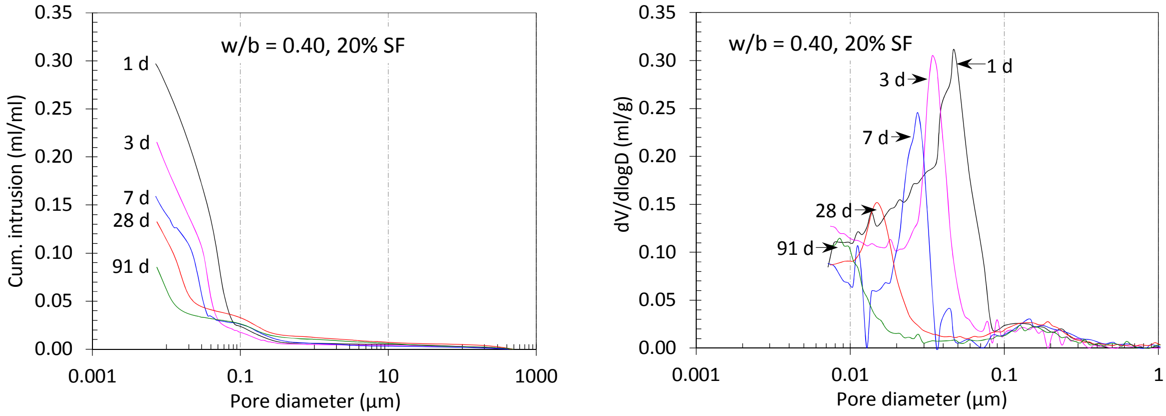

Figure 3.27 Pore size distribution of cement blended with 20% SF at ages from 1 to 91 days, w/b = 0.40

It is clear that the effect of SF on the pore refinement and the total porosity of cement paste is more significant than that of RHA. This is due to the fact that the particle size of SF is much smaller than that of RHA and the degree of reaction of SF is higher than that of RHA. These ultra-fine SF particles contribute to the densification of the paste and therefore, a decrease in the pore size. It should be noted that the pozzolanic reaction of SF occurs earlier and more CH is consumed compared to that of RHA (Figure 3.14). As a result, a higher amount of the CSH gel formed from the pozzolanic reaction between SF and CH will contribute to refine the pore structure, and hence reduce the volume of large pores.

Effect of the RHA fineness The effect of the RHA fineness on the pore size distribution and total porosity of cement paste was investigated in this section. Figure 3.28 and Figure 3.29 show the effect of the mean RHA particle size on the pore structure of pure Portland cement pastes and pastes of cement blended with RHA at the age of 28 days. In general, the porosity of the RHA modified paste decreases with an addition of the finer RHA. Compared to the control sample, the addition of RHA reduces the total porosity in cement paste, except samples containing RHA with a particle size of 15.5 µm. The finer RHA refines the pore structure of cement more significantly than the coarse one, especially at a high RHA content (Figure 3.29).

It is noticed that the effect of RHA on the pore refinement of cement paste does not increase significantly with the mean particle size of RHA less than 5.6 µm. Normally, the addition of a fine mineral admixture will refine the pore structure of cement paste. With the progress of the hydration process, the pore structure of cement paste is further refined by the formation of hydration products and pozzolanic reaction products of the mineral admixture. However, in the case of RHA, a reduction of its particle size possibly accompanies a collapse of the porous structure of RHA. This results in a reduction of the absorbed water in RHA. Therefore, the positive effect of RHA on cement hydration at later stages is limited and the degree of hydration of cement is lower. This leads to a reduction of the extra CSH gel generated from both cement hydration and the pozzolanic reaction of RHA to fill in the pore structure of cement paste. So, the refinement of the pore structure of cement paste may be not increased significantly.

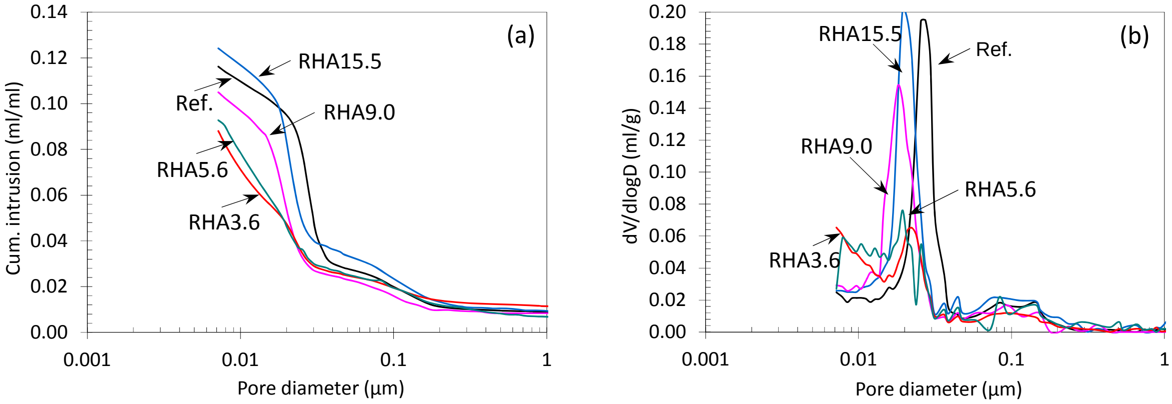

Figure 3.28 Pore structure of cement pastes blended with or without 10% RHA at the w/b ratio of 0.25 at 28 days, the numbers indicate the mean particle sizes of RHA

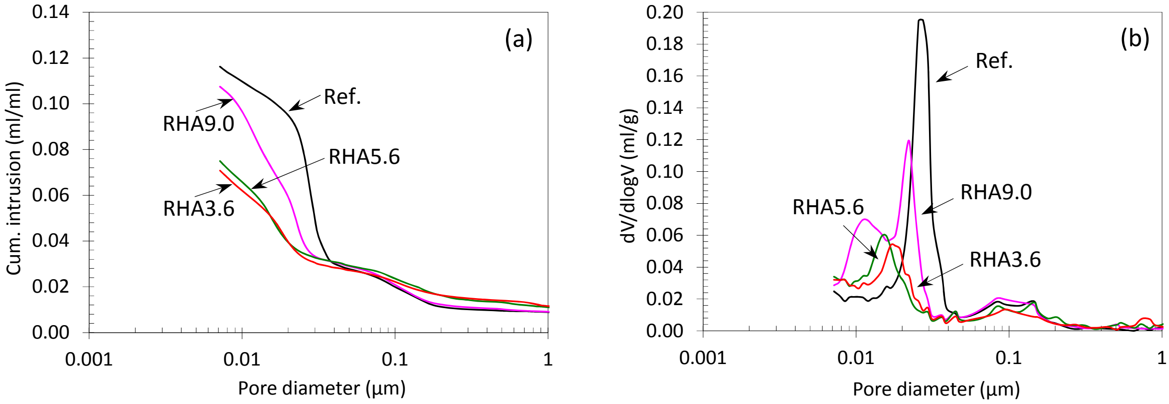

Figure 3.29 Pore structure of cement pastes blended with or without 20% RHA at the w/b ratio of 0.25 at 28 days, the numbers indicate the particle sizes of RHA

3.3.6 The anhydrous cement in cement paste blended with RHA

As discussed in Section 3.3.4, the addition of RHA results in a higher degree of hydration of cement paste at the later stage. However, the result from isothermal calorimetry only shows the effect of RHA on the hydration of cement paste in the short term, i.e. up until 7 days. To further explore the positive effect of RHA on the hydration of cement at later ages, the image analysis can be used to provide this information.

A typical BSE image of the RHA modified paste is shown in Figure 3.30. The colour of RHA particles appears as dark grey ones. The distribution of other phases, i.e. pores, anhydrous cement core, CSH gel, and CH, are also observed in this figure. As discussed previously in Section 3.2.2, only the anhydrous cement was considered by image analysis. From the threshold of grey level of own phases, the area of anhydrous cement cores were determined in order to calculate the degree of hydration of cement in the blended cement paste.

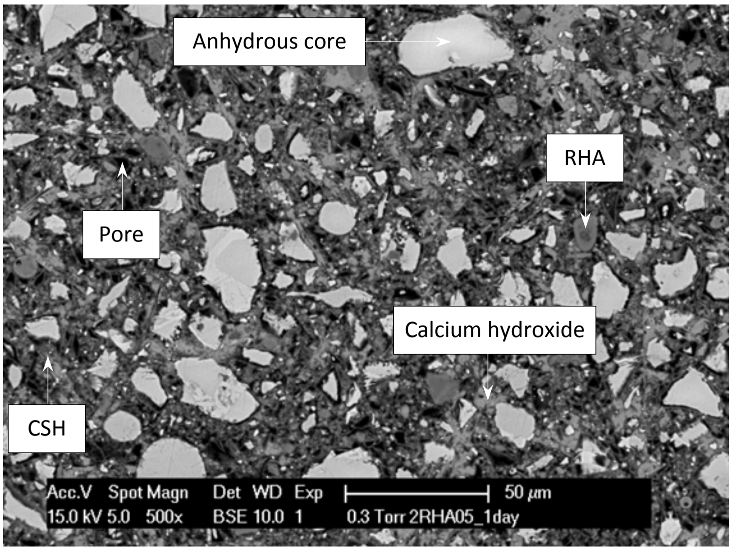

Figure 3.30 SEM image of cement paste contaning 5% RHA at w/b ratio of 0.40 and at 1 day

Figure 3.31 and Figure 3.32 show the percentage of anhydrous cement area and the degree of hydration of cement in the RHA modified samples at w/b ratios of 0.25 and 0.40. It can be seen that adding more RHA leads to a lower percentage of anhydrous cement area and hence a higher degree of hydration of cement. The effect of RHA on increasing the degree of hydration of cement is more significant for low w/b ratio samples. The differences reached in the period from 1 to 7 days hardly change any more at later ages.

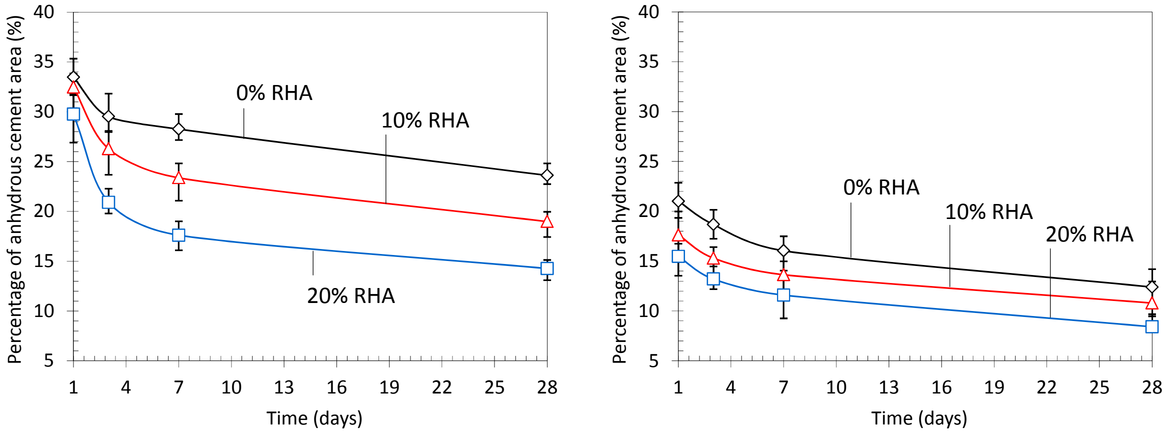

(a) w/b = 0.25 (b) w/b = 0.40

Figure 3.31 Percentage of anhydrous cement in the RHA-modified sample

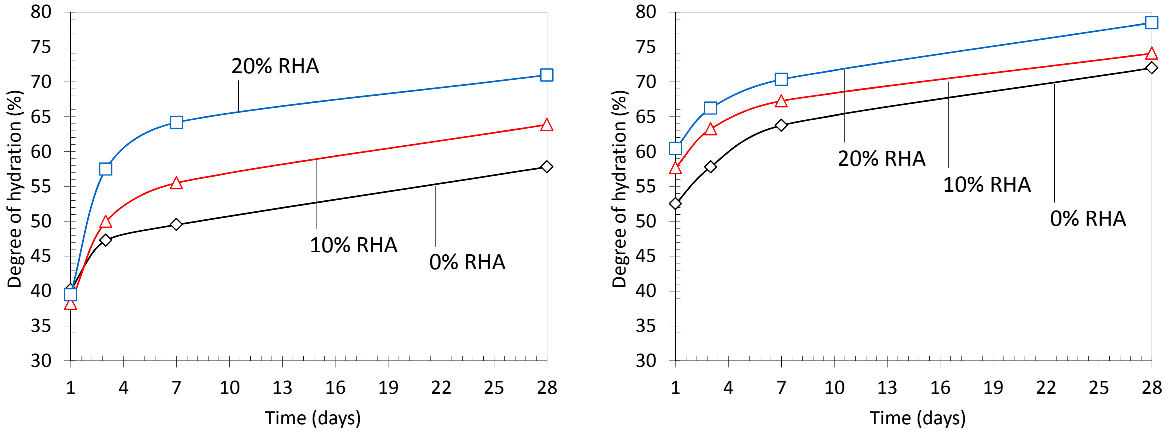

(a) w/b = 0.25 (b) w/b = 0.40

Figure 3.32 Degree of hydration of cement in the RHA-modified sample

Compared to the RHA modified pastes, the addition of SF also increases the degree of hydration of cement, but only before 1 day as observed in Figure 3.33 and Figure 3.34. It is noticed that at a high w/b ratio, although the degree of hydration of cement in both the RHA- and the SF modified pastes is similar at the age of 28 days, the degree of hydration of cement in the RHA modified paste is significant at later ages, i.e. beyond 7 days. At a low w/b ratio, the degree of hydration of cement in the RHA modified paste is much higher than that in the SF modified paste at 28 days, especially with 20% cement replacement. This effect may be caused by the absorbed water in the porous RHA particles as discussed in Section 3.3.4.

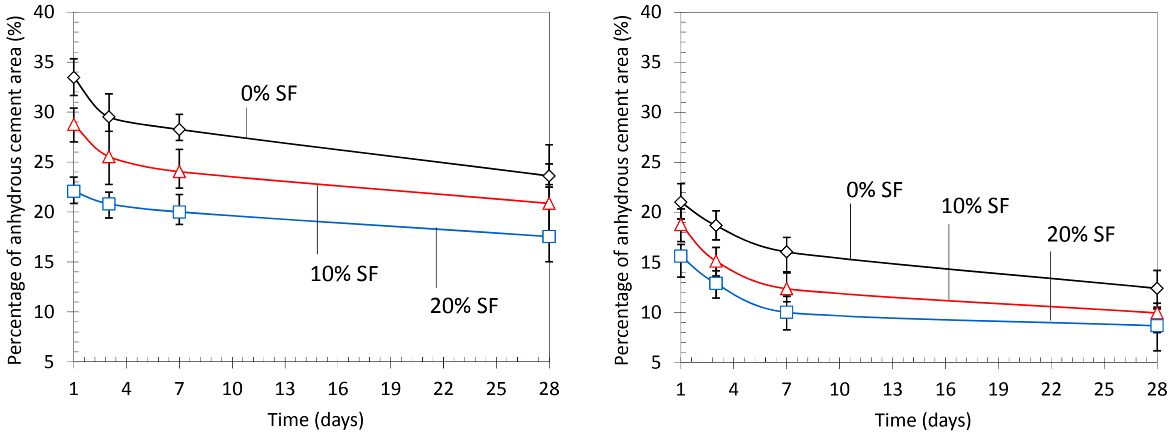

(a) w/b = 0.25 (b) w/b = 0.40

Figure 3.33 Percentage of anhydrous cement in the SF-modified sample

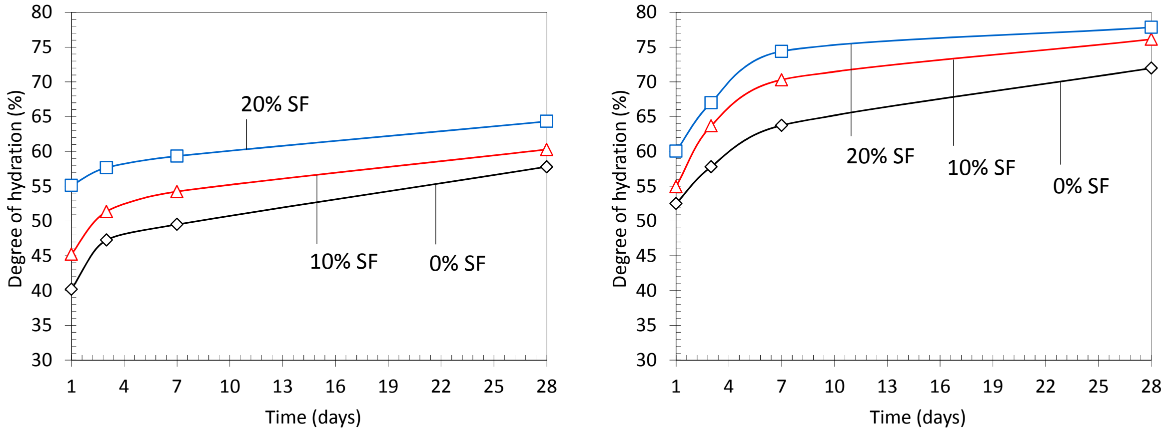

(a) w/b = 0.25 (b) w/b = 0.40

Figure 3.34 Degree of hydration of cement in the SF-modified sample

3.4 Concluding remarks

In this chapter, the effect of RHA on the hydration process and microstructure formation of cement paste was studied experimentally. Based on the experimental results, the following conclusions can be drawn as follows:

- RHA has approximately a same pozzolanic activity as SF if the mean particle size of RHA is smaller than 7.3 µm. The pozzolanic activity of RHA increases when RHA is finer but does not change significantly with the particle size of RHA smaller than 5.6 µm.
- The pozzolanic reaction of RHA occurs later than that of SF. This may be caused by a different particle structure between RHA and SF relating to the accessibility of ions from the surface of particles to the solution and vice versus.

- The addition of RHA delays and lowers the acceleration peak of the hydration of cement paste. The degree of hydration of cement in the RHA modified paste is lower than that in the SF modified paste at early ages or at a high w/b ratio. However, at a low w/b ratio, the degree of hydration of cement in the RHA modified paste is higher than that in the SF modified paste at later ages. This may be caused by the differences in the chemical composition, the particle structure, and the pozzolanic reactivity between RHA and SF.
- The apparent activation energy Ea of cement paste made with either RHA or SF depends on the degree of hydration, the w/b ratio, and the percentage of cement replacement.
- The addition of RHA decreases significantly the amount of calcium hydroxide in cement paste after 3 days.
- The addition of RHA refines the pore structure and reduces total porosity of cement paste. The effect of RHA on the pore structure refinement of cement paste is not significant when the mean particle size of RHA is smaller than 5.6 μm. This may be caused by the collapse of the porous structure of RHA particles.

Based on these results, it is hypothesized that one more mechanism controls the hydration of the RHA modified cement paste in which RHA seems act as an internal curing agent. The porous RHA particles considered as tiny water reservoirs distributes in the whole system. With progress of the cement hydration process, the relative humidity in cement paste drops and the water from these pores will be released and promotes the hydration of cement. This is more significant with the low w/b ratio cement paste.

Although the effect of RHA on the hydration and microstructure development of cement paste was investigated experimentally, the optimum amount of RHA used in cement paste has not been evaluated. This is a very important aspect in terms of designing cement paste and concrete. A very useful solution for this is using the numerical simulation, which is discussed in detail in Chapter 4.

From the experimental studies in this chapter, it is suggested that RHA can be used as a substitute for SF in the low w/b ratio cement paste. This gives rise to the idea that RHA can be used to produce UHPC in which the w/b ratio is very low. Besides, the addition of RHA which acts as an internal curing agent may mitigate the high autogenous shrinkage of UHPC. These aspects are investigated in Chapter 5.

4

Numerical Simulation of the Hydration and Microstructure Development of Cement Paste incorporating Rice Husk Ash

4.1 Introduction

4.1.1 General

The experimental results in Chapter 3 provided valuable clues to explore the mechanism and the effect of RHA on the hydration process and the development of microstructure of cement paste. In fact, however, it is unnecessary and sometimes impossible to investigate experimentally all the aspects because of the scatter of the chemical- and granular-composition of both the cement and the RHA. In this respect, numerical simulation is considered to be a very good tool to support the study of all relevant aspects.

The objective of this chapter is to simulate the effect of RHA on the hydration and microstructure development of cement paste. The simulation was validated by experimental results.

It is well known that simulating cement hydration and its microstructure by numerical modelling is a great challenge. In the past 20 years, several computer-based cement hydration models have been developed [Jennings and Johnson 1986; Bentz and Garboczi 1990; van Breugel 1991; Navi and Pignat 1996; Maekawa *et al.* 1999]. In principle, these models are based on two concepts. One is the spherical growth model [Jennings and Johnson 1986; van Breugel 1991; Navi and Pignat 1996]. The second is the pixel-based model [Bentz and Garboczi 1990]. In this study, simulation of the hydration and microstructure development of cement blend with RHA is proposed with a modified version of the HYMOSTRUC3D model [van Breugel 1991; Koenders 1997; Ye 2003].

4.1.2 HYMOSTRUC3D

HYMOSTRUC3D is designed to simulate the hydration and microstructure development of cement-based systems. It combines the fields of cement chemistry, physics, and stereology. In this model the particle size of the cement, the water-to-cement ratio, the initial curing temperature and the chemical composition of cement are all considered.

In the original HYMOSTRUC model [van Breugel 1991], the hydration of Portland cement pastes were considered. The cement particles are modelled as digitized spheres randomly distributed in a three-dimensional body and the hydrating cement grains are simulated as growing spheres. As cement hydrates, the cement grains gradually dissolve and a porous shell of hydration products is formed around the grain. This results in an outward growth, or "expansion", of the particles. The hydrates around the cement grains firstly cause the formation of small isolated clusters. Big clusters are formed when small cement particles become embedded in the outer shell of other particles, which promotes the outward growth of these particles (Figure 4.1). As hydration progresses, the growing particles become more and more connected and the material changes from the state of a suspension to the state of a porous solid.

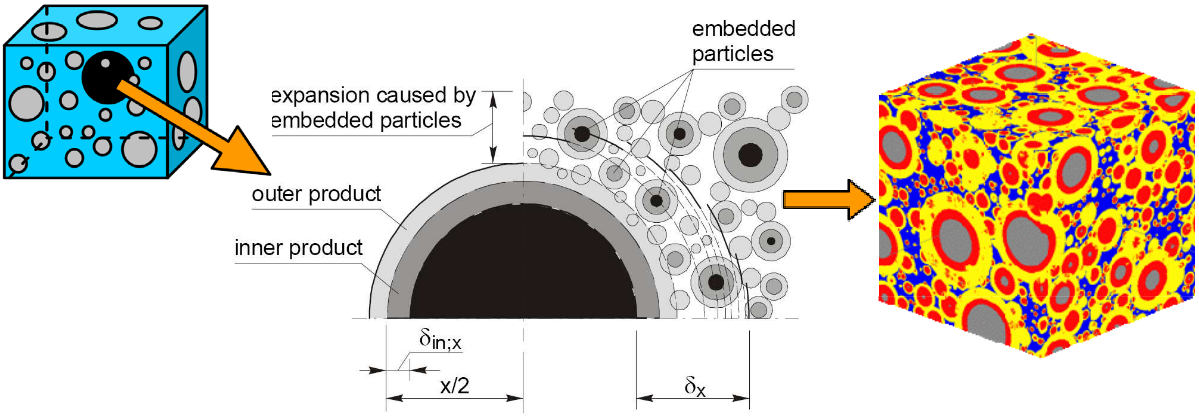

Figure 4.1 Schematic view of HYMOSTRUC3D concept: Growth mechanism of individual particles resulting in a 3D-microstructure [van Breugel 1991]

The rate of penetration of the reaction front in an individual cement particle x at time t_j is computed with a basic rate formula (written in a reduced form):

$$\frac{\Delta\delta_{in;x,j+1}}{\Delta t_{j+1}} = K_0(.)\times\Omega_1(.)\times\Omega_2(.)\times\Omega_3(.)\times F_1(.)\times\left[F_2(.)\times\left(\frac{\delta_{tr}(.)}{\delta_{x,j}}\right)^{\beta_1}\right]^{\lambda} \qquad (4.1)$$

with $\Delta\delta_{in;x,j+1}$ the increase of the penetration depth in time step Δt_{j+1}; K_0(.) the *basic rate factor* (µm/h); δ_{tr}(.) the *transition thickness* (µm), being the total thickness of the product layer $\delta_{x,j}$ at which the reaction for the particle in view changes from a *boundary reaction* ($\lambda = 0$) into a diffusion controlled reaction ($\lambda = 1$). The thickness, at which this change will take place, depends on the type of cement and has been determined by evaluating hydration data obtained with different Portland cements. Three reduction coefficients, Ω_1, Ω_2 and Ω_3, represent the effect of water withdrawal of particles in the shell of a central cement particle, the effect of decrease of available water while emptying of the capillary pores, and the effect of water shortage of the overall system, respectively. β_1 is an empirical constant. The equation that describes the reaction kinetics is called the "Basic Rate Equation". In the basic rate formula (4.1) the effect of the particle size distribution, the w/c ratio and the temperature are now allowed for explicitly. The model parameters $K_0(.)$, $\delta_{tr}(.)$ are the function of chemical composition of the cement. For a full description of the original HYMOSTRUC model, see [van Breugel 1991].

4.1.3 Extensions and modifications of HYMOSTRUC3D

Because the pozzolanic reaction of RHA changes the amount of hydration products of cement, the simulation of the hydration and microstructure development of cement blended with RHA is extended and modified based on the original HYMOSTRUC3D. The chemical reactions and the degree of hydration of four main cement phases, i.e. C_3S, C_2S, C_3A, C_4AF, will be considered explicitly. The model also considers the pozzolanic reaction and the degree of the RHA reaction. The overall scheme of this simulation is shown in Figure 4.2 and will be discussed in details in this chapter.

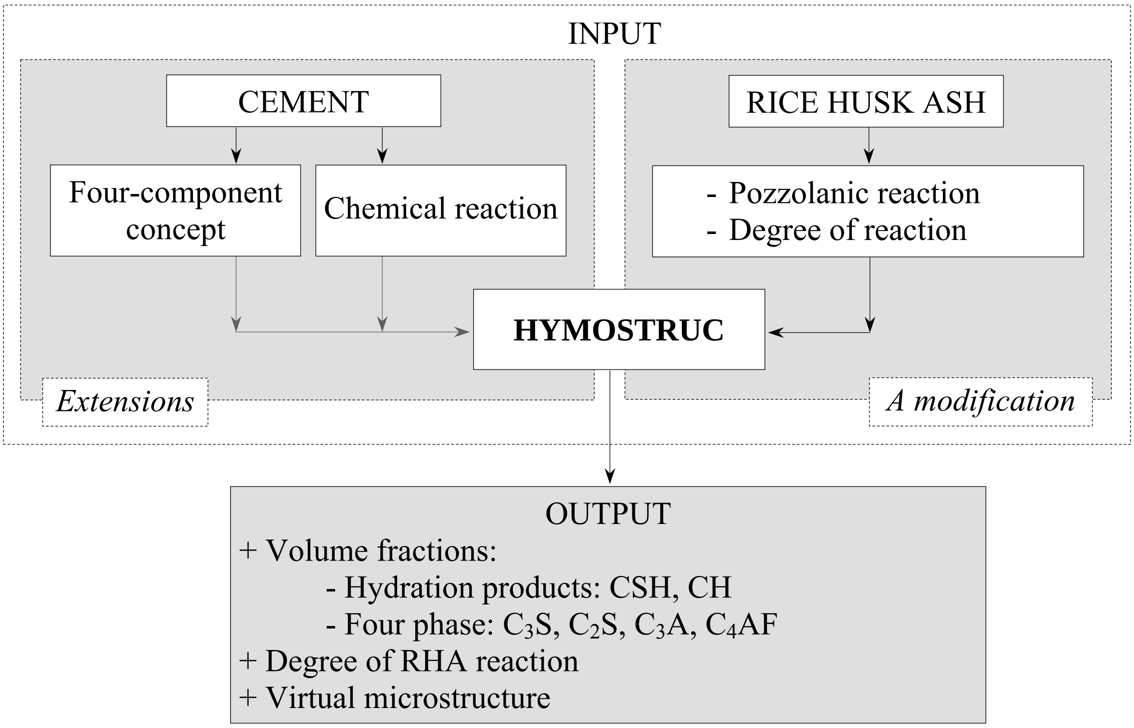

Figure 4.2 Overall scheme of simulation of the hydration process and microstructure development of cement blended with RHA

4.2 Simulation of the hydration and microstructure development of Portland cement systems

The extensions for the simulation of the hydration process and microstructure development of Portland cement will be developed based on the original HYMOSTRUC3D model. These extensions include two main parts:

1) Refinement of the hydration module for Portland cement: The chemical reactions and the degree of hydration of four cement phases, i.e. C_3S, C_2S, C_3A, C_4AF, are taken into account explicitly. This is the so-called four-phase concept. The volume of hydration products of cement, i.e. CSH and CH, is calculated.
2) The microstructure of Portland cement: The virtual microstructure of Portland cement is built up with unhydrated four-phase cement (C_3S, C_2S, C_3A, C_4AF), CSH, CH. The CH phase is assumed to be randomly located as spheres in the voids of the system. The CSH phase is supposed to grow on the surface of cement particles.

4.2.1 The chemical reactions of Portland cement hydration

The volumes of four main cement phases, i.e. C_3S, C_2S, C_3A, C_4AF, and of hydration products over time can be calculated by the chemical equilibrium of cement reactions. In this model the chemical reactions were used as given in equations (4.2)-(4.9) [Bentz *et al.* 1994]. The numbers below each reaction equation indicate the volume units of each phase required to balance that particular chemical reaction. Knowing the molar volumes (Table 4.1) and the reaction stoichiometries, the volume stoichiometries can be calculated for each reaction.

The summary of chemical reactions of cement hydration was used in this model as listed below:

$$\begin{array}{ccccccc} C_3S & + & 5.3H & \rightarrow & C_{1.7}SH_4 & + & 1.3CH \\ 1 & & 1.34 & & 1.521 & & 0.61 \end{array} \tag{4.2}$$

$$\begin{array}{ccccccc} C_2S & + & 4.3H & \rightarrow & C_{1.7}SH_4 & + & 0.3CH \\ 1 & & 1.49 & & 2.077 & & 0.191 \end{array} \tag{4.3}$$

$$\begin{array}{ccccccc} C_3A & + & 3C\bar{S}H_2 & + & 26H & \rightarrow & C_6A\bar{S}_3H_{32} \\ 1 & & 0.833 & & 5.253 & & 8.249 \end{array} \tag{4.4}$$

$$\begin{array}{ccccccc} 2C_3A & + & C_6A\bar{S}_3H_{32} & + & 4H & \rightarrow & 3C_4A\bar{S}H_{12} \\ 1 & & 4.124 & & 0.404 & & 5.269 \end{array} \tag{4.5}$$

$$\begin{array}{ccccccccccc} C_4AF & + & 3C\bar{S}H_2 & + & 30H & \rightarrow & C_6A\bar{S}_3H_{32} & + & CH & + & FH_3 \\ 1 & & 1.739 & & 4.22 & & 5.742 & & 0.259 & & 0.545 \end{array} \tag{4.6}$$

$$\begin{array}{ccccccccccc} 2C_4AF & + & C_6A\bar{S}_3H_{32} & + & 12H & \rightarrow & 3C_4A\bar{S}H_{12} & + & 2CH & + & 2FH_3 \\ 1 & & 2.871 & & 0.844 & & 5.742 & & 0.259 & & 0.545 \end{array} \tag{4.7}$$

$$\begin{array}{ccccc} C_3A & + & 6H & \rightarrow & C_3AH_6 \\ 1 & & 1.21 & & 1.69 \end{array} \tag{4.8}$$

$$\begin{array}{ccccccccc} C_4AF & + & 10H & \rightarrow & C_3AH_6 & + & CH & + & FH_3 \\ 1 & & 1.41 & & 1.17 & & 0.259 & & 0.545 \end{array} \tag{4.9}$$

Table 4.1 Physical properties of cementitious compounds [Bentz *et al.* 1994]

Compound Name	Compound formula	Molar volume (cm^3/mol)
Tricalcium silicate	C_3S	71
Dicalcium silicate	C_2S	52
Tricalcium aluminate	C_3A	89.1
Tetracalcium aluminoferrite	C_4AF	128
Gypsum	$C\bar{S}H_2$	74.2
Calcium silicate hydrate	$C_{1.7}SH_4$	108
Calcium hydroxide	CH	33.1
Ettringite	$C_6A\bar{S}_3H_{32}$	735
Monosulfoaluminate	$C_4A\bar{S}H_{12}$	313
Hydrogarnet	C_3AH_6	150
Iron hydroxide	FH_3	69.8
Water	H	18

in which formulae the standard cement chemistry abbreviations are used:
$C = CaO$, $S = SiO_2$, $A = Al_2O_3$, $F = Fe_2O_3$, $\bar{S} = SO_3$, and $H = H_2O$.

The reduced forms of reactions (4.4) and (4.5), (4.6) and (4.7) can be presented as reactions (4.10) and (4.11), respectively:

$$\begin{array}{ccccccc} C_3A & + & C\bar{S}H_2 & + & 10H & \rightarrow & C_4A\bar{S}H_{12} \\ 1 & & 0.833 & & 2.02 & & 3.513 \end{array} \tag{4.10}$$

$$\begin{array}{ccccccccccc} C_4AF & + & C\bar{S}H_2 & + & 14H & \rightarrow & C_4A\bar{S}H_{12} & + & CH & + & FH_3 \\ 1 & & 0.58 & & 1.97 & & 2.445 & & 0.259 & & 0.545 \end{array} \tag{4.11}$$

In these reactions, the following aspects were accounted for:

1) The time (t_{gyp}), at which gypsum is completely consumed by C_3A and C_4AF, can be determined with eq. (4.12).

$$[(V_{C3A})_0 \times \alpha_{C3A} \times 0.833 + (V_{C4AF})_0 \times \alpha_{C4AF} \times 0.58] \times (t_{gyp}) = (V_{C\bar{S}H2})_0 \tag{4.12}$$

in which $(V_{C3A})_0$, $(V_{C4AF})_0$, $(V_{C\bar{S}H2})_0$ are initial volumes of C_3A, C_4AF, and $C\bar{S}H_2$

2) Total volume of hydration products of cement

In the presence of gypsum, reactions (4.10) and (4.11) dominate over reactions (4.8) and (4.9) [Papadakis *et al.* 1991; Bentz *et al.* 1994]. So, reactions (4.8) and (4.9) take place only after all the gypsum has been consumed.

Before all the gypsum is consumed ($t < (t_{gyp})$), the total volume of hydration products of cement is calculated by the equation (4.13):

$$\begin{aligned} V_{total1} = {} & \alpha_{C3S} \times (V_{C3S})_0 \times (1.521+0.61) + \alpha_{C2S} \times (V_{C2S})_0 \times (2.077+0.191) \\ & + \alpha_{C3A}(V_{C3A})_0 \times (3.513) + \alpha_{C4AF} \times (V_{C4AF})_0 \times (2.445+0.259+0.545) \end{aligned} \tag{4.13}$$

After that ($t \geq (t_{gyp})$), the total volume of hydration products of cement is calculated by the equation (4.14):

$$\begin{aligned} V_{total2} = {} & \alpha_{C3S} \times (V_{C3S})_0 \times (1.521+0.61) + \alpha_{C2S} \times (V_{C2S})_0 \times (2.077+0.191) \\ & + \alpha_{C3A} \times (V_{C3A})_0 \times (1.69) + \alpha_{C4AF} \times (V_{C4AF})_0 \times (1.17+0.259+0.545) \end{aligned} \tag{4.14}$$

3) The volume of the CH phase

From the chemical reactions of cement, it can be seen that the CH phase is produced from the hydration of C_3S, C_2S, and C_4AF. Therefore, the volume of CH can be calculated by equation (4.15):

$$V_{CH} = \alpha_{C3S} \times (V_{C3S})_0 \times (0.61) + \alpha_{C2S} \times (V_{C2S})_0 \times (0.191) + \alpha_{C4AF} \times (V_{C4AF})_0 \times (0.259) \tag{4.15}$$

Therefore, the volume fraction of CH is calculated by equations (4.13) to (4.15):

$$\begin{aligned} &\text{If } (t < (t_{gyp})): && V_{CH} / V_{total1} \\ &\text{Else } (t \geq (t_{gyp})): && V_{CH} / V_{total2} \end{aligned} \tag{4.16}$$

4.2.2 Degree of hydration of four cement phases

The volumes of cement phases and of hydration products of cement with time depend on both the chemical reactions and the degree of hydration of cement phases. In this section, the degree of hydration of cement phases is simulated with a modified version of the HYMOSTRUC3D model.

Hydration curves of individual phases collected from different references are shown in Figure 4.3. From these curves, the rate constant K_0 of the individual phases was determined from the experimental curve as shown in Figure 4.4. It was assumed that the change from a phase boundary to a diffusion controlled reaction occurs at an overall degree of hydration $\alpha \approx 0.2$, cited by [van Breugel 1991]. At this degree of hydration, the transition thickness δ_{tr} is calculated as the thickness $\delta_{ou;x}$ of the outer shell, eq. (4.17) and the penetration depth $\delta_{in;x}$, eq. (4.19).

$$\delta_{ou;x} = R_{ou;x} - \left(\frac{x}{2}\right) \tag{4.17}$$

where $R_{ou;x}$ is the outer radius of the growing central particle, eq. (4.18) with the ratio between the volume of the gel and that of the reactant $\nu = 2.2$ and $\alpha = 0.2$; x is the diameter of the cement particle.

For $R_{ou;x}$ it holds:

$$R_{ou;x} = \left(\frac{x}{2}\right)\times\left[1+\left(\nu-1\right)\times\alpha_x\right]^{\frac{1}{3}} \tag{4.18}$$

and for $\delta_{in;x}$:

$$\delta_{in;x} = \left(\frac{x}{2}\right)\times\left[1-\left(1-\alpha_x\right)^{\frac{1}{3}}\right] \tag{4.19}$$

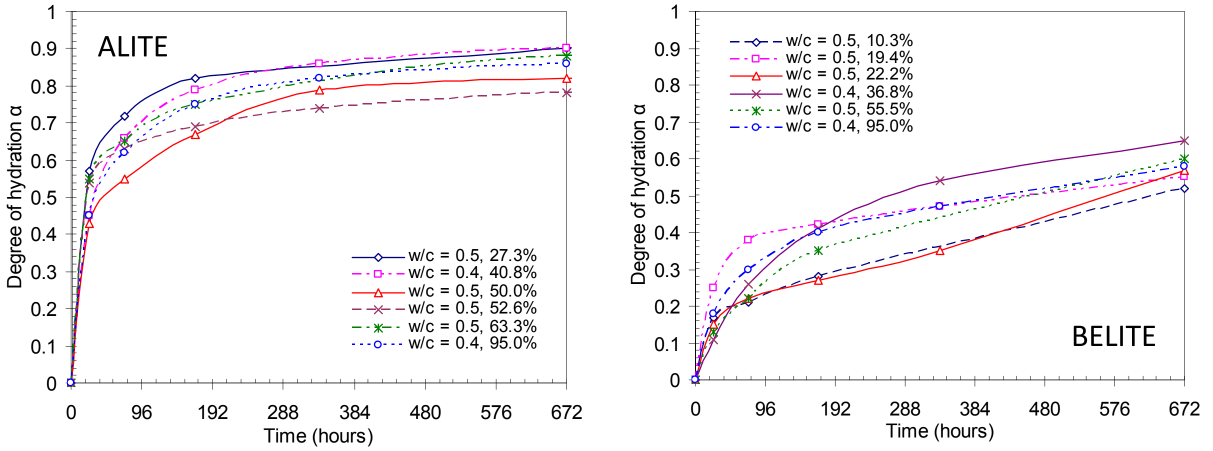

(a) Alite (b) Belite

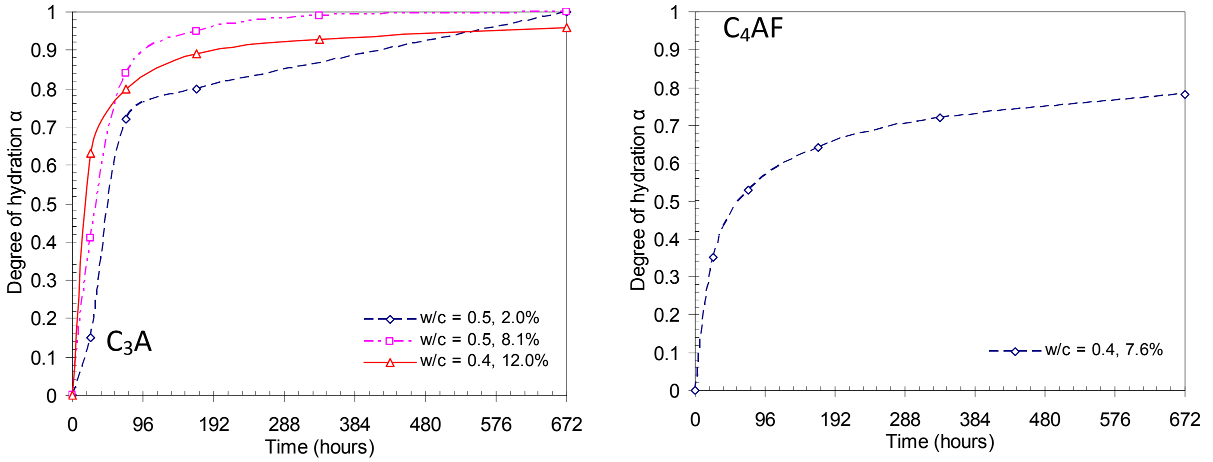

(c) C_3A (d) C_4AF

Figure 4.3 Hydration curves of individual phases in cement paste, collected from different references [Papadakis *et al.* 1991; van Breugel 1991; Escalante-García and Sharp 1998; Maruyama *et al.* 2007; Matsushita *et al.* 2007]

The obtained values of the two independent model parameters K_0 and δ_{tr} of four cement phases are shown in Table 4.2. Based on these values of the rate constant K_0 and the transition thickness δ_{tr}, the empirical constants β_1 and β_2 are determined by using the HYMOSTRUC3D model to fit with experimental hydration curves. The obtained value β_1 is 4 for C_3S, C_2S C_4AF

phases and 8 for the C_3A phase. The other empirical constant β_2 is 2 for all phases. It should be noted that the collected data mainly focus on the hydration of four cement phases in cement pastes with w/c ratios ranging from 0.4 to 0.5 and with a similar particle size distribution. Effects of the w/c ratio and the particle size distribution on hydration of each cement phase are followed the principles of the original HYMOSTRUC3D model. The correlation of K_0 with the content of each cement phase is depicted in Figure 4.5. The correlation of δ_{tr} with the K_0 of cement phases is given in Figure 4.6.

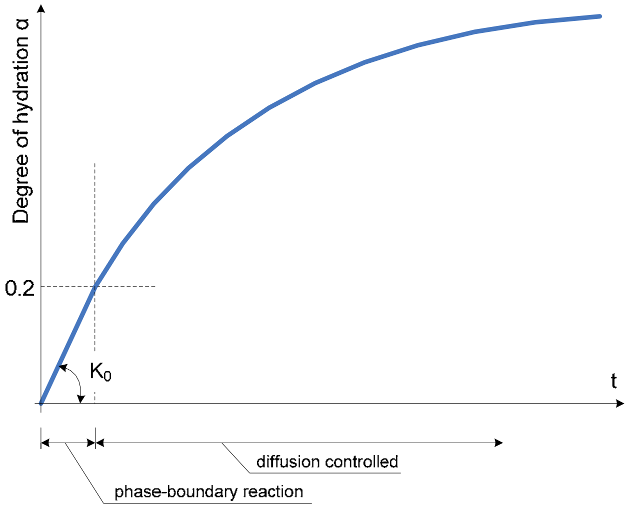

Figure 4.4 Determination of K_0 from an experimental hydration curve

Table 4.2 Two model parameters determined for different cement phases

No.	w/c	%	K0	δ_{tr}	No.	w/c	%	K0	δ_{tr}
		C_3S					C_2S		
1	0.50	0.273	0.078	1.07	7	0.50	0.103	0.0052	1.07
2	0.50	0.408	0.075	1.19	8	0.50	0.208	0.0050	1.31
3	0.40	0.500	0.073	1.31	9	0.40	0.368	0.0047	1.19
4	0.50	0.526	0.073	1.31	10	0.50	0.555	0.0043	1.46
5	0.40	0.633	0.071	1.46	11	0.40	0.950	0.0060	2.10
6	0.40	0.950	0.065	2.10					
		C_3A					C_4AF		
12	0.50	0.081	0.155	1.07	15	0.40	0.076	0.020	1.19
13	0.50	0.020	0.064	1.19					
14	0.40	0.120	0.181	1.19					

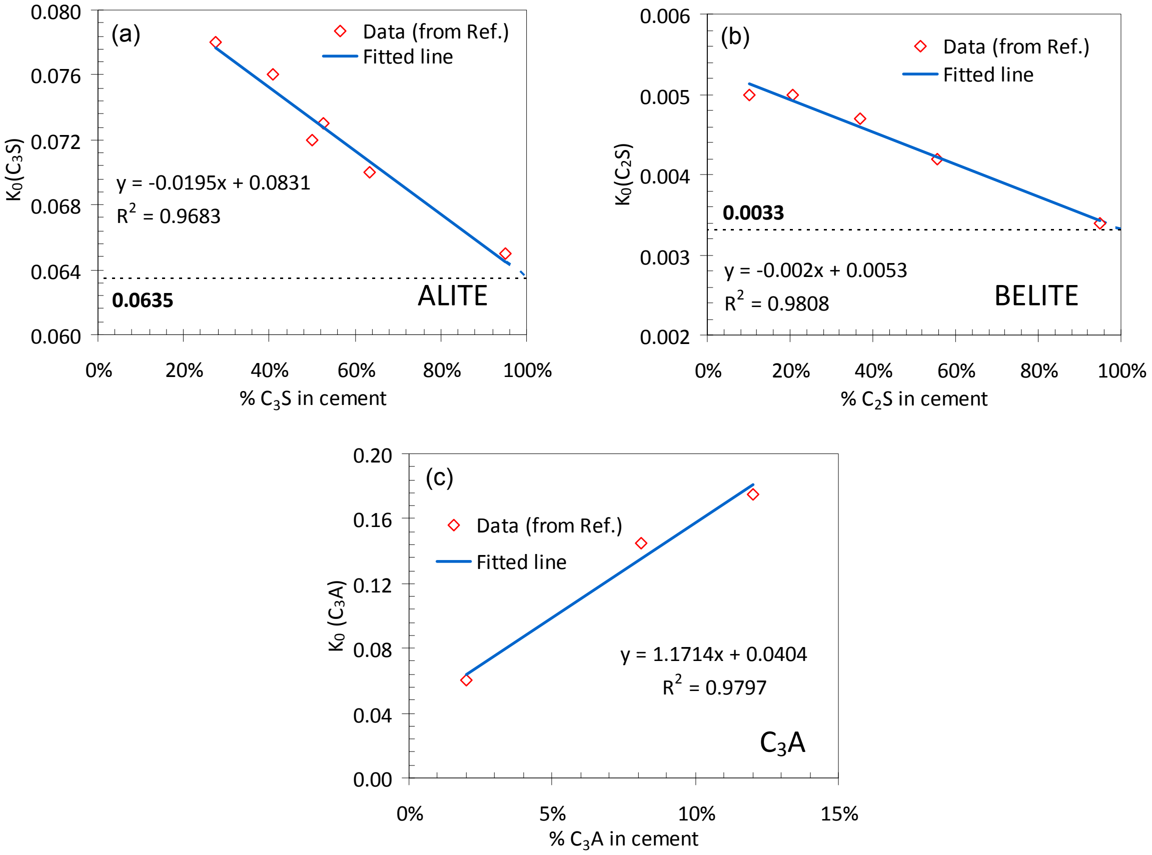

Figure 4.5 The correlation of K_0 with the content of cement phases, (a) C_3S, (b) C_2S, (c) C_3A

From the results in Figure 4.5 and Figure 4.6, the direct correlation of the basic rate factor K_0 with the amount of each phase, and the transition thickness δ_{tr} with K_0 can be determined (Table 4.3, eq. (4.20) to (4.23)).

Table 4.3 Two model parameters K_0 and δ_{tr} of different cement phases

No.	Phase	K_0	δ_{tr}	Equation
1	C_3S	$0.0635 + 0.0195 \times (1 - \%C_3S)$	$2.1199 + 1.4707 \times (1 - \%C_3S)$	(4.20)
2	C_2S	$0.0033 + 0.0020 \times (1 - \%C_2S)$	$2.0730 + 1.1528 \times (1 - \%C_2S)$	(4.21)
3	C_3A	$1.2118 - 1.1714 \times (1 - \%C_3A)$	$2.3280 + 1.2758 \times (1 - \%C_3A)$	(4.22)
4	C_4AF	0.02	1.19	(4.23)

The fact that the K_0 and δ_{tr} values of individual phase exhibit a dependency on the amount of that particular phase in the cement demonstrates that the reaction is affected by reaction with other phases in the cement. The values of K_0 and δ_{tr} for pure cement phases can be determined by the extrapolation if cement is considered to contain only one phase, or 100%. For example, the values of K_0 of the pure C_3S, C_2S and C_3A phases are 0.0635, 0.0033 and 1.2118, respectively (Figure 4.5 and Table 4.3). The values of δ_{tr} of these corresponding phases are 2.1199, 2.0730, 2.3280, respectively (Figure 4.6 and Table 4.3).

It was found that the hydration of cement can be determined from the hydration of C_3S and C_2S phases relative to their mass contributions according to:

$$K_{0(cement)} = (\%C_3S) \times K_{0(C3S)} + (\%C_2S) \times K_{0(C2S)} \tag{4.24}$$

$$\delta_{tr(cement)} = (\%C_3S) \times \delta_{tr(C3S)} + (\%C_2S) \times \delta_{tr(C2S)} \tag{4.25}$$

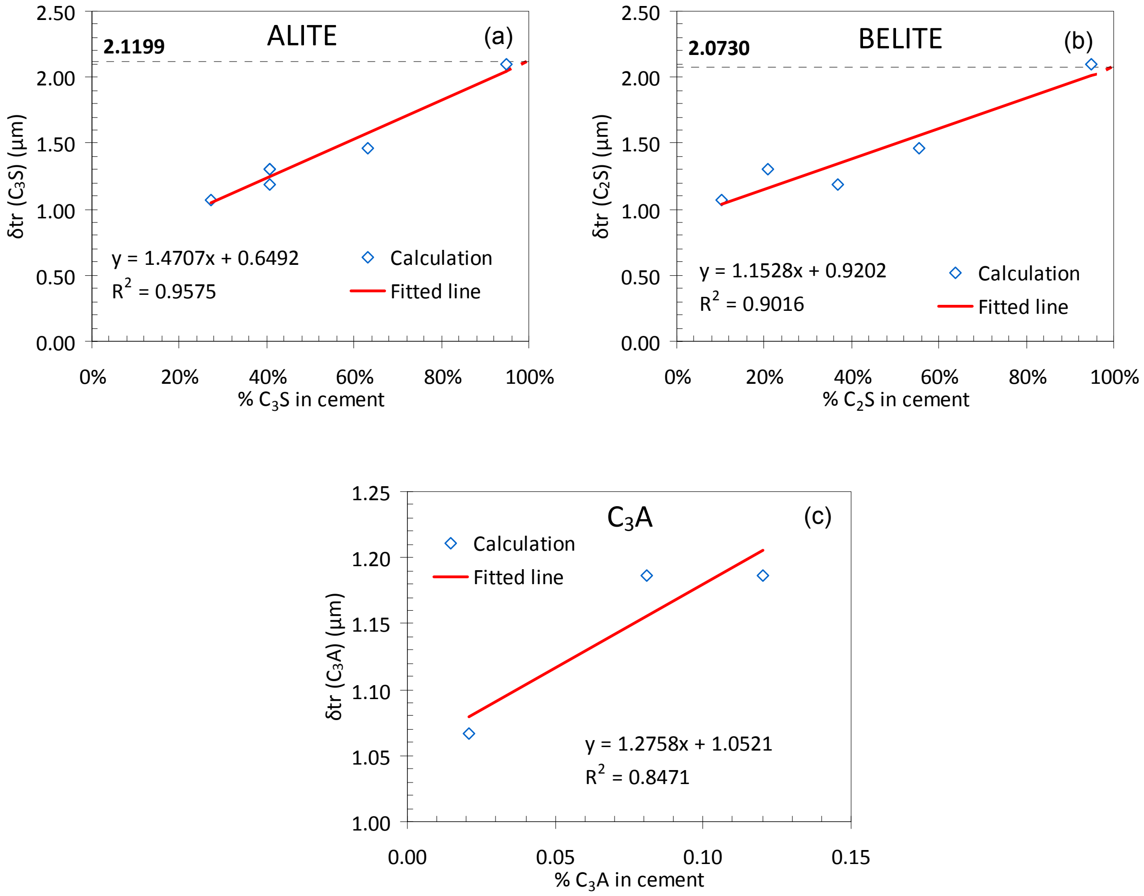

Figure 4.6 The correlation of δ_{tr} with the content of cement phases, (a) C_3S, (b) C_2S, (c) C_3A

4.2.3 Virtual microstructure of cement hydration

In microstructural terms, cement paste is an extremely complex system of solid phases, pores, and water, with a high degree of heterogeneity. The solid phases can be understood as a mixture of unhydrated cement and hydration products. The hydration products of cement are normally separated into two main phases, CH and CSH. Therefore, the virtual microstructure of cement paste is considered as a system of four phases such as CSH and CH phases, unhydrated cement and pores whether or not filled with water. From this consideration, the virtual microstructure of cement hydration with four-phase concept was built up with some assumptions:

- Each cement grain contains four phases and their proportions are kept constant with time of hydration. The degree of hydration of cement is calculated as the average of the four phases C_3S, C_2S, C_3A, and C_4AF (by weight). The growth of cement particles follows the mechanism used in the HYMOSTRUC3D model, in which the cement particles grow concentric-wise due to the formation of reaction products.
- The CH phase is assumed as spherical particles which are randomly distributed in the pore space of the system.

  The volume of the CH phase is calculated from equation (4.15).

  The number of CH particles is assumed to be 20% of the total number of cement particles at the beginning of hydration as suggested by Jennings and Parrott [1986b]. After 1 day of hydration, there is one CH grain for 12.5 grains of C_3S and $\alpha(t) = 1$ there is one CH grain for five grains of C_3S [1986a]. From this data, the number of CH particle generated with time can be calculated following the equation (4.26), as suggested by Navi and Pignat [1996]:

  $$n(t) = n_m (1 - e^{-at}) \tag{4.26}$$

  where n_m is the maximum number of CH grains for complete hydration, a is a constant, and e is equal to 2.718.
- When one CH particle is fully embedded in hydration products of cement, its position and volume is re-distributed randomly in pore spaces of system.

The virtual microstructure of cement paste is generated by a random placement of the cement particles containing four hydrating phases. Two main hydration products are formed during hydration, CSH formed around cement particles and CH formed in the pore spaces (Figure 4.7).

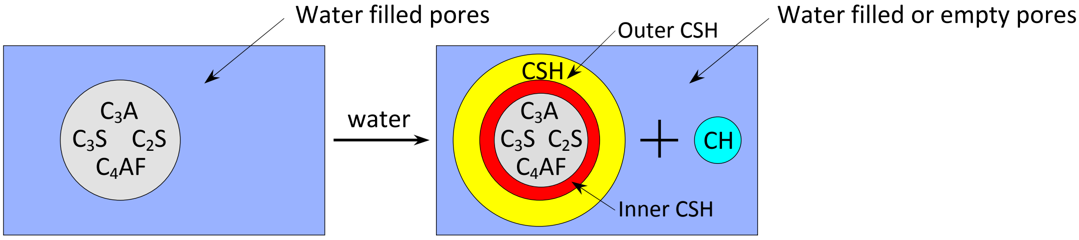

Figure 4.7 Portland cement hydration with the four-phase concept

Because the CH phase is considered independently and separated from the outer shell, the volume of hydration product growing on the surface of cement particles ($\delta_{x,j}$), i.e. CSH, is reduced in comparison with the original HYMOSTRUC3D model, a thinner diffusion layer results in an increase of the rate of penetration of the reaction front in the cement grain. However, that the CH phases are separated and located in the pore spaces constrains the transfer of ions in the solution. In this simulation, this effect can be presented by increasing the density of the CSH layer and a repair factor C_{CH} in the basic rate equation is accounted for this effect (see eq. (4.27)).

$$\frac{\Delta\delta_{in;x,j+1}}{\Delta t_{j+1}}=K_0(.)\times\Omega_1(.)\times\Omega_2(.)\times\Omega_3(.)\times F_1(.)\times\left[F_2(.)\times\left(\frac{\delta_{tr}(.)}{\delta_{x,j}}\right)^{\beta_1}\right]^{\lambda}\times C_{CH} \tag{4.27}$$

The flow chart of the hydration and virtual microstructure development of Portland cement pasteis shown in Figure 4.8.

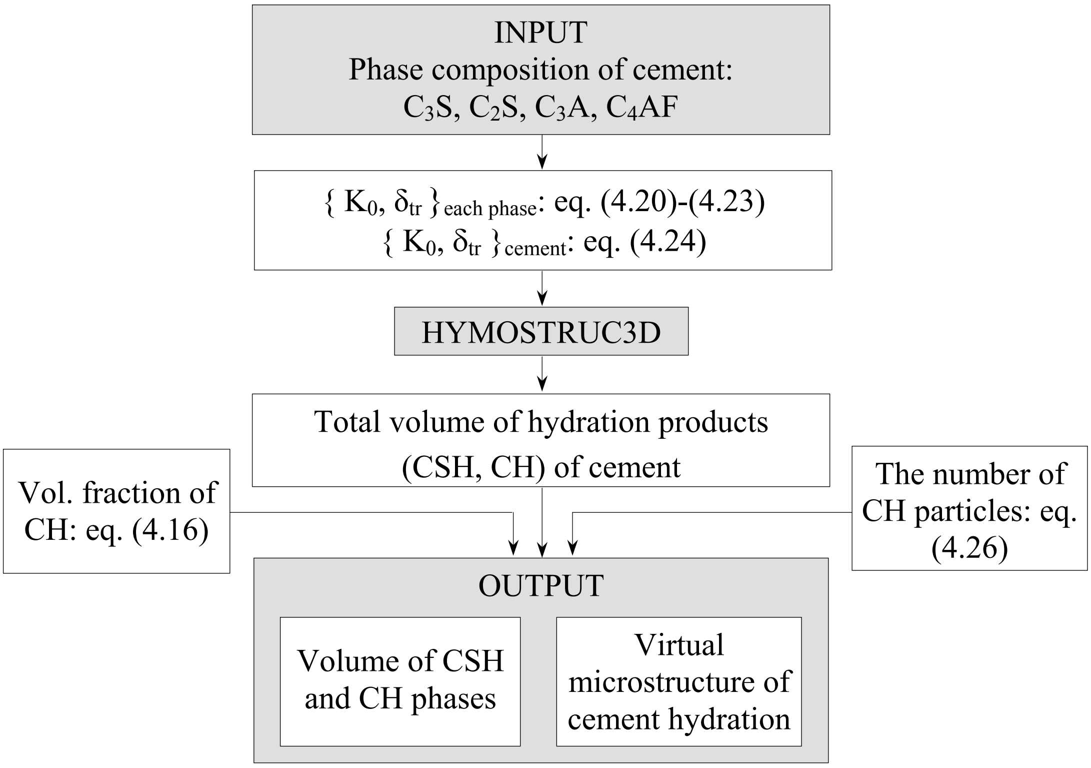

Figure 4.8 Flow chart of the hydration and microstructure development of Portland cement with four- phase concept

4.2.4 Simulation results and validation

In this section, the simulation of Portland cement with four-phase concept is discussed and validated by the experimental results. Table 4.4 shows the properties of the cement used in the simulation. The values of model parameters of K_0 and δ_{tr} of each phase and cement were calculated according to equations (4.20) to (4.25) and presented in Table 4.5.

Degree of hydration of the four cement phases and the cement is shown in the Figure 4.9. The volume fraction of hydration products of cement CSH and CH phases of cement paste with w/c ratio of 0.25 and 0.40 versus time can be seen in Figure 4.10, in which the volume fraction of $Ca(OH)_2$ is compared with TGA results as presented in chapter 3 (part 3.3.3) (Figure 4.10a). As expected the low w/c cement paste has a higher volume fractions of both CH and CSH than those of the higher w/c cement paste (Figure 4.10b).

Table 4.4 The properties of cement CEM I 52.5 N

Chemical composition	Percentage by weight	*Mineral composition* (calculation)	Percentage by weight
CaO	64.0	C_3S =	63.77
SiO_2	20.0	C_2S =	9.24
Al_2O_3	5.0	C_3A =	8.18
Fe_2O_3	3.0	C_4AF =	9.13
SO_3	2.4		
Na_2O	0.3		
LOI	1.3		
Particle size distribution (Rosin-Rammler function)	Value	*Other properties*	Value
n =	0.9338	Specific gravity, kg/m^3	3150
b =	0.0705	Specific surface area, cm^2/g	4500
Maximum size, μm	50		
Minimum size, μm	3	Mean particle size, μm	13.7

Table 4.5 Calculated values of K_0 and δ_{tr} of four phases and cement

No.	Phase	K_0	δ_{tr}	β_1	β_2
1	C_3S	0.0707	1.59	4	2
2	C_2S	0.0051	1.03	4	2
3	C_3A	0.1362	1.15	8	2
4	C_4AF	0.0200	1.19	4	2
5	Cement	0.0456	1.11	4	2

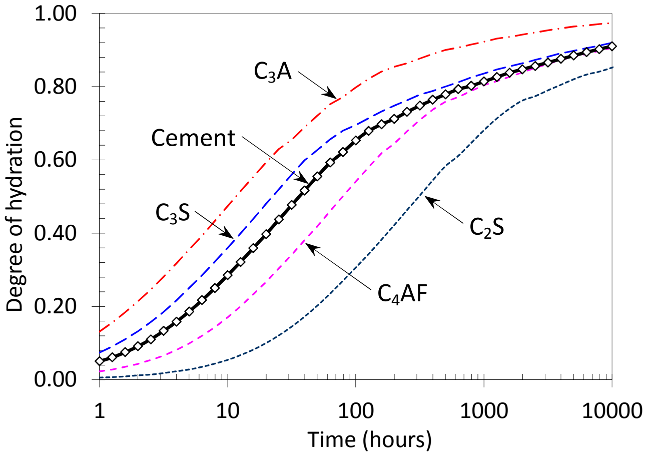

Figure 4.9 Degree of hydration of four phases of cement, w/c = 0.40

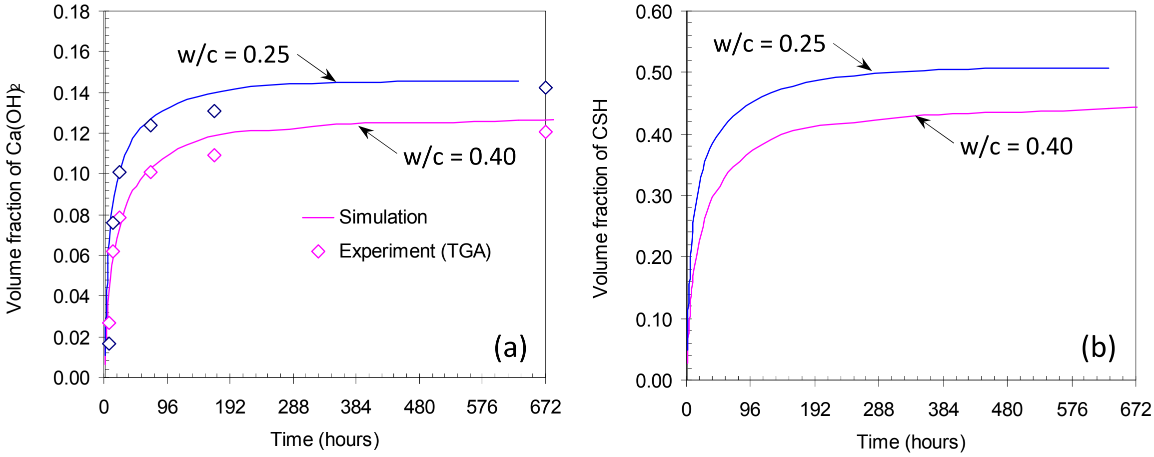

Figure 4.10 Volume fraction of (a) $Ca(OH)_2$ and (b) CSH of cement paste over time, cement CEM I 52.5 N, w/c = 0.25 and 0.40. Experimental data in (a) are taken from the section 3.3.3

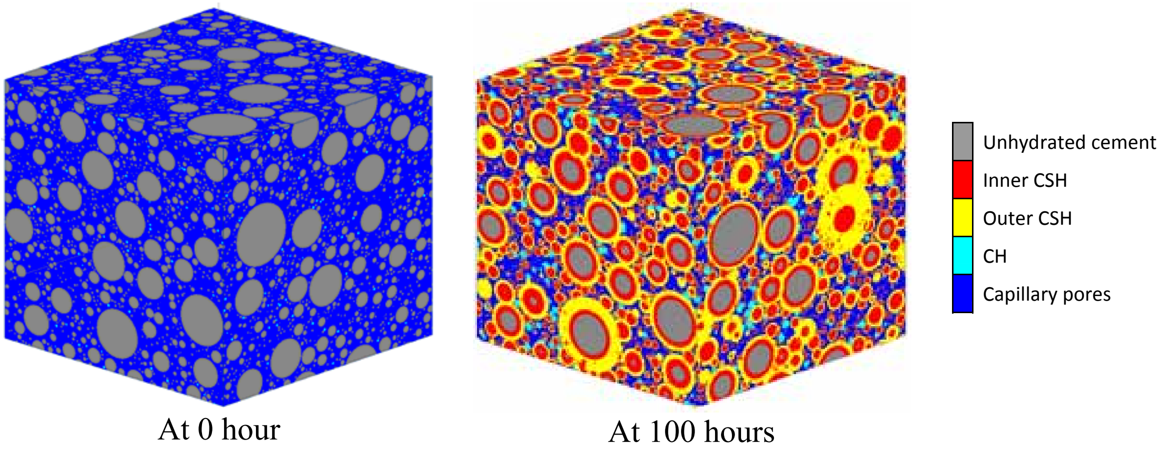

Figure 4.11 3D microstructure of cement hydration with time, green spherical grains indicate CH phase, w/c = 0.40

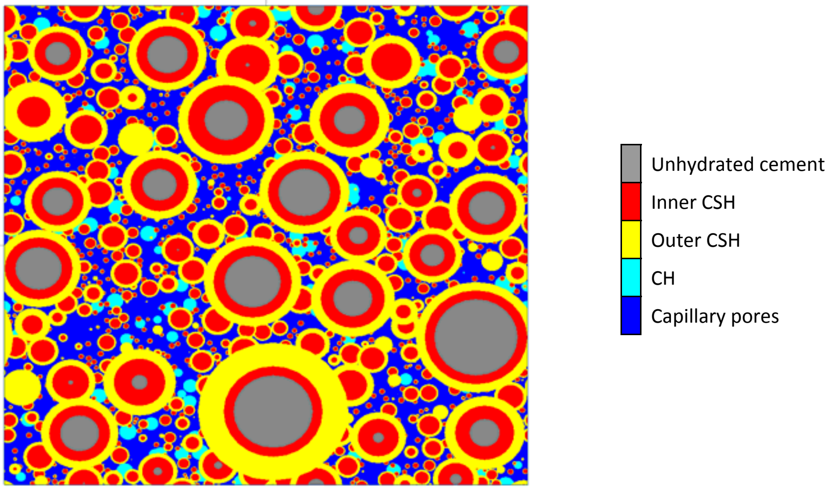

Figure 4.12 2D image of cement hydration after 100 hours, w/c = 0.40

The virtual 3D microstructure of cement paste with w/c ratio of 0.40 at 0 and 100 hours is presented in Figure 4.11 and its 2D microstructure after 100 hours can be seen in Figure 4.12. In this figure, CH particles appear as light blue spheres.

4.3 Simulation of the hydration and microstructure development of cement blended with rice husk ash

As discussed in chapter 3, the addition of RHA in cement paste will lead to a pozzolanic reaction between CH produced from cement hydration and RHA. This pozzolanic reaction results in a reduction of CH content and an increase of CSH content in the system. This is taken into account in the model. In order to simulate the hydration and microstructure development of cement blended with RHA based on the HYMOSTRUC3D model, some modifications were needed in both hydration and microstructural aspects of cement paste, including:

1) The hydration kinetics of cement blended with RHA

   The hydration kinetics of pozzolanic reaction of RHA is accounted for. The progress of the RHA reaction is as similar to that of cement reaction.

2) The microstructure of cement paste blended with RHA

   The virtual microstructure of cement paste is modified due to the addition of RHA. Since RHA reacts with CH and CSH is generated, the capillary- and gel-porosity of the system are changed. This modification is considered in this model.

4.3.1 The pozzolanic reaction of RHA

Because the chemical composition of both SF and RHA is similar (see section 3.2.1), it is assumed that their pozzolanic reactions are similar as well. The pozzolanic reaction and the volume stoichiometries [Bentz *et al.* 2000] of RHA are presented in equation (4.28):

$$\begin{array}{ccccccc} 1.1CH & + & S & + & 2.8H & \rightarrow & C_{1.1}SH_{3.9} \\ 1.35 & & 1 & & 1.87 & & 3.77 \end{array} \qquad (4.28)$$

4.3.2 The calculation of volume of hydration products

The CSH and CH contents are changed by the pozzolanic reaction of RHA according to equation (4.28).

- The volumes of CSH and CH phases at time *t* are calculated based on the stoichiometries of pozzolanic reaction of RHA following equations (4.29) and (4.30), respectively:

$$V_{CSH}(RHA) = 3.77 \times V_{RHA} \times \alpha_{RHA} \qquad (4.29)$$

$$V_{CH}(RHA) = 1.35 \times V_{RHA} \times \alpha_{RHA} \qquad (4.30)$$

in which V_{RHA} is the initial volume of RHA.

- The pozzolanic reaction of RHA will cause a reduction of the CH content (V_{CH}(RHA)) and an increase of the CSH content (V_{CSH}(RHA)). Therefore, the volumes of CSH and CH phases in the whole system can be determined as folows:

$$V_{CSH} = V_{CSH}(OPC) + V_{CSH}(RHA) \tag{4.31}$$

$$V_{CH} = V_{CH}(OPC) - V_{CH}(RHA) \tag{4.32}$$

where V_{CSH}(OPC) and V_{CH}(OPC) are the volumes of CSH and CH phases produced by cement hydration, respectively.

It is noticed that the content of CH in the system at time t depends on both the RHA content and the CH content generated from cement hydration. Two situations can be considered:

1) If the RHA content is too high, there is not enough CH in the system to react with RHA. The degree of the RHA reaction depends on the content of CH available. In this case, there is no CH phase remaining in the system, and the volume of CSH generated due to the pozzolanic reaction of RHA is

$$V_{CSH}(RHA) = (3.77/1.35) \times V_{CH}(OPC) \tag{4.33}$$

2) If the RHA content is low, there is enough CH existing in the system to react with RHA. The degree of the reaction of RHA depends on the pozzolanic activity of the RHA. The volume of the surplus CH phase and the total volume of the CSH phase due to cement hydration and pozzolanic reaction of RHA in the system are calculated with the equations (4.34) and (4.35), respectively.

$$V_{CH} = V_{CH}(OPC) - V_{CH}(RHA) \text{ with } V_{CH}(RHA) = 1.35 \times V_{RHA} \tag{4.34}$$

$$V_{CSH} = V_{CSH}(OPC) + V_{CSH}(RHA) \text{ with } V_{CSH}(RHA) = 3.77 \times V_{RHA} \tag{4.35}$$

4.3.3 The virtual microstructure of cement blended with RHA

A virtual microstructure of cement blended with RHA is built up in which RHA particles, assumed as spheres, are added and randomly distributed in the Portland cement system. The hydration of cement blended with RHA can be illustrated in Figure 4.13. The CSH phase generated from the pozzolanic reaction of RHA will grow on the RHA particles similar to the growth of cement particles with time of hydration. Besides, the CH phase consumed by the pozzolanic reaction of RHA is presented as a reduction of the diameter of CH particles.

In the original HYMOSTRUC3D model, only cement particles were considered. In order to simulate the hydration of cement containing RHA, the characteristics of the paste have to be modified.

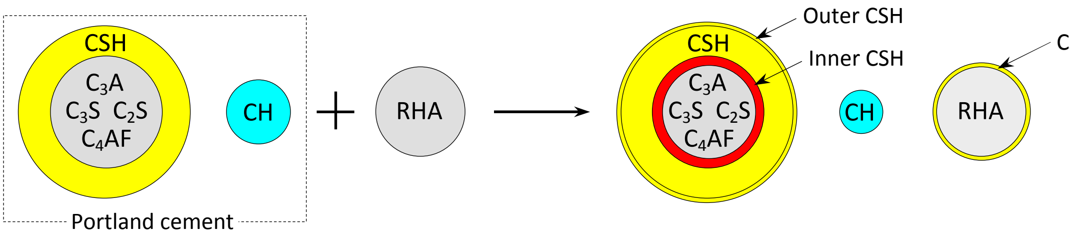

Figure 4.13 Hydration of cement blended with RHA

Particle size distribution (PSD) of cement and RHA

The cumulative particle size distribution of RHA is described like that of cement which uses the Rosin-Rammler function:

$$G_{RHA}(x) = 1 - \exp\left(b_{RHA} \times x^{n_{RHA}}\right) \tag{4.36}$$

where $G_{RHA}(x)$ is the PSD for RHA phase; n_{RHA} and b_{RHA} are the Rosin-Rammler constants. In this case the maximum size of RHA particles is smaller than that of cement particles.

The RHA mass $W_{RHA}(x)$ of the fraction $F_{RHA}(x)$ is obtained by differentiating eq. (4.36) with respect to x:

$$W_{RHA}(x) = \gamma \times b_{RHA} \times n_{RHA} \times x^{n_{RHA}-1} \times e^{-b_{RHA} x^{n_{RHA}}} \tag{4.37}$$

where γ is a correction factor accounting for the establishing the physical consistency of the Rosin-Rammler function [van Breugel 1991].

For the volume $V_{RHA;x}$ of all particles in fraction $F_{RHA;x}$ it holds that:

$$V_{RHA;x} = \frac{W_{RHA}(x)}{\rho_{RHA}} \tag{4.38}$$

where, ρ_{RHA} is the specific mass of RHA.

The number of particles $N_{RHA;x}$ in fraction $F_{RHA;x}$ is found by dividing the volume $V_{RHA;x}$ of fraction $F_{RHA;x}$ by the volume of a single particle $v_{RHA;x}$

$$N_{RHA;x} = \frac{V_{RHA;x}}{v_{RHA;x}} \tag{4.39}$$

in which $v_{RHA;x}$ is considered as a volume of a spherical particle with the diameter of x.

Paste characteristics

The paste is considered to contain cement and RHA particles with the RHA ratio P defined as the mass of RHA relative to the mass of the cement. The w/b ratio ω_b is defined as:

$$\omega_b = \frac{\text{mass of water}}{\text{mass of binder}} \tag{4.40}$$

With this formula, the w/c ratio ω_0 can be expressed as a function of the w/b ratio and the RHA ratio according to:

$$\omega_0 = \omega_b \times (1+P) \tag{4.41}$$

The specific mass ρ_{pa} of a paste containing RHA with a w/b ratio ω_0 can be determined by dividing the mass of the water and binders, i.e. cement and RHA, by the volume of the paste. Elaboration of this leads to the following formula:

$$\rho_{pa} = \frac{\rho_{ce}\left(1+P+\omega_0\right)}{1+\frac{\rho_{ce}}{\rho_{RHA}}\times P+\frac{\rho_{ce}}{\rho_w}\times\omega_0} \tag{4.42}$$

where ρ_{ce}, ρ_{RHA}, ρ_w are the specific masses of cement, RHA and water, respectively.

The (volumetric) density of the paste containing RHA, ζ_{pa}, is defined as the volume of binder V_b relative to the volume of fresh paste V_{pa}. In formula form:

$$\zeta_{pa} = \frac{\text{volume of binder}}{\text{volume of fresh paste}} = \frac{1+\frac{\rho_{ce}}{\rho_{RHA}}\times P}{1+\frac{\rho_{ce}}{\rho_{RHA}}\times P+\frac{\rho_{ce}}{\rho_w}\times\omega_0} \tag{4.43}$$

Cell volume and cell density

In the original HYMOSTRUC model [van Breugel 1991], a cell I_x^c is defined as a cubic space in which the largest cement particle has a diameter x, and further consists of $1/N_{ce;x}$ times the original water volume and of $1/N_{ce;x}$ times the volume of all cement particles smaller than particles x. When the model incorporates RHA, the cell definition can be expressed by:

$$I_x^c = \left(V_w + V_{ce\le x} + V_{RHA\le x}\right)\times N_{ce;x}^{-1} \tag{4.44}$$

where V_w is the initial water volume = $\omega_0.G(\infty)/\rho_w$
$V_{ce\le x} = m_{ce}.\gamma_{ce}.\beta_{ce}.G_{ce}(x)/\rho_{ce}$ = cement volume of particles ≤ x
$V_{RHA\le x} = m_{RHA}.\gamma_{RHA}.\beta_{RHA}.G_{RHA}(x)/\rho_{RHA}$ = RHA volume of particles ≤ x
γ_{ce}, γ_{RHA} are the other correction factors [van Breugel 1991]
$N_{ce;x}$ is the number of cement particles in fraction $F_{ce}(x)$.

Analogous to the volumetric density for paste (4.43), the volumetric cell density ζ_x is defined by:

$$\zeta_x = \frac{\text{volume of binder in cell } I_x^c}{\text{volume of cell } I_x^c} = \frac{\left(V_{ce\le x}+V_{RHA\le x}\right).N_{ce;x}^{-1}}{\left(V_w+V_{ce\le x}+V_{RHA\le x}\right).N_{ce;x}^{-1}} \tag{4.45}$$

Shell density

The shell density of binder $\zeta_{sh;x,d_u}$ is defined as binder volume in a spherical shell with thickness d_u relative to total shell volume.

$$\zeta_{sh;x,d_u} = \frac{\text{binder volume in spherical shell with thickness } d_u}{\text{total shell volume}} = \frac{\zeta_x \times I_x^c - \nu_x}{I_x^c - \nu_x} \tag{4.46}$$

Particle growth during hydration

The growth mechanism describes the mechanism of the outward growth of a central particle *x*, while embedding the particles smaller than the central particle in the growing shell. Figure 4.14 shows the sequential growth of the shell in relation to the increase of the outer radius of the central particle *x* at an arbitrary stage of the hydration process. The particles can be either cement particles, RHA particles or both.

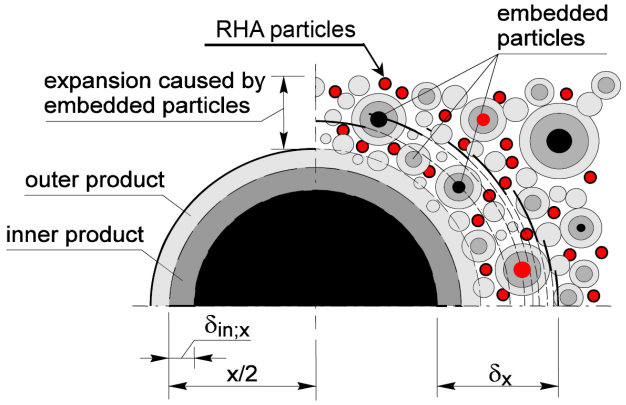

Figure 4.14 Schematic representation of the embedding particle concept

At a particular time, i.e. t = t_j, the degree of hydration of the central RHA particle is $\alpha_x^{RHA}(t)$. The corresponding penetration depth of the reaction front of the filler particles $\delta_{in;x}^{RHA}(t)$ follows from

$$\delta_{in;x}^{RHA}(t) = \left(\frac{x_{RHA}}{2}\right).\left[1-\left\{1-\alpha_x^{RHA}(t)\right\}\right]^{1/3} \tag{4.47}$$

The volume of the outer product $v_{ou;x}^{RHA}(t)$ for the RHA at a degree of hydration *α* can be described as:

$$v_{ou;x}^{RHA}(t) = \left(\nu^{RHA} - 1\right) \times \alpha_x^{RHA}(t) \times v_x^{RHA} \tag{4.48}$$

where ν^{RHA} is the ratio between the volume of the reaction product and dissolved material of RHA, the value of ν^{RHA} is assumed to be 2.2 like that of cement in this case; v_x^{RHA} is the initial volume of a single RHA particle.

The outer radius $R^{RHA}_{ou;x}(t)$ for the RHA particles can be determined according to:

$$R^{RHA}_{ou;x}(t)=\left[\frac{v^{RHA}_{ou;x}(t)}{4\pi/3}+\left(\frac{x_{RHA}}{2}\right)^{3}\right]^{1/3} \tag{4.49}$$

For the thickness of the outer shell for the filler particles $\delta^{RHA}_{ou;x}$ it holds that

$$\delta^{RHA}_{ou;x}(t)=R^{RHA}_{ou;x}(t)-\frac{x_{RHA}}{2} \tag{4.50}$$

Reaction kinetics

For the reaction kinetics of RHA, a similar approach has been adopted as that of cement (see eq. (4.1)). It is assumed that, initially, the rate of reaction of RHA particles is also determined by a phase boundary reaction, and that, after having reached a predefined thickness of the shell of reaction product, this process changes into a diffusion controlled process. The Basic Rate Equation that is proposed has the following shape:

$$\frac{\Delta\delta^{RHA}_{in;x,j+1}}{\Delta t_{j+1}}=K^{RHA}_{0}(.)\times\Omega_1(.)\times\Omega_2(.)\times\Omega_3(.)\times F^{RHA}_{1}(.)\times\left[F^{RHA}_{2}(.)\times\left(\frac{\delta^{RHA}_{tr}(.)}{\delta^{RHA}_{x,j}}\right)^{\beta_1}\right]^{\lambda}\times Po_{RHA} \tag{4.51}$$

where:

K^{RHA}_{0}	: the initial rate constant for the RHA phase.
F^{RHA}_{1}	: the temperature function accounting for the effect of the temperature on the rate of the hydration process of RHA.
F^{RHA}_{2}	: the temperature function accounting for the effect of curing temperature on morphology and formation of structure. This value is operative only in diffusion stage.
Ω_1	: the reduction factor accounting for the water withdrawal on the central RHA particle
Ω_2	: the reduction factor accounting for the water shortage in the pore system.
Ω_3	: the reduction factor accounting for the amount of water in the hydrating mass.
λ	: a factor, depending on the rate controlling mechanism, in which $\lambda = 0$ for phase boundary reaction and $\lambda = 1$ for diffusion controlled reaction.
δ^{RHA}_{tr}	: the transition thickness of RHA particles, being the total thickness of the product layer $\delta_{x,j}$ at which the reaction for the particle in view changes from a boundary reaction ($\lambda = 0$) into a diffusion controlled reaction ($\lambda = 1$).
β_1	: an empirical constant.
Po_{RHA}	: the factor accounting for the reaction of CH phase, produced from the cement, with RHA.

The difference in this equation compared to the original one concerns the inclusion of the factor Po_{RHA}. If the CH content is enough, Po_{RHA} is equal to 1, otherwise Po_{RHA} is reduced with a value of the available CH content relative to the required CH content for the pozzolanic reaction of RHA (see further in the section 4.3.2).

Degree of the RHA reaction

Because the progress of the RHA reaction is assumed to be similar to that of the cement reaction, a similar approach of degree of the RHA reaction has been adopted, i.e. the mass ratio between the amount of RHA that has reacted at time t_j and the total amount of cement at time t = 0 [van Breugel 1991].

$$\alpha^{RHA}(t_j)=\alpha_j^{RHA}=\frac{\text{amount of RHA that has reated at time } t_j}{\text{total amount of RHA at time } t=0} \tag{4.52}$$

It should be noted that the thickness $\delta_{x,j}^{RHA}$ of the shell which surrounds an arbitrary RHA particle *x* is determined by the *degree of reaction of the RHA particle x*. For the increase of the degree of the RHA reaction $\Delta\alpha_{x,j}^{RHA}$ of particle x, a similar increment of the degree of hydration of cement that corresponds to an increase of the penetration depth Δt_j can be derived according to:

$$\Delta\alpha_{x,j}^{RHA}=\left[1-\frac{\delta_{in;x,j-1}^{RHA}}{r_x^{RHA}}\right]^3-\left[1-\frac{\delta_{in;x,j-1}^{RHA}+\Delta\delta_{in;x,j}^{RHA}}{r_x^{RHA}}\right]^3 \tag{4.53}$$

where r_x^{RHA} is the radius of a RHA particle with diameter *x*.

The *degree of hydration of a cell* I_x follows from adding up all the hydrated RHA volumes for all fractions $F_z<F_x$ and dividing this by the sum of the original amount of RHA ($G^{RHA}(x)$). For the degree of hydration at the cell-level for the RHA particles, it holds:

$$\alpha_{<x,j}^{RHA}=\frac{1}{G_{RHA}(x-1)}\sum_{z=x_{minRHA}}^{x_{maxRHA}}\alpha_{z,j}^{RHA}\times W_{RHA}(z) \tag{4.54}$$

where $W_{RHA}(z)$ is the weight of the RHA particles within fraction z.

The *overall degree of the RHA reaction* α_j^{RHA} at time t_j can be considered as a special case of the cell hydration and can, therefore, be calculated using $x = x_{maxRHA}$ for RHA in expressions (4.54).

Effect of state of water

In this part, the effect of the RHA reaction on the factors $\Omega_1(.)$, $\Omega_2(.)$, $\Omega_3(.)$ of the basic rate equation (eq. (4.27) is considered which accounts for different phenomena related to the momentary state of water in the paste [Koenders 2006].

Water withdrawal by embedded particles, reduction factor $\Omega_1(x_{ce}, \alpha_{x,j}^{ce}, \alpha_{x,j}^{RHA})$

The first reduction factor $\Omega_1(.)$ accounts for the hydration of the embedded and still incompletely hydrated cement and/or RHA particles. The still incompletely hydrated cement and RHA particles embedded in the shell of a central cement or RHA particle will withdraw a certain amount of the water needed for further hydration of the central cement or RHA particle. The resulting decrease of the rate of penetration of the reaction front in the central cement particle *x* is accounted for with the reduction factor $\Omega_1(x_{ce}, \alpha^{ce}_{x,j}, \alpha^{RHA}_{x,j})$.

$$\Omega_1 = \frac{\Delta w^{ce}_{x,j}}{\Delta w^{RHA}_{x,j} + m_{ce}.\Delta w^{ce}_{em;x,j} + m_{RHA}.\Delta w^{RHA}_{em;x,j}} \tag{4.55}$$

with $\Delta w^{ce}_{x,j}$ is the amount of water needed for an increase of the degree of hydration $\Delta\alpha_{x,j}$ of the central cement particle x during time step Δt_j; $\Delta w^{ce}_{em;x,j}$, $\Delta w^{RHA}_{em;x,j}$ are the amounts of water required for further hydration of the embedded cement and RHA particles in the shell of the central cement particle.

Effect of water shortage in the pore system: reduction factor $\Omega_2(\alpha^{ce}_j, \alpha^{RHA}_j)$

When considering this concept in view of the RHA phase addition, the parameters that are affected by this addition are the volume of capillary water V_{cap} and pore volume V_{por}. The maximum pore volume in the pore system at an arbitrary degree of hydration α can be calculated according to:

$$V_{por}(\alpha) = V_{cap}(\alpha) + V_{chsh}(\alpha) \tag{4.56}$$

where $V_{cap}(\alpha)$ is the amount of capillary water at a degree of hydration α, and $V_{chsh}(\alpha)$ represents the chemical shrinkage.

$$V_{cap}(\alpha^{ce}_j, \alpha^{RHA}_j) = \frac{\rho_{ce}\left(\omega_0 - 0.4 \times \alpha^{ce}_j \times m_{ce} - w_{RHA} \times \alpha^{RHA}_j \times m_{RHA} \times P\right)}{1 + \omega_0 \times \rho_{ce} + \left(\rho_{ce} / \rho_{RHA}\right) \times P} \tag{4.57}$$

$$V_{chsh}(\alpha^{ce}_j, \alpha^{RHA}_j) = 0.25^2 \times \frac{\rho_{ce}\left(\alpha^{ce}_j \times m_{ce} + \alpha^{RHA}_j \times m_{RHA} \times P\right)}{1 + \omega_0 \times \rho_{ce} + \left(\rho_{ce} / \rho_{RHA}\right) \times P} \tag{4.58}$$

where the chemical shrinkage is assumed to be about 25% of the volume of the chemically bound water.

The diameter of the largest pore in the system can be calculated:

$$\phi_{por}(\alpha^{ce}_j, \alpha^{RHA}_j) = \phi_{max} = \phi_0 \times \exp\left(\frac{V_{por}(\alpha^{ce}_j, \alpha^{RHA}_j)}{a}\right) \tag{4.59}$$

From the capillary water volume V_{cap} and the maximum pore diameter in the system ϕ_{por}, the reduction factor Ω_2 can be derived. For the derivation of this reduction factor, reference is made to the thesis of van Breugel [1991].

Effect of decrease of water content: reduction factor $\Omega_3(\alpha_j^{ce}, \alpha_j^{RHA})$

As the hydration process is progressing, the amount of water available for the chemical reaction with cement and RHA is decreasing. The reduction of the amount of water in the hydrating paste is considered to cause a decrease of the rate of hydration of the cement and RHA phase. With the addition of RHA, the proposed reduction factor has to be adjusted in order to account for the decrease of the water content. This can be achieved by considering the same motivation and conceptual approach as considered as van Breugel [1991].

$$\Omega_3 = \frac{\omega_b - 0.4 \times \alpha_j^{ce} \times m_{ce} - w_{RHA} \times \alpha_j^{RHA} \times m_{RHA}}{\omega_b} \tag{4.60}$$

where ω_b is the w/b ratio of the system.

Capillary- and gel- porosity

The capillary porosity of blended cement paste is calculated from image analysis. The gel porosity ($V_{por,gel}$) takes 28% of the volume of the CSH phase produced from cement hydration ($V_{CSH(OPC)}$) [Powers and Brownyard 1948] and 19% of volume of the CSH phase generated from the pozzolanic reaction of SF [Baroghel Bouny 1996]. In this case, the gel porosity of the CSH phase produced from the pozzolanic reaction of RHA ($V_{CSH(RHA)}$) is considered to be equal to that formed by SF.

$$V_{por,gel} = 0.28 \times V_{CSH(OPC)} + 0.19 \times V_{CSH(RHA)} \tag{4.61}$$

4.3.4 Simulation results and validation

In this section, simulation results for cement blended with RHA were validated by experimental results. The properties of RHA used in this simulation are given in Table 4.6.

Table 4.6 The input data of RHA

Properties	Value	Properties	Value
Cement replacement, %	0-20	*Chemical composition*	
Particle size distribution		Amorphous SiO_2, %	88.00
(Rosin-Rammler function)		Loss on ignition, %	3.8
n =	1.10		
b =	0.07	K_0, µm/h	0.017*
Maximum particle size, µm	50	δ_{tr}, µm	2.92*
Minimum particle size, µm	3		
Specific gravity, kg/m^3	2100	Mean particle size, µm	7.3

(*) The values were derived from the experiment by Khan *et al.* [1985]

The properties of cement, CEM I 52.5 N, used in this validation are taken from Table 4.4. The particle size distribution of cement and RHA, which was determined by laser diffraction and described by a Rosin-Rammler function, is plotted in Figure 4.15. This figure shows that in this example the particle size distribution of the two materials does not differ very much.

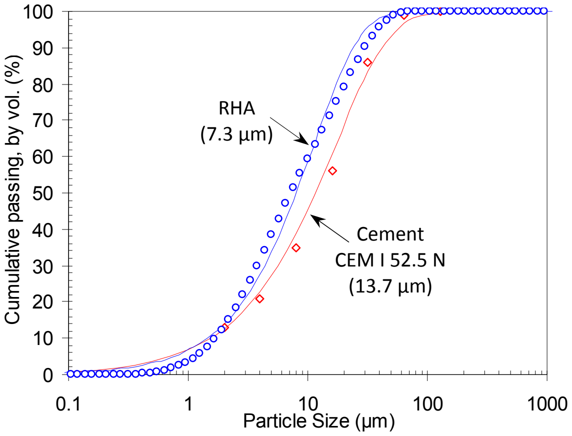

Figure 4.15 Particle size distribution of cement and RHA, determined by laser diffraction (points) and described by a Rosin-Rammler function (solid line)

The simulation result concerning the volume fraction of hydration products and porosity of the paste with 10% RHA and w/b ratio of 0.40 is shown in Figure 4.16. It should be noted that the total volume fraction of unhydrated cement, CH- and CSH- phases, capillary porosity and other hydrates is set to 1.

The virtual 3D-microstructure and 2D-image of cement paste containing 10% RHA with w/b ratio of 0.40 at 0 and 100 hours hydration are presented in Figure 4.17 and Figure 4.18, respectively. In these figures, RHA particles appear as light grey spheres.

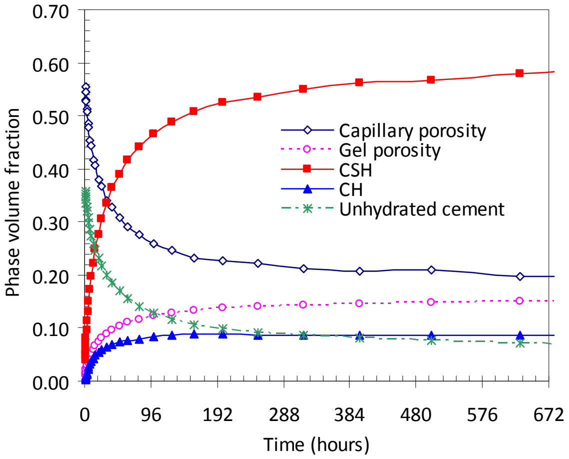

Figure 4.16 Volume fraction of phases in cement paste containing 10% RHA, w/b = 0.40

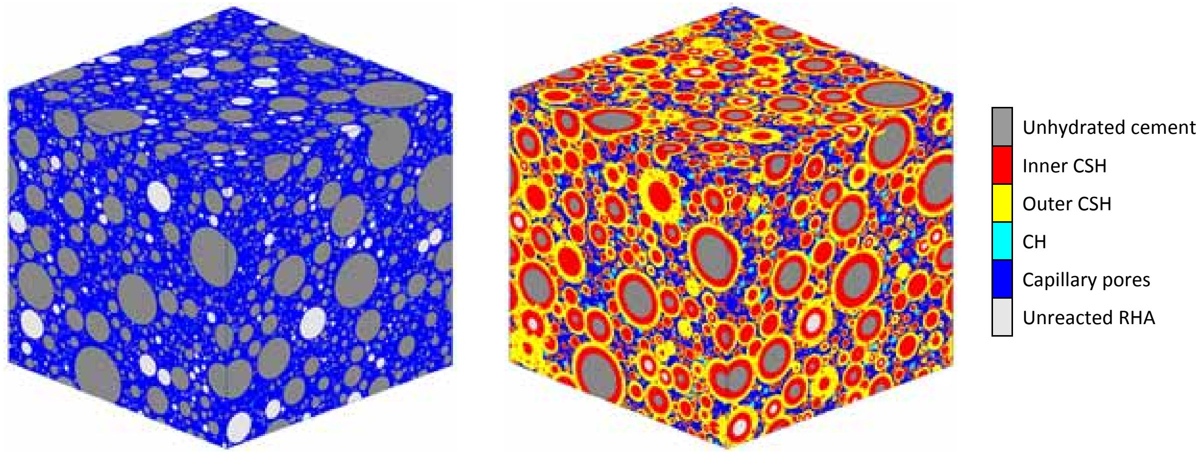

At 0 hour At 100 hours

Figure 4.17 3D microstructure of cement blended with RHA at 0 hour and 100 hours, w/b = 0.40, 10% RHA

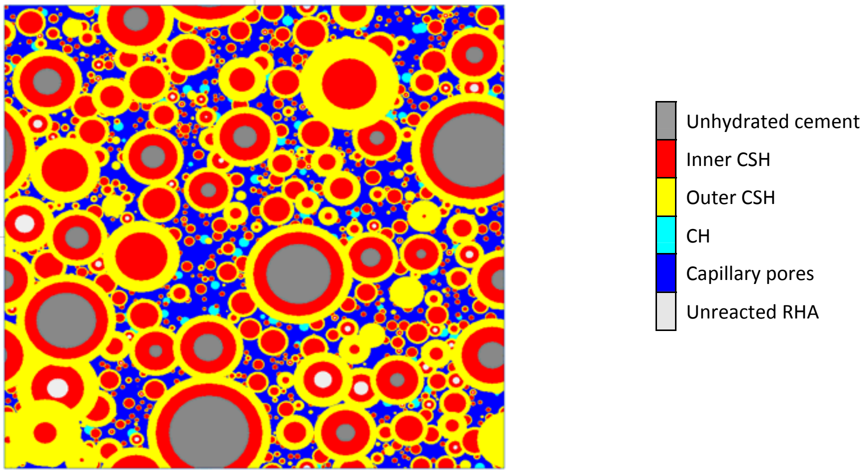

Figure 4.18 2D image of cement blended with RHA at 100 hours, w/b = 0.40, 10% RHA

Effect of the RHA particle size

The particle size of RHA influences its pozzolanic reaction and results in a change of the amounts of CH and CSH phases in the system. With a given chemical composition, the finer RHA has a higher pozzolanic activity than that of the coarser one. It leads to a higher CH content consumed and a higher CSH content produced. As discussed in chapters 2 and 3, the particle size of RHA is determined by the grinding process. Intensive grinding will cause collapse of the RHA-particles and their porous structure. This influences on the hydration of cement. In this section, the effect of particle size of RHA on the degree of reaction of RHA is simulated.

The simulated degree of reaction of RHA and the volume fraction of CH in cement paste containing 10% RHA with different particle sizes are shown in Figure 4.19. It was assumed that these RHAs have only one particle size, i.e. 1, 5, 10, 20, and 50 µm. It is clear that the addition of the finer RHA results in a larger reduction of the CH content than that of the coarser one. In addition, the maximum degree of reaction of RHA depends on its amorphous phase content, i.e. SiO_2. For example, after a certain period of curing, RHA with a particle size of 1 µm reaches its highest degree of reaction of 88%. This value equals the amorphous phase content of RHA, which is able to participate in the pozzolanic reaction. See next paragraph all CH is consumed in the first 10 hours. The degree of reaction of RHA depends on the CH produced from cement hydration at this time. After this point, the volume of CH increases, as there is no RHA for further pozzolanic reaction.

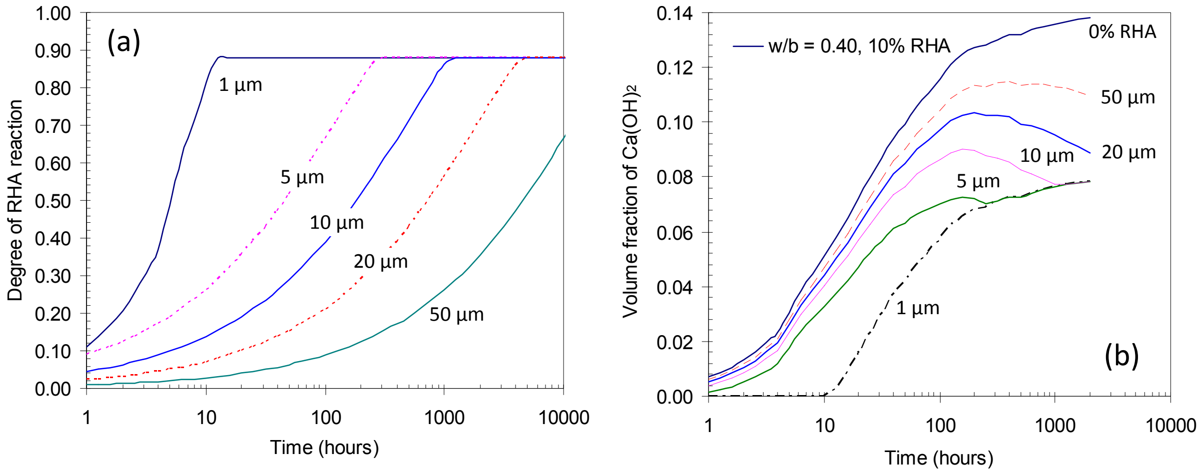

Figure 4.19 Effect of the RHA particle size on (a) degree of reaction of RHA, (b) volume fraction of $Ca(OH)_2$, w/b = 0.40, 10% RHA, 88% amorphous SiO_2 content of RHA

Effect of the amorphous SiO_2 content of RHA

The chemical composition and the amorphous phase content of RHA play important roles in its pozzolanic reaction. In RHA, the amorphous SiO_2 is a main reactive phase and can react with CH to produce CSH. The other phases of RHA are considered inert. The simulation results for cement paste containing 10% RHA with different amounts of the amorphous phase are shown in Figure 4.20. It can be seen that RHA with a higher amorphous SiO_2 content has a higher degree of reaction and consume more CH. Although the degree of reaction of RHA increases with increasing amount of amorphous SiO_2, the amount of CH consumed does not decrease remarkably. This is due to the fact that a low RHA content was used in this case.

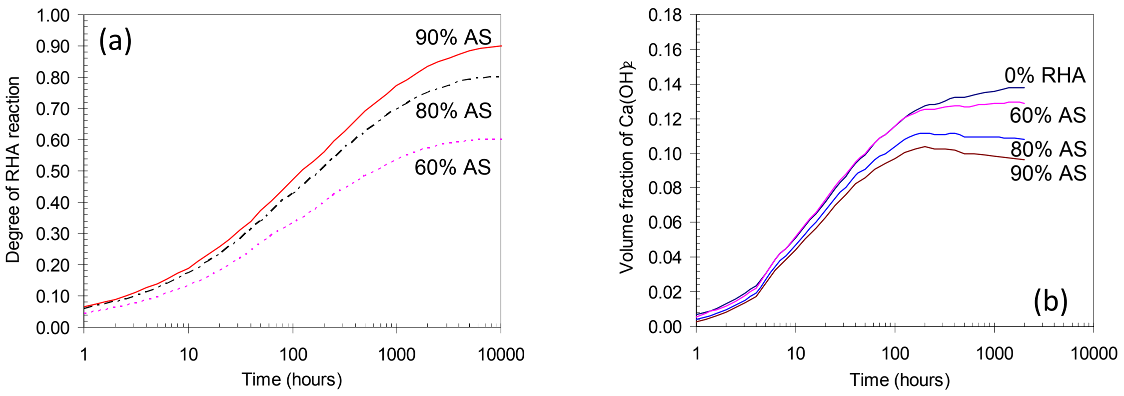

Figure 4.20 Effect of the amorphous SiO_2 content (AS) of RHA on: (a) degree of pozzolanic reaction of RHA; (b) volume fraction of $Ca(OH)_2$, w/b = 0.40, 10% RHA

Effect of the RHA content

The degree of the reaction of RHA is influenced by both the amounts of RHA and CH phase in the system. If the RHA content is high, there may be not enough CH in the system to react with RHA. The extra RHA remains as an inert filler. The degree of reaction of RHA in this case depends on the CH content available to react with RHA. If the RHA content is low, then there is enough CH available in the system. The degree of the reaction of RHA depends on its pozzolanic activity. This can be clearly seen in Figure 4.21. There is enough CH in the system to react with RHA as long as the RHA content is below 20%. However, at the cement replacement level of 30%, RHA cannot react completely after 1000 hours because of a lack of available CH. The RHA reaction depends on the rate of CH formation. The effect of RHA contents on the volume of CH of system is shown in Figure 4.22. It is obvious that a higher amount of RHA will consume more CH.

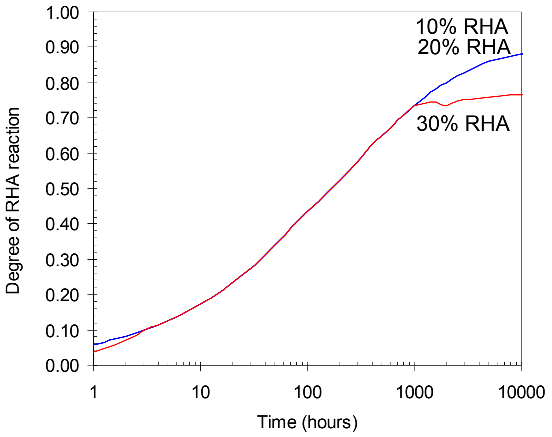

Figure 4.21 Degree of reaction of RHA with different RHA contents, w/b = 0.40

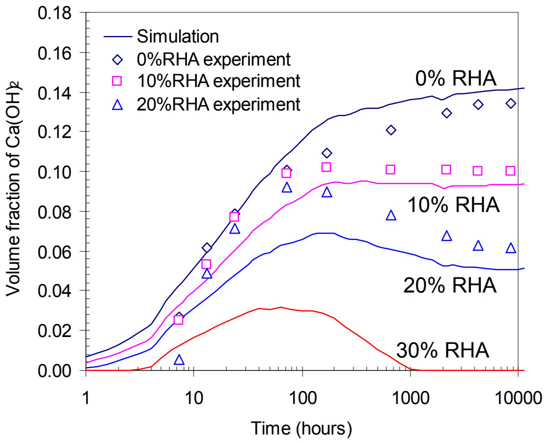

Figure 4.22 Volume fraction of $Ca(OH)_2$ of cement paste containing different RHA contents vs. time, w/b = 0.40

Degree of the RHA reaction and validation

In order to validate the simulation and test result, data presented by Khan [1985] was used. In that study, the pozzolanic reaction of RHA with the C_3S paste was performed. The Blaine specific surface of C_3S was 0.3 m^2/g. The RHA contains 82% SiO_2 and has a BET specific surface area of 60 m^2/g. The C_3S/RHA ratio of 3 and the w/b ratio of 0.40 were used. The comparison of the degree of reaction of RHA between simulation and test result is depicted in Figure 4.23. Interestingly, the presentation of result shows different effects. It can be seen that the simulation result seems fit very well with the experimental data when the paragraph is presented in the linear scale, but in the logarithmic scale there is a difference between simulation and experimental data in the early period. In this study, the degree of reaction of RHA in the early period is focused and the paragraph presented in the logarithmic scale is considered.

The difference between simulation and experimental data in the early period in this case may be caused by the assumption in the simulation that RHA reacts with CH immediately after CH produced from cement hydration. In fact, the experimental result shows that the pozzolanic reaction occurs later, i.e. after 10 hours of hydration. The onset of the pozzolanic reaction should be studied further to validate the model, i.e. the pozzolanic reaction of RHA with CH will affect the hydroxyl concentration of the pore water and the resulting pH of the pore solution will thus be used as an indicator to determine a time at which the RHA becomes active. Nevertheless, the simulation result is in a good agreement with Khan's test data after 100-hour hydration.

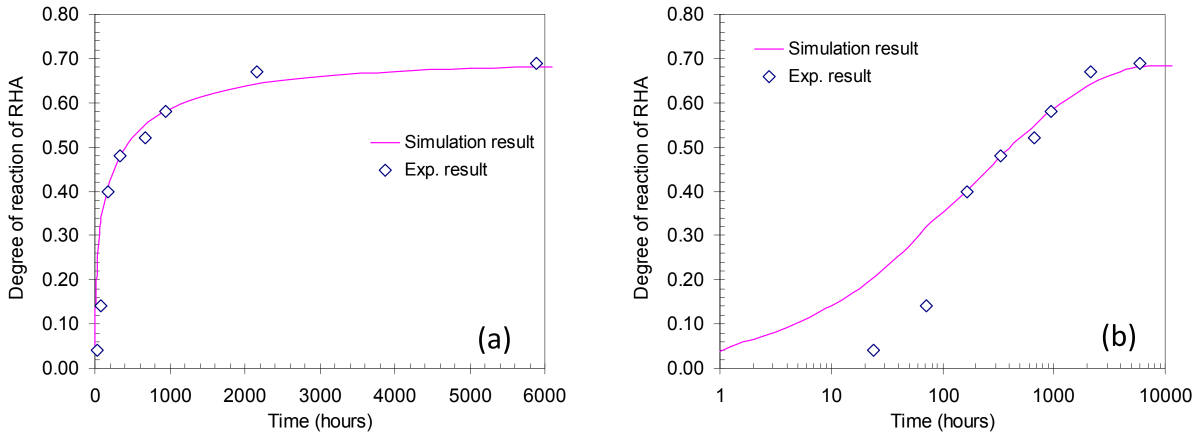

Figure 4.23 Simulation and experimental data [Khan *et al.* 1985] of degree of reaction of RHA; w/b = 0.40; 25% RHA. Paragraphs presented in the (a) linear scale and (b) logarithmic scale

4.4 Concluding remarks

In this chapter, the hydration and microstructure development of cement blended with RHA was simulated and developed with a modified version of the HYMOSTRUC3D model. In fact, the HYMOSTRUC3D model is an 'open' model which contains many modules describing many phenomena of cement hydration. To modify this system in order to simulate the hydration of blended binder systems, it is very important to keep the consistency of all these phenomena.

In this simulation, the chemical reactions and the degree of hydration of four main cement phases, i.e. C_3S, C_2S, C_3A, C_4AF, were modeled explicitly in order to calculate the volume of reaction products, i.e. CSH and CH, with time of hydration. The virtual microstructure of Portland cement was built up with the four-phase cement particles. The CH phase is randomly located as spheres in the voids of system. The CSH phase is supposed to grow on the surface of cement particles and RHA particles.

The effect of RHA with different particle sizes, amorphous phases of RHA, and RHA replacement contents on the hydration and microstructure development of cement paste were dealt with. However, the effects of the alkali content, the internal curing, and the unburnt carbon content of RHA has not been considered in this simulation.

Based on the simulation results and validations by the experimental results in this chapter, the following conclusions can be drawn:

- An optimal RHA content, i.e. less than 30%, used in cement paste was found from simulation. The extra RHA has no contribution to the pozzolanic reaction.

- The pozzolanic reaction of RHA is influenced by the particle size of RHA. The finer RHA reacts with CH faster and more CSH is generated. However, the maximum degree of reaction of RHA depends on its amount of amorphous phase, not on the size of RHA particle. After reaching the maximum degree of reaction, a constant amount of CH is consumed by the pozzolanic reaction of RHA and the amount of CH in the system increases with time of hydration.

5

Experimental Study of Ultra-High Performance Concrete incorporating Rice Husk Ash

5.1 Introduction

Experimental studies on the hydration process and microstructure formation of cement paste presented in Chapter 3 show that RHA can be used as a substitution for SF in low w/b ratio cement pastes. This gives rise to the idea that RHA can be used to produce UHPC in which the w/b ratio is very low. Besides, the addition of RHA, which seems to act as an internal curing agent, can mitigate the high autogenous shrinkage that is generally observed in UHPC. These aspects are the objectives of this chapter.

In this chapter, the optimization of the packing density of the UHPC granular mixtures was investigated. The UHPC mixtures were designed based on the result of the packing studies. The properties of UHPC, such as the workability, the compressive strength, and autogenous shrinkage were dealt with. From these results, the hypothesized internal water curing of RHA for UHPC will be further discussed.

5.2 Materials and Methods

5.2.1 Materials

The materials used in this chapter were the same as those used to study the hydration process and microstructure development of cement paste discussed in Chapter 3. One more constituent, silica sand with a particle size ranging from 100 to 300 μm, was employed. The type of superplasticizer was changed to Glenium ACE30, condensed 30%. The morphology of silica sand used in this study is shown in Figure 5.1. It can be seen that the shape of these particles is predominantly round.

5.2.2 Methods

All mixtures were prepared in a 20-liter Hobart mixer. The volume of each batch was 3.5 litres. After mixing, the mixtures were cast into 40×40×40 mm^3 cubes for a compression test. All mixtures were vibrated for 1 minute using a vibrating table with a frequency of 2500 cycles/min. After casting, the samples with moulds were cured in a fog room (20±2^{o}C, RH>95%) for one day. After demoulding, the samples were still stored in the fog room until the day of testing.

For microstructural studies and thermogravimetric analysis, the preparation of sample and the testing program were the same as those applied for cement paste (see Section 3.2.2).

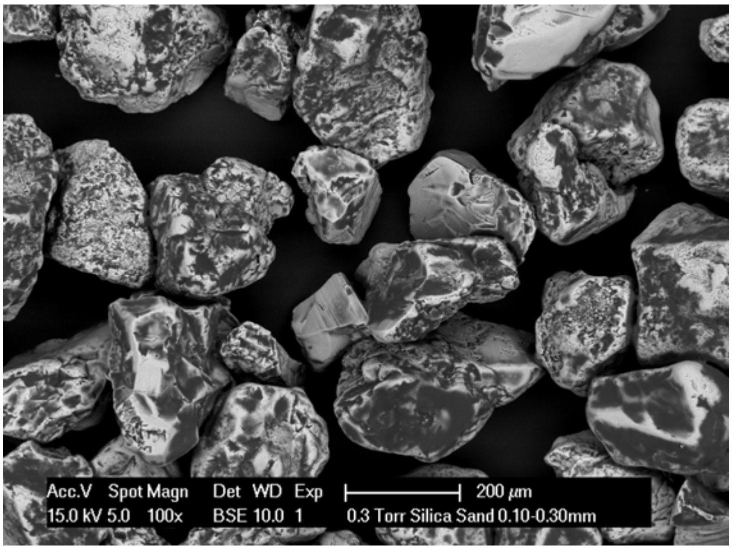

Figure 5.1 Morphology of silica sand with a size range from 100 to 300 μm used in this study

In order to explore the interface transition zone (ITZ) in detail by BSE imaging, images with a magnification of 1000× were captured. The thickness of the ITZ was determined by analysing the variation in the grey level. A total number of 12 to 15 images were captured in this study for each sample. The ITZs between the sand particles and cement paste were analysed. The size of sand particles ranged between 100 and 300 μm. Each image was subdivided into 20 frames with a length of 30 μm and the left side of each frame was put along the surface of sand particles (Figure 5.2). The grey level of each frame was obtained by using the software, ImageJ. The average result of the grey level analyses of all the frames will be used to predict the thickness of the ITZ between the aggregate and the cement paste (Figure 5.3).

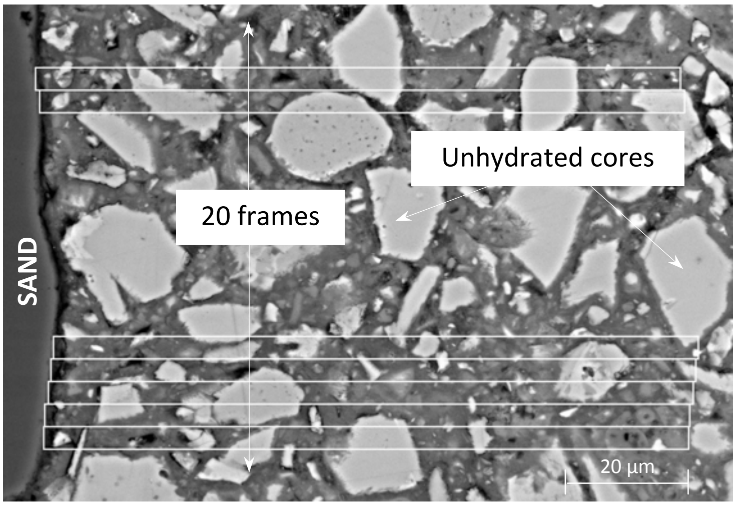

Figure 5.2 BSE image of UHPC, sand particle is on left,
the left side of white frames put along the surface of sand particles

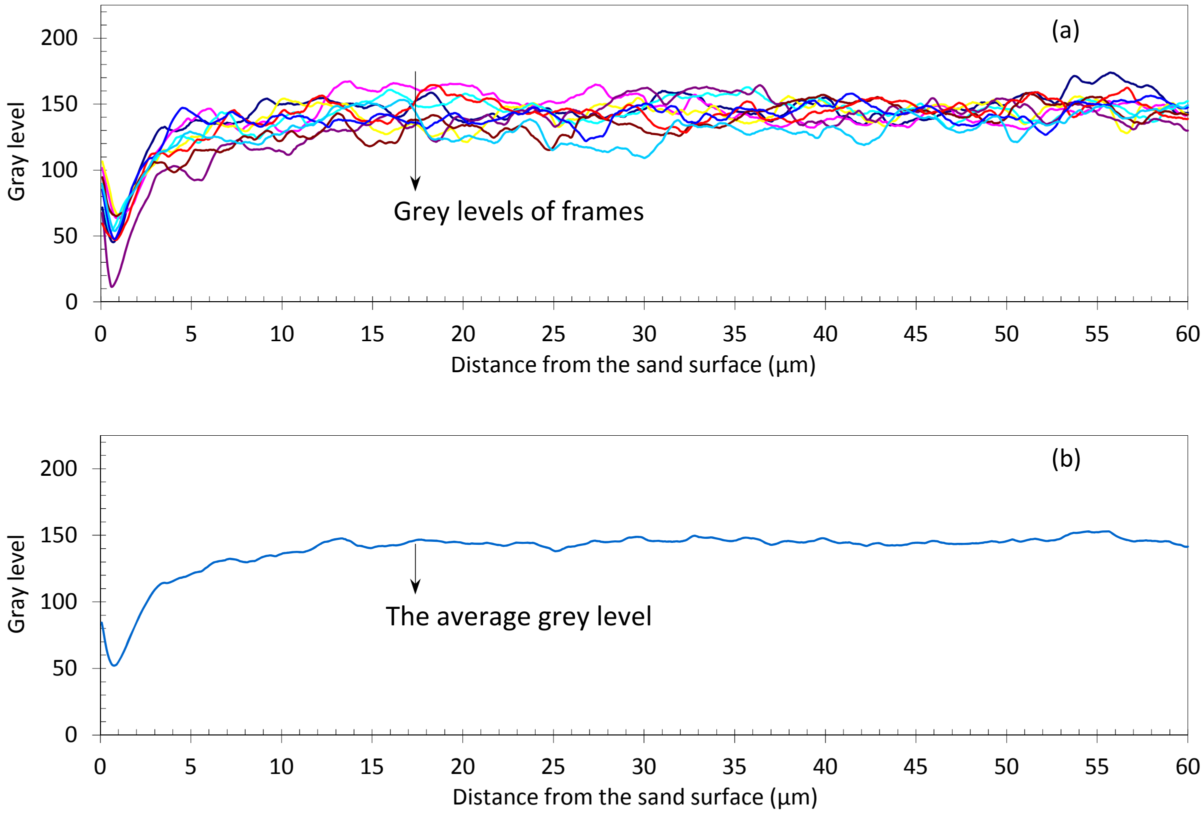

Figure 5.3 The grey levels of frames (a) and the average grey level (b)

In addition, the degree of hydration of cement in UHPC pastes can be determined according to the stereology analysis as discussed in Section 3.2.2 in which with sufficient sampling, the volume fraction can be assumed to be equal to the area fraction in BSE images and the degree of hydration of cement can be calculated from the percentage of anhydrous Portland cement.

5.3 Packing density and UHPC compositions

5.3.1 Packing density

One of the very important key issues of designing UHPC is the enhancement of its density by optimization of the granular mixture [Richard and Cheyrezy 1995]. When the packing of the system is optimized, the porosity of the system is lowest and the strongest matrix is obtained. Because of optimizing the granular mixture, more fine particles will fill in the voids of the system. These fine particles expel water from the voids and water is more homogenously distributed in the system. This will improve the workability of mixture.

In this study, the packing of granular mixtures was predicted by using the packing model developed by Larrard [1999]. This method has been used successfully to design UHPC [de Larrard and Sedran 1994]. The mixing energy method was applied to verify the packing density of the wet mixtures.

Particle packing theory - the De Larrard model

Two models have been developed by De Larrard: the linear packing model (LPM) and the compressible packing model (CPM). Both models require the particle size distribution (PSD) to be measured for all constituent materials. In the first model, the *virtual packing density* for one particle size class is considered. It is a theoretical concept that is only a component of the achievable density of an actual mixture. In this respect, a class of large grains is dominant when it fills all the spaces available in such a way that adding a few smaller grains would merely fill the voids between large grains without forcing these large particles apart. Additionally, a class of small grains is dominant when it consumes more space than the voids available between the large particles.

The overall virtual packing density γ_i for a mixture of one particle size class i with independent β_i values is defined by the following equation, in which the loosening effect a_{ij} and the wall effect b_{ij} are taken into account.

$$\gamma_i = \frac{\beta_i}{1 - \sum_{j=1}^{i-1}\left[1 - \beta_i + b_{ij}\beta_i\left(1 - \frac{1}{\beta_j}\right)\right]y_j - \sum_{j=i+1}^{n}\left[1 - a_{ij}\frac{\beta_i}{\beta_j}\right]y_j} \tag{5.1}$$

where the value y_i represents the volume fraction retained in each size class i.

The *loosening effect* (a_{ij}) describes an effect whereby the introduction of small particles pushes apart larger particles.

$$a_{ij} = \sqrt{1 - \left(1 - \frac{d_j}{d_i}\right)^{1.02}} \tag{5.2}$$

where d_i, d_j represent the average particle diameters of the i^{th} and j^{th} size class, respectively, in which d_i is larger than d_j ($d_i > d_j$).

The *wall effect* (b_{ij}) describes an effect that larger particles cause the voids in the system. These voids are too small to be filled by other particle classes.

$$b_{ij} = 1 - \left(1 - \frac{d_i}{d_j}\right)^{1.50} \tag{5.3}$$

The *compressible packing model* (CPM) is built based on the selection of LPM which is appropriate for the particular compaction method. As proposed by De Larrard [1999], a constant related to the manner in which the mixture is compacted, the so-called compaction index *K*, is accounted for in this model. As explained by De Larrard, LPM can be considered as a special case for which the compaction index, K = ∞. The calculation process of the packing density of the combination of the constituent materials using CPM is similar to that using LPM but accounting for a compaction index *K*.

$$K = \sum_{i=1}^{n} K_i = \sum_{i=1}^{n} \frac{\dfrac{y_i}{\beta_i}}{\dfrac{1}{\Phi} - \dfrac{1}{\gamma_i}} \tag{5.4}$$

where Φ represents the percentage of solid in the mixture.

Application of the De Larrard model

In this section, the packing density of the ternary system of sand - cement - RHA is calculated following the CPM model. The physical properties and particle size distribution (PSD) of these materials are given in Table 5.1.

The packing density α of each constituent material was chosen as indicated in Table 5.2, in which these values of sand, cement and RHA were got from [Jones *et al.* 2002], of SF from [de Larrard and Sedran 1994]. The compaction index for all constituent materials was fixed at 12.5, as suggested by Jones *et al.* [2002].

From the PSD and chosen values of packing density α for each constituent material, the packing density of the ternary system of sand - cement - RHA was calculated. The result is shown in Figure 5.4. It can be seen that the packing density of this granular mixture is optimized at the sand/binder ratio ranging from 0.45 to 0.55. The increase of RHA contents only improves the packing density of the granular mixture when RHA combines with cement. On the contrary, the addition of SF increases the packing density of the ternary system of sand - cement - SF as seen in Figure 5.5. It should be noted that the calculated packing density of the RHA mixture is smaller than that of the SF mixture at a same cement replacement percentage.

Table 5.1 Physical characteristics of materials used in grading design

Property		Material type			
		Sand 0.1-0.3 mm	Cement CEM I 52.5 N	RHA	SF
Relative density, ρ, kg/m^3		2650	3150	2100	2200
Bulk density, ρ_0, kg/m^3		1500	1100	300	500-600
PSD, µm	Mean size, di, µm *	Fraction retained, y_i, % by volume			
630					
500	561.2				
400	447.2	1			
250	316.2	27			
180	212.1	58			
125	150.0	13.4			
90	106.1	0.5			
63	75.3	0.1	1	0.99	
32			13	4.24	0.24
16			30	16.29	0.96
8.0			21	22.67	1.19
4.0			14	24.85	1.35
2.0			8	19.57	0.76
1.0			13	9.75	0.22
0.5				2.65	4.86
0.25					14.37
0.12					34.68
0.06					32.88
0.03					8.50
Mean size, d(50)**		223 µm	13.7 µm	5.6 µm	0.15 µm

(*) $\log(d_i) = 0.5(\log(d_{upper}) + \log(d_{lower}))$

(**) The size for which there is 50 % of the volume of particles passing.

Table 5.2 Packing density of each constituent material

Property	Material type			
	Sand 0.1-0.3 mm	Cement CEM I 52.5 N	RHA	SF
LPM, Packing density, α	0.478	0.388	0.364	0.640
Compaction index, K	12.5	12.5	12.5	12.5

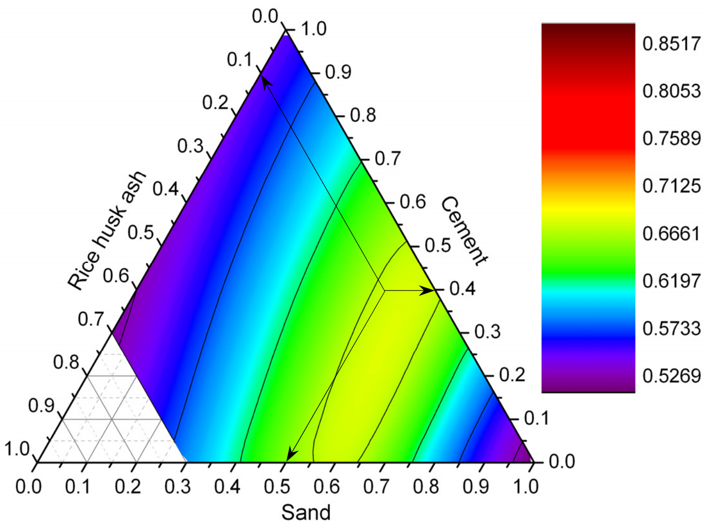

Figure 5.4 Packing density of a ternary system of sand - cement - RHA

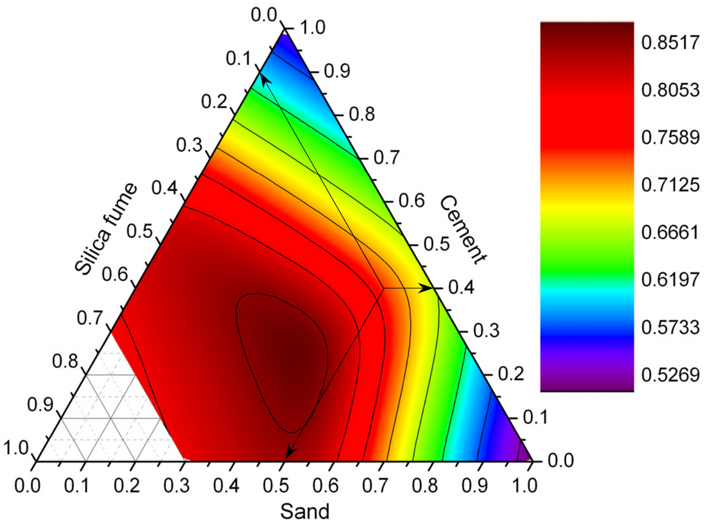

Figure 5.5 Packing density of a ternary system of sand - cement - SF

Experimental method - Mixing energy

The measurement of the maximum packing density of mixture incorporating fine powders (<100 µm) in particular the ultra-fine materials like SF, is difficult because they have a large surface energy and are very susceptible to adhering to one another. Moreover, the packing density of mixtures is also influenced by the conditions (dry, wet, the use of superplasticizer etc.) of the packing structure. Therefore it is important that the maximum packing density of the particles is measured under the same conditions as those in which the particles will be used in concrete and in the model.

With regard to the techniques to determine, the maximum packing density of particles, some common methods have been used, i.e. water demand, proctor test, centrifugal consolidation, rheology measurements, etc. In this study, the method to determine the water demand through mixing energy which was developed by Marquardt [2001] for measuring the maximum packing density was applied. This method was later recommended by Fennis [2008,2011] which was used for measuring the maximum packing density of the fine aggregates (>100 µm). The measurement system and the mixing procedure are shown in Figure 5.6 and Figure 5.7. Each mixture consisted of 1500 grams of powder. The mixing procedure started by mixing the dry powders with a certain amount of total mixing water and a fixed dosage of superplasticizer in a three-litre Hobart mixer for one minute. After two minutes rest and scraping, mixing was continued with a constant water supply of ± 0.3 ml/s until the maximum power consumption was reached. The amount of water in the mixture at the maximum power consumption was used to calculate the packing density.

Figure 5.6 The system to determine the packing density of concrete mixtures by mixing energy

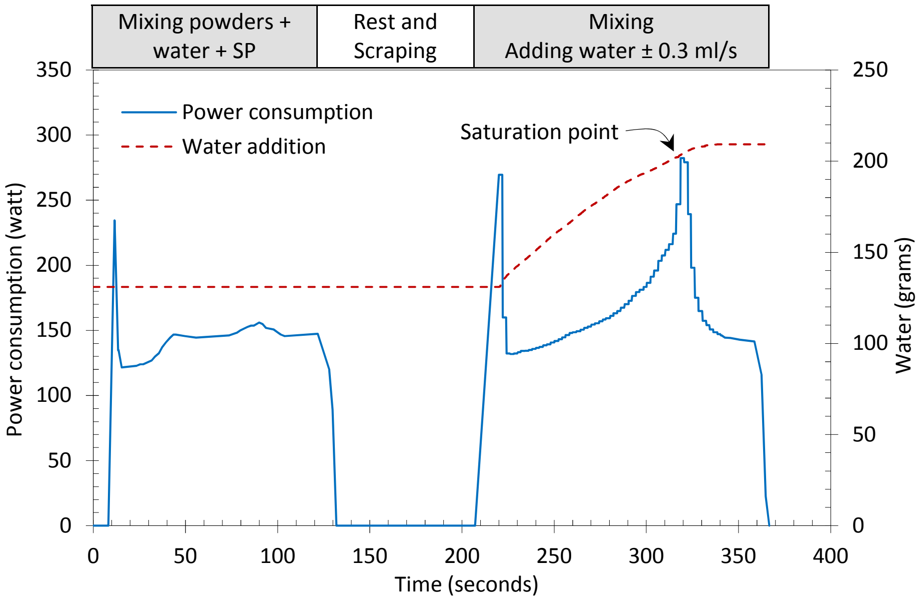

Figure 5.7 Power consumption and water supply during the mixing process of mixture

In this experiment, only 20% cement replacement by SF was chosen. The results of measured and calculated packing densities are shown in Figure 5.8. The calculated values are derived from Figure 5.5. It is clear that both the calculated and measured results give an optimized packing density at the same sand / (sand + cement + SF) ratio of 0.50. From this result, it was suggested that the optimization of packing density of UHPC granular mixtures can be predicted by using the CPM model.

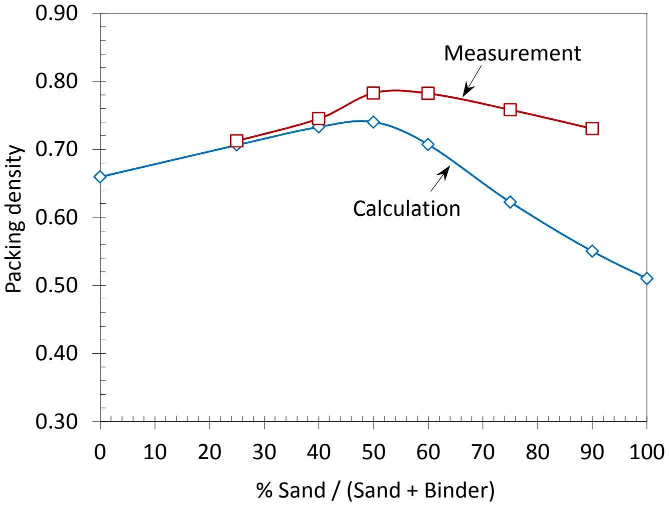

Figure 5.8 Packing density of ternary system of sand - cement - SF, w/b = 0.30, 20% SF

According to the calculated values as seen in Figure 5.4, the optimization of packing density of the ternary system of sand - cement - RHA is obtained at the sand / (sand + binder) ratio of 0.50 and with the RHA contents between 0 and 40%. The similar result can also be seen with the ternary system of sand - cement - SF (Figure 5.5).

5.3.2 UHPC compositions

Based on the results of the optimized packing density of granular mixtures, UHPC mixtures were designed with a sand / (sand + binder) ratio of 0.50. The water to binder (w/b) ratio of the mixtures was fixed at 0.18 by the weight of the binder.

Regarding the effect of the RHA content and the fineness of RHA on the properties of UHPC, UHPC compositions were prepared as given in Table 5.3. Besides, these mixtures were also studied in comparison with those of the control sample and the SF modified samples. The effect of the combination of RHA and SF on the properties of UHPC was also accounted for. The binder herein is a total of the cement and either RHA or SF.

Table 5.3 UHPC compositions used in this study, values calculated by weight

Aspect to be investigated	Amount of cement, kg/m^3	w/b ratio (by weight)	Sand/binder ratio (by weight)	RHA (% by weight)	SF (% by weight)	The mean particle size of RHA (μm)
- Effect of RHA	1140	0.18	1	0	0	
	1010	0.18	1	10	0	5.6
	885	0.18	1	20	0	5.6
	765	0.18	1	30	0	5.6
- Effect of SF	1010	0.18	1	0	10	
	885	0.18	1	0	20	
	765	0.18	1	0	30	
	645	0.18	1	0	40	
- Effect of fineness of RHA	885	0.18	1	20	0	3.6-5.6-6.3-9.0-15.5
- Effect of blend of RHA and SF	885	0.18	1	10	10	5.6
	765	0.18	1	20	10	5.6
	645	0.18	1	30	10	5.6
	530	0.18	1	40	10	5.6
	885	0.18	1	5	15	5.6
	885	0.18	1	15	5	5.6

5.4 Experimental methods

5.4.1 Mixing, workability and casting

All mixtures were prepared in a 20-litre Hobart mixer. The volume of each batch was 3.5 litres. Figure 5.9 shows the mixing procedure.

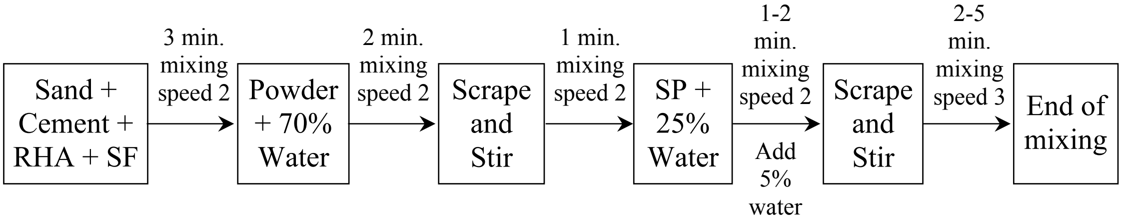

Figure 5.9 Mixing procedure for UHPC

The workability of all mixtures was determined by means of the flow table test [Standards 1998]. The flow values were kept in the range between 210 and 230 mm by using different superplasticizer amounts.

Mixtures were casted into the 40×40×40 mm^3 cubes for compression test. All mixtures were vibrated for 1 minute using a vibrating table with a frequency of 2500 cycles/min.

To study the hydration and the microstructure of UHPC, test samples for ESEM, MIP, TGA investigations were prepared in the same way as those used for cement paste as described in Section 3.2.2.

5.4.2 Curing

After casting, samples were cured in a fog room (20±2°C, RH>95%) for one day. After demoulding, the samples were stored in the fog room until the day of testing.

5.5 Workability of UHPC mixtures

The amount of superplasticizer of mixtures with 0-30% RHA and 0-40% SF for achieving a flow value from 210 mm to 230 mm is shown in Figure 5.10. The figure shows that if more RHA is added, a higher amount of superplasticizer is required. Especially the required amount of superplasticizer increased dramatically with the addition of 30% RHA. This is caused by the porous structure of RHA. A portion of mixing water and superplasticizer will be absorbed in the pores of RHA particles. Therefore, with a same amount of mixing water, a higher required amount of superplasticizer needed to attain a given workability.

It was found that the addition of 10% and 20% SF has a positive effect on the workability of the mixtures. This was explained by the spherical shape of SF particles, which act as a lubricant. However, when more than 20% SF is added, the required amount of superplasticizer increases dramatically to 1.43% and 2.38% for 30% and 40% SF, respectively.

The higher required amount of superplasticizer of mixtures when a higher RHA content is added is caused by the high specific surface area of RHA. For example, the cement CEM I 52.5 N and RHA have specific surface areas of 0.45 m^2/g and about 20 m^2/g, respectively. Therefore, the total surface area of the blend of cement and RHA strongly depends on the RHA content. When 20% cement is replaced by RHA, the total surface area of 1 g of this blend is 4.36 m^2. This value will be almost double, 8.27 m^2/g with 40% RHA. The similar negative effect also occurs with the addition of SF. In addition, RHA has a porous structure which absorbs a certain amount of mixing water. This makes the workability of mixtures worse at a higher RHA content when the total amount of mixing water is kept constant. It is the reason why a very high amount of superplasticizer was needed to compensate for this negative effect to attain a given workability.

Owing to the fact that the addition of 10% SF much improves the workability of UHPC mixture significantly, the total cement replacement level by using the blend of RHA and SF can be further extended, i.e. up to 50% in which the RHA content is 40%, as seen in Figure 5.10.

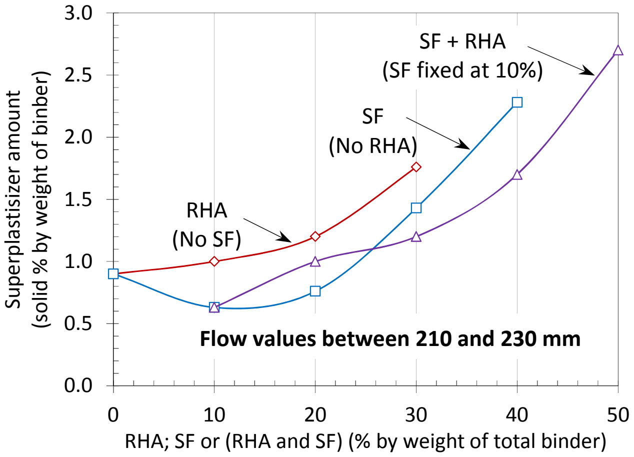

Figure 5.10 Amount of superplasticizer of UHPC mixtures vs. % RHA, % SF or % (RHA+SF), for achieving a constant flow value of mixtures between 210 and 230 mm; w/b = 0.18, $d_{RHAmean}$ = 5.6 µm

It should be noted that the very high amount of superplasticizer used to keep the workability will cause a negative effect on the properties of UHPC mixtures, i.e. delaying the setting. In this respect, the cement replacement percentages of 20% RHA, 30% SF, and 40% blend of RHA and SF, respectively, were considered as the 'maximum' percentages in this study. Higher percentages would result in detrimental effects on the setting of UHPC mixtures.

5.6 Hydration and microstructure formation

In Chapter 3, the effect of RHA on the hydration process and microstructure formation of cement paste with w/b ratios ranging from 0.25 to 0.60 was studied. The results showed the potential of using RHA as a substitute for SF in low w/b ratio cement pastes. This is a very important clue for investigations of using RHA in making UHPC. In this section, the effect of RHA on the hydration process and microstructure formation of UHPC is investigated. It is noted that in this study the w/b ratio of UHPC mixtures was chosen to be very low, i.e. 0.18 compared to that used in cement paste.

5.6.1 Microstructural observations

Figure 5.11 to Figure 5.13 show the BSE images of the control sample with only Portland cement and samples containing RHA and SF.

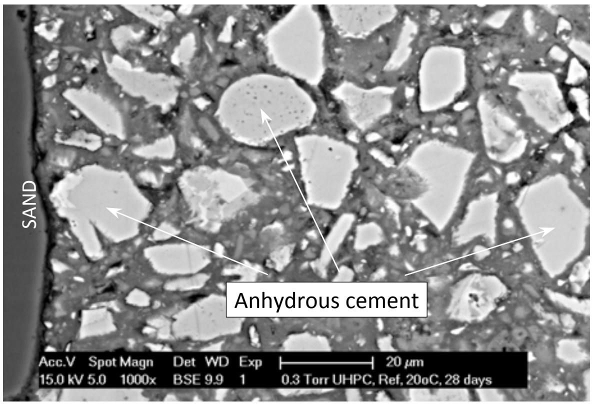

Figure 5.11 BSE image of the control sample at 28 days, w/b = 0.18

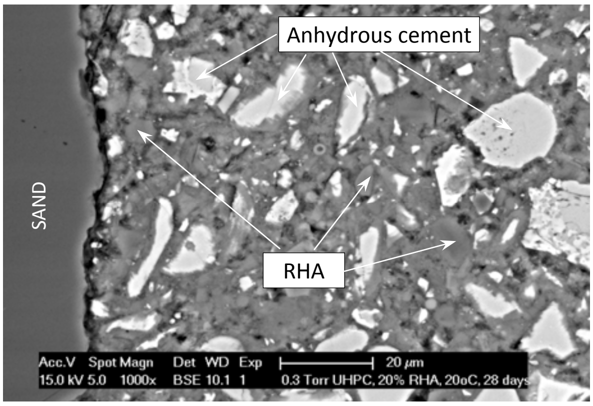

Figure 5.12 BSE image of the RHA modified sample at 28 days, $d_{RHAmean}$ = 5.6 µm, w/b = 0.18, 20% RHA

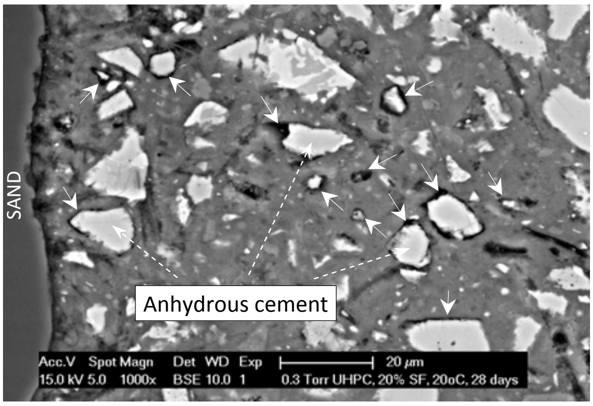

Figure 5.13 BSE image of the SF modified sample at 28 days; white-solid arrows indicate the hollow-shell pores, w/b = 0.18, 20% SF

Normally, in the control paste without either RHA or SF, hollow shells are formed due to the dissolution of cement grains in the early period and become filled with fresh hydration products at a later period [Pratt and Ghose 1983; Scrivener 1989; Kjellsen *et al.* 1997]. Kjellsen et al. [1997] suggested that hollow shells are refilled by CSH in hollow-shell separations outside larger alite particles and the other hydrates, mainly CH, in smaller completely hollow shells. It is observed in this study that the larger hollow-shell pores were found in the SF modified sample only, and not in the control sample or the RHA modified sample. These hollow-shell pores even persist at the later stages. The cement grains formed hollow shells with remnant anhydrous cores, which are marked with arrows (Figure 5.13). Moreover, the smaller hollow-shell pores can be seen clearly in the SF modified sample but not extensively in the control sample or the RHA modified sample.

5.6.2 Degree of hydration of cement in UHPC by image analysis

From the obtained BSE images, the percentage of anhydrous cement in the paste of UHPC and the corresponding degree of hydration of cement was calculated. The results are shown in

Figure 5.14 and Figure 5.15, respectively. In general, the degree of hydration of cement in UHPC samples is relative low, ranging from 0.30 to 0.40 after 91 days. It is noticed that the degree of hydration of cement in the RHA modified sample is increased significantly at later stages; i.e. after 7 days, even higher than that in the SF modified sample at 91 days.

The effect of RHA on the hydration of cement can be explained by the porous structure of RHA. RHA particles may absorb a certain amount of free water into their pores during mixing. On the one hand, this absorbed water lowers the degree of hydration of cement at an early stage because less water is available to react with the cement grains, especially in low w/b ratio mixtures. On the other hand, the pores in RHA particles act as water reservoirs. With the progress of hydration of cement process, the relative humidity in the bulk cement paste drops and the absorbed water in RHA will be released from these reservoirs to promote the hydration of cement and thus the degree of hydration of cement increases further at the later stages (see Figure 5.15). The absorbed water can also increase the pozzolanic reaction of Ca^{2+} with silica ions from RHA inside its cellular spaces [Hwang and Chandra 1997; Lin and Hwang 1997]. Furthermore, the lower concentration of Ca^{2+} caused by the pozzolanic reaction will lead to an enhancement of the hydration of cement.

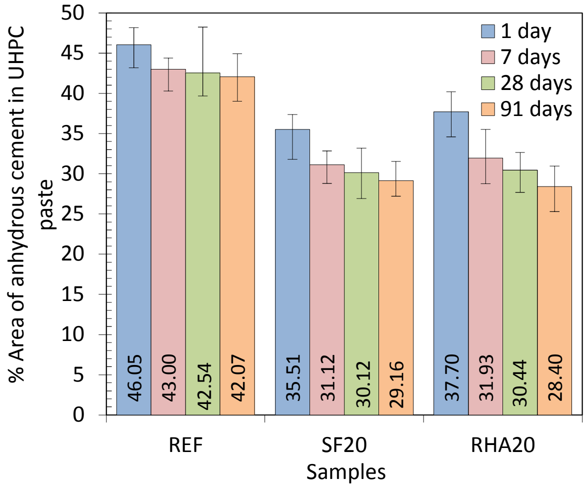

Figure 5.14 Percentage of anhydrous cement area in paste of UHPC at 1, 7, 28 and 91 days, $d_{RHAmean} = 5.6$ µm

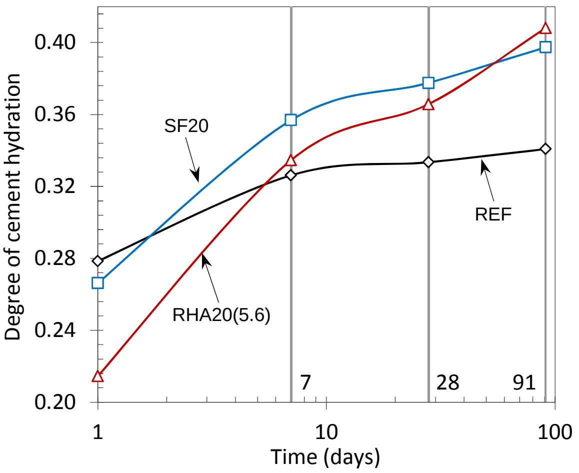

Figure 5.15 Degree of hydration of cement in UHPC over time, $d_{RHAmean} = 5.6$ µm

5.6.3 The thickness of the interfacial transition zone between the sand particles and paste in UHPC

The properties of interfacial transition zone (ITZ) between the cement paste and aggregate have a big effect on the properties of the concrete. Normally, the microstructure of ITZ is partly influenced by the 'wall effect' in the vicinity of aggregate surfaces, and this region may extend some 50 µm from the interface into the cement paste [Maso 1996]. With the addition of mineral admixtures, in particular silica fume, the transition zone decreases markedly in thickness and is more homogeneous and dense [Maso 1996]. In this work, the effect of RHA on the ITZ microstructure in UHPC was studied by examining the SEM images. Following the proposed method to determine the thickness of the ITZ between sand particles and paste in UHPC by considering the change in the grey level in these images in Section 5.2.2, the results of ITZ thicknesses of the control sample, RHA, and SF samples are shown in Figure 5.16.

It can be apparently observed that the thickness of ITZ of the control sample without either RHA or SF is very small, i.e. about 4-5 μm, and the addition of RHA or SF does not influence this ITZ. This is ascribed to the absence of coarse aggregate in UHPC. In this study, sand with particle sizes ranging from 100-300 μm was used as the main aggregate, which strongly reduces the 'wall effect' and the resulting thickness of ITZ. Moreover, with such a small sand particle size and a very small thickness of ITZ, the effect of mineral admixtures such as SF or RHA in reducing the ITZ thickness will not be significant. For this reason, the thickness of the ITZ of all samples obtained in this study was similar and very small.

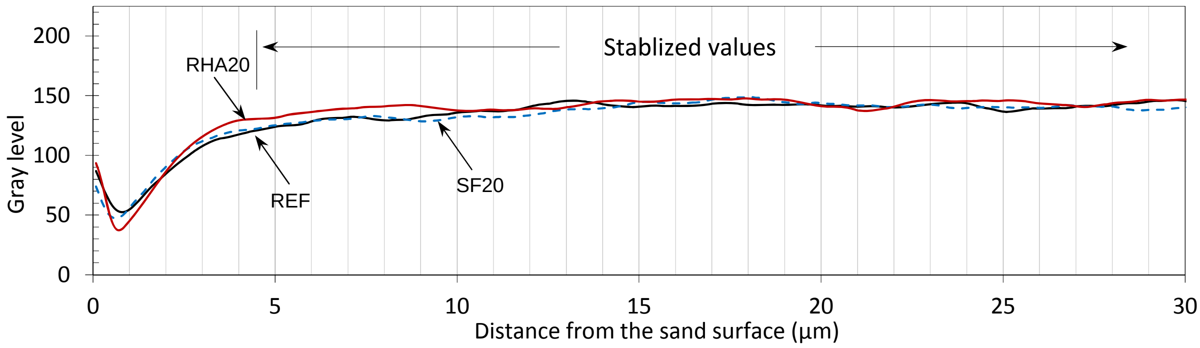

Figure 5.16 Grey level of the interfacial zone between sand and cement paste at 28 days, $d_{RHAmean} = 5.6$ μm

5.6.4 Pore structure

Pore size distribution and total porosity of UHPC samples that were measured by MIP at the ages of 1, 7, 28, and 91 days are provided in Figure 5.17 and Table 5.4. It was found that the first peak of the differential curve, which is called a 'critical pore diameter' [Ye 2003], of the control sample is below 0.04 μm at any age. The addition of RHA gives a pore refinement and a reduction of the total porosity of UHPC due to the filler effect and the pozzolanic reaction of RHA particles. The critical pore diameter of the RHA modified sample decreases from 0.04 μm at 1 day to 0.01 μm at 28 days and to less than 0.01 μm at 91 days.

It can be seen in Table 5.4 that the total porosity of both the RHA and SF modified samples is lower than that of the control sample. Apparently, the total porosity of the RHA modified sample is higher than that of the SF modified sample because both the filler effect and pozzolanic reaction of RHA are less significant than those of the SF modified samples.

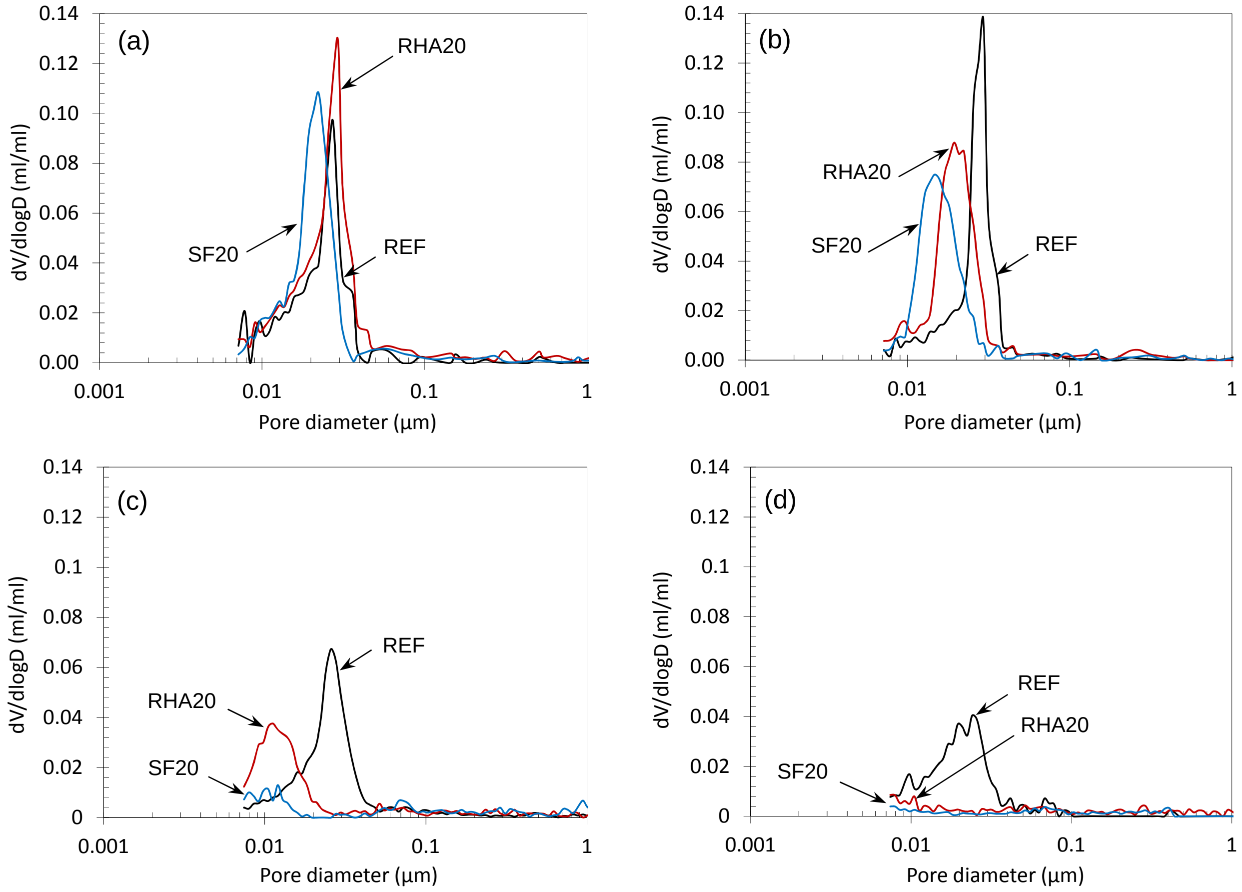

Figure 5.17 Pore size distribution of UHPC samples including sand particles at (a) 1 day, (b) 7 days, (c) 28 days and (d) 91 days, $d_{RHAmean}$ = 5.6 µm

Table 5.4 Porosity of UHPC samples at the different ages from 1 to 91 days

	Porosity of UHPC samples at the different ages, %			
	1 day	7 days	28 days	91 days
REF	11.15	8.13	7.5	6.95
RHA20	10.32	7.63	5.76	4.92
SF20	9.18	6.49	4.55	3.98

5.6.5 The calcium hydroxide content

In this section, the effect of RHA on the reduction of the calcium hydroxide content is evaluated. It was assumed that the silica sand particles are inert. The TGA was performed on ground UHPC samples, in which silica sand particles were included.

Figure 5.18 shows the calcium hydroxide content of UHPC samples over time. It can be seen that the CH content of the control sample increases with time. The addition of both RHA and SF strongly reduce the CH content but the effect of SF is more pronounced than that of RHA at later ages.

The amount of calcium hydroxide in the RHA modified sample was relatively low compared to that in the control sample and the SF modified sample at the early ages up to 7 days. This may be caused by the low degree of hydration of cement in the RHA modified sample (see Figure 5.15) because RHA absorbs a certain amount of mixing water and thus less water is available in the system for cement to react. This leads to a small amount of CH generated from cement hydration and a slow pozzolanic reaction of RHA. The CH content in the RHA modified sample decreases significantly after 7 days. Compared to the SF, the reactivity of the RHA appears less significant at later ages. For example, the addition of RHA gives reductions of 45% and 65% of the calcium hydroxide content in UHPC at the ages of 28 and 91 days, respectively. These corresponding CH reduction values in the SF modified sample are 70% and 90%. This can be attributed to the difference in their amorphous SiO_2 content and particle characteristics, which was also suggested by Zhang *et al.* [1996].

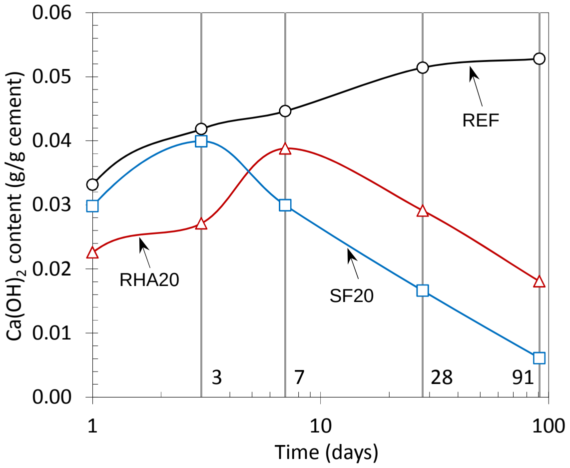

Figure 5.18 Amount of calcium hydroxide in UHPC samples over time, $d_{RHAmean}$ = 5.6 µm

5.7 Compressive strength

As mentioned in Chapter 1 and 2, UHPC is defined worldwide as concrete with a compressive strength of at least 150 MPa. Therefore, compressive strength is a very important issue to evaluate the possibility of using RHA in producing UHPC. In this section, the effect of RHA, in combination with or without SF, on the compressive strength of UHPC is studied.

5.7.1 Effect of RHA contents

The results of the workability of UHPC mixtures in Section 5.5 show that the maximum contents of RHA and SF used to meet the requirement of the flowability of UHPC mixtures were 20 and 30%, respectively. These contents are considered as maximum values to study the effect of RHA and SF on the development of the compressive strength of UHPC. The results are shown in Figure 5.19. It can be seen that the addition of RHA increases the compressive strength of UHPC compared to that of the control sample. Besides, at a high cement replacement level, the compressive strength of the RHA modified samples is even slightly higher than that of the SF modified samples at later ages.

It is also noticed that at a high cement replacement level, i.e. 20%, the compressive strength of the RHA modified sample is low at early ages but high at high ages. This may be caused by the lack of a portion of the mixing water which is absorbed in RHA for the cement to hydrate at the early ages. This leads to a low compressive strength of the RHA modified sample compared to that of the control sample at 3 and 7 days. However, with progress of the hydration process, the relative humidity in the mixture drops and the absorbed water in RHA will be released to the surrounding of the cement matrix to promote the hydration of cement and thus increase the compressive strength of UHPC at later ages.

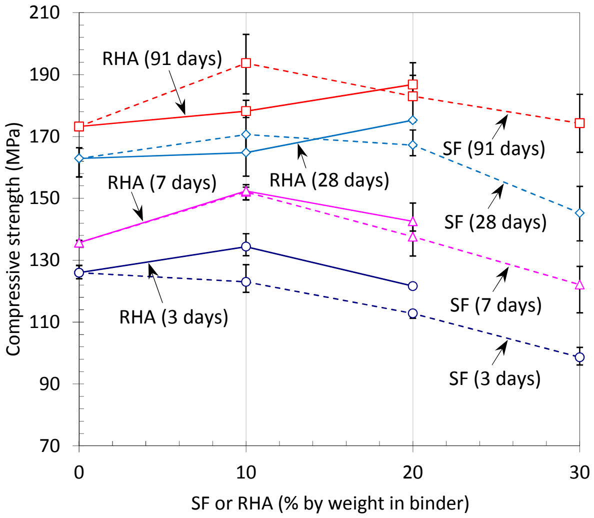

Figure 5.19 Compressive strength of UHPC samples vs. % SF (dotted line) or % RHA (solid line), w/b = 0.18, $d_{RHAmean}$ = 5.6 µm

On the contrary, the compressive strength of SF modified samples is highest with 10% SF content. The addition of higher SF contents, especially beyond 20%, gives a reduction to the compressive strength of UHPC. This is due to the fact that using over 20% SF might cause the agglomerates due to the very large specific surface of SF. Increasing the superplasticizer content to lubricate the SF particles and to break the agglomerates in this case, i.e. over 20% SF, is difficult because the water content used in UHPC is very limited. It reduces the positive effects of SF in terms of filler- and pozzolanic- effects in UHPC and results in a reduction of the compressive strength of SF modified samples.

5.7.2 Effect of fineness of RHA

As discussed in Chapter 1 and Chapter 2, the fineness is one of the most important properties of RHA which relates to both the physical - and the chemical - effects, i.e. the porous structure, the filler effect, the pozzolanic reaction of RHA, the grinding energy, and the workability of the mixture. This was demonstrated in Chapter 3 and the RHA particle size of 5.6 µm was found to be 'optimal' in terms of the specific surface area, the pozzolanic activity, and the pore structure of the RHA modified paste. In this section, the effect of the RHA fineness on the workability and the compressive strength of UHPC mixtures was studied. The cement replacement percentage was fixed at 20%. Five types of RHA with the different mean particle sizes from 3.6 µm to 15.5 µm were chosen as used in experimental studies in Chapter 3.

Table 5.6 shows the required amount of superplasticizer of UHPC mixtures for achieving a flow value from 210 to 230 mm. It can be seen that the fineness of RHA strongly influences the workability of UHPC mixtures. The mixture using the RHA with the mean particle size of 15.5 µm requires a very high amount of superplasticizer (higher 4% solid by weight of binder). However, this amount dramatically reduces when the mean particle size of RHA decreases from 15.5 µm to 9.0 µm. Mixtures using RHA with a mean particle size of less than 6.3 µm require a similar amount of superplasticizer. It should be noted that in the size range from 5.6 µm to 15.5 µm, the specific surface area of RHA increases but the total pore volume and the average width of pore decreases (Table 5.5). This means that the grinding process may only separate the particles through the big pores. This increases the surface outside of the RHA particles and does not significantly collapse the porous structure of RHA particles as illustrated in Figure 5.20. Intensive grinding will partly collapse the porous structure of RHA (see Figure 5.20c). This results in a reduction of specific surface area and total pore volume of RHA (Table 5.5) and a lower required amount of superplasticizer for the RHA mixture. This change can be seen when the mean particle size of RHA decreases from 5.6 to 3.6 µm in Table 5.6.

Table 5.5 Properties of different types of RHA relating to their pore structure

Property	Different types of RHA				
Mean particle sizes, µm	3.6	5.6	6.3	9.0	15.5
Specific surface area (BET nitrogen absorption), m^2/g	15.0	20.6	19.7	18.3	13.4
Average pore width (BJH absorption)	18.12	20.94	-	23.73	26.49
Total pore volume, cm^3/g	0.0610	0.0863	-	0.0876	0.0975

Table 5.6 The required amount of superplasticizer used in UHPC mixtures, % solid by weight of binder

The RHA modified mixtures					The SF modified mixture	The control mixture
RHA3.6	RHA5.6	RHA6.3	RHA9.0	RHA15.5		
0.89	1.15	1.20	1.75	> 4.00	0.76	0.90

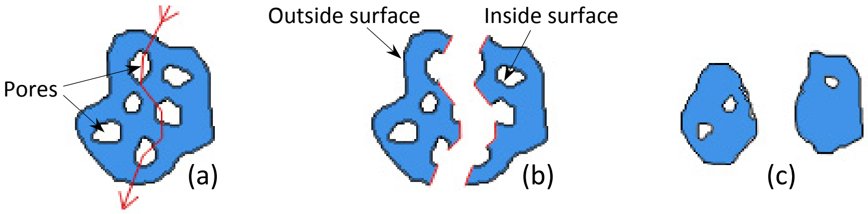

Figure 5.20 Different stages of grinding for the RHA particles: (a) original, (b) ground without collapsing the porous structure, and (c) ground with collapsing the porous structure

From the result of the workability of the RHA modified mixtures, the RHA with the mean particle size of 15.5 µm was not used in the study of the packing density and the compressive strength development of UHPC. This is due to the fact that the mixture containing this RHA required a very high amount of superplasticizer.

Figure 5.21 shows the result of the measured packing density of the UHPC mixtures containing 20% RHA with different mean particle sizes from 3.6 µm to 9.0 µm. It is clear that the addition of the finer RHA improves the packing density of the UHPC mixtures. It is noticed that the measured packing density value of the RHA modified mixtures is closer to that of the SF mixture compared to the calculated values (see Figure 5.4, Figure 5.5, and Figure 5.22). This could be due to the assumption in the calculation that the particle size of SF is very small, i.e. 0.15 µm. However, in fact these SF particles are easy to make agglomerates to become 'big particles' in the presence of water, which reduces the filler effect of SF in the mixture.

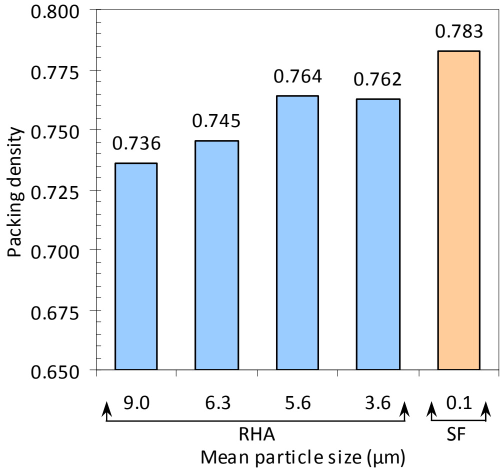

Figure 5.21 The measured packing density of the UHPC mixtures containing 20% RHA with different mean particle sizes from 3.6 µm to 9.0 µm, w/b = 0.18

The effect of the fineness of RHA on the compressive strength of UHPC over time is shown in Figure 5.23, in which the numbers indicate the different mean RHA particle sizes.

It can be seen that the compressive strength of UHPC increases with decreasing of the mean RHA particle size. The development of the compressive strength of the RHA6.3 sample is similar to that of the control sample after 7 days. The compressive strength of these two samples was over 150 MPa at the age of 28 days. In addition, the development of the compressive strength of the RHA modified samples is larger than that of the SF modified sample when the mean particle size of RHA is smaller than 5.6 µm especially with the mean particle size of 3.6 µm. The higher compressive strength of the RHA3.6 sample compared to that of other samples is possibly due to the better filler effect (see Figure 5.21) and the internal water curing of RHA. The porous structure of RHA with the mean particle size of 3.6 µm may be collapsed as discussed above. However, this collapse may not occur completely and a part of the porous structure of RHA still remains as illustrated in Figure 5.20c. This allows RHA to absorb a portion of the mixing water albeit that this amount of absorbed water is less than that of other RHAs. This absorbed water promotes the hydration of cement and contributes to a higher compressive strength of the RHA3.6 sample.

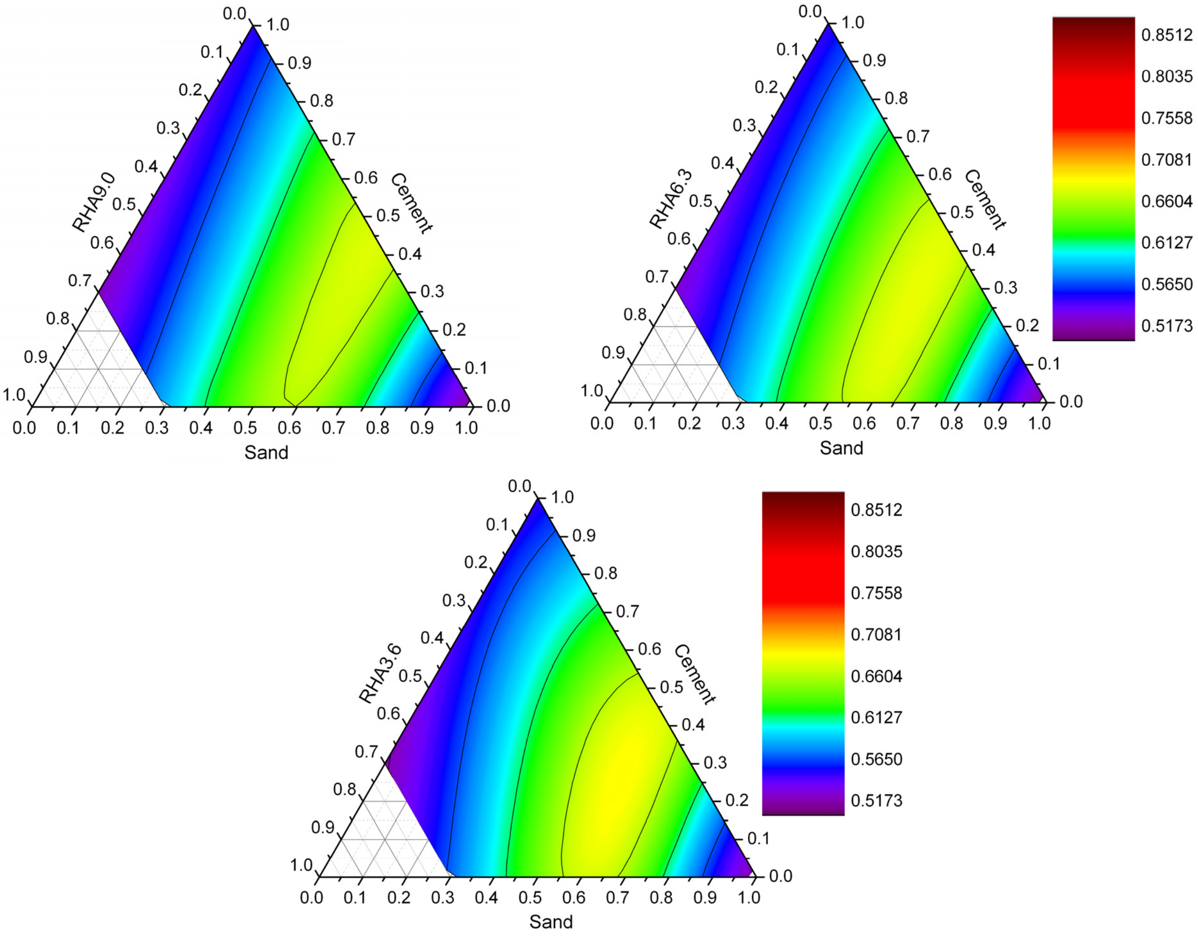

Figure 5.22 The calculated packing density of the ternary system of sand - cement - RHA with different mean particle sizes of RHA of 3.6, 6.3, and 9.0 µm

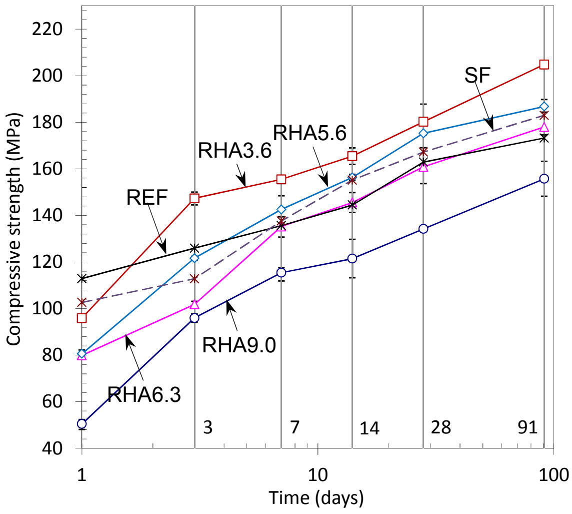

Figure 5.23 Development of the compressive strength of UHPC samples over time; 20% cement replacement by either RHA or SF; the numbers indicate the different mean particle sizes of RHA; w/b = 0.18

It should be noted that the mixture containing the coarser RHA requires a higher amount of superplasticizer. This may be due to the fact that the coarser RHA contains more big pores and absorbs a higher amount of mixing water than the fine RHA. In addition, although the flow value of mixtures was kept between 210 mm and 230 mm, the RHA modified mixtures with the mean particle size beyond 6.3 µm was observed to be difficult to cast. With regard to the grinding energy consumption, this energy cost increases dramatically from 3 to 7.5 kWh/kg when the mean size of RHA particle reduces from 5.6 µm to 3.6 µm. Therefore, the reasonable mean size of RHA used to make UHPC was proposed to be in the range between 5.6 and 6.3 µm in terms of energy consumption, the workability, and the compressive strength of UHPC mixtures.

5.7.3 Effect of a combination of RHA and SF

Based on the results of the workability experiments with UHPC mixtures, it was recognized that the addition of a small amount of SF, i.e. 10%, can improve the workability of the RHA modified mixtures. This can increase the total amount of the cement replacement up to 40%. Therefore, in this section, the effect of a combination of RHA and SF on the compressive strength of UHPC was investigated, in which SF was fixed at 10%. The result is shown in Figure 5.24.

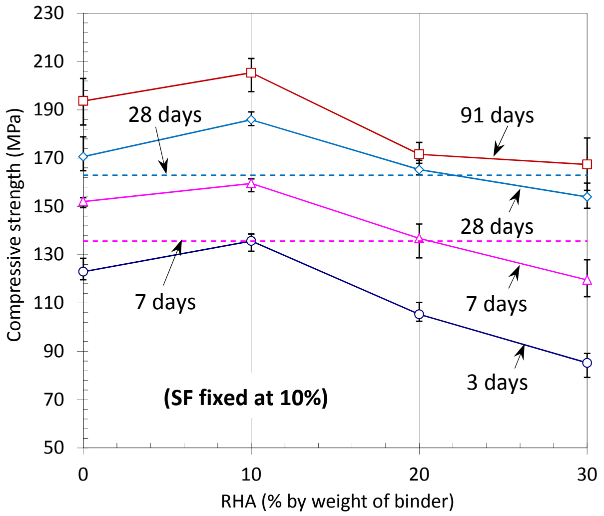

Figure 5.24 Compressive strength of UHPC samples vs. % RHA (solid line); the control sample (dotted line), the SF content was fixed at 10%, w/b = 0.18, $d_{RHAmean}$ = 5.6 µm

It is observed that the compressive strength of UHPC containing up to 10% RHA is higher than that of the control sample. Beyond this amount, the addition of RHA decreases the compressive strength of UHPC. However it is noticed that the 28-day compressive strength of all samples was in excess of 150 MPa. This shows the benefit of using RHA in combination with SF to make UHPC, which is that the RHA content can increase up to 30% by weight and the total cement replacement percentage can reach to 40% in this case.

Interestingly, as presented in Figure 5.24, the compressive strength of the UHPC sample using the blend of 10% RHA and 10% SF can attain 185 MPa and 205 MPa at the ages of 28 days and 91 days, respectively. The UHPC sample containing this combination shows a higher compressive strength than those of the control sample and of samples using other blends. There must be a synergic effect between RHA and SF on the compressive strength of UHPC.

To further investigate this effect, the total cement replacement percentage by the combination of RHA and SF was kept at 20% and SF was replaced by RHA from 0 to 100%. The compressive strength of UHPC samples versus the RHA/(RHA + SF) ratio is shown in Figure 5.25.

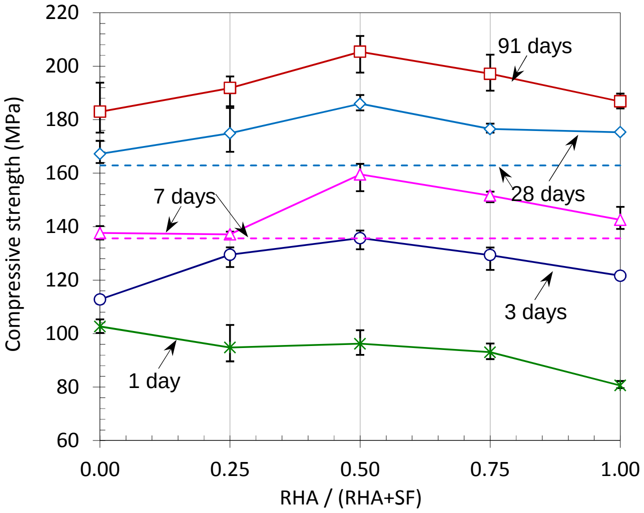

Figure 5.25 Compressive strength of UHPC samples vs. the RHA/(RHA+SF) ratio (solid line); the control sample without either RHA or SF (dotted line) at the ages from 1 day to 91 days, w/b = 0.18, $d_{RHAmean}$ = 5.6 µm

It is clear that using the combination of 10% RHA and 10% SF gives a synergic effect on the compressive strength of UHPC. It seems that the addition of a higher amount of SF shows a greater effect on the compressive strength of UHPC at a very early age, i.e., at 1 day, whereas the effect of the addition of RHA is larger at later ages, i.e., after 3 days. This can be explained by the better packing density of the granular mixture (Section 5.3.1) and the higher degree of hydration of cement (Section 5.6.2) to improve the compressive strength of UHPC with the addition of SF at early ages. However, at later ages the positive effect of internal water curing of RHA is significant as discussed in the previous section (Section 5.7.1).

5.8 Autogenous shrinkage

As discussed in Chapter 2, UHPC has large shrinkage values. However unlike normal concrete, autogenous shrinkage makes a large portion of the total shrinkage in UHPC. This is due to the very low w/b ratio and the very high amount of SF used in UHPC which causes a high self-desiccation during the hydration of cement progress. Nearly all the researchers who are studying chemical shrinkage, relative humidity changes and pore water pressure in low w/b ratio systems have drawn the identical conclusion: a major reason for the early-age cracking sensitivity of High-Strength and High-Performance Concrete (HSC/HPC) is self-desiccation, which is extremely pronounced in mixes with a low w/b ratio resulting in increased autogenous shrinkage [Kovler and Jensen 2007]. In this respect, internal curing is considered an effective solution for the shrinkage and mechanical behaviour for the low permeability of low w/b ratio systems.

The analysis from Chapter 2 in combination with experimental results in Chapter 3, as well as the result tests of the compressive strength of UHPC in this chapter proved a positive effect of RHA on the hydration of cement and the compressive strength at later ages. Based on these results, it was suggested that RHA may act as an internal water curing agent for UHPC. This is very important for the use of RHA in making UHPC, in which RHA has a potential to mitigate the autogenous shrinkage of UHPC and to improve the compressive strength of UHPC. The possibility for using RHA to mitigate autogenous shrinkage of UHC is the objective of this section.

5.8.1 Method and compositions

The autogenous shrinkage of UHPC mixtures was measured following the ASTM C1698 standard [ASTM Standard 2009], in which three sealed corrugated moulds of 440 mm Ø28.5 mm were determined for each mix composition. After preparing and mixing, each mixture was carefully filled into three sealed corrugated tubes. The apparatus used to measure the autogenous shrinkage is shown in Figure 5.26. According to this standard, the length of samples is started measuring at the time of the final setting of the mixture. All samples and the dilatometer were kept in a thermostatically controlled room during the whole test. The surrounding temperature was maintained at 23±1°C.

The mix compositions used to determine autogenous shrinkage of UHPC are given in Table 5.7.

Figure 5.26 The dilatometer bench with accessories used to determine autogenous shrinkage of UHPC mixtures

Table 5.7 Mix compositions of UHPC used to study autogenous shrinkage

Mixture	Amount of cement, kg/m^3	w/b ratio (by weight)	Sand/binder ratio (by weight)	RHA (% by weight)	SF (% by weight)	The mean particle size of RHA (µm)
REF	1140	0.18	1	0	0	
RHA10(5.6)	1010	0.18	1	10	0	5.6
RHA20(5.6)	885	0.18	1	20	0	5.6
SF10	1010	0.18	1	0	10	
SF20	885	0.18	1	0	20	
RHA20(9.0)	885	0.18	1	20	0	9.0
RHA20(3.6)	885	0.18	1	20	0	3.6

5.8.2 Effect of RHA contents

Figure 5.27 and Figure 5.28 show the curves for the development of autogenous shrinkage of UHPC containing different amounts of RHA and SF, respectively, versus time. Generally, the autogenous shrinkage of all samples is very high at a very early age, particularly in the first twelve hours from the final set time, and then remains more or less constant afterwards.

When a higher amount of RHA is added, i.e. 20%, the autogenous shrinkage of UHPC is significantly reduced compared to the control sample without RHA. After the first twelve hours from the final set, the RHA modified samples show only a very small increase in autogenous shrinkage. In addition, after reaching the age of 10 days, the autogenous shrinkage of the RHA modified samples was further mitigated. Especially the autogenous shrinkage of the 20% RHA modified sample was even completely eliminated after 15 days. Meanwhile, the autogenous shrinkage of SF samples increases with increasing of SF content as discussed in Section 2.1.8.

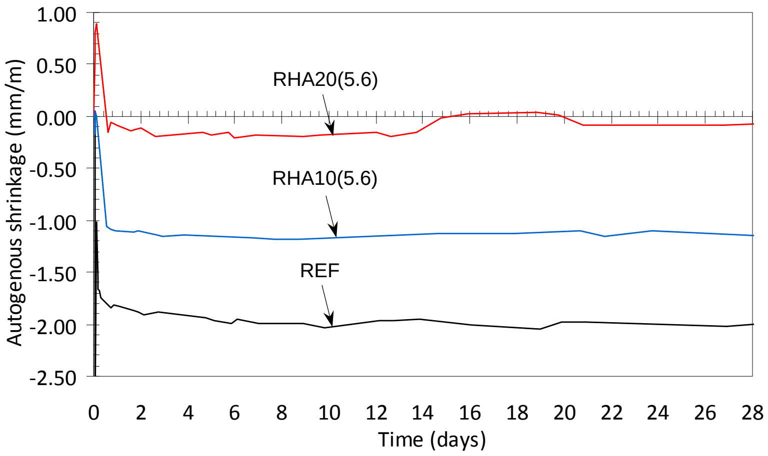

Figure 5.27 Autogenous shrinkage of UHPC mixtures containing different amounts of RHA measured from the final setting time, $d_{RHAmean}$ = 5.6 µm, w/b = 0.18

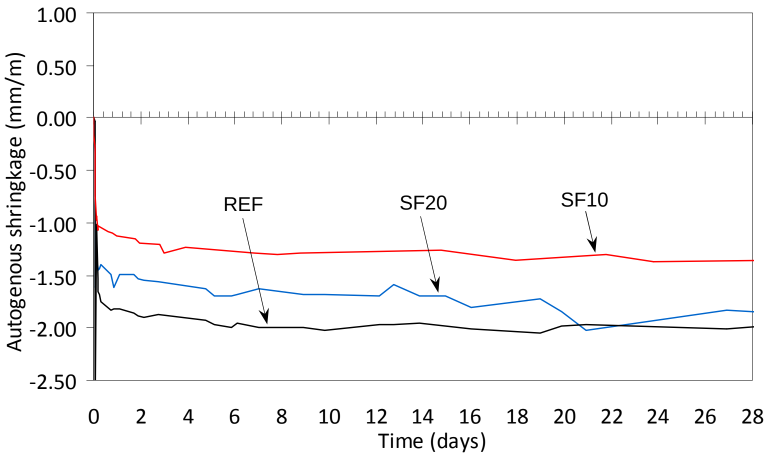

Figure 5.28 Autogenous shrinkage of UHPC mixtures containing different amounts of SF measured from the final setting time, w/b = 0.18

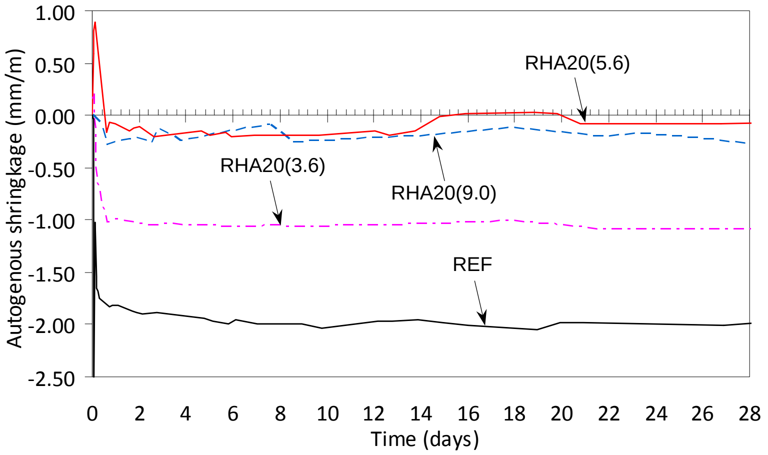

Figure 5.29 Autogenous shrinkage of UHPC mixtures containing RHA with different mean particle sizes measured from the final setting time, w/b = 0.18

5.8.3 Effect of fineness of RHA

The mitigation of autogenous shrinkage of UHPC was proposed by the internal water curing of RHA, which in turn depends on the porous structure of RHA. As discussed in Section 5.8.2, the porous structure of RHA is influenced by the degree of grinding. At a certain degree of grinding, the porous structure of RHA can be collapsed. Therefore, the effect of the fineness of RHA on autogenous shrinkage should be evaluated. The result is depicted in Figure 5.29. It is clear that RHA particles are particularly effective in mitigating the autogenous shrinkage of UHPC when the mean size of RHA particles ranges between 5.6 µm and 9.0 µm. The sample containing the RHA with a smaller particle size, i.e. 3.6 µm, shows a higher autogenous shrinkage. This may be caused by the collapse of the porous structure as mentioned in Section 5.7.2, which reduces the amount of the absorbed water in RHA. The less absorbed water will reduces the positive effect of RHA particles to mitigate the autogenous shrinkage of UHPC. This result implies that the benefit of RHA on reducing the autogenous shrinkage can be achieved when the mean particle size is bigger than 5.6 µm.

5.8.4 Discussion

In this section, the discussion is separated into three aspects including the effect of RHA on (1) the hydration process and microstructure formation of UHPC, (2) the compressive strength development of UHPC, and (3) the autogenous shrinkage of UHPC. The detail of the discussion of these aspects can be seen as follows:

1) Effect of RHA on the hydration process and microstructure formation of UHPC

Because the addition of RHA increases the degree of hydration of cement at later ages (Figure 5.15), it may be attributed to the porous structure of RHA particles as discussed earlier. The mechanism is proposed to be similar to the suggestion from Weber and Reinhardt [1997] and Van Breugel *et al.* [1999] when using the water-saturated lightweight aggregates (LWA) and from Jensen and Hansen [2001,2002] when using superabsorbent polymer (SAP) particles for internal curing of concrete. The effect of RHA on the mitigation of autogenous shrinkage of cement paste [de Sensale *et al.* 2008] and of UHPC in this study also supports this idea.

In sum, the experimental results suggest the internal water curing of RHA in UHPC. The further discussion can be seen in the next discussion section of the effect of RHA on autogenous shrinkage of UHPC. However, more studies are needed in this aspect to show whether this holds.

One of the other interesting features is that the hollow-shell pores, especially the larger hollow-shells, mainly appear in the SF modified sample, not in the control sample or the RHA modified sample. This can be explained in several ways. Normally, in the control paste without either RHA or SF, hollow shells are formed by the dissolution of cement grains at the early period and become filled with fresh hydration products at a later period [Pratt and Ghose 1983; Scrivener 1989; Kjellsen *et al.* 1997]. Kjellsen *et al.* [1997] suggested that hollow shells are refilled by C-S-H in hollow-shell separations outside larger alite particles and by the other hydrates, mainly calcium hydroxide (CH), in smaller completely hollow shells. However, in the systems containing SF, this is observed to a much lower extent and many hollow shells may persist also at later ages. Possibly, this may be caused by the fact that there are a large number of ultra-fine SF particles with a mean size of 0.1 µm, i.e. about 100,000 particles [Chatterji *et al.* 1982], attached around each cement particle. Clearly, this number depends on the size of the cement and SF particles, the w/b ratio, and the SF content in the mixture. However, this creates a dense SF layer to constrain both water to percolate through this layer to hydrate the cement cores, and ions from the cement cores to migrate outward to the pore solution. The resistance to these flows of water and ions would increase with an increase in the thickness of the SF layer, i.e. with a very low w/b ratio of UHPC. It means that the refilling process of hydration products in previous established hollow shells of larger alite particles formed in the SF system will be delayed and remain at the later period. Additionally, the highly reactive SF particles available in the whole system will consume CH generated from cement hydration, which reduces the refilling ability of CH in smaller completely hollow shells formed previously. This result is also very similar with that observed by Kjellsen and Atlassi [1999].

In the RHA modified system, RHA particles with the size of about 5.6 μm are as about one-third smaller than those of cement particles but fifty times bigger than that of SF particles, and thus distribute randomly in the system rather than contact the surface of cement particles (Figure 5.12). Besides, it can be observed that the degree of hydration of cement in the RHA system is relatively low compared with that of the control sample up until 7 days (Figure 5.15) and the pozzolanic reaction of RHA is slow (Figure 5.18). This leads to an assumption that the microstructure development of cement in the RHA modified sample is similar to that of the control sample. Although the pozzolanic reaction of RHA is significant after 7 days (Figure 5.18), the degree of hydration of cement is not much increased, especially from 14 days to 28 days (Figure 5.15). Therefore, the larger hollow-shells in the RHA modified sample may be refilled by CSH as in the control sample. The only presumably different feature is that some smaller completely hollow shells may not be entirely refilled because of the lack of CH phases due to the pozzolanic reaction of RHA.

2) Effect of RHA on the compressive strength development of UHPC

Regarding the compressive strength of the RHA modified sample, the experimental results (Figure 5.19) show the positive effect of RHA on increasing the compressive strength of UHPC at later ages. It should be noted that only normal curing conditions were applied in this study. The pozzolanic reaction is thus not enhanced strongly compared with the elevated temperature curing condition and the hydration of cement at a very low w/b ratio is a slow process in early ages. In this respect, the improvement of the compressive strength of UHPC by using RHA may be explained by the enhancement of the packing density of granular mixtures, the internal water curing of RHA, and the lower effective w/b ratio of the RHA mixture.

One of the most important principles of making UHPC is the optimization of the particle packing of granular mixtures [Richard and Cheyrezy 1995], especially with the normal curing applied in this study. In fact, because the degree of hydration of cement in this concrete is relatively low (Figure 5.15), the filler effect of mineral admixtures, such as SF which was found by Detwiler and Mehta [1989], is primarily responsible for the strength improvement in low w/b ratio mixtures. In this respect, the substitution of cement by RHA with a smaller particle size will improve the packing density of the granular mixture and thus increase the resulting compressive strength of UHPC. This leads to a higher compressive strength of the RHA modified sample compared to that of the control sample at a same degree of hydration of cement but the results show a lower compressive strength of the RHA modified sample in the early ages, i.e. before 7 days (Figure 5.19). This is ascribed to less available water in the system for the cement to hydrate because RHA absorbs a certain amount of water during mixing. However, this absorbed water, as discussed above, will promote the hydration of cement at later ages and thus increase the compressive strength of UHPC. In addition, the higher compressive strength of the RHA modified sample can possibly be attributed to a reduction of the effective w/b ratio in the RHA mixture, as a portion of free water is adsorbed by RHA and retained in its pores [Sugita *et al.* 1997].

It is noticed that the development of the compressive strength of the RHA is even slightly higher than that of the SF modified sample at later ages, i.e. beyond 3 days. This is achieved despite the fact that the RHA particles are less suitable to obtain a very dense packing and these particles are less reactive than SF particles. Similar results were also obtained by Zhang *et al.* [1996]. This seems consistent with the MIP (Figure 5.17) and the TGA (Figure 5.18) results, in which SF provides a more significant pore refinement and consumes more $Ca(OH)_2$, respectively, than RHA does. Therefore, this larger improvement of the compressive strength of UHPC by adding RHA is suggested by the contribution of the internal water curing of RHA and the lower effective w/b ratio of the RHA mixture compared to that of the SF mixture. In addition, it should also be noted that the positive effects of SF have been concerned with the technical point of view. For example, the ultra-fine SF particles easily exhibits agglomerates even up to several hundreds of micrometres in diameter [Mitchell *et al.* 1998]. This reduces the positive effect of SF not only on the optimization of the packing density of granular mixtures, but also on the pozzolanic reaction of SF. Secondly, the addition of SF causes a high volume of hollow-shell pores in the system and these hollow shells cannot be recorded from the intrusion of mercury because of the ‘ink-bottle’ effect [Kjellsen and Atlassi 1999]. Kjellsen and Atlassi [1999] suggested that the porosity constituted by hollow shells may represent approximately 20% of the total porosity when the mixture contains 10% SF and a w/b ratio of 0.25. It means that SF still has some drawbacks, which influences its roles in improving the properties of UHPC in comparison with RHA.

3) Effect of RHA on the autogenous shrinkage of UHPC

The above results show the positive effect of using RHA on mitigating autogenous shrinkage of UHPC. Besides, the reduction of autogenous shrinkage of UHPC by using RHA is not only a proof of the effectiveness of internal water curing, it is also a potential in the beneficial practical consequence.

Normally, at a low w/b, the available water will be consumed rapidly (a few days maximum), and water from the RHA particles will then be thought to be consumed. In the other studies [Zhutovsky *et al.* 2004; Mechtcherine *et al.* 2008], the water is stored in particles, i.e. LWAs and SAPs, which are several orders of magnitude larger, and might be expected to retain water over a significant time-scale. In the case of RHA, with such a small particle size, the water from RHA will probably be available very quickly, and may also become exhausted in a few days. However, in fact, the experimental results provided evidence that the internal water curing of RHA still remains effective at later ages. This can be explained by several reasons as below.

The specific pore volume of ground RHA with a mean particle size of 5.6 μm is approximately 0.086 cm^3/g. It is assumed that the water will fill all these pores. Theoretically because 20% RHA was added corresponding to about 220 kg RHA/m^3 concrete, the total absorbed water by RHA is about 18.9 l/m^3 UHPC. The extra water for internal curing of UHPC by super-absorbent polymers (SAP) ranges from 33 - 64 l/m^3 UHPC [Mechtcherine *et al.* 2008]. Thus, the absorbed water in RHA in UHPC is also significant. In addition, the distribution of water reservoirs also plays an important role for internal curing because it relates to the effective distance for transporting water to the vicinity of these water reservoirs [Kovler and Jensen 2007]. At a lower w/b ratio in particular for UHPC, the microstructure of cement paste is very dense which constrains the water from reservoirs to migrate to the surroundings. This means that the water reservoirs should be separated into smaller ones to enhance the effectiveness of using internal curing agents in the system. In this respect, RHA is an appropriate candidate.

The size of pores in RHA particles, i.e. from 5 to 60 nm in diameter (see Figure 5.30), is much smaller than that of SAP particles which is about 450 µm [Mechtcherine *et al.* 2008] and that of LWAs (about 10-20 µm [Zhutovsky *et al.* 2004]). According to Kelvin's equation [Lura *et al.* 2003], this size range of pores in RHA particles corresponds to the change of relative humidity (RH) in the cement matrix from 81.9 to 98.0%. The effectiveness of water released from inside of the pores of RHA particles to the surrounding cement matrix depends on the suction force, which in turn depends on the porosity and RH in cement paste [Kovler and Jensen 2007]. At early ages, the RH in the cement paste with a w/c ratio of 0.25 is still higher than 87%, which corresponds to the RHA pore diameter of 8.5 nm, before 7 days [Wittmann 1969]. Thus only water in the big pores, i.e. about 8.5 nm in diameter, of RHA particles can be released. A certain amount of water still remains in the smaller pores and gradually releases at later ages, even after 28 days at which the RH decreases to 78% [Wittmann 1969]. This process is illustrated in Figure 5.32.

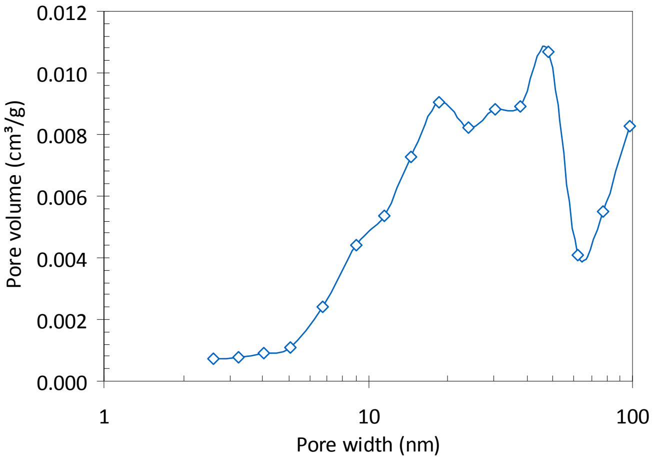

Figure 5.30 Pore size distribution of the RHA powder, $d_{RHAmean} = 5.6$ µm

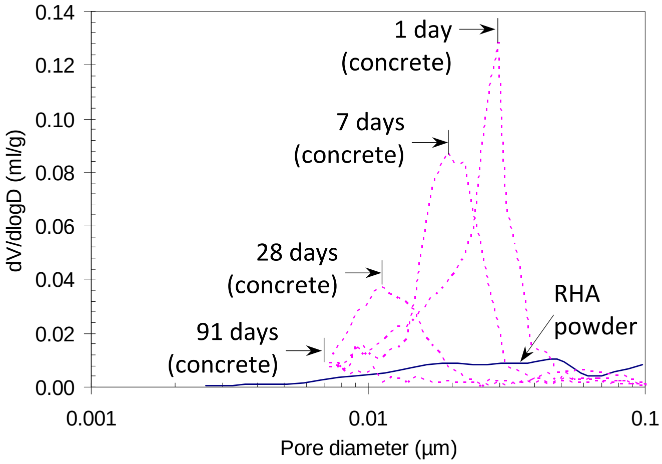

Figure 5.31 Pore size distribution of RHA modified samples including sand particles at (a) 1 day, (b) 7 days, (c) 28 days and (d) 91 days, and of the RHA powder, $d_{RHAmean} = 5.6$ µm

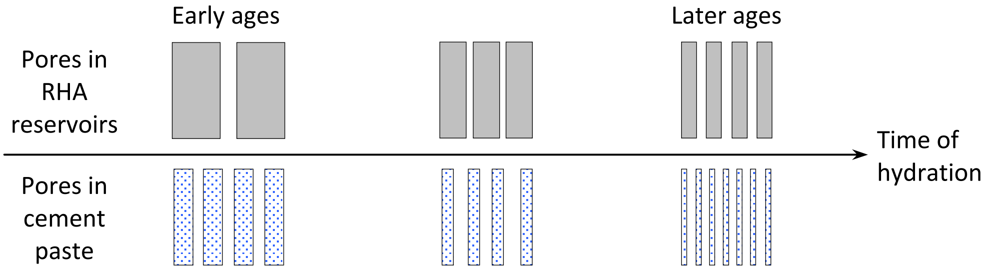

Figure 5.32 Illustration of the potential for the internal water curing of RHA with time of hydration; dots indicate water-filled pores within the hydrating cement paste whereas grey indicates empty pores.

Furthermore, small pores i.e. smaller than 8.5 nm in diameter, in the RHA particles remain water-filled for a longer period of time and in their saturated state are available to promote the hydration of cement. This contributes to a higher compressive strength achieved at later ages of the RHA modified sample. This phenomenon is also observed with high performance mortar using pre-wetted lightweight aggregates by Bentz and Stutzman [Bentz and Stutzman 2008].

From the above discussion, the internal water curing by RHA is only a hypothesis based on some preliminary experimental results. More studies are needed in this aspect to show whether this holds.

5.9 Concluding remarks

In this chapter, the effect of RHA on the packing density, the workability, the compressive strength, and autogenous shrinkage of UHPC mixtures was studied. Based on the experimental results and discussion, the following conclusions can be drawn:

- Optimization of the packing density of UHPC granular mixtures containing RHA can be predicted by using the Compressible Packing Model.
- The use of the finer RHA reduces the high water demand of the RHA modified mixtures. This may be caused by the collapse of the porous structure of RHA particles at a high degree of grinding and reduces the resulting absorbed water content in RHA during mixing.
- RHA can be used as a supplementary cementitious material in producing UHPC.
- The addition of RHA increases the degree of hydration of cement in UHPC at later ages.
- The thickness of ITZ between sand particles and cement paste in UHPC is very small and is not influenced by the presence of RHA.
- The maximum RHA content used to make UHPC was found to be 20% by weight of binder in regard to the workability and the compressive strength. In combination with 10% SF, the maximum RHA content used in UHPC can reach up to 30% and the total cement replacement increases to 40%. This result also shows the benefits of using RHA in making UHPC in terms of the cost and sustainability.

- There is a synergic effect between RHA and SF on the workability and the compressive strength of UHPC. The compressive strength of UHPC containing this combination can attain 185 MPa and 205 MPa at the ages of 28 days and 91 days, respectively, under normal curing conditions.
- The appropriate mean particle size of RHA in making UHPC was suggested to be from 5.6 to 6.3 µm in terms of the energy consumption for grinding RHA, the workability and the compressive strength of UHPC.
- The addition of RHA mitigates autogenous shrinkage of UHPC. The positive effect of RHA on autogenous shrinkage is possibly attributed to the absorbed water in the porous structure of RHA during mixing and the distribution of this water in the whole system. The water absorption capacity in the porous structure of RHA is about 18.9 l/m^3 UHPC with the cement replacement level of 20% by RHA. Because of the wide size range of RHA pores, the internal water curing of RHA can be effective not only at the early ages but also at later ages which can be observed by the experimental results.
- The effective mean particle size of RHA on mitigating autogenous shrinkage of UHPC mixtures was suggested to be from 5.6 to 9.0 µm.

6

Retrospection, Conclusions and Further Research

6.1 Retrospection

UHPC has become one of the promising concretes of the 21st century because of its high strength, low permeability, excellent durability characteristics, and high fluidity. However, regarding the material constituents, the use of a high amount of SF to make UHPC will cause some apparent disadvantages in terms of the high cost and the limited availability. This constrains the applications of SF in making UHPC especially in developing countries. It also gives a motivation for searching for other materials with similar functions to replace SF. Among the mineral admixtures used in concrete, RHA, an agricultural waste material, was found to be a very suitable potential substitute with respect to its properties and its available quantity. Therefore, the overall objective of the research, i.e. the possibility of using RHA as a mineral admixture to make UHPC, was proposed.

Compared with SF, from a technical point of view RHA has some disadvantages in terms of its effect on the workability and the packing density. It is hard to think of using RHA to substitute for SF to make UHPC with these disadvantages. However, the results from this research reveal that the use of RHA to make UHPC is feasible technically, environmentally, and economically compared to SF. The following analysis and evaluations of these aspects will be given in detail below.

A brief summary on UHPC and the drawbacks of using SF was discussed in the literature review in Chapter 2. In addition, a review of the properties of RHA and its effects on the hydration process and microstructure development as well as the compressive strength was also dealt with. This overview revealed some clues for using RHA to replace SF in low w/b ratio mixtures. Both RHA and SF have a similar chemical composition and very high specific surface area but their particle size, shape and particle structure are different. This leads to the different effects on the hydration and microstructure development of cement paste. The experimental studies in Chapter 3 demonstrated these differences. One of the very important results observed in Chapter 3 is that the addition of RHA in low w/b ratio cement pastes increases the degree of cement hydration at later stages. This may be attributed to the absorbed water from the porous RHA particles. These water-saturated RHA particles will act as water reservoirs distributed throughout the system. With progress of the hydration process, the water from these pores will be released and will promote the hydration of the cement.

Additionally, it was also found that the fineness of RHA strongly influences the hydration and microstructure development of cement paste. In fact, the fineness of RHA is depended on the grinding process. Intensive grinding will cause the collapse of the RHA particles and their porous structure. This collapse causes a reduction of water absorption by RHA, and thus the positive effect of RHA on both the hydration and the microstructure of cement paste are decreased. The experimental results found that there is an appropriate fineness of RHA, i.e. 5 µm, with regard to the grinding energy, the pozzolanic activity of RHA, the hydration and the microstructure of cement paste.

The combination of experimental results and the numerical simulation is very useful in evaluating the effect of RHA on the hydration process and microstructure development of cement paste. Modelling of these aspects was developed in Chapter 4 with a modified version of the HYMOSTRUC3D model. The simulation results show that there is an optimum amount of RHA used in cement paste. An extra amount of RHA makes no contribution to the pozzolanic reaction between RHA and CH produced from cement hydration. This result is very important in designing UHPC mixtures containing RHA.

The other key issue in designing UHPC mixtures is the optimization of the packing density of UHPC granular mixtures. This feature was dealt with in Chapter 5, in which the packing density of the ternary system of sand-cement-RHA was predicted by using the Compressible Packing Model which was developed by De Larrard [1999]. Based on the optimization of the packing density of granular mixtures and the optimum content of RHA found in Chapter 4, UHPC mix compositions using RHA were given. The effect of RHA on the properties of UHPC, such as the workability, the compressive strength and the autogenous shrinkage, is the objective of the experimental studies in Chapter 5.

It was found from the results in Chapter 5 that the finer RHA particles improve the workability of UHPC mixtures. This may be caused by the partial collapse of the porous structure of RHA particles at a certain degree of grinding. This leads to a reduction of the amount of absorbed water in the RHA particles. Therefore, more free water available in the system can make the mixture more workable.

In addition, the experimental results demonstrated that the addition of RHA increases the compressive strength of UHPC compared to that of the control sample. Besides, the compressive strength of the RHA modified samples is even higher than that of the SF modified samples, especially at later ages and with a high cement replacement level. This confirms that RHA can be used as a mineral admixture to produce UHPC. A synergic effect between RHA and SF was also found to improve both the workability and the compressive strength of UHPC. This leads to an increase of the total cement replacement percentage to make UHPC, which is very important for the sustainable development of the construction industry.

A high autogenous shrinkage is one of the disadvantages of UHPC. This is because of self-desiccation caused by the very low w/b ratio and the use of a high amount of SF. In the experimental studies, it was observed that the addition of RHA mitigates the autogenous shrinkage of UHPC mixtures. This positive effect is possibly attributed to the absorbed water in the porous structure of RHA, which influences the distribution of water and compensates for the drop of relative humidity in concrete during the hydration process.

6.2 Conclusions

In this thesis, the possibility of using RHA to make UHPC was investigated by both experimental studies and numerical simulation. The general conclusions of this research are given as follows:

- The addition of RHA increases the degree of hydration of cement at the later period. This positive effect of RHA on the hydration of cement is possibly attributed to the pozzolanic reaction and the absorbed water in the porous structure of RHA.
- The apparent activation energy (*Ea*) of cement blended with RHA was found to depend on the degree of hydration, the w/b ratio and the RHA content.
- A numerical model for cement hydration with a modified version of the HYMOSTRUC3D model was developed to evaluate the effect of RHA on the hydration and microstructure development of cement paste. In this model, the hydration kinetics of chemical reactions of four main cement components, i.e. C_3S, C_2S, C_3A, C_4AF, was taken into account. The effect of particle size, the amorphous phase of RHA and the RHA content on the hydration and microstructure development of cement paste was dealt with and validated. Through the study, an optimum amount of RHA in cement paste, i.e. less than 30%, was found. The extra RHA makes no contribution to its pozzolanic reaction.
- The packing density of UHPC granular mixtures containing RHA was optimized by using the Compressible Packing Model.
- The fineness of RHA influences the hydration and microstructure development of cement paste. A mean particle size of RHA, i.e. 5.6 µm, was found to be appropriately used in cement paste in terms of the pozzolanic activity of RHA, the degree of cement hydration, and the refinement of the pore structure of cement paste.
- The addition of RHA increases the compressive strength of UHPC compared to that of a control sample. In particular, the compressive strength of the RHA modified samples is higher than that of the SF modified samples at later ages. This was ascribed to the absorbed water in the porous RHA particles which act as water reservoirs. This water will be released during the hydration progress to promote the hydration of cement and result in a higher compressive strength of UHPC at later ages. The maximum RHA content used to make UHPC was found to be 20% by weight of binder in this study.
- The addition of the finer RHA reduces the high water demand of the RHA modified mixtures. The appropriate mean particle size of RHA to make UHPC is suggested to be in the range from 5.6 µm to 6.3 µm with regard to the energy consumption for grinding RHA, the workability, and the compressive strength of UHPC.
- There is a synergic effect between RHA and SF on the workability and the compressive strength of UHPC. The compressive strength of UHPC made by 10% RHA and 10% SF can reach 185 MPa and 205 MPa at the ages of 28 days and 91 days, respectively under normal curing conditions. Moreover, in combination with 10% SF, the total cement replacement level by the blend of RHA and SF can reach up to 40%. This result shows the benefits of using RHA in terms of the cost and sustainable development in the UHPC production.
- The addition of RHA mitigates autogenous shrinkage of UHPC mixtures. Obviously, RHA acts as an internal curing agent in UHPC. The positive effect of RHA on autogenous shrinkage is possibly attributed to its porous structure. The water absorption capacity in the

porous structure of 20% RHA used in one cubic meter of UHPC was approximately 18.9 litres. It was also found that the effective mean particle size of RHA to mitigate autogenous shrinkage of UHPC mixtures was suggested in the range of 5.6 µm to 9.0 µm.

6.3 Further research

From this study, several aspects of the experiments and numerical simulation of using RHA to make UHPC are recommended for further research:

1) Mechanism of internal water curing of RHA in UHPC

   The use of internal water curing is a very important method to enhance the properties of concrete, especially at low w/b ratio mixes [Kovler and Jensen 2007; Bentz and Weiss 2011]. Light-weight aggregates have been used successfully in high performance concretes where the finer LWAs were found to be more effective than the coarse ones [Kovler and Jensen 2007; Bentz and Weiss 2011]. With decreasing the w/b ratio, the microstructure of mixtures becomes denser and the effective distance of internal curing from 'water reservoirs' to the surroundings is limited. Therefore it is essential to separate 'big water reservoirs' into 'smaller ones' to improve the effectiveness of internal curing in very/ultra high performance concretes. Additionally, these tiny water reservoirs should be well distributed in the whole system. In this respect, RHA becomes a very good candidate for use as an internal curing agent for UHPC.

   Furthermore, the size of pores in RHA particles ranges from 6 to 60 nm in diameter. According to the Kelvin equation, this size range of pores corresponds to the change of relative humidity in the cement matrix between 81.9 and 98%. Besides, the relative humidity of cement paste with the w/c ratio of 0.25 is still over 87% up to 7 days of hydration [Wittmann 1969]. Therefore, only water in big pores, i.e. 8.5 nm in diameter, of RHA particles can be released. A certain amount of water still remains in the smaller pores to promote the hydration of cement at later ages, even after 28 days when the RH drops to about 78%. Unfortunately, the mechanism of how water can be absorbed and de-absorbed in such small pores of the RHA particles still remains unclear. In this respect, the additional absorbed water in the porous RHA particles should be calculated. This is very important in designing concrete mixtures containing RHA.

2) Modelling of hydration and microstructure development of cement paste containing RHA

   The effects of the pH of pore solution, the unburnt carbon content and the internal water curing of RHA on the hydration and microstructure development of cement paste should be evaluated.

   From the hydration process and the built-up microstructure of the blended system, the permeability, the tensile strength, compressive strength, and autogenous shrinkage of concrete will be simulated.

3) Durability of UHPC incorporating RHA

   Concrete is the most available and widely used construction material in the world. Despite the good properties of concrete, some durability problems, mostly related to the structure of the hardened concrete, can occur during a structure's lifetime. This reduces the service life of the total construction. Problems such as chloride penetration, carbonation, alkali silica reactions, structural cracks, damage due to accidents, explosions or earthquakes, etc. will cause the deterioration and/or a reduction in strength of the concrete. Therefore, this reduces the service life or, even worse, results in an unsafe situation for the structures' users.

It is well known that a reduction in the w/b ratio and the use of pozzolans are proper ways to produce a denser, more impermeable matrix [Bentz *et al.* 2000]. This helps to increase the resistance of concrete to the attack of harmful substances. Besides, the increase in the service life of concrete made from blended cements containing pozzolans would further reduce the amount of Portland cement. In this respect, the use of RHA in concrete is promising. It is suggested that RHA greatly improves the durability characteristics [Mehta and Folliard 1995; De Sensale 2010]. In particular, non-air-entrained concrete containing RHA exhibited a significantly higher frost resistance than similar mixtures containing SF. Additionally, the general decrease in capillary porosity associated with the pozzolanic reaction, the porous structure of RHA may to some extent serve as an air void system, acting as a pressure relief when subjected to freezing and thawing. RHA is in this sense unique compared to fly ash, slag and SF [Sandberg 1995]. Unfortunately, to date, there has been no investigation concerning the effect of RHA on the durability of UHPC where the w/b ratio is very low, i.e. from 0.08 to 0.25. This point should be given more attention.

4) Combination of RHA and other mineral admixtures in producing UHPC in terms of sustainable development

Pozzolans are powders used in concrete in relatively large amounts and mainly used as cement replacements in order to enhance early and long term performance. The use of these materials reduces the cost of concrete production and increases environmental benefits. The utilization of very high amounts of cement in producing UHPC, about 900-1000 kg/m^3 [Richard and Cheyrezy 1995] not only affects the production costs, but also has negative effects on the heat of hydration and may cause shrinkage problems. Due to their pozzolanic nature, some materials, such as fly ash, slag and RHA, are beneficial mineral admixtures for concrete. Replacing cement with mineral admixtures seems to be a feasible solution to these problems. Furthermore, the combination of mineral admixtures may also have positive effects on the durability of concrete.

In this research, it was found that the maximum cement replacement level by RHA in producing UHPC was 20%, but in combination with 10% SF, the maximum of total cement replacement level can reach up to 40%. The main reason constraining the increase of the RHA content used in making UHPC is the high water demand of RHA-modified mixtures. In fact, it is well known that the addition of some fine powders such as blast furnace slag and fly ash can improve the workability of fresh concrete [Lange *et al.* 1997; Ferraris *et al.* 2001]. This gives rise to the idea that the total cement replacement level can be expected to increase further by using RHA combined with these powder additions. Indeed, it was revealed that UHPC can be made with a total cement replacement content of 75% by a ternary system of slag cement-RHA-SF [Nguyen and Ye 2011]. This is an important contribution to the sustainable development of UHPC using RHA. In other words, it also opens a door for using a combination of RHA with other mineral admixtures in producing UHPC. This aspect should be investigated exhaustively.

References

AFGC-SETRA (2002). Ultra High Performance Fibre-Reinforced Concretes, Interim Recommendations, Paris, France, AFGC publication.

Aïtcin P.-C. (1998). High Performance Concrete, Taylor & Francis (eds).

Aïtcin P.-C. (2000). Cements of yesterday and today, concrete of tomorrow, Cement and Concrete Research 30(9) 1349-1359.

ASTM Standard (2009). Test method for autogenous strain of cement paste and mortar, ASTM C1698-09, Vol. 04.02, West Conshohocken, PA.

Bache H.H. (1981). Densified cement/Ultra fine particle based materials, CBL Report No. 40, Aalborg Portland, PO Box 165, DK-9100, Aalborg, Denmark, 35 p.

Baroghel Bouny V. (1996). Texture and moisture properties of ordinary and high-performance cementitious materials, International RILEM Conference on Concrete: from Material to Structure, J.-P. Bournazel and Y. Malier (eds), Arles, France, pp. 144-165.

Bentz D.P., Coveney P.V., Garboczi E.J., Kleyn M.F., Stutzman P.E. (1994). Cellular automaton simulations of cement hydration and microstructure development, Modeling Simulated Materials Science and Engineering 2(4) 783-808.

Bentz D.P., Garboczi E.J. (1990). A digitized simulation model for microstructural development, Proceeding of NIST/ACerS Conference on Advances in Cementitious Materials, Gaithersburg, MD, American Ceramic Society, Westerville, OH, pp. 211-226.

Bentz D.P., Jensen O.M., Coats A.M., Glasser F.P. (2000). Influence of silica fume on diffusivity in cement-based materials: I. Experimental and computer modeling studies on cement pastes, Cement and Concrete Research 30(6) 953-962.

Bentz D.P., Stutzman P.E. (2008). Internal curing and microstructure of high-performance mortars, Internal Curing of High Performance Concrete: Lab and Field Experiences, ACI SP256-07, Detroit: American Concrete Institute, pp. 81-90.

Bentz D.P., Weiss W.J. (2011). Internal Curing: A 2010 State-of-the-Art Review (NISTIR 7765), U.S. Department of Commerce (eds), 82 p.

Bhatty J.I., Reid K.J. (1985). Use of thermal analysis in the hydration studies of a Type I Portland cement produced from mineral tailings, Thermochimica Acta (91) 95-105.

Blais P.Y., Couture M. (1999). Precast, prestressed pedestrian bridge - World's first Reactive Powder Concrete structure, PCI Journal 44(5) 60-71.

Boateng A.A., Skeete D.A. (1990). Incineration of rice hull for use as a cementitious material: the Guyana experience, Cement and Concrete Research 20(5) 795-802.

Boddy A.M., Hooton R.D., Thomas M.D.A. (2000). The effect of product form of silica fume on its ability to control alkali-silica reaction, Cement and Concrete Research 30(7) 1139-1150.

Bonneau O., Pouline C., Dugat J., Richard P., Aïtcin P.C. (1996). Reactive Powder Concretes: From theory to practice, Concrete International 18(4) 47-49.

Bui D.D. (2001). Rice husk ash as a mineral admixture for High Performance Concrete, PhD Thesis, Delft University of Technology, Delft.

Bui D.D., Hu J., Stroeven P. (2005). Particle size effect on the strength of rice husk ash blended gap-graded Portland cement concrete, Cement and Concrete Composites 27(3) 357-366.

Buitelaar P. (2004). Ultra High Performance Concrete: Developments and Applications during 25 years, Plenary session, Proceeding of the 1st International Symposium on Ultra High Performance Concrete, Kassel, Germany, 29 p.

Chandra S., Bergqvist H. (1997). Interaction of silica colloid with Portland cement, Proceeding of the 10th International Congress of the Chemistry of Cement, 3, 3ii106, 6 p.

Chandrasekhar S., Pramada P.N., Raghavan P., Satyanarayan K.G. (2002). Microsilica from rice husk as a possible substitute for condensed silica fume for high performance concrete, Journal of Materials Science letters (21) 1245-1247.

Chandrasekhar S., Satyanarayana K.G., Pramada P.N., Raghavan P., Gupta T.N. (2003). Review processing, properties and applications of reactive silica from rice husk - An overview, Journal of Materials Science 38(15) 3159-3168.

Chatterji S., Thaulow N., Christensen P. (1982). Puzzolanic activity of byproduct silica-fume from ferro-silicom production, Cement and Concrete Research 12(6) 781-784.

Cheyrezy M., Maret V., Frouin L. (1995). Microstructural analysis of Reactive Powder Concrete, Cement and Concrete Research 25(7) 1491-1500.

Chindaprasirt P., Rukzon S. (2008). Strength, porosity and corrosion resistance of ternary blend Portland cement, rice husk ash and fly ash mortar, Construction and Building Materials 22(8) 1601-1606.

Cook D. (1984). Rice husk ash cements: their development and applications, United Nations Industrial development organization, Vienna.

Cook D.J. (1986). Rice husk ash, In: Concrete Technology and. Design, Cement Replacement Materials, Swamy R.N. (eds), Vol. 3, Surrey University Press, London, pp. 171-196.

Cook D.J., Pama R.P., Damer S.A. (1976). The behaviour of concrete and cement paste containing rice husk ash, Conference Proceeding on Hydraulic Cement Paste, Cement & Concrete Association, London, pp. 268-282.

Cook R.A., Hover K.C. (1993). Mercury porosimetry of cement-based materials and associated correction factors, ACI Materials Journal 90(2) 152-161.

Cook R.A., Hover K.C. (1999). Mercury porosimetry of hardened cement pastes, Cement and Concrete Research 29(6) 933-943.

Coutinho J.S. (2003). The combined benefits of CPF and RHA in improving the durability of concrete structures, Cement and Concrete Composites 25(1) 51-59.

D'Aloia L., Chanvillard G. (2002). Determining the "apparent" activation energy of concrete: Ea - numerical simulations of the heat of hydration of cement, Cement and Concrete Research 32(8) 1277-1289.

Dalhuisen D.H., Stroeven P., Bui D.D., Quy N.T. (1996). Replacement of condensed silica fume by rice husk ash for the production of high strength concrete in developing countries, Proceeding of International Conference on the Utilization of High Strength/High Performance Concrete, Pont et Chaussées, Paris, pp. 235-243.

de Larrard F. (1999). Concrete mixture proportioning: A scientific approach, Modern Concrete Technology Series, E&FN Spon (Eds).

de Larrard F., Sedran T. (1994). Optimization of ultra-high-performance concrete by the use of a packing model, Cement and Concrete Research 24(6) 997-1009.

de Sensale G.R. (2010). Effect of rice-husk ash on durability of cementitious materials, Cement and Concrete Composites 32(9) 718-725.

de Sensale G.R., Ribeiro A.B., Gonçalves A. (2008). Effects of rice husk ash on autogenous shrinkage of Portland cement pastes, Cement and Concrete Composites 30(10) 892-897.

Detwiler R.J., Mehta P.K. (1989). Chemical and physical effects of silica fume on the mechanical behavior of concrete, ACI Material Journal 86(6) 609-614.

Diamond S. (1971). A critical comparison of mercury porosimetry and capillary condensation pore size distributions of Portland cement pastes, Cement and Concrete Research 1(5) 531-545.

Diamond S., Leeman M.E. (1995). Pore size distributions in hardened cement paste by SEM image analysis. Material Research Society Symposia, Vol. 370, Microstructure of cement-based systems/bonding and interfaces in cement-based materials, S. Diamond et al. (eds), pp. 217-226.

Diamond S., Sahu S. (2006). Densified silica fume: particle sizes and dispersion in concrete, Materials and Structures 39(9) 849-859.

Diamond S., Sahu S., Thaulow N. (2004). Reaction products of densified silica fume agglomerates in concrete, Cement and Concrete Research 34(9) 1625-1632.

Domone P.L., Soutsos M.N. (1995). Properties containing of high-strength concrete mixes PFA and GGBS, Magazine of Concrete Research 47(173) 355-367.

Droll K. (2004). Influence of additions on ultra high performance concretes - grain size optimization, Proceeding of the 1st International Symposium on ultra high performance concrete, Kassel, Germany, pp. 285-301.

Dudziak L., Mechtcherine V. (2008). Mitigation of volume changes of Ultra-High Performance Concrete (UHPC) by using Super Absorbent Polymers, Proceeding of the 2nd International Symposium on Ultra High Performance Concrete, Kassel University, Kassel, Germany, pp. 425-432.

Escalante-García J.I., Sharp J.H. (1998). Effect of temperature on the hydration of the main clinker phases in portland cements: Part I- Neat cements, Cement and Concrete Research 28(9) 1245-1257.

FAO (2010). Rice market monitor. http://www.fao.org/es/ESC/common/ecg/71/en/RMM-Jun09.pdf [online] [Accessed 18 Oct. 2010].

Feng Q., Yamamichi H., Shoya M., Sugita S. (2004). Study on the pozzolanic properties of rice husk ash by hydrochloric acid pretreatment, Cement and Concrete Research 34(3) 521-526.

Fennis S.A.A.M. (2008). Measuring water demand or packing density of micro powders: comparison of methods, TUDelft Repository (http://repository.tudelft.nl/view/ir/uuid:9f1a716d-d669-4ce5-9fae-1afefac2c168/).

Fennis S.A.A.M. (2011). Design of ecological concrete by particle packing optimization, PhD thesis, Delft University of Technology, Delft, the Netherlands.

Ferraris C.F., Obla K.H., Hill R. (2001). The influence of mineral admixtures on the rheology of cement paste and concrete, Cement and Concrete Research 31(2) 245-255.

Ganesan K., Rajagopal K., Thangavel K. (2008). Rice husk ash blended cement: Assessment of optimal level of replacement for strength and permeability properties of concrete, Construction and Building Materials 22(8) 1675-1683.

Gao R., Liu Z.-M., Zhang L.-Q., Stroeven P. (2006). Static properties of reactive powder concrete beams, Key Engineering Materials (302-303) 521-527.

Habeeb G.A., Fayyadh M.M. (2009). Rice husk ash concrete: the effect of RHA average particle size on mechanical properties and drying shrinkage, Australian Journal of Basic and Applied Sciences 3(3) 1616-1622.

Habel K., Viviani M., Denarié E., Brühwiler E. (2006). Development of the mechanical properties of an Ultra-High Performance Fiber Reinforced Concrete (UHPFRC), Cement and Concrete Research 36(7) 1362-1370.

Haines P.J. (2002). Principles of thermal analysis and calorimetry, The Royal Society of Chemistry: London, O.T. Sorensen and J. Rouquerol (Eds).

Hansen P.F., Pedersen E.J. (1977). Maturity computer for controlled curing and hardening of concrete, Nordisk Betong 1(19) 21-25.

Hwang C.L., Chandra S. (1997). The use of Rice husk ash in concrete, In: Waste materials used in concrete manufacturing, William Andrew Publishing/Noyes (eds), pp. 184-234.

Hwang C.L., Wu D.S. (1989). Properties of cement paste containing rice husk ash, Proceeding of the 3rd CANMET ACI International Conference on Fly Ash, Silica Fume, Slag and Natural Pozzolans in Concrete, SP114-35, Trondheim, Norway, V. M. Malhotra (eds), pp. 733-762.

Ismail M.S., Waliuddin A.M. (1996). Effect of rice husk ash on high strength concrete, Construction and Building Materials 10(7) 521-526.

James J., Subba Rao M. (1986). Reaction product of lime and silica from rice husk ash, Cement and Concrete Research 16(1) 67-73.

Jayakumar K. (2004). Role of Silica fume Concrete in Concrete Technology, Proceeding of the 1st International Symposium on UHPC. Kassel, Germany, pp. 165-174.

Jennings H.M., Parrott L.J. (1986a). Microstructural analysis of hydrated alite paste, Part 1: Porosity, Journal of Materials Science 21(11) 4048-4052.

Jennings H.M., Parrott L.J. (1986b). Microstructural analysis of hydrated alite paste, Part 2: Microscopy and reaction products, Journal of Materials Science 21(11) 4053-4059.

Jennings H.M., Johnson S.K. (1986). Simulation of microstructure development during the hydration of a cement compound, Journal of the American Ceramic Society 69(11) 790-795.

Jensen O.M., Hansen P.F. (2001). Water-entrained cement-based materials: I. Principles and theoretical background, Cement and Concrete Research 31(4) 647-654.

Jensen O.M., Hansen P.F. (2002). Water-entrained cement-based materials: II. Experimental observations, Cement and Concrete Research 32(6) 973-978.

Jones M., Zheng L., Newlands M. (2002). Comparison of particle packing models for proportioning concrete constitutents for minimum voids ratio, Materials and Structures 35(5) 301-309.

Jungwirth J., Muttoni A. (2004). Structural Behavior of Tension Members in UHPC, Proceeding of International Symposium on Ultra High Performance Concrete, Kassel, Germany, pp. 533-544.

Kada-Benameur H., Wirquin E., Duthoit B. (2000). Determination of apparent activation energy of concrete by isothermal calorimetry, Cement and Concrete Research 30(2) 301-305.

Khan M.H., Mohan K., Taylor H.F.W. (1985). Pastes of tricalcium silicate with rice husk ash, Cement and Concrete Research 15(1) 89-92.

Kjellsen K., Lagerblad B., Jennings H. (1997). Hollow-shell formation - An important mode in the hydration of Portland cement, Journal of Materials Science 32(11) 2921-2927.

Kjellsen K.O., Atlassi E.H. (1999). Pore structure of cement silica fume systems: Presence of hollow-shell pores, Cement and Concrete Research 29(1) 133-142.

Kjellsen K.O., Detwiler R.J. (1992). Reaction kinetics of Portland cement mortars hydrated at different temperatures, Cement and Concrete Research 22(1) 112-120.

Koenders E.A.B. (1997). Simulation of volume changes in hardening cement-based materials, Delft University of Technology, Delft, the Netherlands.

Koenders E.A.B. (2006). Stereology-based modelling of blended cement microstructures - Implementation in HYMOSTRUC, Report Nr 25.5-06-09, Project Nr 3.05.06, Delft University of Technology, the Netherlands.

Kovler K., Jensen O.M. (2007). Internal Curing of Concrete, State-of-the-art Report of RILEM Technical Committee 196-ICC.

Lange F., Mörtel H., Rudert V. (1997). Dense packing of cement pastes and resulting consequences on mortar properties, Cement and Concrete Research 27(10) 1481-1488.

Laskar A.I., Talukdar S. (2008). Rheological behavior of high performance concrete with mineral admixtures and their blending, Construction and Building Materials 22(12) 2345-2354.

Le T.T. (2008). Ultra high performance fibre reinforced concrete paving flags, PhD thesis, Liverpool, University of Liverpool, UK.

Lea F.M. (2004). Lea's Chemistry of Cement and Concrete, Butterworth-Heinemann (eds).

Lin L.K., Hwang C.L. (1997). Characteristics and hydration mechanism of rice husk ash cement paste, Proceeding of the 10th International Congress on the Chemistry of Cement, Gothenburg, Vol. 3, 3ii108, 4 p.

Locher F.W., Richartz W., Sprung S. (1976). Erstarren von Zement' (in German), Zement Kalk Gips 29(10) 435-442.

Long G., Wang X., Xie Y. (2002). Very-high-performance concrete with ultrafine powders, Cement and Concrete Research 32(4) 601-605.

Loukili A., Khelidj A., Richard P. (1999). Hydration kinetics, change of relative humidity, and autogenous shrinkage of ultra-high-strength concrete, Cement and Concrete Research 29(4) 577-584.

Lubbers A.R. (2003). Bond performance between ultra high performance concrete and prestressing strands, MSc thesis, Ohio University.

Lura P., Jensen O.M., van Breugel K. (2003). Autogenous shrinkage in high-performance cement paste: An evaluation of basic mechanisms, Cement and Concrete Research 33(2) 223-232.

Luxán M.P., Madruga F., Saavedra J. (1989). Rapid evaluation of pozzolanic activity of natural products by conductivity measurement, Cement and Concrete Research 19(1) 63-68.

Ma J., Dietz J., Dehn F. (2003). Ultra High Performance Self Compacting Concrete, The 3rd International Symposium on Self-Compacting Concrete, Reykjavik, Iceland, pp. 136-142.

Ma J., Schneider H. (2002). Properties of Ultra-High-Performance Concrete, Leipzig Annual Civil Engineering Report (LACER), pp. 25-32.

Ma W., Sample D., Martin R., Brown P.W. (1994). Calorimetric study of cement blends containing Fly Ash, Silica Fume, and Slag at elevated temperatures, Cement, Concrete and Aggregates 16(2) 93-99.

Maekawa K., Chaube R., Kishi T. (1999). Modelling of concrete performance: hydration, microstructure formation, and mass transport, E&PN Spon (Eds), London.

Mahmud H.B., Majuar E., Zain M.F.M., Hamid N.B.A.A. (2009). Mechanical properties and durability of normal and water reduced high strength grade 60 concrete containing rice husk ash, Journal of Advanced Concrete Technology 79(1) 21-30.

Malhotra V.M., Ramachandran V.S., Feldman R.F., Aitcin P.C. (1987). Condensed-Silica Fume in Concrete, CRC Press (Eds), Inc., Florida.

Marquardt I. (2001). Ein Mischungskonzept für selbstverdichtenden Beton auf der Basis der Volumenkenngrößen und Wasseransprüche der Ausgangsstoffe, Rostock, Germany, University of Rostock.

Marsh B.K., Day R.L. (1988). Pozzolanic and cementitious reactions of fly ash in blended cement pastes, Cement and Concrete Research 18(2) 301-310.

Maruyama I., Matsushita T., Noguchi T. (2007). Numerical modeling of Portland cement hydration based on particle kinetic model and multi-component concept, Proceeding of the 12th International Congress of the Chemistry of Cement (ICCC), TH1-08.3, 12 pp.

Maso J.C. (1996). Interfacial Transition Zone in Concrete: RILEM Reports, Taylor & Francis (Eds).

Matsushita T., Hoshino S., Maruyama I., Noguchi T., Yamada K. (2007). Effect of curing temperature and water to cement ratio on hydration of cement compounds, Proceeding of the 12th International Congress of the Chemistry of Cement (ICCC), TH2-07.3, 12 pp.

Mechtcherine V., Dudziak L., Hempel S. (2008). Mitigating early age shrinkage of Ultra-High Performance Concrete by using Super Absorbent Polymers (SAP), In: Creep, shrinkage and durability mechanics of concrete and concrete structures, Taylor & Francis (Eds), pp. 847-853.

Mehta P.K. (1983). Pozzolanic and cementitious by-products as mineral admixtures for concrete - A critical review, ACI Special Publication (79) 1-46.

Mehta P.K. (1994). Rice husk ash - a unique supplementary cementing material, Advances in Concrete Technology (2nd edition), CANMET, V.M. Malhotra (eds), pp. 419-444.

Mehta P.K. (2002). Greening of the concrete industry for sustainable development, Concrete International 24(7) 23-28.

Mehta P.K. (2009). Global concrete industry sustainability, Concrete International 31(02) 45-48.

Mehta P.K., Folliard K.J. (1995). Rice husk ash - A unique supplementary cementing material: Durability aspects, Proceeding of the 2nd CANMET/ACI International Symposium, ACI SP 154-28, Las Vegas, Nevada, USA, pp. 531-541.

Midgley H.G. (1979). The determination of calcium hydroxide in set Portland cements, Cement and Concrete Research 9(1) 77-82.

Mills R.H. (1966). Factors influencing cessation of hydration in water cured cement pastes, Symposium on structure of Portland cement paste and concrete, Special report 90, Highway Research Board, Washington, pp. 406-424.

Mindess S., Young J.F., Darwin D. (2003). Concrete: Prentice-Hall, Upper Saddle River, New Jersey, USA.

Mitchell D.R.G., Hinczak I., Day R.A. (1998). Interaction of silica fume with calcium hydroxide solutions and hydrated cement pastes, Cement and Concrete Research 28(11) 1571-1584.

Möser B., Pfeifer C. (2008). Microstructure and durability of Ultra-High Performance Concrete, Proceeding of the 2nd International Symposium on UHPC, Fehling.et al. (eds), Kassel, Germany, pp. 417-424.

Nair D.G. (2006). Sustainable-affordable housing for the poor in Kerala, PhD thesis, Delft University of Technology, Delft, the Netherlands.

Navi P., Pignat C. (1996). Simulation of cement hydration and the connectivity of the capillary pore space, Advanced Cement Based Materials 4(2) 58-67.

Nguyen V.T., Guo Z., Ye G., van Breugel K. (2009). Activation energy of cement blended with silica fume, The 29th Cement and Concrete Science Conference, Leeds, UK, pp. 149-152.

Nguyen V.T., Ye G. (2011). The use of rice husk ash to produce ultra high performance concrete in sustainable construction, The International Conference on Advances in Construction Materials through Science and Engineering, and the 65th RILEM week, 5-7 Sept. 2011, Hong Kong, China SAR.

Nguyen V.T., Ye G., van Breugel K., Guo Z. (2010a). Activation energy of cement blended with rice husk ash. The 2nd International Conference on Sustainable Construction Materials and Technologies, Ancona, Italy, pp. 383-392.

Nguyen V.T., Ye G., van Breugel K., Guo Z., Bui D.D. (2010b). Influence of rice husk ash fineness on the hydration and microstructure of blended cement paste, The 7th International Symposium on Cement and Concrete (ISCC2010). Jinan, China, 325-332.

Nicole P.H., Monteiro P.J.M., Carasek H. (2000). Effect of silica fume and rice husk ash on alkali-silica reaction, ACI Materials Journal 97(4) 486-492.

Ordóñez L.M., Payá J., Coats A.M., Glasser F.P. (2002). Reaction of rice husk ash with OPC and Portlandite, Advances in Cement Research 14(3) 113-119.

Papadakis V.G. (1999). Experimental investigation and theoretical modeling of silica fume activity in concrete, Cement and Concrete Research 29(1) 79-86.

Papadakis V.G., Vayenas C.G., Fardis M.N. (1991). Physical and chemical characteristics affecting the durability of concrete, ACI Materials Journal 8(2) 186-196.

Perry V. (2006). Ductal® - A revolutionary new material for new solutions, Association of Professional Engineers and Geoscientists of the Province of Manitoba (APEGM) [download http://www.apegm.mb.ca/pdnet/papers/ductal.pdf] [Accessing date 20th Nov. 2010].

Powers T.C., Brownyard T.L. (1948). Studies of the physical properties of hardened Portland cement paste, PCA Bull Portland Cement Association, No. 22.

Pratt P.L., Ghose A. (1983). Electron microscope studies of Portland cement microstructures during setting and hardening, Philosophical Transactions of the Royal Society A: Mathematical 310(1511) 93-103.

Racky P. (2004). Cost-effectiveness and sustainability of UHPC, Proceeding of the 1st International Symposium on Ultra High Performance Concrete, Kassel, Germany, pp. 797-805.

Real C., Alcalá M.D., Criado J.M. (1996). Preparation of silica from rice husks, Journal of the American Ceramic Society 79(8) 2012-2016.

Reda M.M., Shrive N.G., Gillott J.E. (1999). Microstructural investigation of innovative UHPC, Cement and Concrete Research 29(3) 323-329.

Richard P., Cheyrezy M. (1994). Reactive powder concretes with high ductility and 200 - 800 MPa compressive strength, ACI Special Publication, SP144-24, pp. 507-518.

Richard P., Cheyrezy M. (1995). Composition of reactive powder concretes, Cement and Concrete Research 25(7) 1501-1511.

Rodríguez G.S. (2006). Strength development of concrete with rice-husk ash, Cement and Concrete Composites 28(2) 158-160.

Rossi P. (2005). Development of new cement composite materials for construction, Proceeding of the Institution of Mechanical Engineers, Part L: Journal of Materials: Design and Applications 219(1) 67-74.

Rougeau P., Borys B. (2004). Ultra High Performance Concrete with ultrafine particles other than silica fume. Proceeding of the 1st International Symposium on Ultra High Performance Concrete, Kassel, Germany, pp. 213-225.

Sadrekarimi A. (2004). Development of a Light Weight Reactive Powder Concrete, Journal of Advanced Concrete Technology 2(3) 409-417.

Sandberg P. (1995). Resistance of non air-entrained rice hull ash concrete to freezing and thawing in saline environment, Proceeding of the 2nd CANMET/ACI International Symposium on Advances in Concrete Technology, SP154-06, Las Vegas, Nevada, USA, pp. 95-101.

Sata V., Jaturapitakkul C., Kiattikomol K. (2007). Influence of pozzolan from various by-product materials on mechanical properties of high-strength concrete, Construction and Building Materials 21(7) 1589-1598.

Schindler A.K. (2004). Effect of temperature on hydration of cementitious materials, ACI Materials Journal 101(1) 72-81.

Schmidt M. (2006). Von der Nanotechnologie zum Ultra-Hochfesten Beton, Ultra high performance concrete - 10 years of research and development at the University of Kassel, Ibausil, Weimar, 2006, Tagungsband, S. 2-1405 - 2-1416, Kassel University Press GmbH, Kassel, pp. 98-110.

Schmidt M., Fehling E. (2005). Ultra-high-performance concrete: research development and application in Europe, The 7th International Symposium on the Utilization of High-strength/High-performance concrete. American Concrete Institute, Washington DC, USA, SP 228-4, pp. 51-78.

Schmidt M., Fehling E., Teichmann T., Bunje K., Bornemann R. (2003). Ultra-High Performance Concrete: Perspective for the precast concrete industry, Concrete Precasting Plant and Technology 69(3) 16-29.

Scrivener K.L. (1989). The Microstructure of Concrete, In: Materials Science of Concrete I, J.P. Skalny (eds), pp. 127-162.

Siddique R. (2008). Rice husk ash, In: Waste materials and by-products in concrete, Springer, pp. 235-264.

Sivakumar G., Ravibaskar R. (2009). Investigation on the hydration properties of the rice husk ash cement using FTIR and SEM, Applied Physics Research 1(2) 71-77.

Skalny J.P., Young J.F. (1980). Mechanisms of Portland cement hydration, The 7th International Congress of the Chemistry of Cement, Paris, II-1/3 - II-1/45.

Spasojevic A. (2008). Structual implications of ultra-high performance fibre-reinforced concrete in bridge design, PhD thesis, Lausanne, Switzerland.

Standards (1998). BS 4551-1:1998, Methods of testing mortars, screeds and plasters, Physical Testing, 32 pp.

Stovall T., de Larrard F., Buil M. (1986). Linear packing density model of grain mixtures, Powder Technology 48(1) 1-12.

Sugita S., Shoya M., Tokuda H. (1992). Evaluation of pozzolanic activity of rice husk ash, Proceeding of the 4th International Conference on Fly ash, Slag and Silica Fume in Concrete, Vol. 1, ACI SP 132-28, Istanbul, Turkey, pp. 495-512.

Sugita S., Yu Q., Shoya M., Tsukinaga Y., Isojima Y. (1997). On the semi-industrial production of highly reactive rice husk ash and its effect on cement and concrete properties, Proceeding of the 10th International Congress of the Chemistry of Cement., Gothenburg, Vol. 3, ii109, 1997, 9 pp.

Swamy R.N. (1986). Cement Replacement Materials- Vol. 3, Concrete Technology and Design, Surrey University Press.

Tafraoui A., Escadeillas G., Lebaili S., Vidal T. (2009). Metakaolin in the formulation of UHPC, Construction and Building Materials 23(2) 669-674.

Taylor H.F.W. (1997). Cement Chemistry, Thomas Telford (Eds), London.

Urhan S. (1987). Alkali silica and pozzolanic reactions in concrete, Part 1: Interpretation of published results and an hypothesis concerning the mechanism, Cement and Concrete Research 17(1) 141-152.

van Breugel K. (1991). Simulation of hydration and formation of structure in hardening cement-based materials, PhD thesis, Delft University of Technology, the Netherlands.

van Breugel K., de Vries J., Takada K. (1999). Low water/binder ratio concretes with low cracking risk by using LWA, Proceeding of International Conference Dundee, pp. 255-264.

van Breugel K., Ye G. (2004). Analyses of hydration processes and microstructural development of UHPC through numerical simulation, Proceeding of the 1st International Symposium on Ultra-High Performance Concrete. Kassel, Germany, pp. 253-264.

Vande Voort T., Suleiman M., Sritharan S. (2008). Design and Performance Verification of UHPC Piles for Deep Foundations, Final Report, Iowa DOT, IHRB Project TR-558, CTRE Project 06-264, Iowa Dept. of Transportation, Ames, IA, 224 p. [http://www.intrans.iastate.edu/reports/tr-558_uhpc_piles.pdf] (Accessing date: 10th Nov. 2010).

Vernet C., Lukasik J., Prat E. (1998). Nanostructure, porosity, permeability, and diffusivity of Ultra High Performance Concrete, Proceeding of International Symposium on HPC and RPC, In: P.-C. Aitcin and Y. Delagrave (Eds). Sherbrooke, Canada, pp. 17-35.

Waller V., de Larrard F., Roussel P. (1996). Modeling the temperature rise in massive high performance concrete Structures, Proceeding of the 4th International Symposium on Utilization of High-strength/High-performance Concrete, Paris, France, pp. 415-421.

Weber S., Reinhardt H.W. (1997). A new generation of high performance concrete: concrete with autogenous curing, Advanced Cement Based Materials 6(2) 59-68.

Wen-yu J., Ming-zhe A., Gui-ping Y., Jun-min W. (2004). Study on Reactive Powder Concrete used in the sidewalk system of the Qinghai-Tibet railway bridge, International Workshop on Sustainable Development and Concrete Technology, Beijing, China, pp. 333-338.

Wittmann F.H. (1969). Physikalische Messungen an Zementstein, Habilitationsarbeit, TU München

Wolsiefer Sr. J. (2007). The measurement and analysis of silica fume particle size distribution and de-agglomeration of different silica fume product forms, The 9th CANMET/ACI Fly Ash Conference, ACI Special Publication, SP-242-10, pp. 111-132.

Wu Z.-Q., Young J.F. (1984a). Formation of calcium hydroxide from aqueous suspensions of tricalcium silicate, Journal of the American Ceramic Society 67(1) 48-51.

Wu Z.-Q., Young J.F. (1984b). The hydration of tricalcium silicate in the presence of colloidal silica, Journal of Materials Science 19(11) 3477-3486.

Ye G. (2003). Experimental study and numerical simulation of the microstructure and permeability of cementitious materials, PhD thesis, Delft University University, Delft, the Netherlands.

Young J.F. (1972). A review of the mechanisms of set-retardation in Portland cement pastes containing organic admixtures, Cement and Concrete Research 2(4) 415-433.

Yu Q., Sawayama K., Sugita S., Shoya M., Isojima Y. (1999). The reaction between rice husk ash and $Ca(OH)_2$ solution and the nature of its product, Cement and Concrete Research 29(1) 37-43.

Zhang M.H., Lastra R., Malhotra V.M. (1996). Rice-husk ash paste and concrete: Some aspects of hydration and the microstructure of the interfacial zone between the aggregate and paste, Cement and Concrete Research 26(6) 963-977.

Zhang M.H., Malhotra V.M. (1996). High performance concrete incorporating rice husk ash as a supplementary cementing materials, ACI Materials Journal 93(6) 629-636.

Zhutovsky S., Kovler K., Bentur A. (2004). Influence of cement paste matrix properties on the autogenous curing of high-performance concrete, Cement and Concrete Composites 26(5) 499-507.

Appendix

A1 Effect of RHA and SF on the kinetic of cement hydration

A1.1 Effect of RHA contents at 20°C curing

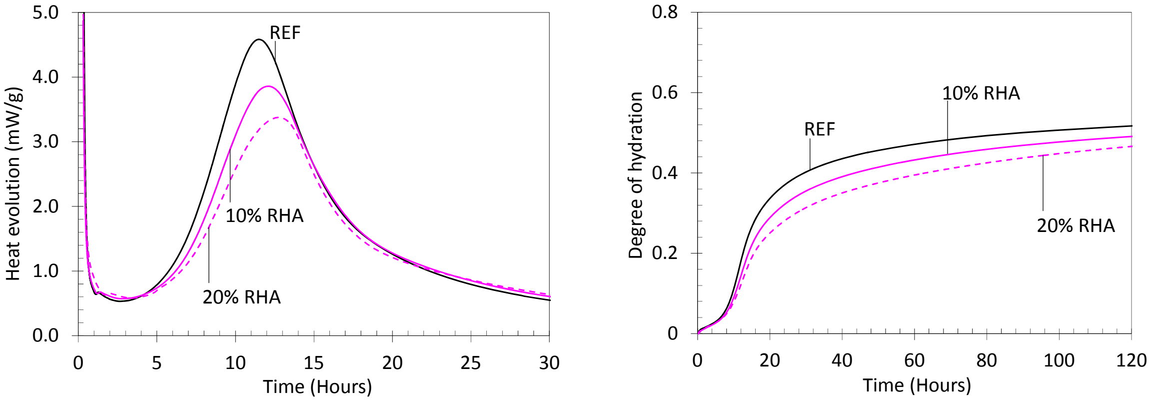

Figure A1.1 Heat evolution and degree of hydration of cement made with RHA, w/b = 0.25

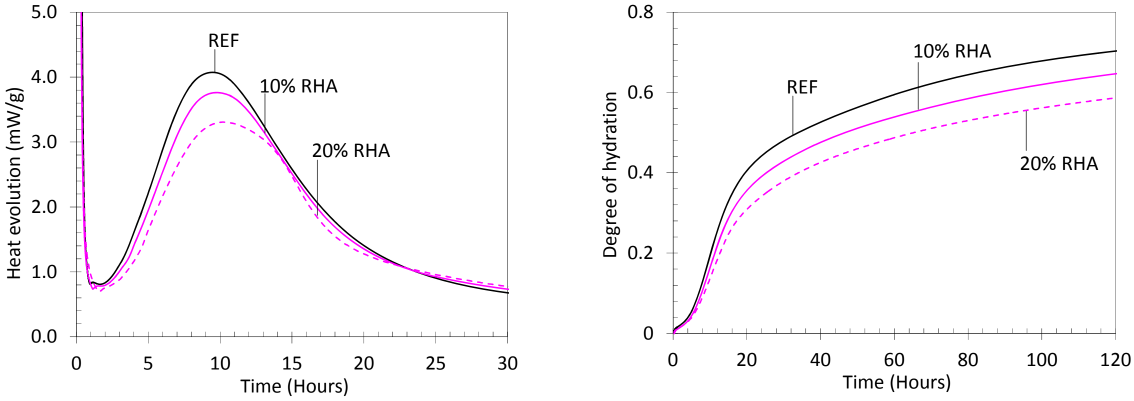

Figure A1.2 Heat evolution and degree of hydration of cement made with RHA, w/b = 0.40

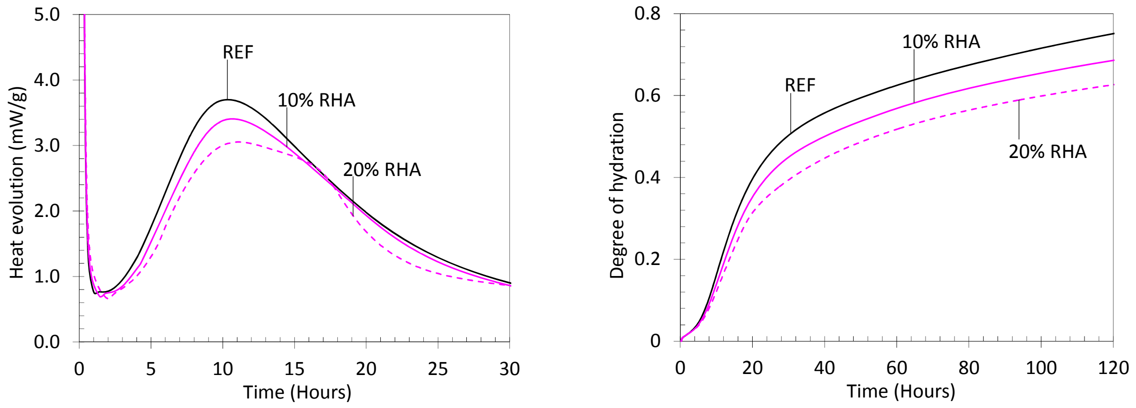

Figure A1.3 Heat evolution and degree of hydration of cement made with RHA, w/b = 0.60

A1.2 Effect of SF contents at 20°C curing

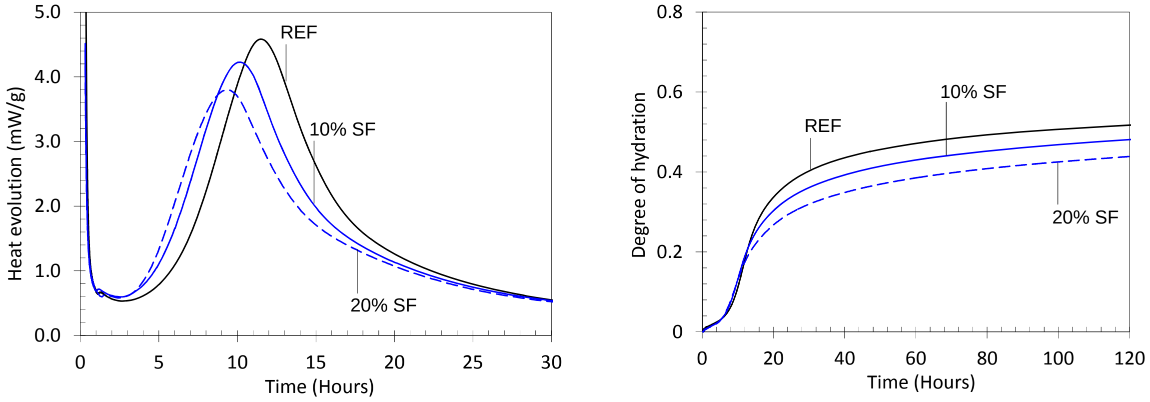

Figure A1.4 Heat evolution and degree of hydration of cement made with SF, w/b = 0.25

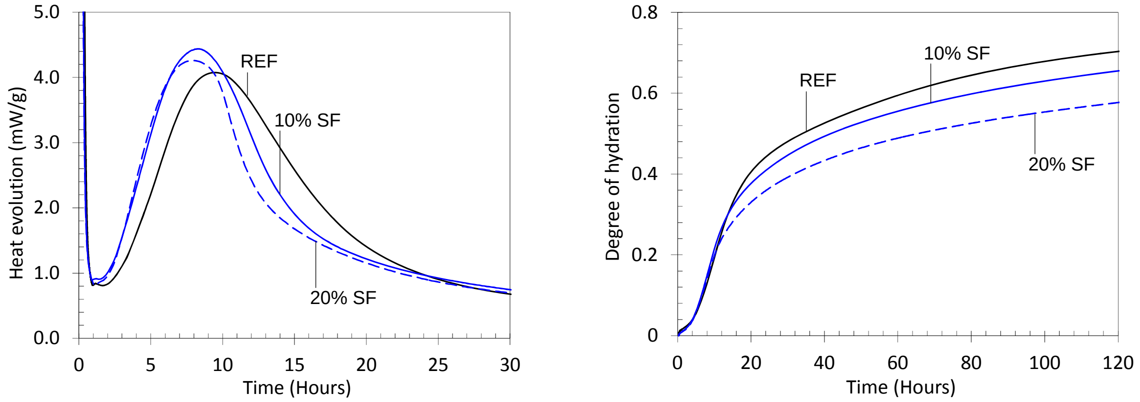

Figure A1.5 Heat evolution and degree of hydration of cement made with SF, w/b = 0.40

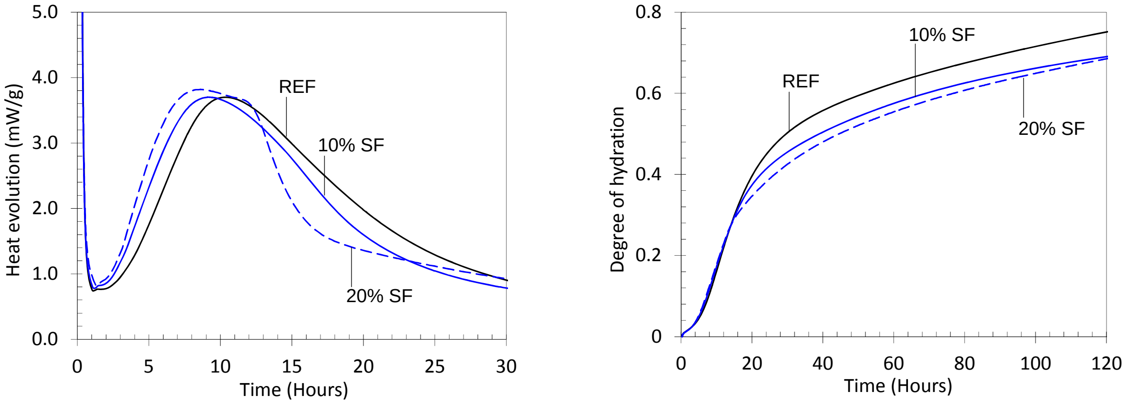

Figure A1.6 Heat evolution and degree of hydration of cement made with SF, w/b = 0.60

A1.3 Effect of curing temperature on heat evolution of cement paste made with RHA

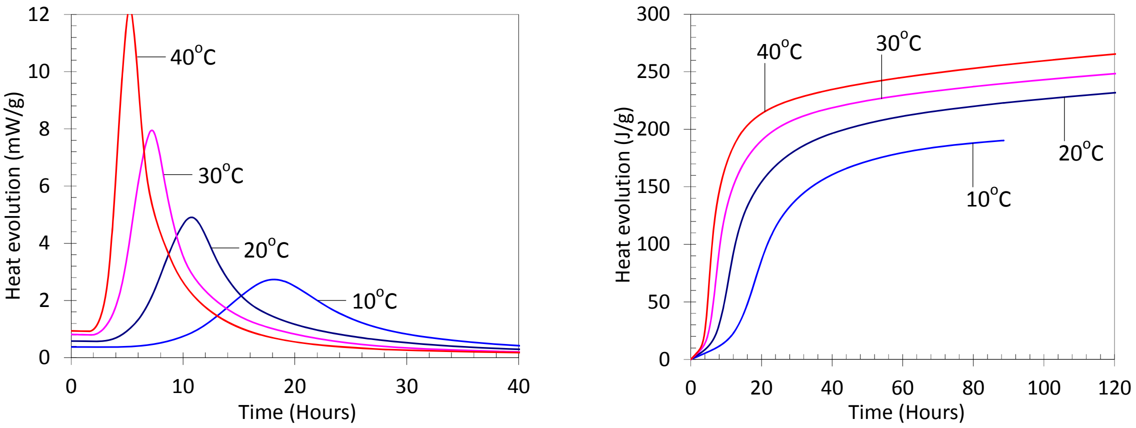

Figure A1.7 Heat evolution of cement paste made with 0% RHA, w/b = 0.25

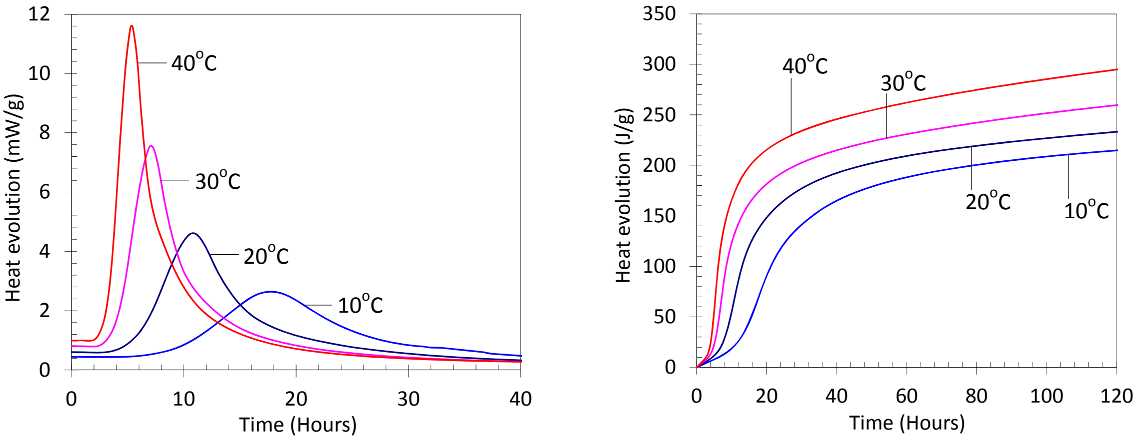

Figure A1.8 Heat evolution of cement paste made with 5% RHA, w/b = 0.25

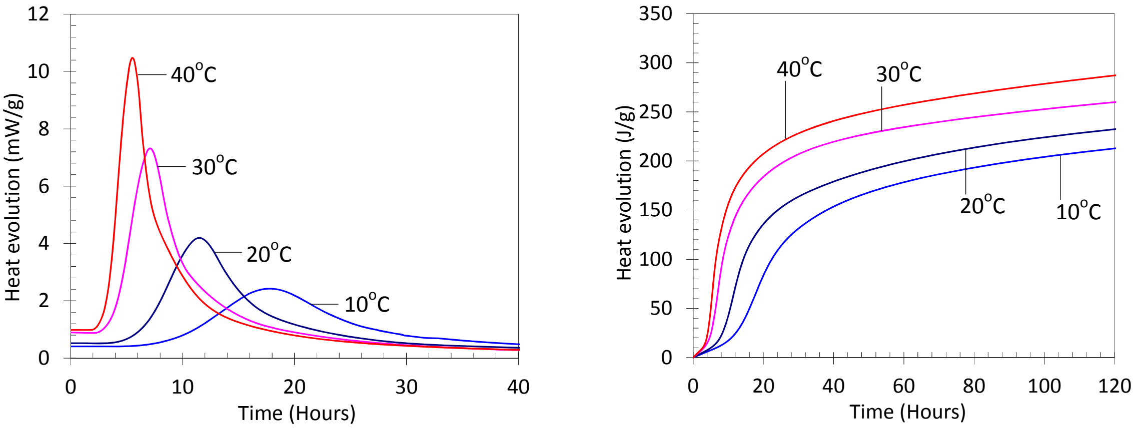

Figure A1.9 Heat evolution of cement paste made with 10% RHA, w/b = 0.25

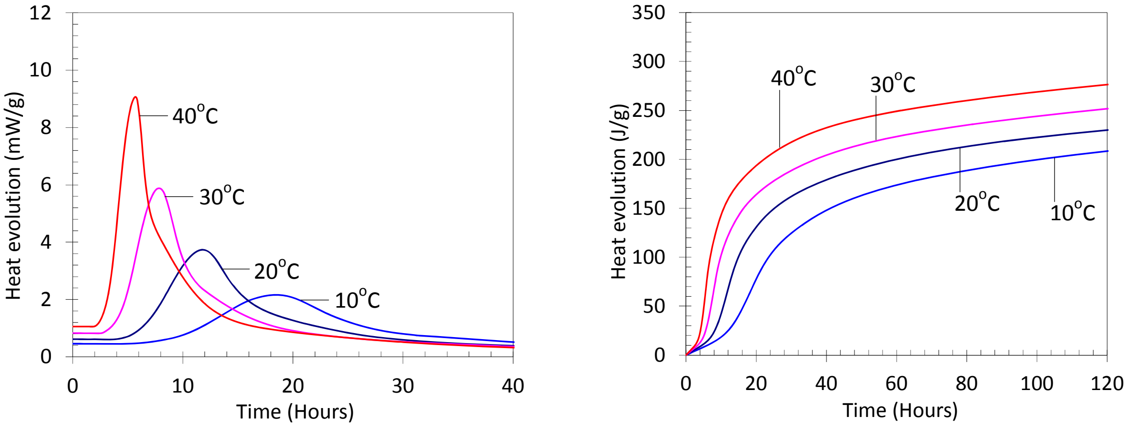

Figure A1.10 Heat evolution of cement paste made with 20% RHA, w/b = 0.25

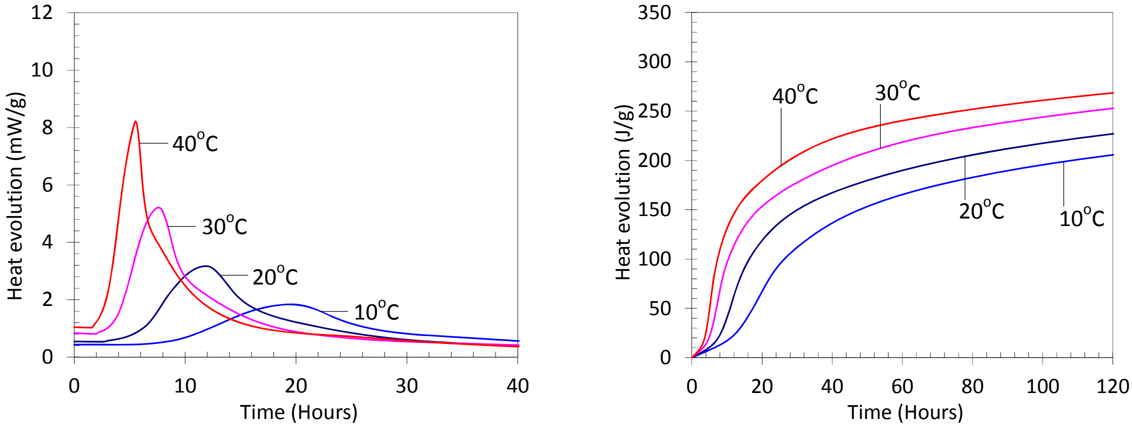

Figure A1.11 Heat evolution of cement paste made with 30% RHA, w/b = 0.25

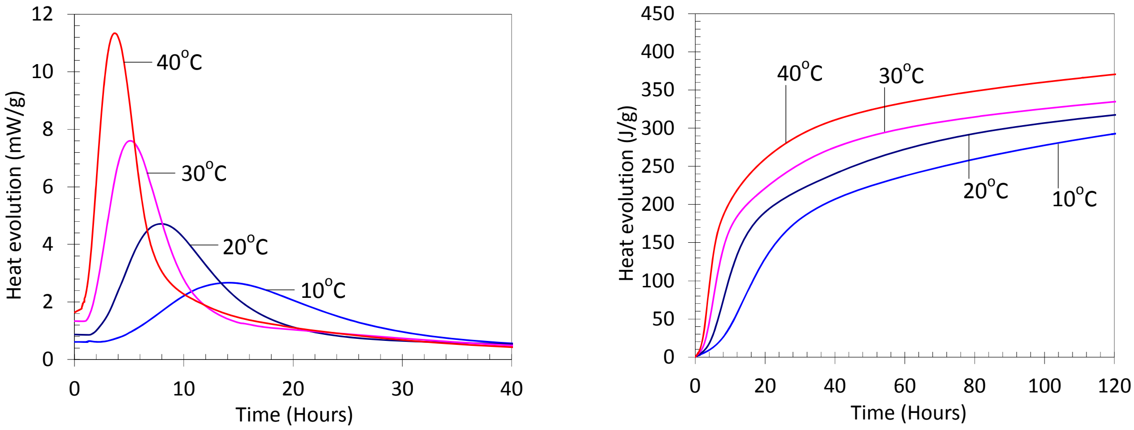

Figure A1.12 Heat evolution of cement paste made with 0% RHA, w/b = 0.40

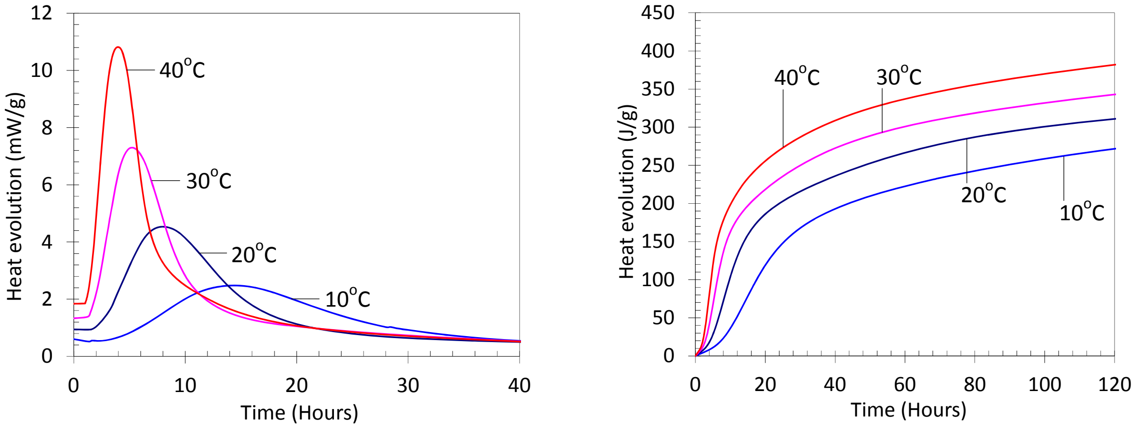

Figure A1.13 Heat evolution of cement paste made with 5% RHA, w/b = 0.40

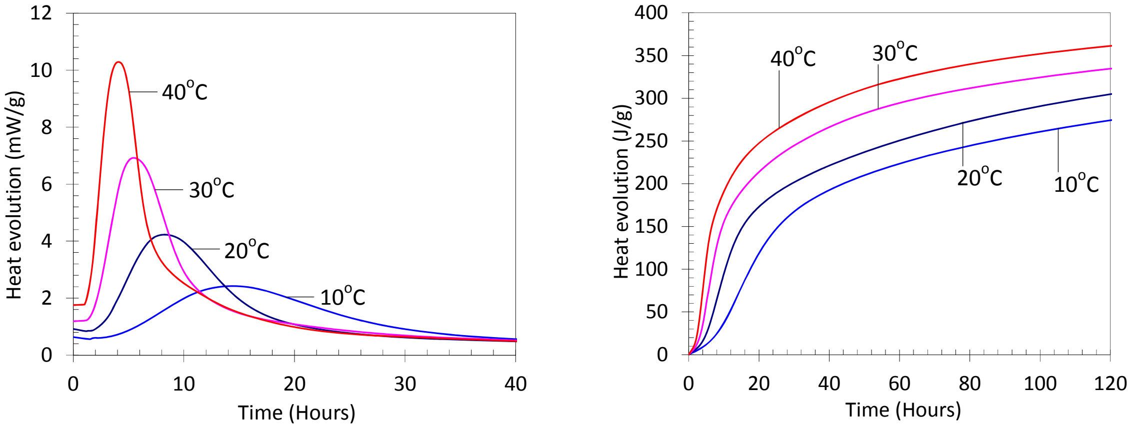

Figure A1.14 Heat evolution of cement paste made with 10% RHA, w/b = 0.40

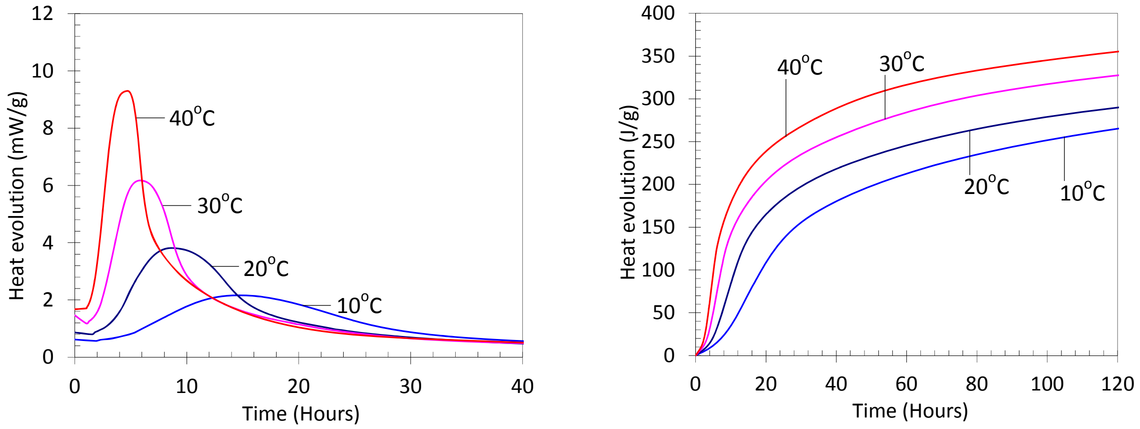

Figure A1.15 Heat evolution of cement paste made with 20% RHA, w/b = 0.40

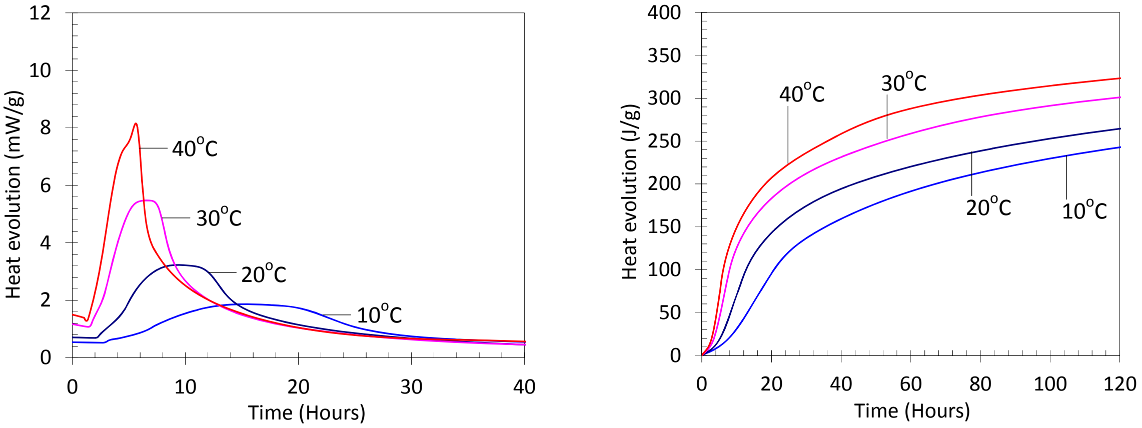

Figure A1.16 Heat evolution of cement paste made with 30% RHA, w/b = 0.40

A1.4 Effect of curing temperature on heat evolution of cement paste made with SF

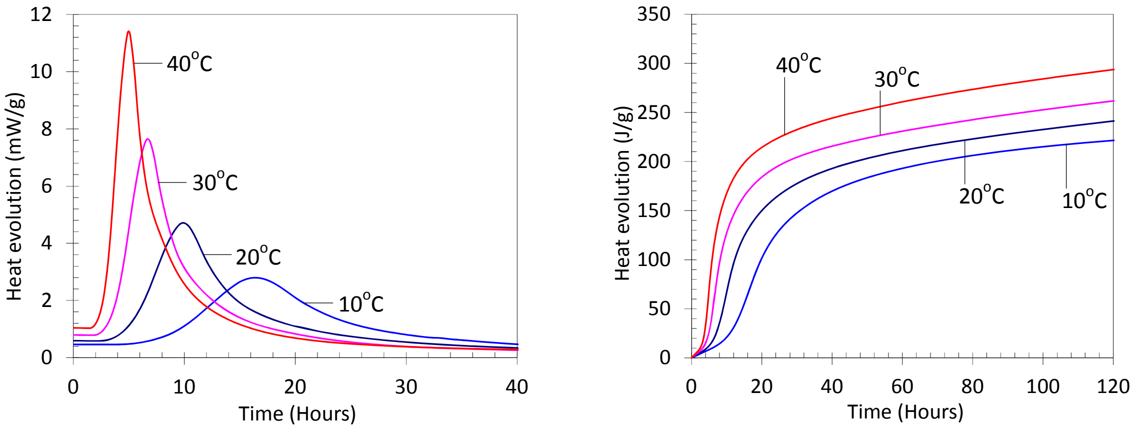

Figure A1.17 Heat evolution of cement paste made with 5% SF, w/b = 0.25

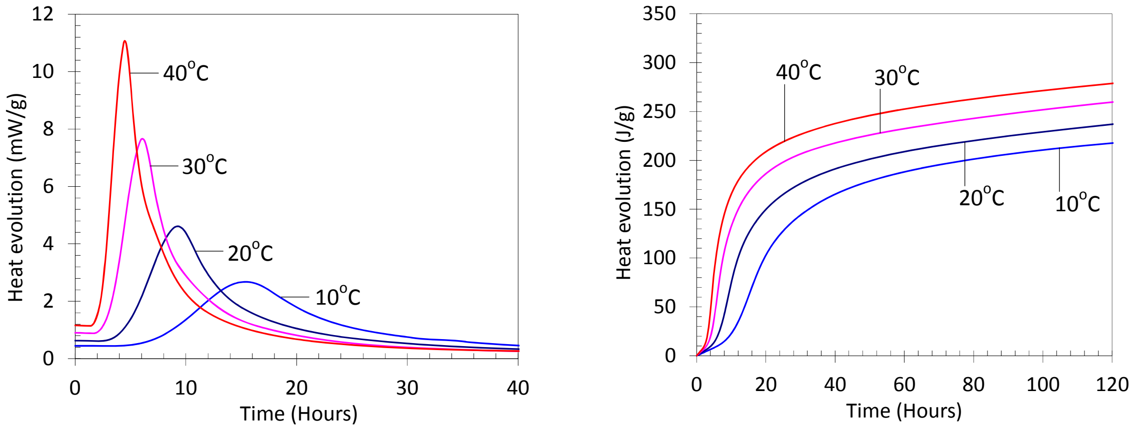

Figure A1.18 Heat evolution of cement paste made with 10% SF, w/b = 0.25

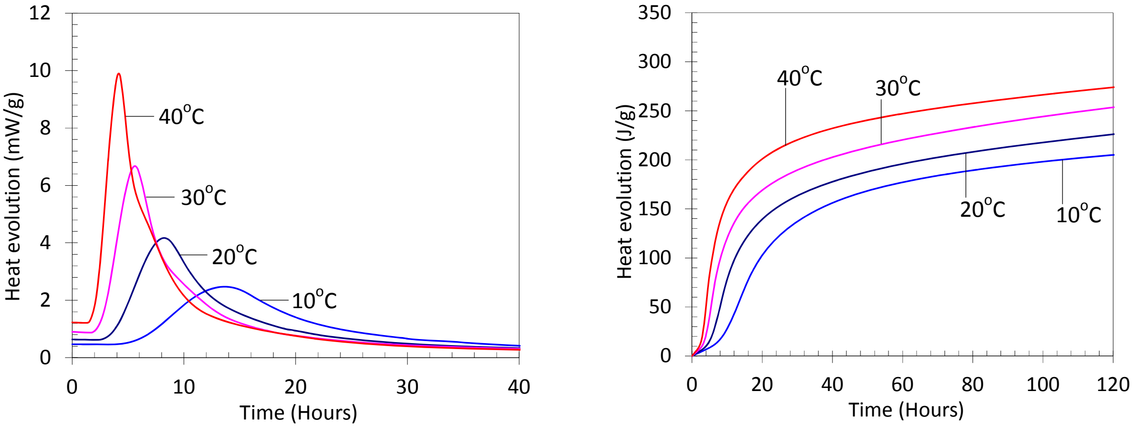

Figure A1.19 Heat evolution of cement paste made with 20% SF, w/b = 0.25

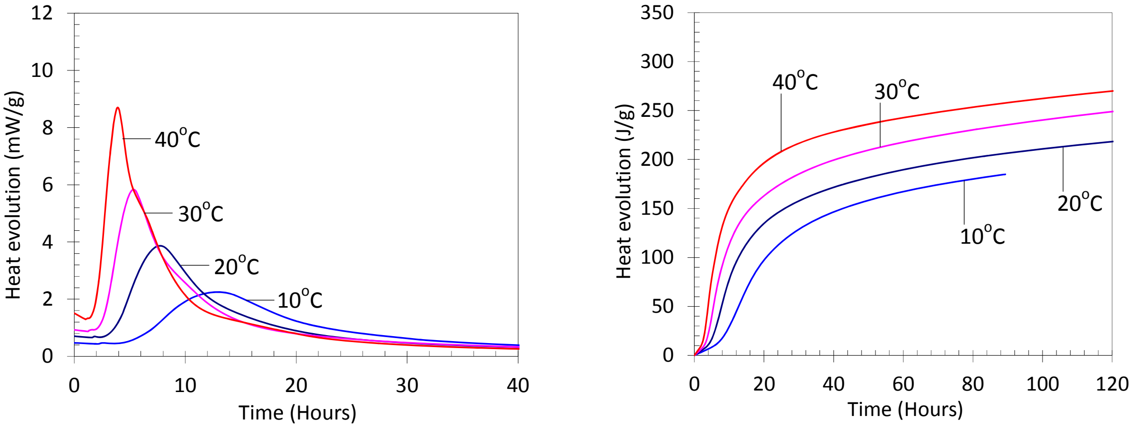

Figure A1.20 Heat evolution of cement paste made with 30% SF, w/b = 0.25

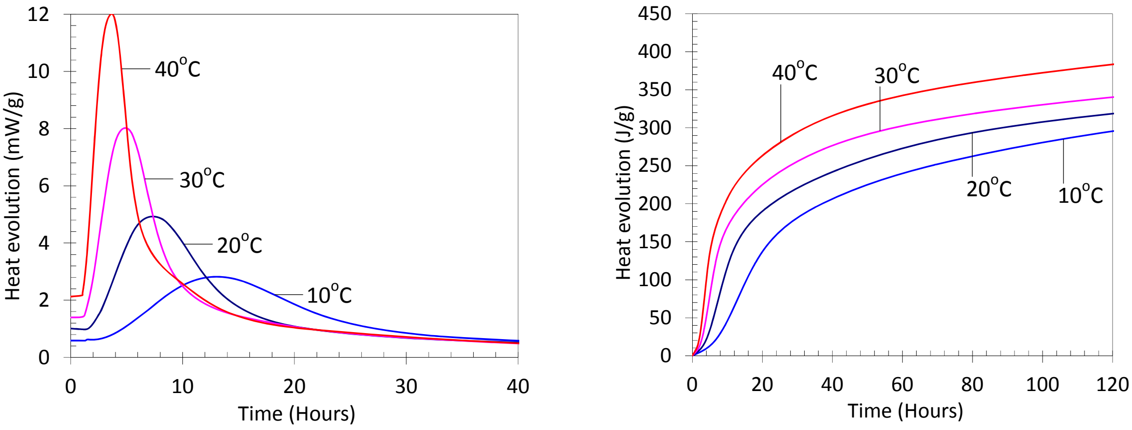

Figure A1.21 Heat evolution of cement paste made with 5% SF, w/b = 0.40

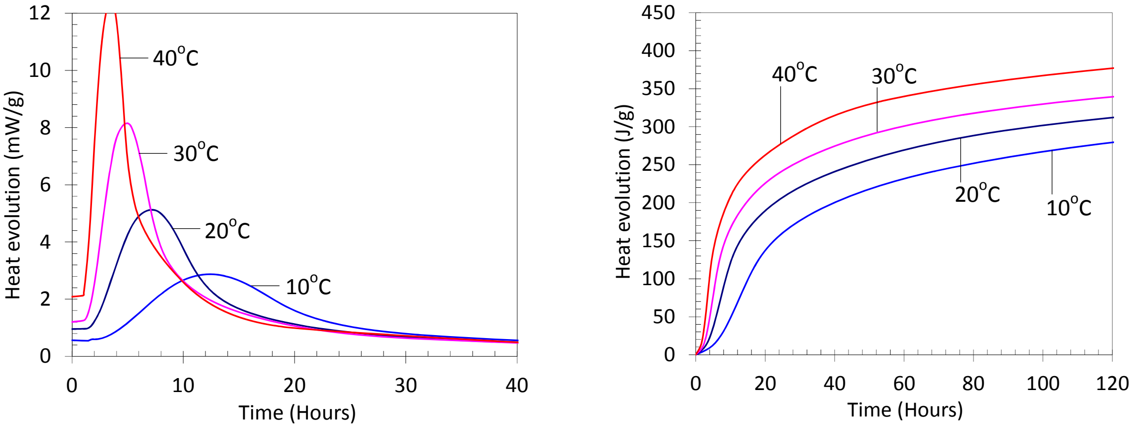

Figure A1.22 Heat evolution of cement paste made with 10% SF, w/b = 0.40

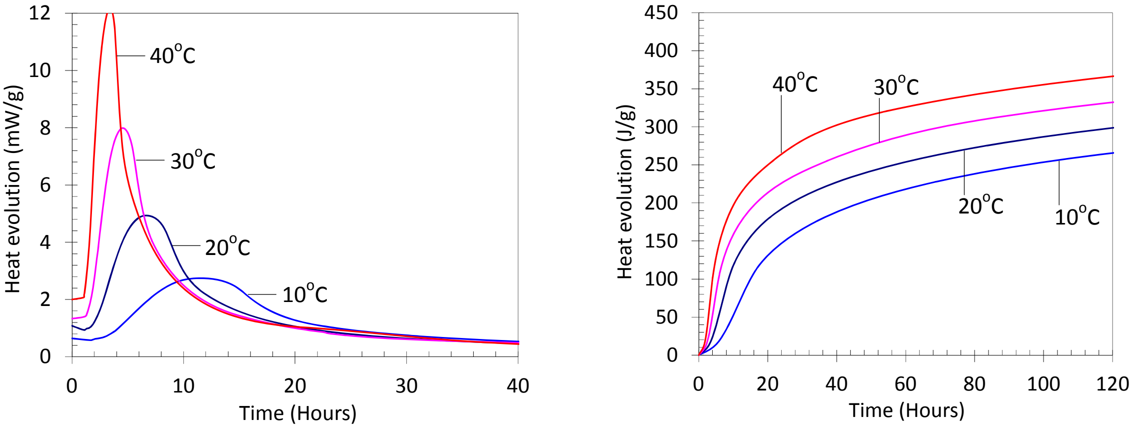

Figure A1.23 Heat evolution of cement paste made with 20% SF, w/b = 0.40

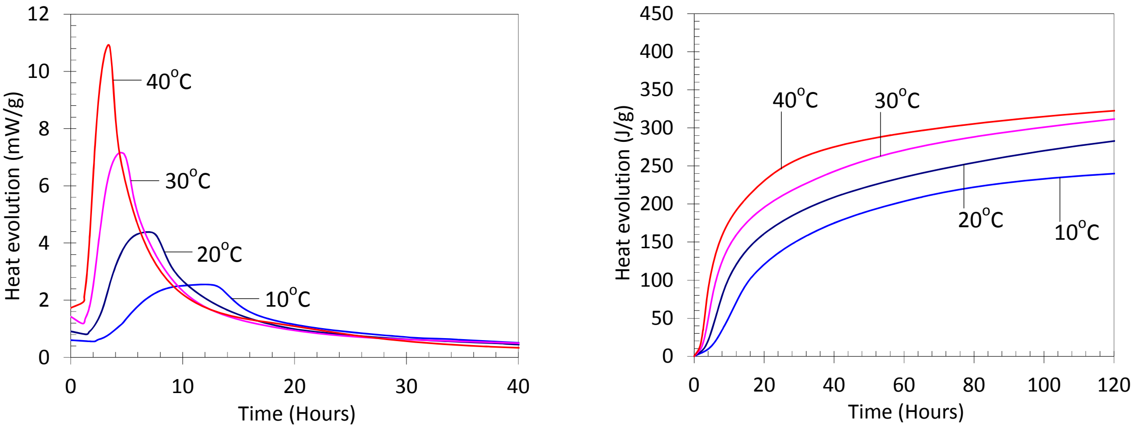

Figure A1.24 Heat evolution of cement paste made with 30% SF, w/b = 0.40

A1.5 Apparent activation energy (Ea) of cement blended with RHA

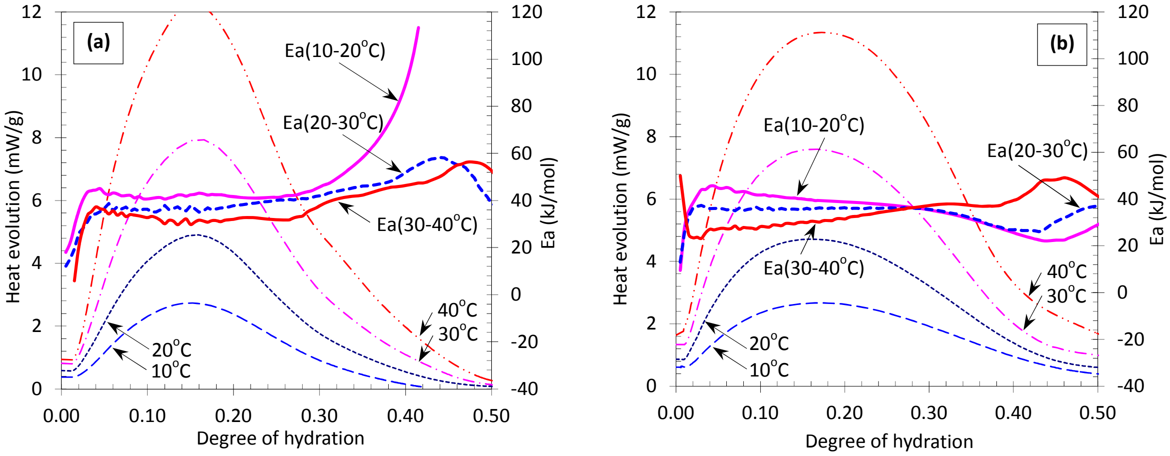

Figure A1.25 Heat evolution and the calculated *Ea* of control samples without RHA, w/b = 0.25 (a) and 0.40 (b)

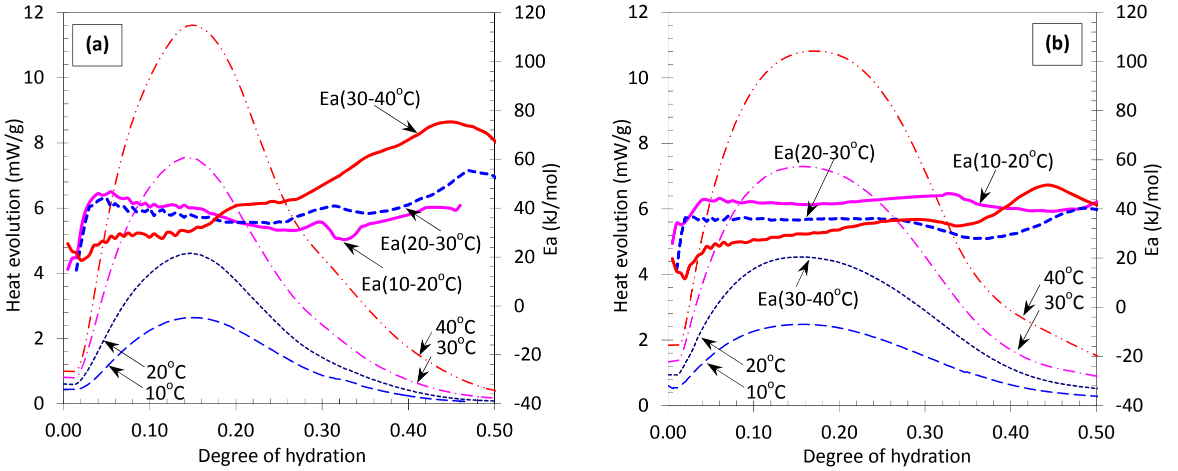

Figure A1.26 Heat evolution and the calculated *Ea* of samples with 5% RHA, w/b = 0.25 (a) and 0.40 (b)

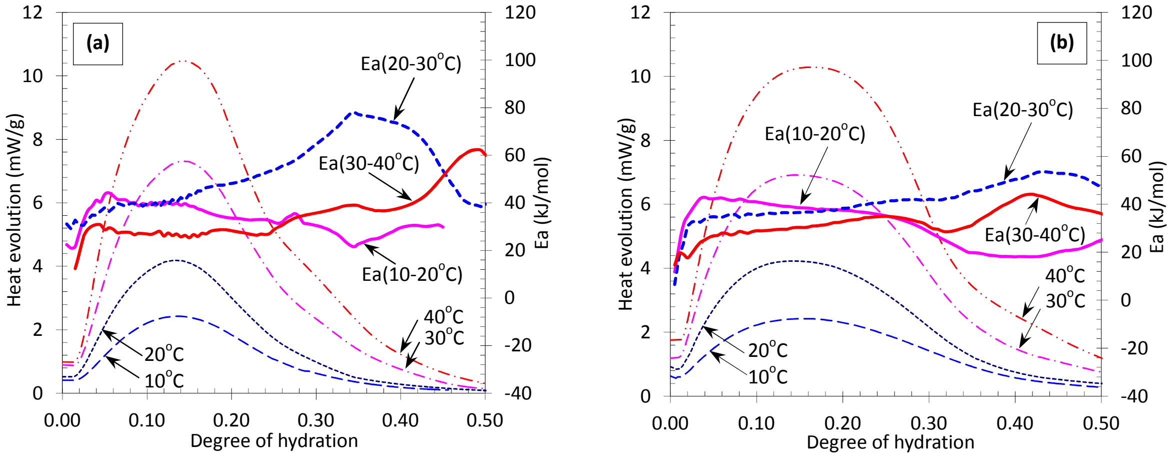

Figure A1.27 Heat evolution and the calculated *Ea* of samples with 10% RHA, w/b = 0.25 (a) and 0.40 (b)

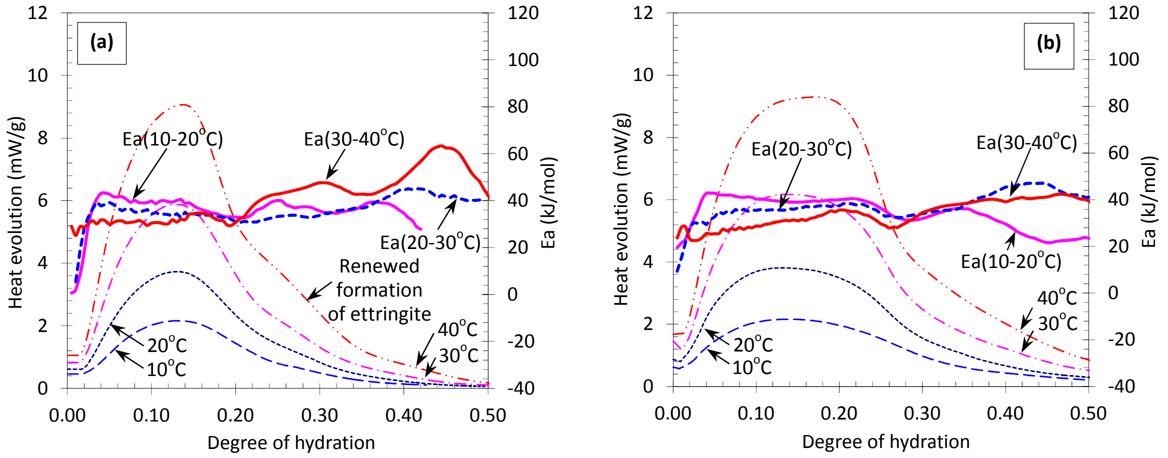

Figure A1.28 Heat evolution and the calculated *Ea* of samples with 20% RHA, w/b = 0.25 (a) and 0.40 (b)

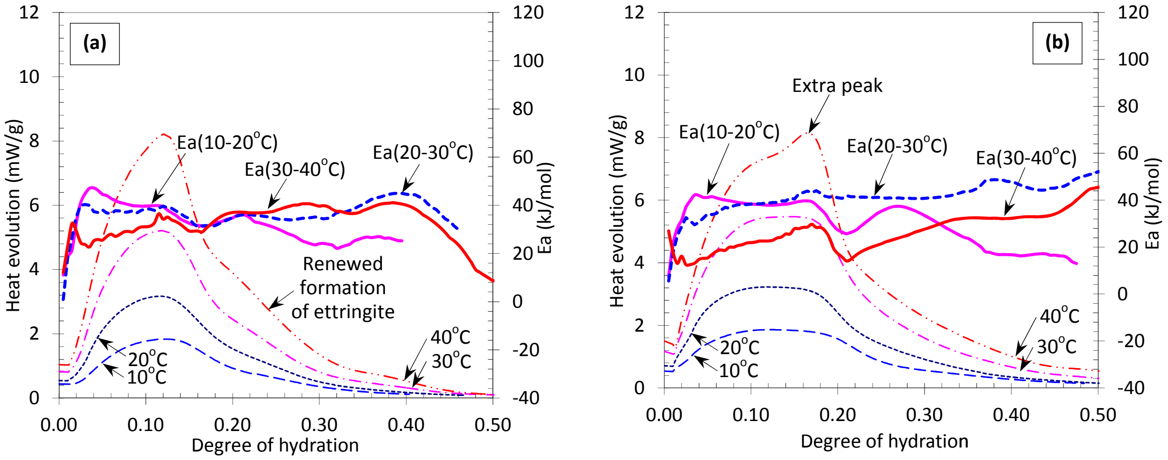

Figure A1.29 Heat evolution and the calculated *Ea* of samples with 30% RHA, w/b = 0.25 (a) and 0.40 (b)

A1.6 Apparent activation energy (Ea) of cement blended with SF

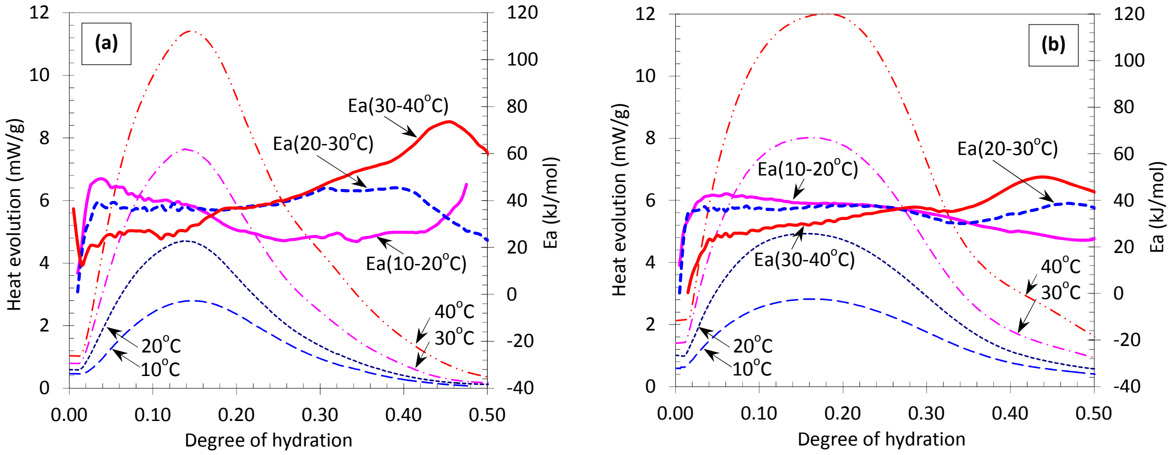

Figure A1.30 Heat evolution and the calculated *Ea* of samples with 5% SF, w/b = 0.25 (a) and 0.40 (b)

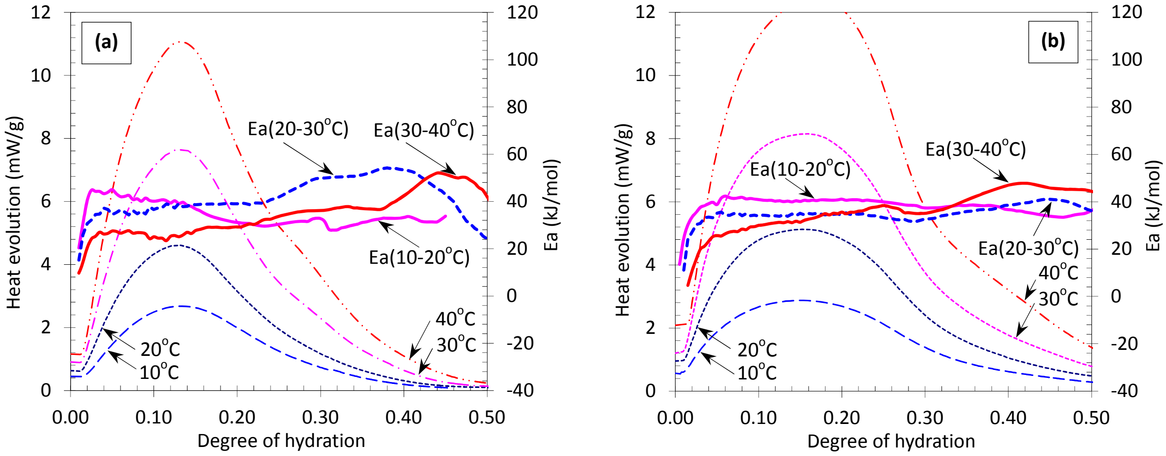

Figure A1.31 Heat evolution and the calculated *Ea* of samples with 10% SF, w/b = 0.25 (a) and 0.40 (b)

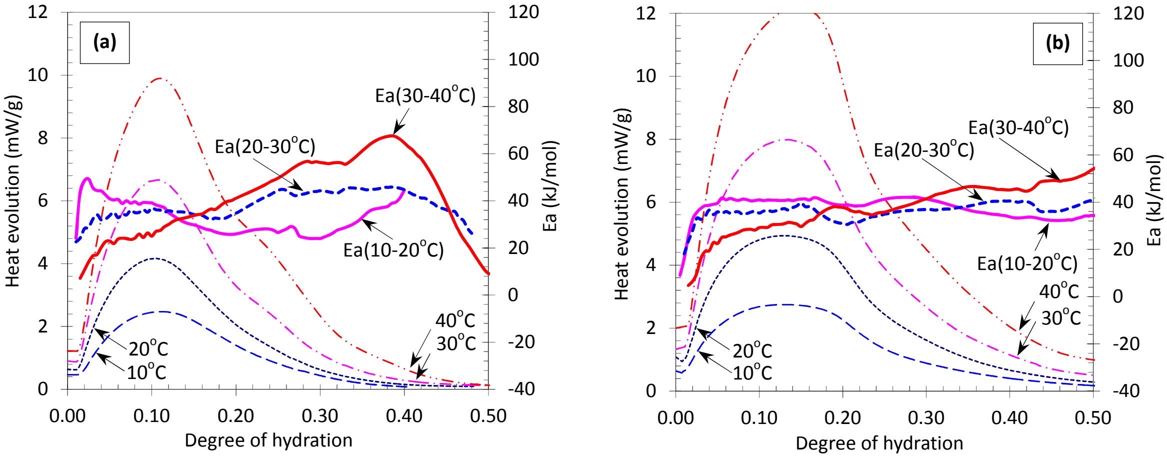

Figure A1.32 Heat evolution and the calculated *Ea* of samples with 20% SF, w/b = 0.25 (a) and 0.40 (b)

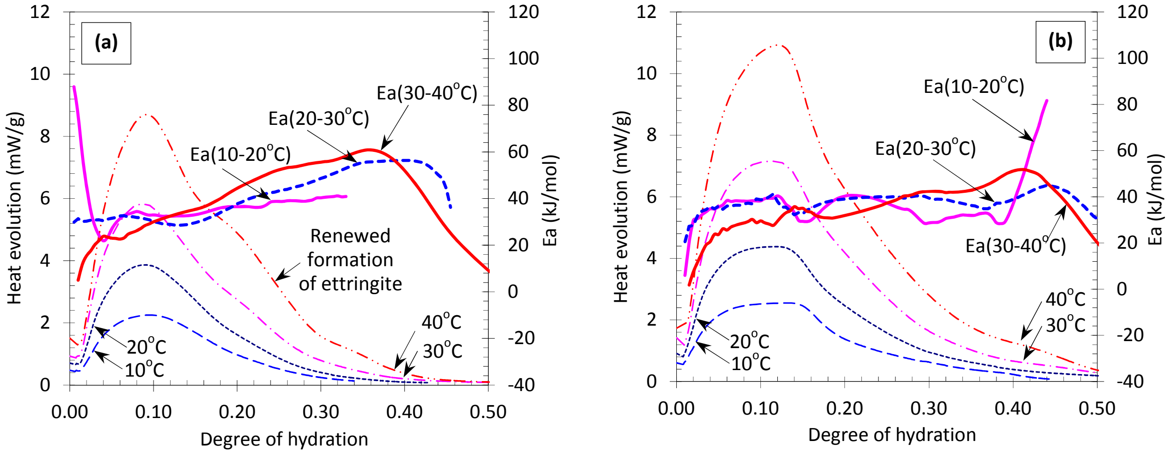

Figure A1.33 Heat evolution and the calculated *Ea* of samples with 30% SF, w/b = 0.25 (a) and 0.40 (b)

A2 Effect of RHA and SF on the pore size distribution of cement paste

A2.1 Effect of RHA contents with different w/b ratios

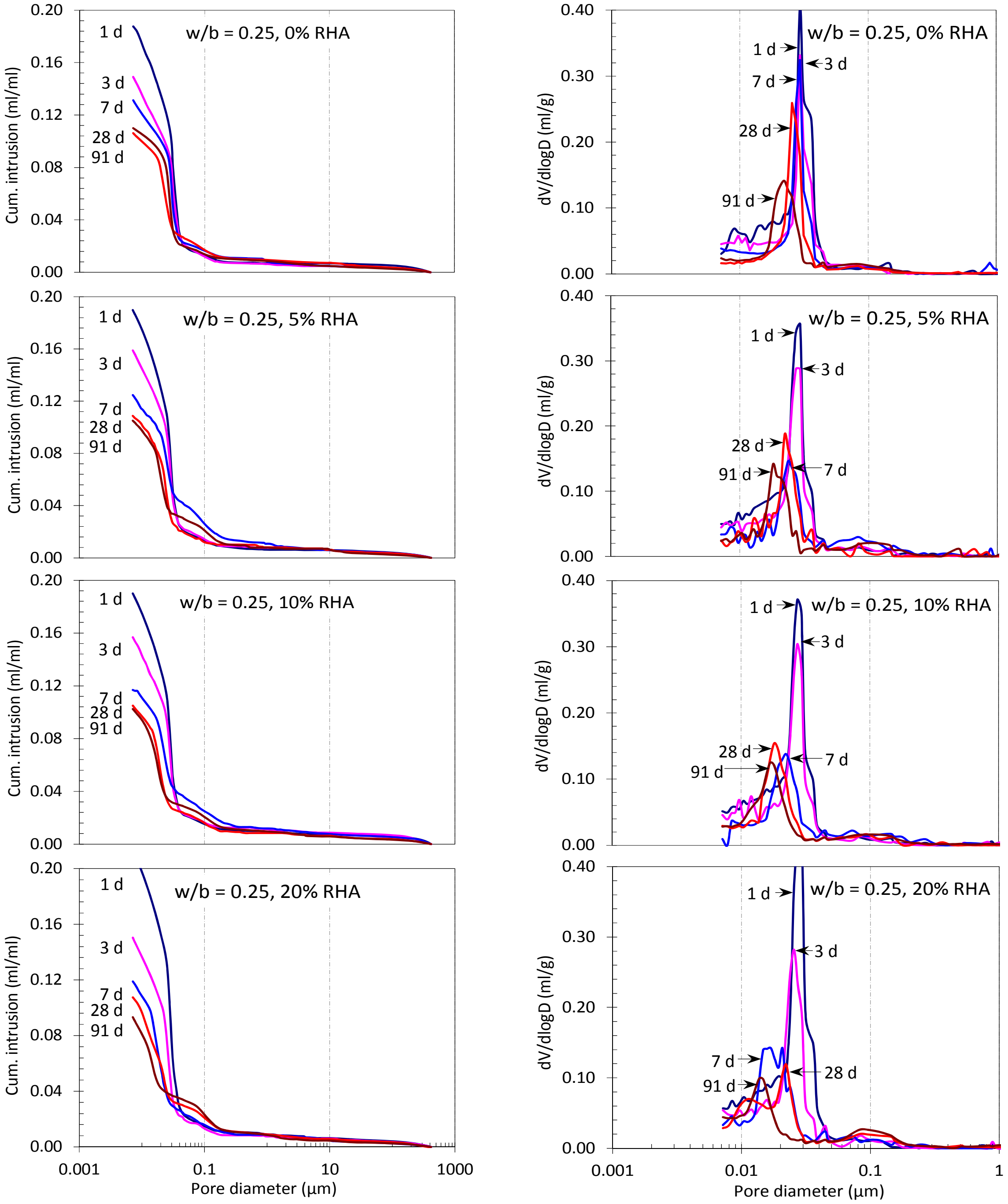

Figure A2.1 Pore size distribution of cement made with 0, 5, 10 and 20% RHA at the ages from 1 to 91 days, w/b = 0.25

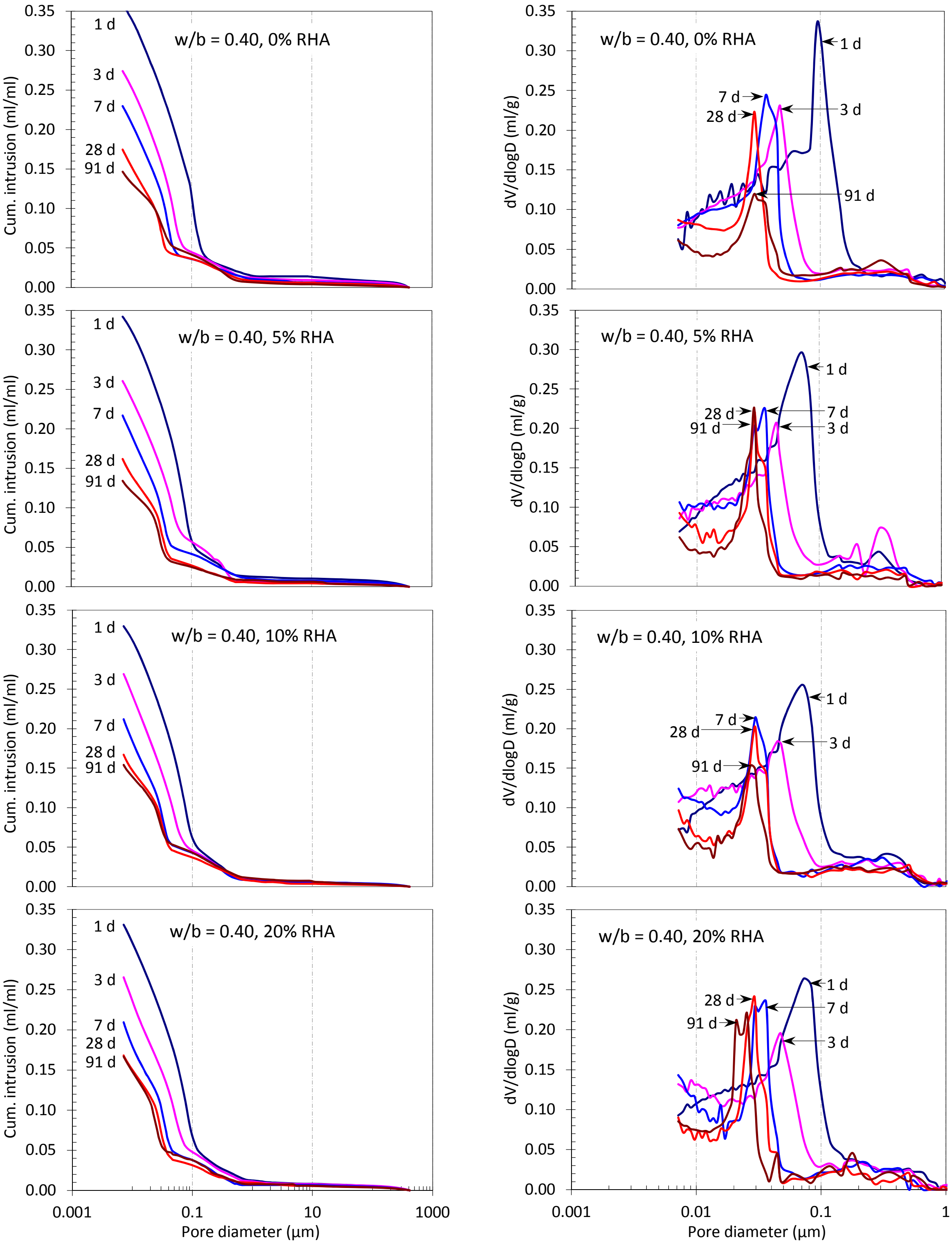

Figure A2.2 Pore size distribution of cement blended with 0, 5, 10 and 20% RHA at the ages from 1 to 91 days, w/b = 0.40

A2.1 Effect of SF contents with different w/b ratios

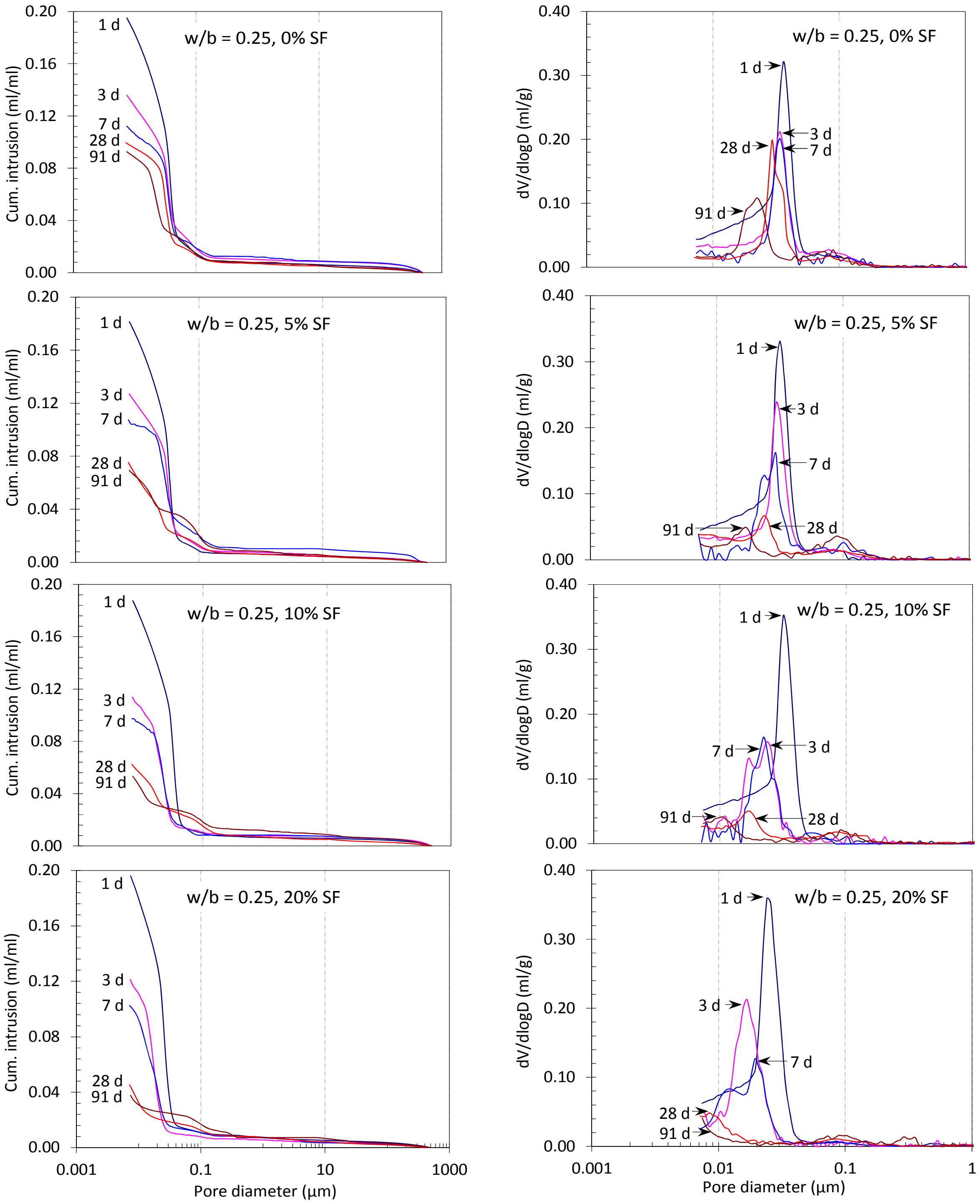

Figure A2.3 Pore size distribution of cement blended with 0, 5, 10 and 20% SF at the ages from 1 to 91 days, w/b = 0.25

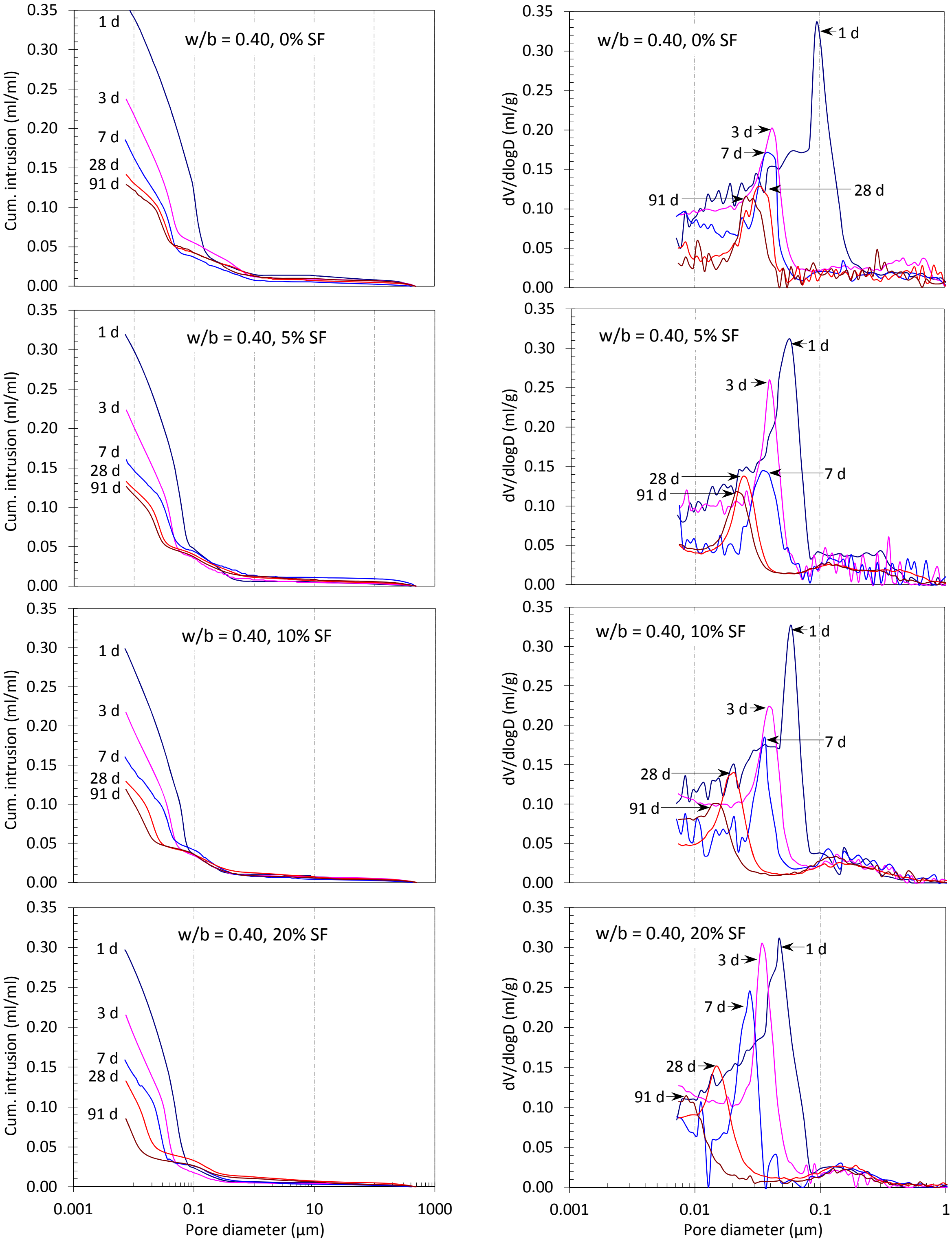

Figure A2.4 Pore size distribution of cement blended with 0, 5, 10 and 20% SF at the ages from 1 to 91 days, w/b = 0.40

Summary

Ultra High Performance Concrete (UHPC) has become one of the promising concretes in the 21st century because of its high fluidity, high strength, low permeability, and excellent durability characteristics. However, regarding the material constituents, the use of a high amount of silica fume (SF) to make UHPC will cause some apparent disadvantages in terms of the high cost and the limited availability. This constrains the applications of SF for making UHPC, especially in developing countries. It also gives a motivation for searching for other materials with similar functions to replace SF. Among the mineral admixtures used in concrete, Rice Husk Ash (RHA), an agricultural waste material, was found to be a very suitable potential substitution with respect to its properties and its available quantity. Therefore, the overall objective of the research, i.e. the possibility of using RHA as a mineral admixture to make UHPC, was proposed.

In order to reach such goals, the experimental studies focus on the influence of RHA, not only on the hydration and microstructure development of cement paste at a low w/b ratio, but also on autogenous shrinkage and the compressive strength of UHPC. In the experimental program, isothermal calorimetry, mercury intrusion porosimetry, scanning electron microscopy and thermogravimetric analysis were used to study the hydration process and the microstructural development. The sealed corrugated moulds were used to measure the autogenous shrinkage of UHPC mixtures. In the numerical simulation, the effect of RHA on the hydration and microstructure development of cement paste was simulated and verified in order to optimize the use of RHA in cement paste.

Compared with SF, from a technical point of view RHA has some disadvantages in terms of its effect on the workability and the packing density. However, the results from this research reveal that the use of RHA to make UHPC is feasible both technically, environmentally and economically.

The experimental studies on the hydration and microstructure development of cement paste demonstrated one of the very important results that the addition of RHA in low w/b ratio cement pastes increases the degree of cement hydration at later stages. This may be attributed to the absorbed water from the porous RHA particles. These water-saturated RHA particles seem to act as water reservoirs distributed throughout the system. With the progress of the hydration process, the water from these pores will be released and will promote the hydration of the cement.

Additionally, it was also found that the fineness of RHA strongly influences the hydration and microstructure development of cement paste. In fact, the fineness of RHA is determined by the grinding process. Intensive grinding will cause the collapse of the RHA particles and their porous structure. This collapse causes a reduction of water absorption by RHA, and thus the positive effect of RHA on both the hydration and the microstructure of cement paste will be less. The experimental results showed that there is an appropriate fineness of RHA, i.e. 5 µm, with regard to the grinding energy, the pozzolanic activity of RHA, the hydration and the microstructure of cement paste.

The combination of experimental results and the numerical simulation is very useful in evaluating the effect of RHA on the hydration process and microstructure development of cement paste. Modelling of these aspects was developed with a modified version of the HYMOSTRUC3D model. The simulation results show that there is an optimum amount of RHA used in cement paste. An extra amount of RHA makes no further contribution to the pozzolanic reaction between RHA and CH produced from cement hydration. This result is very important in designing UHPC mixtures containing RHA.

The optimization of the packing density of UHPC granular mixtures, the effect of RHA on the workability, compressive strength, and autogenous shrinkage were dealt with in the experimental studies on UHPC. It was found that the finer RHA particles improve the workability of UHPC mixtures. This may be caused by the partial collapse of the porous structure of RHA particles at a certain degree of grinding. This leads to a reduction of the amount of absorbed water in the RHA particles. Therefore, more free water available in the system can make the mixture more workable.

In addition, the experimental results demonstrated that the addition of RHA increases the compressive strength of UHPC compared to that of the control sample. Besides, the compressive strength of the RHA modified samples is even higher than that of the SF modified samples, especially at later ages and with a high cement replacement. This confirms that RHA can be used as a mineral admixture to produce UHPC. A synergic effect between RHA and SF was also found to improve both the workability and the compressive strength of UHPC. This leads to a higher amount of the total cement replacement to make UHPC, which is very important for the sustainable development of the construction industry.

A high autogenous shrinkage is one of the disadvantages of UHPC. This is because of self-desiccation caused by the very low w/b ratio and the use of a high amount of SF. In the experimental studies, it was observed that the addition of RHA mitigates the autogenous shrinkage of UHPC mixtures. The effective mean particle size of RHA to mitigate autogenous shrinkage of UHPC mixtures was suggested in the range of 5.6 µm to 9.0 µm. This positive effect is possibly attributed to the absorbed water in the porous structure of RHA, which influences the distribution of water and compensates for the drop of relative humidity in concrete during the hydration process.

Samenvatting (Dutch summary)

Ultra High Performance Concrete (UHPC) is uitgegroeid tot een van de veelbelovende betonsoorten in de 21e eeuw vanwege de hoge vloeibaarheid, hoge sterkte, lage permeabiliteit en uitstekende duurzaamheidseigenschappen. Silica fume (SF) is een belangrijk bestanddeel van UHPC. De toepassing van een hoog gehalte SF bij de productie van UHPC heeft echter nadelen, zoals hoge kosten en beperkte beschikbaarheid. Dit beperkt het gebruik van SF bij het vervaardigen van UHPC, vooral in ontwikkelingslanden. Bovendien creëert het motivatie voor het zoeken naar andere materialen met vergelijkbare functies die SF kunnen vervangen. Naast de minerale toevoegingen die in het beton worden gebruikt blijkt Rice Husk Ash (RHA), een agrarisch afvalmateriaal, een zeer geschikte potentiële vervanging van SF te zijn, zowel voor wat betreft de eigenschappen van het materiaal als de beschikbare hoeveel-heid. De algemene doelstelling van dit onderzoek betreft dan ook de mogelijkheid om RHA als een mineraaltoevoeging te gebruiken voor het produceren van UHPC.

De experimentele studies in dit onderzoek richten zich op de invloed van RHA of verschillende eigenschappen van cementsteen. De focus ligt niet alleen op de hydratatie en de ontwikkeling van de microstructuur in cementsteen bij een lage water-bindmiddelfactor, maar ook op de autogene krimp en de druksterkte van UHPC. In het experimentele programma is gebruik gemaakt van isotherme calorimetrie, kwikporositeitsmetingen, microscopisch onderzoek (ESEM) en thermogravimetrische analyse (TGA) om het hydratatieproces en de ontwikkeling van de microstructuur te bestuderen. Om de autogene krimp van de UHPC mengsels te meten zijn de verzegelde gegolfde gietvormen gebruikt. Met behulp van numerieke simulaties is het effect van RHA op de hydratatie en microstructuurontwikkeling gesimuleerd om het gebruik van RHA in cementsteen te optimaliseren.

Vergeleken met SF heeft RHA, vanuit technisch oogpunt, een aantal nadelen voor wat betreft de verwerkbaarheid en dichtheid. Dit onderzoek heeft aangetoond dat het gebruik van RHA om UHPC te maken zowel technisch, ecologisch en economisch haalbaar is.

De experimentele studies naar de hydratatie en de ontwikkeling van de microstructuur tonen aan, dat de toevoeging van RHA in cementsteen met een lage water-bindmiddelfactor de hydratatiegraad van cement in latere stadia verhoogt. Dit kan mogelijk worden toegeschreven aan het geabsorbeerde water dat uit de poreuze RHA deeltjes kan vrijkomen. Deze met water verzadigde RHA deeltjes lijken te fungeren als waterreservoirs, verspreid door het verhardende systeem. Bij de voortgang van het hydratatieproces zal het water uit de poriën worden vrijgegeven en zo de hydratatie van het cement bevorderen.

Daarnaast is ook geconstateerd dat de fijnheid van RHA sterk van invloed is op de hydratatie en microstructuurontwikkeling van de cementsteen. De fijnheid van RHA wordt in feite bepaald door het maalproces. Intensief malen zal leiden tot het ineenklappen van de poriën in de RHA deeltjes. Dit ineenklappen van de poriën veroorzaakt een vermindering van de waterabsorptie door RHA, waardoor het positieve effect van RHA op zowel de hydratatie als de microstructuur van de cementsteen minder is. De experimentele resultaten tonen aan dat er een optimale fijnheid bestaat voor RHA, namelijk 5 micrometer, waarin verdisconteerd zijn de maalenergie, de puzzolane activiteit van RHA, de hydratatie en de microstructuur van de cementsteen.

De combinatie van experimentele resultaten en numerieke simulatie is zeer nuttig bij het evalueren van het effect van RHA op het hydratatieproces en de microstructuurontwikkeling van de cementsteen. Het modelleren van deze aspecten is gedaan met een aangepaste versie van het HYMOSTRUC3D model. De simulatieresultaten laten zien dat er een optimale hoeveelheid RHA is die voor het vervaardigen van cementsteen gebruikt kan worden. Een extra hoeveelheid RHA levert geen verdere bijdrage aan de puzzolane reactie tussen de RHA en de calcium hydroxide afkomstig uit de cementhydratatie. Dit resultaat is van groot belang voor het ontwerpen van UHPC mengsels met RHA.

De optimalisatie van de dichtheid van UHPC mengsels, het effect van RHA op de verwerkbaarheid, druksterkte en autogene krimp zijn behandeld in de experimentele studies over UHPC. Fijnere RHA deeltjes leiden tot een betere verwerkbaarheid van UHPC mengsels. Dit kan het gevolg zijn van het gedeeltelijke ineenklappen van de poreuze structuur van de RHA deeltjes bij een bepaalde mate van malen. Hierdoor is de hoeveelheid geabsorbeerd water in de RHA deeltjes minder, waardoor de toegenomen hoeveelheid vrij water beschikbaar in het systeem leidt tot een beter verwerkbaar mengsel.

Bovendien tonen de experimentele resultaten aan dat door de toevoeging van RHA de druksterkte van UHPC, vergeleken met referentiemengsels zonder RHA, wordt vergroot. Tevens is de druksterkte van een RHA-gemodificeerd proefstuk groter dan die van een SF-gemodificeerd proefstuk, voornamelijk op latere leeftijd en bij een hoge cementvervanging. Dit bevestigt dat RHA gebruikt kan worden als minerale toevoeging aan UHPC. Een synergie-effect tussen RHA en SF blijkt zowel de verwerkbaarheid als de druksterkte van UHPC te verbeteren. Dit leidt tot een grotere hoeveelheid cement die vervangen kan worden om UHPC te maken, wat heel belangrijk is voor de duurzame ontwikkeling van het bouwen, met name in landen waar rijstkaf ruim voor handen is.

Een grote autogene krimp is een van de nadelen van UHPC. De oorzaak hiervan is zelfuitdroging die het gevolg is van de zeer lage water-bindmiddelfactor en het gebruik van een hoog gehalte aan SF. In het experimentele onderzoek is waargenomen dat de toevoeging van RHA de autogene krimp van UHPC mengsels vermindert. De effectieve gemiddelde deeltjesgrootte van RHA om autogene krimp van UHPC mengsels te verminderen ligt in de range van 5,6 μm tot 9,0 μm. Dit positieve effect is mogelijk toe te schrijven aan het geabsorbeerde water in de poreuze structuur van RHA, die de verdeling van het water in het systeem beïnvloedt en de daling van de relatieve vochtigheid in beton tijdens de hydratatieproces compenseert.

Tóm tắt (Vietnamese summary)

Do có các đặc tính như độ chảy cao, cường độ cao, độ thấm thấp, và độ bền tuyệt vời nên bê tông tính năng siêu cao (BTTNSC) đã và đang trở thành một trong những loại bê tông đầy triển vọng ở thế kỷ 21. Tuy vậy, xét theo khía cạnh nguyên vật liệu cấu thành, thì loại bê tông này cũng có nhược điểm cơ bản đó là khi chế tạo cần phải sử dụng một lượng lớn silica fume là một sản phẩm có giá thành cao và nguồn cung ứng hạn hẹp. Điều này đã hạn chế việc sử dụng silica fume trong chế tạo BTTNSC, đặc biệt ở các nước đang phát triển, đồng thời cũng là động lực cho việc tìm kiếm vật liệu với các tính năng tương tự silica fume để thay thế loại sản phẩm đắt và tương đối hiếm này. Trong số các phụ gia khoáng dùng trong bê tông thì tro trấu, một loại phế thải nông nghiệp, được đánh giá là rất triển vọng và phù hợp để thay thế silica fume dựa trên các tính chất kỹ thuật của nó cũng như nguồn cung cấp. Do vậy, mục tiêu chính của đề tài được đặt ra là nghiên cứu khả năng sử dụng tro trấu như là một phụ gia khoáng nhằm chế tạo BTTNSC.

Để đạt được mục tiêu này, đề tài đã tiến hành các nghiên cứu thực nghiệm về sự ảnh hưởng của tro trấu không chỉ đến quá trình thủy hóa và sự phát triển vi cấu trúc của hồ xi măng với tỷ lệ nước/xi măng thấp, mà còn đến độ tự co và cường độ nén của BTTNSC. Để thực hiện các nghiên cứu thực nghiệm về thủy hóa và phát triển vi cấu trúc của hồ xi măng, đề tài đã sử dụng các phương pháp phân tích hóa lý như đo nhiệt theo phương pháp đẳng nhiệt, đo độ rỗng theo phương pháp thấm thủy ngân, phân tích bằng kính hiển vi điện tử quét, và phân tích nhiệt vi sai. Đề tài đã sử dụng các khuôn gắn kín dưới dạng các ống nhựa xoắn gấp nếp để đo độ tự co của hỗn hợp BTTNSC. Trong phần mô phỏng kỹ thuật số, sự ảnh hưởng của tro trấu đến quá trình thủy hóa và phát triển vi cấu trúc của hồ xi măng đã được mô phỏng và kiểm chứng bằng thực nghiệm để xác định lượng tro trấu tối ưu sử dụng trong hồ xi măng.

So sánh với silica fume trên khía cạnh tính chất kỹ thuật, thì tro trấu có hiệu quả thấp hơn trong việc cải thiện tính công tác và độ đặc chắc của hỗn hợp. Tuy vậy, các kết quả của nghiên cứu này đã chứng minh rằng việc sử dụng tro trấu để chế tạo BTTNSC là hoàn toàn khả thi về mặt kỹ thuật, môi trường và kinh tế.

Một trong những kết quả quan trọng nhất của các nghiên cứu thực nghiệm về thủy hóa và phát triển vi cấu trúc của hồ xi măng là phát hiện về sự gia tăng mức độ thủy hóa ở giai đoạn muộn của hồ xi măng có tỷ lệ nước/xi măng thấp, khi trong hồ xi măng có mặt tro trấu. Nguyên nhân làm tăng mức độ thủy hóa có thể là do lượng nước bổ sung nằm trong các lỗ rỗng của các hạt tro trấu. Các hạt tro trấu bão hòa nước này dường như đóng vai trò các bể chứa nước phân bố

khắp trong thể tích của bê tông. Cùng với tiến trình thủy hóa, nước trong lỗ rỗng này sẽ được giải phóng và sẽ thúc đẩy sự thủy hóa của xi măng.

Các kết quả thực nghiệm cũng chỉ ra rằng độ mịn của tro trấu có ảnh hưởng lớn đến sự thủy hóa và sự phát triển vi cấu trúc của hồ xi măng. Trên thực tế, độ mịn của tro trấu phụ thuộc vào quá trình nghiền. Quá trình nghiền này đến một mức độ nào đấy sẽ gây phá hủy cấu trúc rỗng của các hạt tro trấu. Sự phá hủy này dẫn đến việc giảm độ hút nước của tro trấu và do đó làm giảm tác dụng có lợi của tro trấu đến sự thủy hóa và phát triển vi cấu trúc của hồ xi măng. Các kết quả thực nghiệm đã chứng tỏ rằng tro trấu có một độ mịn hợp lý, khoảng 5 µm, dựa trên sự đánh giá về các khía cạnh như năng lượng nghiền, độ hoạt tính của tro trấu, sự thủy hóa và vi cấu trúc của hồ xi măng.

Khi đánh giá ảnh hưởng của tro trấu đến quá trình thủy hóa và phát triển vi cấu trúc của hồ xi măng thì sự kết hợp các kết quả thực nghiệm với mô phỏng kỹ thuật số là giải pháp rất hữu hiệu. Trong luận án này, việc mô phỏng để xem xét các khía cạnh ảnh hưởng nói trên được phát triển trên cơ sở cải tiến mô hình HYMOSTRUC3D. Các kết quả mô phỏng kỹ thuật số cho thấy khi đưa tro trấu vào hồ xi măng sẽ tồn tại một hàm lượng sử dụng tối ưu. Với lượng dùng lớn hơn hàm lượng tối ưu, tro trấu không làm tăng mức độ phản ứng puzơlanic giữa tro trấu với $Ca(OH)_2$ tạo thành do xi măng thủy hóa. Kết quả này có một ý nghĩa rất quan trọng trong việc thiết kế hỗn hợp BTTNSC sử dụng tro trấu.

Công trình nghiên cứu này còn bao gồm các nghiên cứu thực nghiệm về tối ưu hóa sự sắp xếp các hỗn hợp hạt của BTTNSC, sự ảnh hưởng của tro trấu đến tính công tác, cường độ nén, và độ tự co của BTTNSC. Kết quả chỉ ra rằng, sử dụng tro trấu với các hạt mịn hơn sẽ cải thiện tính công tác của hỗn hợp BTTNSC. Điều này có thể do sự phá hủy một phần cấu trúc rỗng của các hạt tro trấu khi nghiền đến một độ mịn nhất định và do đó làm giảm lượng nước nằm trong các lỗ rỗng của các hạt tro trấu. Kết quả là lượng nước tự do trong hỗn hợp tăng lên, làm tăng tính công tác của hỗn hợp bê tông.

Bên cạnh đó, các kết quả thực nghiệm cũng chứng tỏ rằng việc đưa thêm tro trấu vào hỗn hợp bê tông đã làm tăng cường độ nén của BTTNSC so với cường độ của mẫu đối chứng. Cường độ nén của các mẫu BTTNSC chứa tro trấu này thậm chí cao hơn so với cường độ nén của các mẫu BTTNSC chứa silica fume, đặc biệt ở tuổi muộn và với lượng thay thế xi măng lớn. Điều này đã khẳng định rằng tro trấu có thể sử dụng như một phụ gia hoạt tính để chế tạo BTTNSC. Nghiên cứu thực nghiệm về BTTNSC còn thu được một kết quả thú vị là tro trấu và silica fume có tác dụng tương hỗ trong việc cải thiện tính công tác và cường độ nén của BTTNSC. Điều này mở ra khả năng sử dụng hàm lượng phụ gia khoáng lớn hơn để hay thế xi măng, giúp giảm đáng kể lượng dùng xi măng trong BTTNSC, góp phần quan trọng vào sự phát triển bền vững của công nghiệp xây dựng.

Một nhược điểm lớn của BTTNSC là độ tự co lớn. Nguyên nhân gây ra độ tự co lớn là sự tự sấy khô do sử dụng tỷ lệ nước/chất kết dính rất thấp và lượng dùng silica fume rất cao. Các nghiên cứu thực nghiệm đã cho thấy rằng đưa thêm tro trấu vào hỗn hợp BTTNSC làm giảm đáng kể độ tự co của bê tông. Kích thước hạt trung bình từ 5.6 đến 9.0 µm là cỡ hạt tối ưu của tro trấu sử dụng để giảm độ tự co của BTTNSC. Nguyên nhân làm giảm độ tự co có thể là ở lượng nước bổ sung nằm trong cấu trúc rỗng của các hạt tro trấu vì lượng nước này làm tăng độ đồng nhất của sự phân bố nước trong hệ thống và góp phần chống lại sự suy giảm độ ẩm tương đối trong bê tông do quá trình thủy hóa gây ra.

List of publications

Journals

1. **V.T. Nguyen**, G. Ye, K. van Breugel, A.L.A Fraaij, D.D. Bui, The study of using rice husk ash to produce ultra high performance concrete, *Construction and Building Materials* 25(4) (2011) 2030-2035.
2. **V.T. Nguyen**, G. Ye, K. van Breugel, O. Copuroglu, Hydration and microstructure of ultra high performance concrete incorporating rice husk ash, *Cement and Concrete Research* 41(11) (2011) 1104-1111.

Conferences

1. **V.T. Nguyen**, Z. Guo, G. Ye, K. van Breugel, Activation energy of cement blended with silica fume, In Proceeding of *the 29th Cement and Concrete Science Conference*, Leeds, UK, 7-9 Sept. 2009, ISBN: 13 978-0-85316-281-0, pp. 149-152
2. **V.T. Nguyen**, G. Ye, K. van Breugel, D.D. Bui, Influence of rice husk ash fineness on the hydration and microstructure of blended cement paste, In Proceeding of *the 7th International Symposium on Cement and Concrete (ISCC2010),* Jinan, China, 9-12 May 2010, ISBN: 978-7-119-06783, pp. 325-332
3. **V.T. Nguyen**, G. Ye, K. van Breugel, Z. Guo, D.D. Bui, Hydration process of rice husk ash and silica fume in cement paste by means of isothermal calorimetry, In Proceeding of *the Sixth International Conference on Concrete under Severe Conditions Environment and Loading (CONSEC'10)*, Taylor & Francis Group (Eds.), Yucatan, Mexico, 7-9 Jun. 2010, ISBN: 978-0-415-59317-5, Vol. 1, pp. 1521-1528.
4. **V.T. Nguyen**, G. Ye, K. van Breugel, Z. Guo, Activation energy of cement blended with rice husk ash, In Proceeding of *the Second International Conference on Sustainable Construction Materials and Technologies*, Ancona, Italy, 28-30 Jun. 2010, ISBN: 978-1-4507-1490-7, Vol. 1, pp. 383-392
5. **V.T. Nguyen**, G. Ye, K. van Breugel, The possibility of using rice husk ash to produce ultra high performance concrete, In Proceeding of *the 8th fib International PhD Symposium in Civil Engineering*, Lyngby, Denmark, 20-23 Jun. 2010, ISBN: 9788778773012, pp. 437-442

6. **V.T. Nguyen**, G. Ye, K. van Breugel, H.H. Pham, The possibility of using combination of rice husk ash and silica fume to produce ultra high performance concrete with a reduced cement content, In Proceeding of *the 1st International Conference on Sustainable Construction Materials: Design, Performance and Application*, Wuhan, China, 10-12 Aug. 2010, ISBN 978-7-900503-05-3, pp. 763-769
7. **V.T. Nguyen**, G. Ye, K. van Breugel, D.D. Bui, Study the hydration and the microstructure of cement blended with Rice husk ash in comparison with Silica fume, In Proceeding of *the 1st International Conference on Sustainable Construction Materials: Design, Performance and Application*, Wuhan, China, 10-12 Aug. 2010, ISBN 978-7-900503-05-3, pp. 770-776
8. **V.T. Nguyen**, G. Ye, K. van Breugel, Effect of rice husk ash on autogenous shrinkage of ultra high performance concrete, In Proceeding of *the International RILEM Conference on Use of Superabsorbent Polymers and Other New Additives in Concrete*, RILEM (Eds.), Proceedings PRO 74, Lyngby, Denmark, 15-18 Aug. 2010, ISBN: 978-2-35158-104-9/e-ISBN: 978-2-35158-105-6, pp. 293-304
9. **V.T. Nguyen**, G. Ye, K. van Breugel, H.H. Pham, Synergic effect of rice husk ash and silica fume on compressive strength of ultra high performance concrete, In Proceeding of *the International Conference on Material Science and 64th RILEM Annual Week*, RILEM (Eds.), Proceedings PRO 77, Aachen, Germany, 6-10 Sept. 2010, ISBN: 978-2-35158-110-0/e-ISBN: 978-2-35158-111-7, Vol. III, pp. 255-263
10. **V.T. Nguyen**, G. Ye, K. van Breugel, Internal curing of ultra high performance concrete by using rice husk ash, In Proceeding of *the International Conference on Material Science and 64th RILEM Annual Week*, RILEM (Eds.), Proceedings PRO 77, Aachen, Germany, 6-10 Sept. 2010, ISBN: 978-2-35158-110-0/e-ISBN: 978-2-35158-111-7, Vol. III, pp. 265-274
11. **V.T. Nguyen**, G. Ye, K. van Breugel, Effect of rice husk ash on hydration and microstructure of ultra high performance concrete, In Proceeding of *the 30th Cement and Concrete Science Conference*, Birmingham, UK, 13-15 Sept. 2010, ISBN: 978-0-70442-797-6, pp. 51-54
12. **V.T. Nguyen**, G. Ye, K. van Breugel, D.D. Bui, Improving service life of concrete by using rice husk ash, In Proceeding of *the 2nd International Symposium on Service Life Design for Infrastructure*, RILEM (Eds.), Proceedings PRO 70, Delft, The Netherlands, 4-6 Oct. 2010, ISBN: 978-2-35158-096-7/e-ISBN: 978-2-35158-097-4, Vol. 2, pp. 841-848
13. **V.T. Nguyen**, H.H. Pham, T.T. Le, G. Ye, M.N. Soutsos, C.I. Goodier, Ultra high performance concrete using waste materials for high-rise buildings, In Proceeding of *Franco-Vietnamese Conference CIGOS-2010 on High Rise Buildings and Underground Structure*, 18-19 Nov. 2010, Paris, France, R46, 9 pp.
14. **V.T. Nguyen**, G. Ye, D.D. Bui, Study the hydration process of Portland cement blended with rice husk ash by means of isothermal calorimetry, In Proceeding of *the 13th International Congress on the Chemistry of Cement (ICCC)*, Madrid, Spain, 3-8 Jul. 2011, ISBN: Obra completa 84-7292-399-7, Area 4, p. 287
15. **V.T. Nguyen**, G. Ye, Study hydration and microstructure of ultra high performance concrete using rice husk ash, In Proceeding of *the 13th International Congress on the Chemistry of Cement (ICCC)*, Madrid, Spain, 3-8 Jul. 2011, ISBN: Obra completa 84-7292-399-7, Area 4, p. 256
16. **V.T. Nguyen**, Q. Zhang, G. Ye, Modeling the hydration of cement blended with rice husk ash, In Proceeding of *the 13th International Congress on the Chemistry of Cement (ICCC)*, Madrid, Spain, 3-8 Jul. 2011, ISBN: Obra completa 84-7292-399-7, Area 6, p. 353

17. **V.T. Nguyen**, G. Ye, K. van Breugel, D.D. Bui, Influence of fineness of rice husk ash in producing ultra high performance concrete, In Proceeding of *the 9th Symposium on High Performance Concrete- Design, Verification and Utilization*, Rotorua, New Zealand, 7-11 Aug. 2011, ISBN: 978-0-473-19028-6, Session 8, 8.3, p. 113
18. **V.T. Nguyen**, G. Ye, The Use of rice husk ash to produce ultra high performance concrete in sustainable construction, In Proceeding of *the International Conference on Advances in Construction Materials through Science and Engineering, and the 65th RILEM week,* Hong Kong, China SAR, 5-7 Sept. 2011, ISBN: 978-2-35158-116-2/e-ISBN: 978-2-35158-117-9, p. 207
19. G. Ye**, V.T. Nguyen**, Using rice husk ash to mitigate the autogenous shrinkage in ultra high performance concrete, In Proceeding of *International Workshop on Sustainable and Science-Driven Engineering of Cement-based Materials,* Beijing, China, 18-19 Jul. 2011, pp. 187-194

Curriculum vitae

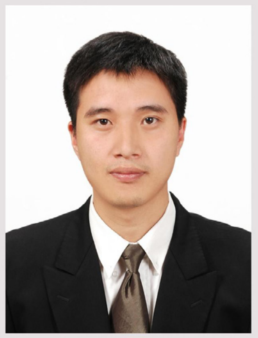

Name:	Nguyen Van Tuan
Date of birth:	May 11th, 1977
Place of birth:	Thai Binh, Vietnam
Email:	tuan.rang@gmail.com

Sept. 1995 - Jun. 2000	Undergraduate studies of Civil Engineering (Field of study: Technology of Building Materials) National University of Civil Engineering, Hanoi, Vietnam
Dec. 2000 - present	Lecturer at the Department of Building Materials, National University of Civil Engineering, Hanoi, Vietnam
Sept. 2001 - Oct. 2004	Graduate studies of Civil Engineering (Honor) National University of Civil Engineering, Hanoi, Vietnam
Apr. 2007 – Jun. 2011	PhD-studies of structural engineering and materials at section of Materials and Environment, Faculty of Civil Engineering and Geosciences, Delft University of Technology, Delft, the Netherlands